Contribution à l'étude de la turbulence dans les fluides et les plasmas

Wouter J.T. Bos

Mémoire présenté pour l'obtention du diplôme

d'habilitation à diriger des recherches par

Wouter Bos

du Laboratoire de Mécanique des Fluides et d'Accoustique
Ecole Centrale de Lyon, Université de Lyon, CNRS

Contribution à l'étude de la turbulence dans les fluides et les plasmas

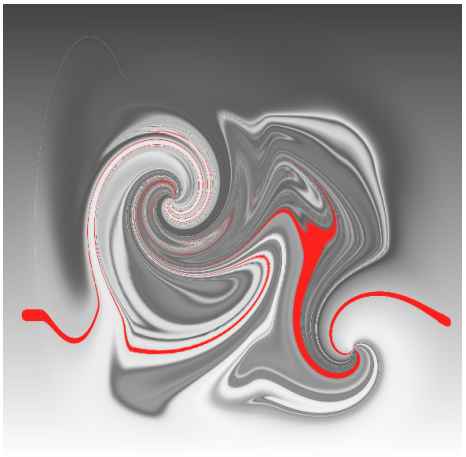

Soutenu le 29 Juin 2012

après l'avis de:

MM.	Dominique	Escande
	William	Matthaeus
Mme	Annick	Pouquet

devant le jury composé de :

MM.	Jean-Pierre	Bertoglio
	Dominique	Escande
	Jean-Noël	Gence
	Jean-François	Pinton
Mme	Annick	Pouquet
M.	Kai	Schneider

Contents

Part I

Contributions to the description of turbulence in fluids and plasmas

Introduction

Turbulence is a fascinating mixture of randomness and coherence. On the one hand, the randomness of the phenomenon naturally motivates the use of a statistical characterization of the turbulent flow properties and the search for theories that can describe and predict these statistics. The coherence, on the other hand, makes it tempting to look at the intriguing beauty of instantaneous vorticity fields and to identify generic mechanisms that describe the dynamics of coherent flow structures. Both approaches are complementary, but in general it is hard to transpose concepts of one approach to the other. For this to be successful, statistical theories should be able to describe the statistical imprint of coherence and generic mechanisms of the dynamics of coherent structures should be characterized statistically. The rapid increase of computational resources and the development of advanced experimental techniques have helped the research community to obtain a detailed description of individual flow-structures, and instantaneous flow realizations. The simulations of turbulence which are carried out and the data obtained from experiments yield a wealth of information, and most statistics are now accessible. However, the accumulation of information does not directly increase our understanding of turbulent flows.

The understanding of a phenomenon is a mixture of intuition based on simple phenomenological models and the development of theories which explain (and ideally predict) the features observed in simulations and experiments. In the case of turbulence, the development of a theory is a long-lasting quest and no entirely satisfactory theory is available which takes into account all features of a turbulent flow. In the following chapter we will highlight the reason for this: the strong nonlinear mode coupling and the inherent Lagrangian character of turbulent movement.

The closest mankind has come to a theory of turbulence is the Direct Interaction Approximation (DIA) which is discussed in detail in chapter 2. However, as soon as one considers problems involving anisotropy or inhomogeneity, the application of DIA-based theories becomes immediately a formidable task. Complex flows have however many features in common with isotropic turbulence, in particular with respect to the interaction between scales, and the study of isotropic turbulence does significantly contribute to a better understanding of turbulent flows in general. In chapter 3 isotropic turbulence is studied using DIA-based approaches. Armed with the understanding of these flows, we can now address more complicated systems. In the second part of the manuscript, chapters 4–6, we investigate the dynamics of plasma turbulence and two-dimensional turbulence in wall-bounded geometry. The presence of plasma density gradients, strong magnetic fields and confining walls considerably complicates the description of the flow properties. In these chapters we will therefore mainly rely on

Direct Numerical Simulations and we try to understand the flow features using phenomenological models and parametric studies.

First, in the following pages, an outline is given of the main results presented in this manuscript.

Outline

This outline summarizes the results presented in the following six chapters. Some key results are presented and references are given to the relevant journal articles.

Chapter 1: Turbulence and the strength of the nonlinearity

The Reynolds number is defined as

$$R_L = \frac{UL}{\nu}, \tag{1}$$

with L a typical lengthscale characterizing the size of the largest (energetically important) flow structures and U the rms velocity. The physical interpretation is that R_L number measures the ratio between inertial effects and viscous effects. If we write the Navier-Stokes equations as

$$\partial_t \boldsymbol{u} = \boldsymbol{N} + \nu \Delta \boldsymbol{u}, \tag{2}$$

with $\boldsymbol{N} = -(\boldsymbol{u} \cdot \nabla \boldsymbol{u} + \nabla p)$, then the Reynolds number could be alternatively defined by

$$R_* = \frac{\sqrt{< \boldsymbol{N} \cdot \boldsymbol{N} >}}{\sqrt{< (\nu \Delta \boldsymbol{u}) \cdot (\nu \Delta \boldsymbol{u}) >}}. \tag{3}$$

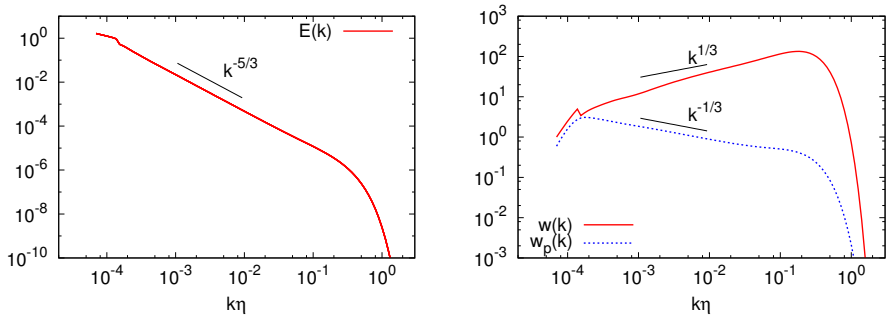

Figure 1: Left: the energy spectrum for a forced turbulent flow at a Taylor-scale Reynolds number $R_\lambda = 4000$. Right: the spectrum of the mean square nonlinearity for the same flow and the spectrum of the pressure gradient.

If we define the power spectrum of the mean-square nonlinearity and of the viscous term such that

$$\begin{aligned} \int w(k)dk &= <|\boldsymbol{N}|^2> \\ \int \Upsilon(k)dk &= <|\nu\Delta\boldsymbol{u}|^2>, \end{aligned} \tag{4}$$

one can define the scale-dependent Reynolds number,

$$R_*(k) = \sqrt{\frac{w(k)}{\Upsilon(k)}}. \tag{5}$$

As observed in Figure 1, the nonlinear term scales as

$$w(k) \sim U^2\epsilon^{2/3}k^{1/3}. \tag{6}$$

Substituting this and Kolmogorov scaling, $E(k) \sim \epsilon^{2/3}k^{-5/3}$, into the Reynolds number (5), it is found that the Kolmogorov scale is not only a function of the energy dissipation and viscosity, but also of the large-scale sweeping velocity. We know from observation in experiments and simulations that this is not the case, and something in the above reasoning is not correct. The problem is related to a key-feature of Kolmogorov's theory, namely the locality of interaction is only satisfied in the Lagrangian reference frame, where the influence of large-scale sweeping is eliminated. This shows the importance of the Lagrangian description of turbulence if one is interested in its multi-scale character.

Chapter 2: The Direct Interaction Approximation

The DIA is a perturbation method. The influence of the nonlinearity on the dynamics of the flow is treated perturbatively. The obvious problem is that this nonlinearity is not small, and perturbation methods only work adequately in the limit of a small perturbation around a certain equilibrium state. In a turbulent flow a large number of triads (velocity fluctuations at three different positions in wavenumber space) are involved in the nonlinear interaction. The influence of one individual triad compared to the cumulative influence of all possible triads should become infinitesimally small if the total number of triad interactions tends to infinity. This ratio of the influence of one individual triad, compared to the cumulative influence of all other triads is the small parameter used in the DIA. A peculiarity of this perturbation approach is that we perturb about the actual state that is unknown and not about a known linear solution. DIA can treat systems which are far from Gaussian, as long as the weak-dependence and maximum randomness conditions are fullfilled.

The derivation of triple and quadruple correlations of a nonlinear evolving quantity (such as the velocity) is described in section 2.3. Whereas this procedure for the derivation of triple correlations is relatively well known, the procedure to derive the expression for quadruple correlations is not.

The DIA applied to the velocity in a Eulerian reference frame yields results which do not agree with Kolmogorov's phenomenological theory about energy

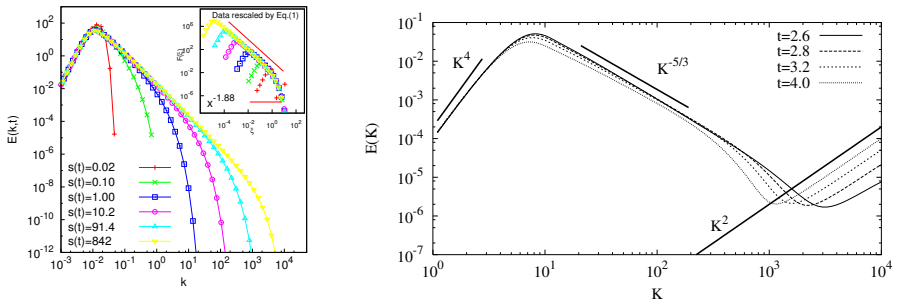

Figure 2: Left: when a turbulent flow develops from an intial state in which the energy is confined at the large scales, the energy spectrum is given by a self-similar form different from classical Kolmogorov scaling. Right: a flow governed by the truncated Euler equations can have an energy spectrum which exhibits a Kolmogorov inertial range in coexistence with modes in thermal equilibrium at the smallest wave-lengths [2].

transfer. The reason is that DIA involves multiple time-correlations which measure the time-scale on which distinct Fourier-modes interact, and in the Eulerian reference frame, decorrelation is dominated by large-scale sweeping. The sweeping time-scale is however not the time-scale which determines the energy transfer and the time-correlations measured in the Eulerian reference frame are therefore not the appropriate ones to describe the local (in scale space) energy tranfer on which Kolmogorov's theory is based. This problem of DIA can be solved by recasting the approximation into a Lagrangian reference frame. This shows that the scale-locality assumption of Kolmogorov is directly linked to the Lagrangian character of the time-correlation of the Fourier modes.

In order to obtain a single-time description, one can use an assumption for the functional dependence of the time-correlations. The unknown quantity to specify is then a Lagrangian memory time which can be specified in several ways. We proposed a procedure, yielding the Lagrangian Markovianized Field Approximation (LMFA), in which this time-scale is determined using the analogy between the fluid particle displacement and the advection of a non-diffusive passive scalar [1].

Chapter 3: Studies on the dynamics of isotropic turbulence

The statistical equilibrium state of a set of Fourier modes governed by the Galerkin-truncated Euler equations is thermal equilibrium with an equipartition of energy between the modes. The nonlinearity of the Navier-Stokes equations is identical to the nonlinearity of the Euler equations and one can therefore expect that if the energy distribution of a turbulent flow is far from this equilibrium, the nonlinearity will act in such a way as to approach it. In the initial stage, this will generate a transient self-similar energy distribution which is not the same as the one observed for constant flux cascades. The steeper slope, with

a power-law exponent of order 1.89, has not yet been described by a simple dimensional analysis [3] (Figure 2, left).

At later times, when the energy is transported to scales fine enough for the viscous stress to act, an equilibrium will be observed (for high enough Reynolds numbers) between the flux towards the small scales and the viscous dissipation of energy at these scales. Exactly the same equilibrium is observed in the Galerkin-truncated Euler equations, where the *thermalized modes* act on the non-equilibrium modes as an eddy viscous process [2] (Figure 2, right).

The energy piles thus up at the largest wavenumbers for the three-dimensional truncated system. Two-dimensional turbulence shows a tendency to transfer the energy to the smallest wavenumbers. The way the energy accumulates at the low-wave-number end can be regulated by adding a friction. If this friction becomes very localized in space, by using a high-order hypo-friction, the energy sink acts like a wavenumber truncation [4] and bottlenecks at the large scales of the flow are observed.

The energy transfer in three-dimensional turbulence is considered in more detail in sections 3.2 and 3.3. First we consider the time-reversibility of the nonlinearity. The Euler equations are invariant under the simultaneous change $t \to -t$ and $\boldsymbol{u} \to -\boldsymbol{u}$. This implies that if in an Euler flow we change the sign of the velocity at every point of space, the flow will evolve backwards to its initial condition. This symmetry is not retained by the Navier-Stokes equations in the dissipation range since the viscous term does not share the same symmetry. To what extent the Navier-Stokes equations retain this reversibility is an important issue in Large Eddy Simulations [5].

Subsequently we link the energy-flux to the normalized dissipation rate $\epsilon L/U^3$, in order to explain the variability of the latter in different flow situations [6]. In another study we link the energy flux to the physical-space third-order structure function. This quantity and its normalized value, the skewness, are investigated as a function of the Reynolds number and it is shown that the Reynolds-number corrections to asymptotic scaling laws are of the order of the intermittency corrections, which makes it complicated to disentangle the two types of corrections [7].

Adding a periodically fluctuating forcing to the large scales, the filter properties of the turbulent energy cascade can be evaluated. The energy cascade acts as a low-pass filter with a characteristic frequency dependence proportional to ω^{-3}, with ω the frequency [8]. In a follow-up investigation we show how one can construct a multiple scale turbulence model which takes into account the non-local interactions which are responsible for the filtering-characteristics of the energy cascade [9].

The last section of chapter 3 discusses the phenomenon of depletion of nonlinearity. It is observed that turbulence displays the perhaps surprising property, that it locally tends to a state in which the strength of the nonlinear term is reduced, compared to a random ensemble of independent Fourier modes with the same kinetic energy (see Figure 3). This depletion of nonlinearity seems to be a quite general property of systems containing a quadratic nonlinearity. We tested the concept of depletion of nonlinearity for the case of a passive scalar advected by turbulence. The scalar equation is linear, but the advection term plays for the scalar a similar role as the nonlinearity of the Navier-Stokes equations with respect of the coupling of different modes. It was found that also the dynamics of the scalar tend to a state depleted of advection. In particular in

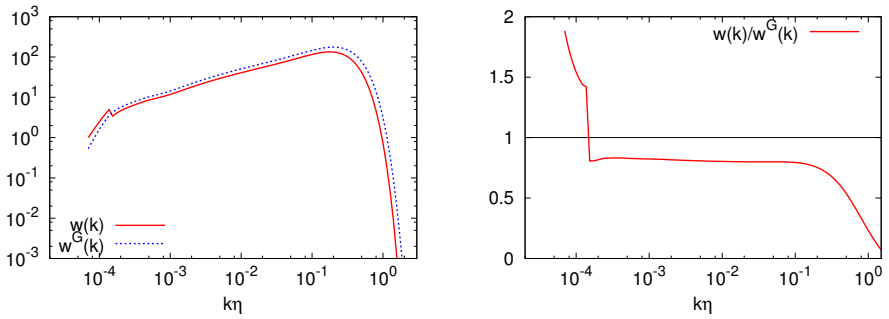

Figure 3: Left: spectrum of the nonlinear term (as in figure 1.3) and the same spectrum computed assuming the velocity-field to consist of independent (Gaussian) Fourier modes. Right: the ratio of the two spectra.

the small scales of the scalar it was observed that the strength of the advection term was reduced substantially compared to its Gaussian estimate.

Chapter 4: Magnetized plasmas and two-dimensional turbulence

In chapter 4 a brief introduction is given to the fluid models that can be used to describe a fusion plasma. It is shown how one can derive a fluid description, starting from the kinetic equation for the distribution function of the space-velocity evolution of the particles constituting a plasma. The two-fluid description due to Hasegawa and Wakatani, relevant to describe the dynamics of the edge turbulence of tokamaks, is introduced and it is shown how to simplify this description to a charge neutral MHD description. The influence of a strong magnetic field on a conducting fluid or plasma is recalled, focusing on the tendency towards a 2.5-dimensional dynamics [10], see Figure 4.

This 2.5-dimensional dynamics is equivalent to the mixing of a passive scalar in two-dimensional turbulence. We therefore also present an investigation on this latter subject in Chapter 4, in which we link the scaling of the velocity-scalar cross-correlation to the Lagrangian velocity correlation time [11].

Chapter 5: Lagrangian statistics in 2D fluid and plasma turbulence

In Chapter 5 we present results for the Lagrangian acceleration, which is the right hand side of the Navier Stokes equations, evaluated on a trajectory. $\boldsymbol{X}(\boldsymbol{x},t)$,

$$\boldsymbol{a}(\boldsymbol{X},t) = -\frac{1}{\rho}\nabla p(\boldsymbol{X},t) + \nu\Delta\boldsymbol{u}(\boldsymbol{X},t) + \boldsymbol{f}(\boldsymbol{X},t). \tag{7}$$

The dominant contribution to the acceleration is the pressure gradient. The PDF of the acceleration will therefore closely ressemble the PDF of the pressure gradient. It is argued that even in a Gaussian velocity field the acceleration is

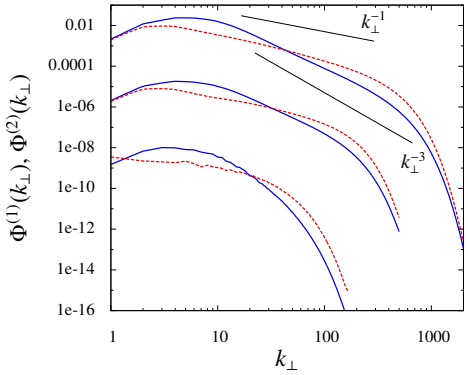

Figure 4: Quasi-static MHD turbulence behaves as two-and-a-half-dimensional turbulence. The perpendicular velocity advects the parallel velocity as were it a passive scalar. This behavior is illustrated by considering the energy spectra. The energy spectra of the perpendicular velocity (solid lines) display a steep inertial range behavior with a spectral exponent of the order three or four, as is usual for two-dimensional turbulence. The spectrum of the third velocity component (dotted lines) displays a Batchelor-type behavior, as is expected in the case of advection by a velocity field with a steep energy distribution. The lower two curves are obtained using DNS, the upper four curves are EDQNM results.

not Gaussian. Intermittency can thus not straightforwardly be measured by the non-Gaussianity of the velocity-time increments or the Lagrangian acceleration. A more precise definition is needed if one wants to employ the term intermittency to denote the anomalous features of turbulence [12].

The origin of the non-Gaussian shape of the acceleration PDFs is investigated in drift-wave turbulence. The interesting feature of the latter system is that it contains an adjustable parameter (unlike the Navier-Stokes equations), which allows to regulate the correlation time of the Lagrangian dynamics. This was done systematically and the influence on the shape of the PDFs was assessed [13].

In further studies, we addressed the influence of walls on the acceleration by performing simulations of decaying [14] and forced [15] two-dimensional turbulence in which we compared the statistics of a flow in a periodic domain with the statistics of a flow in a wall bounded domain. We showed that the differences in shape in the PDFs between the wall-bounded and periodic geometry are a robust feature and that the entrophy level influences strongly the shape of the PDFs.

An additional question on the statistical distribution of the acceleration is its link to regions of strong vorticity, or strong shear layers. The link between flow topology and acceleration was studied in reference [16]. In order to separate the flow in topologically distinct regions the Okubo-Weiss criterion was used. It was shown that, to some extent, the origin of the characteristic shape of the PDFs can be attributed to the intermittency of the flow topology. A large part of the flow is topologically quiescent, and the Lagrangian acceleration in this part is strongly peaked around zero. The contributions of the topologically more active

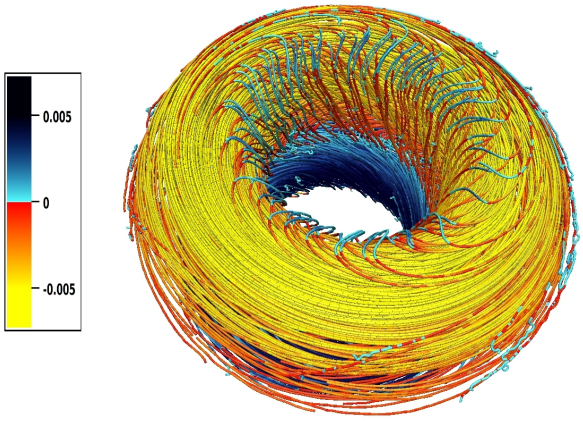

Figure 5: Velocity field in a toroidal fusion plasma, as obtained by our simulations. The streamlines, which show the direction of the velocity field, are coloured using the value of the toroidal velocity.

regions leads to tails that are raised. Considering these topologically more active regions by themselves, the PDFs are close to exponential, as would be expected for Gaussian velocity fields.

Chapter 6: Self-organization in magnetohydrodynamic turbulence

In turbulence certain quantities are conserved by the governing equations in the absence of viscosity. For the three-dimensional hydrodynamic case these invariants are the energy and the helicity. In the case of MHD, more invariants can be identified. The inviscid invariants determine the dynamics of the system (in a statistical sense). As a function of the initial conditions, one can predict in certain cases towards which state a system evolves. We investigated these dynamics in a system of two-dimensional MHD, confined by isolating boundaries [17].

In a subsequent study we investigated the generation and transport of angular momentum in two-dimensional MHD. We showed that a two-dimensional MHD flow, confined in non-circular boundaries is spun-up rapidly and this effect is even more important when the initial magnetic energy is increased [18, 19].

The exciting study of the influence of the geometry and transport coefficients on the toroidal rotation of fusion plasmas is presented in section 6.3. This topic is exciting since plasmas in toroidal fusion confinement devices are known to rotate for a reason which is not well understood. This rotation, seems to be an important ingredient in a transition to a much-improved confinement state and may be a prerequisite for future toroidal nuclear reactors (such as ITER) to function. In Figure 5 we show results of the flowfield generated through visco-resistive instabilities in toroidal geometry, in which the shape of the boundaries

and the magnetic field are chosen similar to tokamak geometry. It is shown that, when raising the Lundquist number, a dominantly toroidal velocity field is spontaneously generated. If the up-down symmetry of the cross-section is broken, toroidal angular momentum is generated [20].

Chapter 1

Turbulence and the strength of the nonlinearity

1.1 A description in scale space

The Navier-Stokes equations for incompressible, unit density flow, read as

$$\partial_t \boldsymbol{u} + \boldsymbol{u} \cdot \nabla \boldsymbol{u} = -\nabla p + \nu \Delta \boldsymbol{u}, \qquad \nabla \cdot \boldsymbol{u} = 0. \tag{1.1}$$

The nonlinearity of the Navier-Stokes equations gives rise to a wide range of interacting different length-scales in a turbulent flow. To describe this multi-scale dynamics of turbulence, one needs an appropriate scale-space description. Different complete orthonormal bases are available to describe the multi-scale character of turbulent flows. Examples are the Fourier-, wavelet- and Chebyshev-decomposition. The Chebyshev decomposition is convenient to study wall-bounded flow-geometries confined between parallel planes, the wavelet- decomposition allows a simultaneous scale-position description and the Fourier-description is the optimal basis to describe the scale-space distribution of general statistically homogeneous vector-fields. In the following chapters, a substantial part of the work focuses on homogeneous turbulence such that the Fourier description is adopted to decribe the flow.

Let us briefly discuss the Navier-Stokes equations in Fourier-space. If one wants to determine the pressure for a given velocity field, one needs to solve the Laplace equation, obtained by taking the divergence of (1.1), yielding

$$\Delta p = -\nabla \cdot (\boldsymbol{u} \cdot \nabla \boldsymbol{u}). \tag{1.2}$$

To solve this equation one needs to integrate over the whole space domain. However, if we Fourier-transform this last equation, and use the fact that a derivation with respect to $\boldsymbol{x}$ becomes a multiplication by $i\boldsymbol{k}$, we obtain

$$\hat{p} = \frac{i\boldsymbol{k}}{k^2} \cdot \widehat{(\boldsymbol{u} \cdot \nabla \boldsymbol{u})}. \tag{1.3}$$

The pressure is thus the non-solenoidal part of the nonlinear term.[1] This allows

[1] A solenoidal vector field is a field which is incompressible. The divergence is thus zero.

us to write the Fourier-transformed Navier-Stokes equations as,

$$\left(\partial_t + \nu k^2\right) u_i(\boldsymbol{k}) = -\frac{i}{2} P_{ijm}(\boldsymbol{k}) \iint u_j(\boldsymbol{p}) u_m(\boldsymbol{q}) \delta(\boldsymbol{k}-\boldsymbol{p}-\boldsymbol{q}) d\boldsymbol{p} d\boldsymbol{q}. \tag{1.4}$$

where summation over repeated indices is implied and the operator $P_{ijm}(\boldsymbol{k})$ is given by

$$P_{ijm}(\boldsymbol{k}) = k_j P_{im}(\boldsymbol{k}) + k_m P_{ij}(\boldsymbol{k}) \quad \text{with} \tag{1.5}$$

$$P_{ij}(\boldsymbol{k}) = \delta_{ij} - k_i k_j k^{-2}. \tag{1.6}$$

This operator removes the non-solenoidal part from the Navier-Stokes nonlinearity, which is the role of the pressure. The viscous term becomes a multiplication of the velocity of mode $\boldsymbol{k}$ by νk^2, and is thus determined locally in Fourier space. The fact that the pressure has been eliminated from equation (1.1) by using the incompressibility constraint is an important advantage of the Fourier-space formulation. Furthermore, the scale interaction is directly visible in the convolution integral, which displays the dependence on the wavevectors $\boldsymbol{p}$, $\boldsymbol{q}$, that take values everywhere in Fourier-space. It is this term, incorporating both the advection and the pressure term, that generates the multi-scale dynamics.

A particular useful quantity to quantify the multi-scale activity of the Fourier modes is the energy spectrum, which is defined as the kinetic energy distribution between scales, such that[2]

$$\int_0^\infty E(k) dk = \frac{1}{2}\overline{u_i u_i}, \tag{1.9}$$

where the overline denotes a suitable average. The wavenumber k is here related to the scale size of a turbulent structure. Rigorously, $2\pi/k$ is the wavelength of a continuous periodic wave. In order to get an intuitive understanding of dynamics and for general hand-waving phenomenology, it is often convenient to use a description of a turbulent flow consisting of eddies [21]. There is no generally accepted and precise definition of an eddy. Following Tennekes and Lumley [21], we can use the following tentative definition: *An eddy of wavenumber k may be thought of as some disturbance containing energy in the vicinity of k.* The ensemble of eddies of wavenumber k will then constitute a band in the energy spectrum, *cf.* Figure 1.1.

Since in Fourier space the divergence is proportional to the scalar product of the wavevector and the vector, the solenoidal part of the vector field is perpendicular to the wave vector. The non-solenoidal, or potential, part of the vector is parallel to the wavevector. The pressure, which is the scalar product of the wavevector and the nonlinearity (multiplied by ik^{-2}), is therefore the non-solenoidal part of the latter.

[2]The kinetic energy contained by a Fourier mode is given by $u_i(\boldsymbol{k})u_i(\boldsymbol{k})^*/2$. For quanties which are real in physical space (which is the case for the velocity) the Fourier transform is an even function of the wave-vector, such that $u_i(\boldsymbol{k})^* = u_i(-\boldsymbol{k})$. The average total energy of all wave-vectors together is then

$$\frac{1}{2}\overline{u_i u_i} = \frac{1}{2}\int \overline{u_i(\boldsymbol{k}) u_i(-\boldsymbol{k})} d\boldsymbol{k}. \tag{1.7}$$

If we are only interested in the distribution over scales, or equivalently the wavenumber, and not in the directional dependence, we can move to spherical coordinates, writing,

$$\frac{1}{2}\int \overline{u_i(\boldsymbol{k}) u_i(-\boldsymbol{k})} d\boldsymbol{k} = \int_0^\infty \left[\int_0^{2\pi} \int_0^{\pi} \frac{1}{2} \overline{u_i(\boldsymbol{k}) u_i(-\boldsymbol{k})} k^2 \sin(\theta) d\theta d\phi \right] dk. \tag{1.8}$$

The term in square brackets is the energy spectrum $E(k)$.

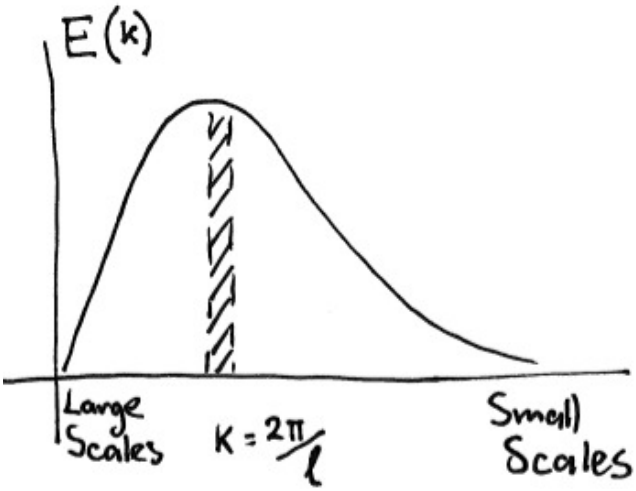

Figure 1.1: The energy spectrum gives the scale distribution of the kinetic energy. The wavenumber k corresponds to the wavenumber of a base-function (a sine-function in the case of Fourier-series). The inverse of the wavenumber is thus proportional to the wave-length. Phenomenologically, if one considers all *eddies* of a typical size, they will together contribute to a band in the energy spectrum.

An eddy is then a localized structure, similar in shape to a wavelet (*e.g.* [22]), but with this difference that we give a physical meaning to an eddy, related to a flow structure. Whereas a wavelet is simply a mathematical tool to describe a localized disturbance of a certain size, an eddy is a flow structure which can be sheared, dissipated, advected and rotated. The eddy-concept is in my opinion important for the physical understanding of a turbulent flow, but one should always be extremely careful in using the eddy-concept to predict flow properties. Rather should they be considered a cartoon picture to explain *a posteriori* concepts which are derived more rigorously using theories applied to the dynamics of Fourier modes (or other base functions such as wavelets). For example, the concept of scale-local interactions can be illustrated using a cartoon of a large eddy advecting a small eddy without distorting it (see Figure 1.2) but the validity of the concept should be tested by considering scale-locality functions, rigorously defined in Fourier-space [23]. The intrinsic triadic character induced by the nonlinear mode-coupling does then show that the picture is more complicated than the cartoon suggested (see for example the debate on the local transfer driven by nonlocal interactions [24, 25, 26]).

In our investigations we try to follow the following approach: results are obtained using simulations of the discretized partial differential equations or using an adapted closure model, and subsequently results are interpreted using intuitive concepts, which are suitable for general handwaving. We stress here that this handwaving without the supporting results is considerably less valuable.

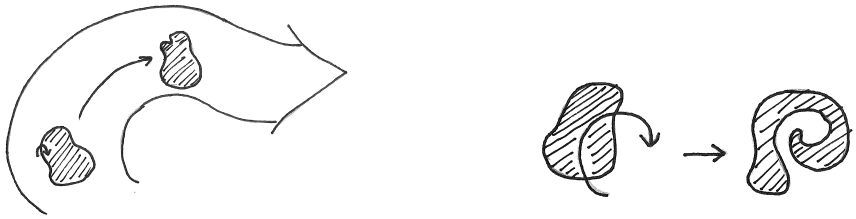

Figure 1.2: Cartoon of the concept of scale locality, as applied to the mixing of a scalar blob. Left: eddies much larger than the blob-size will advect the blob without distorting it, whereas much smaller scales will only nibble-off the boundaries. Right: an eddie of comparable size will efficiently deform the blob.

1.2 Scale-dependence of the nonlinear interaction

Closure theories, simulations and experiments all indicate that at high Reynolds numbers, the energy spectrum contains a range that is, to a good approximation, given by [27]:

$$E(k) \sim \epsilon^{2/3} k^{-5/3}, \tag{1.10}$$

in which ϵ is the energy flux among scales, equal to the dissipation rate of kinetic energy in the statistically stationary case. This inertial range extends roughly from $k_0 \sim 2\pi/L$ to $k_\eta \sim 2\pi/\eta$, in which η is the scale where the viscous effects become important. The above scaling, due to Kolmogorov, reflects the local character of the energy flux through scales from the large scales, where the energy is injected by some large scale instability, to the small scales where viscous stresses become important. In what now follows we will explain that this inertial range behavior is intrinsically reflecting the Lagrangian character of the underlying energy transfer mechanism. For this we will start by considering the scale dependence of the Reynolds number.

The Reynolds number is defined as

$$R_L = \frac{UL}{\nu}, \tag{1.11}$$

with L a typical lengthscale characterizing the size of the largest (energetically important) flow structures and U the rms velocity. The physical interpretation that we find in every textbook on fluid dynamics is that the Reynolds number measures the ratio between inertial effects and viscous effects. If we write the Navier-Stokes equations as

$$\partial_t \boldsymbol{u} = \boldsymbol{N} + \nu \Delta \boldsymbol{u}, \tag{1.12}$$

with $\boldsymbol{N} = -(\boldsymbol{u} \cdot \nabla \boldsymbol{u} + \nabla p)$, then the Reynolds number could be alternatively defined by

$$R_* = \frac{\sqrt{< \boldsymbol{N} \cdot \boldsymbol{N} >}}{\sqrt{< (\nu \Delta \boldsymbol{u}) \cdot (\nu \Delta \boldsymbol{u}) >}}, \tag{1.13}$$

which is a more precise (but far less practical) measure of the ratio of the effects of inertia and viscosity. Note that we take both the advection and pressure term

together in this definition of the inertial effects, which seems logical in the light of equation (1.4). Taking in this definition of the Reynolds number only the advection term would not change qualitatively the picture that we are about to describe.

If on the largest scales, of order L and with typical velocity U, all the velocity gradients are of order U/L, and the second derivatives of order U/L^2, then it is easy to see that $R_* \sim R_L$. The Reynolds number gives thus the ratio of the strength of the inertial effects to the viscous effects *at the large scales*. The direct effects of viscous stresses are indeed not directly influencing the dynamics of the large scales in very large Reynolds number turbulence. But how does this ratio evolve as a function of scale? Let us for simplicity consider the isotropic case. In scale space we can rigorously define

$$w(k) = 4\pi k^2 < \boldsymbol{N}(\boldsymbol{k}) \cdot \boldsymbol{N}(-\boldsymbol{k}) >, \tag{1.14}$$

which is the power spectrum of the mean-square nonlinearity defined such that

$$\int w(k)dk =< |\boldsymbol{N}|^2 > . \tag{1.15}$$

It represents the distribution over scales of the strength of the inertial effects. Similarly we can define the scale distribution of the viscous contribution to the Navier-Stokes equation,

$$\Upsilon(k) = 4\pi k^2 < \nu k^2 \boldsymbol{u}(\boldsymbol{k}) \cdot \boldsymbol{u}(-\boldsymbol{k}) \nu k^2 > = 2\nu k^4 E(k), \tag{1.16}$$

$$\int \Upsilon(k)dk = < |\nu \Delta \boldsymbol{u}|^2 > . \tag{1.17}$$

How does this Reynolds number,

$$R_*(k) = \sqrt{\frac{w(k)}{\Upsilon(k)}}, \tag{1.18}$$

behave as a function of scale?

Closure theories[3], that will be introduced in the next chapter, give for the spectrum $w(k)$,

$$w(k) \sim U^2 \epsilon^{2/3} k^{1/3}. \tag{1.19}$$

Results are given in Figure 1.3. In the inertial range we therefore have

$$R_*(k) = \sqrt{\frac{U^2 \epsilon^{2/3} k^{1/3}}{\nu^2 \epsilon^{2/3} k^{7/3}}} = \frac{U}{\nu k}. \tag{1.20}$$

In which we used Taylor's relation $\epsilon \sim U^3/L$ to relate ϵ, L, U. At the scale at which inertia and viscous effects become comparable this Reynolds number should become of order unity. Solving $R_*(k) = 1$ we find

$$k_* = \frac{U}{\nu} = R_L^{1/4} k_\eta. \tag{1.21}$$

[3]We expect that simulations and experiments should give the same result, but this quantity has not been significantly studied at present so that we rely on our closure results. All the results presented in this chapter are obtained using closures which will be discussed in chapter 2. In the present chapter the results only serve as an illustration of the ideas and the tool which is used to obtain them is not so relevant. The advantage of closure is that high Reynolds numbers can be considered such that clear scaling ranges are visible.

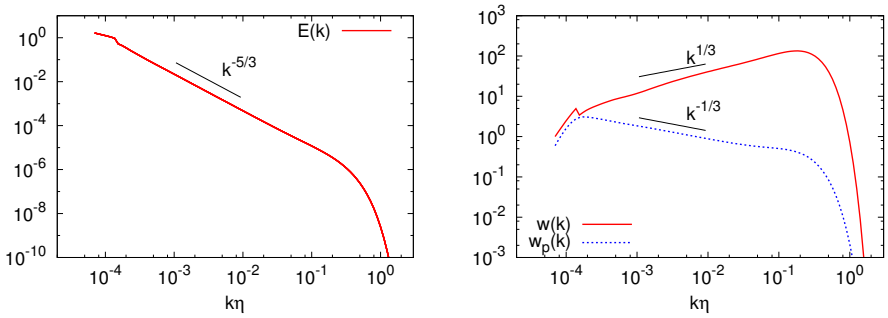

Figure 1.3: Left: the energy spectrum for a forced turbulent flow at a Taylor-scale Reynolds number $R_\lambda = 4000$. Right: the spectrum of the mean square nonlinearity for the same flow and the spectrum of the pressure gradient. All results in this chapter are obtained using a closure of the Eddy-Damped Quasi-Normal Markovian type. See section 2.5 on the details of this approach.

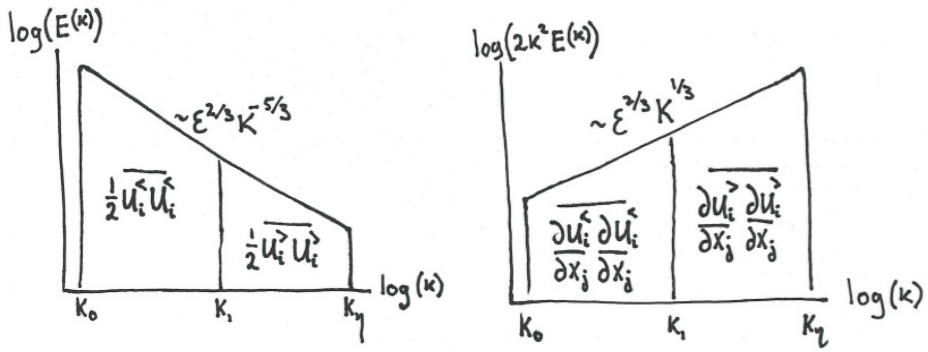

Figure 1.4: Left: we consider a model energy spectrum and we arbitrarily divide the scales into large scales and small scales. Right: the enstrophy spectrum, characterizing the mean square value of the velocity gradients is obtained by multiplying the energy spectrum by k^2.

in which $k_\eta = \epsilon^{1/4}/\nu^{3/4}$ is the Kolmogorov scale. The scale k_* should determine the beginning of the dissipation range. It is very interesting that the scale k_* which is the scale at which the viscous effects become dominant is much larger than the Kolmogorov scale k_η for very high Reynolds numbers, since k_η is also defined as the scale where the viscous effects become dominant. We would therefore have expected that $k_* \approx k_\eta$, independent of the Reynolds number. This paradoxical result brings us immediately to a key issue in the description of scale interactions and Kolmogorov's inertial range theory.

Let us introduce an arbitrary separation of velocity into large $\boldsymbol{u}^<$ and small $\boldsymbol{u}^>$ scales,

$$\boldsymbol{u} = \boldsymbol{u}^< + \boldsymbol{u}^>. \tag{1.22}$$

For convenience we assume that the energy distribution of the turbulent flow that we consider is given by a long inertial range distribution, extending from

k_0 to k_η:

$$\begin{aligned} E(k) = &\quad C_k \epsilon^{2/3} k^{-5/3} \qquad \text{for} \quad k_0 < k < k_\eta \\ = &\quad 0 \qquad\qquad\qquad \text{elsewhere,} \end{aligned} \tag{1.23}$$

with C_k the Kolmogorov constant. Arbitrarily, scales $\boldsymbol{u}(\boldsymbol{k})$ with $|\boldsymbol{k}| \equiv k < k_1$ are considered large scales and scales with $k > k_1$ are considered small. At the very high Reynolds number we consider in this example we have chosen k_1 such that $k_0 \ll k_1 \ll k_\eta$ as illustrated in Figure 1.4.

We can compute the magnitude of the energy of the large and small scales, respectively, as

$$\begin{aligned} \frac{1}{2}\overline{u_i^< u_i^<} = \int_{k_0}^{k_1} E(k)dk &= \frac{2}{3} C_k \epsilon^{2/3} \left(k_0^{-2/3} - k_1^{-2/3} \right) \\ &\approx \frac{2}{3} C_k \epsilon^{2/3} k_0^{-2/3} \\ \frac{1}{2}\overline{u_i^> u_i^>} = \int_{k_1}^{k_\eta} E(k)dk &\approx \frac{2}{3} C_k \epsilon^{2/3} k_1^{-2/3}, \end{aligned} \tag{1.24}$$

and for the magnitude of the square of the gradients, which is given by the integral of the enstrophy spectrum, $2k^2 E(k)$ we have,

$$\begin{aligned} \overline{\frac{\partial u_i^<}{\partial x_j} \frac{\partial u_i^<}{\partial x_j}} = \int_{k_0}^{k1} 2k^2 E(k)dk &= \frac{3}{2} C_k \epsilon^{2/3} \left(k_1^{4/3} - k_0^{4/3} \right) \\ &\approx \frac{3}{2} C_k \epsilon^{2/3} k_1^{4/3} \\ \overline{\frac{\partial u_i^>}{\partial x_j} \frac{\partial u_i^>}{\partial x_j}} = \int_{k_1}^{k_\eta} 2k^2 E(k)dk &\approx \frac{3}{2} C_k \epsilon^{2/3} k_\eta^{4/3}. \end{aligned} \tag{1.25}$$

Since we considered $k_0 \ll k_1 \ll k_\eta$, we have therefore

$$\frac{|\boldsymbol{u}^<|}{|\boldsymbol{u}^>|} \gg 1 \quad \text{and} \quad \frac{|\nabla \boldsymbol{u}^>|}{|\nabla \boldsymbol{u}^<|} \gg 1. \tag{1.26}$$

The advection term can then be roughly estimated by

$$\boldsymbol{u} \cdot \nabla \boldsymbol{u} = (\boldsymbol{u}^> + \boldsymbol{u}^<) \cdot (\nabla \boldsymbol{u}^> + \nabla \boldsymbol{u}^<) \tag{1.27}$$

$$\approx \boldsymbol{u}^< \cdot \nabla \boldsymbol{u}^>, \tag{1.28}$$

which immediately shows the coupling of large and small scales which dominates the dynamics of the advection term. The small scale gradients are swept around by large scale velocity fluctuations.

In the beginning of this section we mentioned that the inertial range is directly related to the energy transfer among different length-scales. The sweeping interactions just described are *not* the interactions which govern the energy transfer. This can be illustrated by adding a large uniform velocity $\boldsymbol{U}_0$ to the velocity field. This should not change the energy transfer, but it does change the value of $\boldsymbol{u} \cdot \nabla \boldsymbol{u} \to (\boldsymbol{u} + \boldsymbol{U}_0) \cdot \nabla \boldsymbol{u}$. We should therefore not use Kolmogorov's scaling in evaluating $R_*(k)$, since the latter characterizes the sweeping interaction and not the energy transfer.

If we place ourselves in a reference frame in which the inter-scale transfer is clearly decoupled from the large-scale sweeping effect, the energy transfer should be more correctly evaluated. Therefore we consider the dynamics in a Lagrangian reference frame [28]. Doing so, we have

$$D_t \boldsymbol{u} = -\nabla p + \nu \Delta \boldsymbol{u}. \tag{1.29}$$

In this Lagrangian frame the nonlinear interaction is given by the pressure gradient and not by the advection, which has become part of the material time derivative $D/D_t \equiv (\partial_t + \boldsymbol{u} \cdot \nabla)$. We recall here that the pressure term is part of the nonlinear interaction, as is clear from relation (1.3). We can now define a new dimensionless (Reynolds-number-like) quantity, in which it is not the complete nonlinear term (advection plus pressure gradient) which is compared to the viscous term, but only the pressure gradient term. We therefore introduce the mean-square pressure gradient spectrum,

$$w_p(k) = 4\pi k^2 < \nabla p(\boldsymbol{k}) \cdot \nabla p(-\boldsymbol{k}) >, \tag{1.30}$$

and since in the inertial range (see Figure 1.3 (right)),

$$w_p(k) \sim \epsilon^{4/3} k^{-1/3}, \tag{1.31}$$

we now have

$$R_*(k) = \sqrt{\frac{w_p(k)}{2\nu k^4 E(k)}} \sim \frac{\epsilon^{1/3} k^{2/3}}{\nu k^2}. \tag{1.32}$$

In this case the Reynolds number is order unity around the Kolmogorov scale, so that $k_* \sim k_\eta$ as we would expect it. The Lagrangian description is therefore most natural if we want to consider the importance of scale interactions with respect to energy transfer without considering the effect of sweeping by the large scales. Kolmogorov scaling is thus directly tied to the Lagrangian dynamics of a turbulent flow[4]. This is important in the formulation of a statistical theory of turbulence (chapter 2). Chapter 5 focuses on the Lagrangian statistics obtained in two-dimensional turbulence and in plasma turbulence.

1.3 Multi-scale dynamics of the scalar field

The evolution equation for the advection of a scalar quantity with a diffusivity α is

$$\partial_t \theta + \boldsymbol{u} \cdot \nabla \theta = \alpha \Delta \theta. \tag{1.33}$$

We consider in the remainder only passive scalars such as small temperature fluctuations or dye concentration, meaning that the scalar quantity does not influence the velocity field. The above equation is linear in the sense that every term in the equation is proportional to θ. No quadratic terms appear and also, no nonlocally determined terms like the pressure appear. However, the advection term involves both the velocity field and the scalar field and hereby

[4]Note that we can evaluate the Reynolds number based on the pressure gradient equally well in the Eulerian frame and it is therefore not a completely Lagrangian quantity. But the fact that we decouple the pressure gradient from the advection term in evaluating the strength of the nonlinearity is only a logical thing to do if one considers the Lagrangian dynamics.

the scalar displays a multiscale dynamics, like the turbulent velocity. This is clear if we consider the convolution term in the Fourier transform of the above equation,

$$\left(\partial_t + \alpha k^2\right) \theta(\boldsymbol{k}) = -ik_i \iint u_i(\boldsymbol{p})\theta(\boldsymbol{q})\delta(\boldsymbol{k}-\boldsymbol{p}-\boldsymbol{q})d\boldsymbol{p}d\boldsymbol{q}. \tag{1.34}$$

Since this equation is slightly less complicated than the Navier-Stokes equations, but contains the same multi-scale character, it can be hoped that an understanding of the dynamics of a scalar leads to deeper insights into the dynamics of the Navier-Stokes equations. This is not certain. Changing an equation can help understand the influence of certain effects, but often the behavior of the modified system changes completely with respect to the system governed by the original equations. A good example is the equation that was proposed by J.M. Burgers [29] as a one dimensional equivalent of Navier-Stokes,

$$\frac{\partial u}{\partial t} + u\frac{\partial u}{\partial x} = \nu \frac{\partial^2 u}{\partial x^2}. \tag{1.35}$$

The nonlinearity in this equation has the same structure as the Navier-Stokes equations, but the absence of the regularizing pressure term leads to the formation of shocks in the evolution of the velocity u. These discontinuities lead to an inertial range behavior proportional to k^{-2} for the energy spectrum of Burgers' equations, whereas "naive" Kolmogorov arguments would yield a $k^{-5/3}$ wavenumber dependence. We mention an interesting investigation on this subject [30] which shows that closure can correctly predict this shock-dominated Burgers-turbulence. On one hand, the scalar advection problem has in common with the Burgers dynamics that no pressure is present in the equation. On the other hand the multiscale-dynamics of the passive scalar share the scaling properties with Navier-Stokes turbulence with respect to the constant flux inertial range. Indeed, we can consider the multi-scale distribution of passive scalar variance, given by $E_\theta(k)$, the scalar spectrum, defined such that

$$\int_0^\infty E_\theta(k)dk = \frac{1}{2}\overline{\theta^2}. \tag{1.36}$$

It was suggested by Obukhov and Corrsin [31, 32] that the scalar spectrum scales as

$$E_\theta(k) \sim \epsilon_\theta \epsilon^{-1/3} k^{-5/3}. \tag{1.37}$$

And this scaling is akin to Kolmogorov's constant flux inertial range (1.10).

Let us now reconsider the issue that was discussed in section 1.2. How can we define a scale dependent Péclet number? Classically, the Péclet number is defined as

$$Pe = \frac{UL}{\alpha}, \tag{1.38}$$

and the interpretation is that it measures the ratio of the strength of the advection, compared to diffusion. Clearly we can redefine a scale dependent Péclet number, analogously to equation (1.39),

$$Pe_*(k) = \sqrt{\frac{w_\theta(k)}{2\alpha k^4 E_\theta(k)}}, \tag{1.39}$$

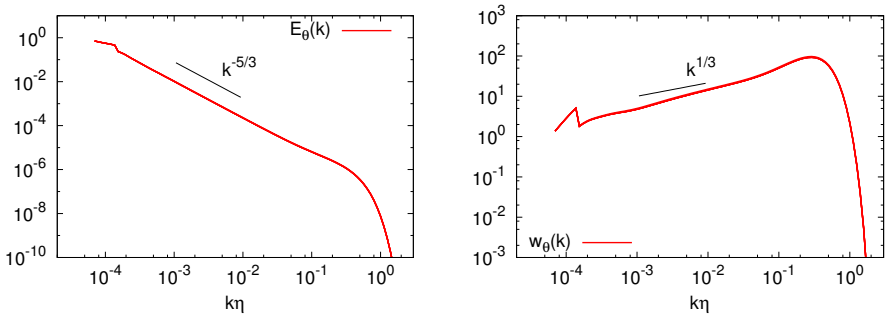

Figure 1.5: Left: scalar variance spectrum at a $R_\lambda = 4000$ and $Pr = 1$. A clear Corrsin-Obukhov scaling range is present. Right: spectrum of the advection term for the same case.

with

$$w_\theta(\boldsymbol{k}) = 4\pi k^2 \left\langle \left(\widehat{\boldsymbol{u}\cdot\nabla\theta}(\boldsymbol{k})\right)\left(\widehat{\boldsymbol{u}\cdot\nabla\theta}(-\boldsymbol{k})\right)\right\rangle, \tag{1.40}$$

such that

$$\int w_\theta(k)dk = \overline{(\boldsymbol{u}\cdot\nabla\theta)^2}. \tag{1.41}$$

The spectra $E_\theta(k)$ and $w_\theta(k)$ for unit Prandtl number (which means that the diffusivity α is equal to the viscosity ν), are shown in Figure 1.5.

Closure predicts (as for the mean-square nonlinearity spectrum in Figure 1.3) that the spectrum of the mean-square advection scales proportional to $k^{1/3}$. More precisely, the scaling is

$$w_\theta(k) \sim U^2\epsilon_\theta\epsilon^{-1/3}k^{1/3}. \tag{1.42}$$

Substituting this scaling and the Corrsin-Obukhov scaling (1.37) in the above expression for $Pe_*(k)$ and determining where the effects of diffusion and inertia become comparable, we find exactly the same problem as for the velocity dynamics: large-scale sweeping dominates the advection of the small scales. What was our solution for the velocity? We reformulated our problem in the Lagrangian frame. What happens if we do that for the scalar? In that case the equation becomes

$$\frac{D\theta}{Dt} = \alpha\Delta\theta. \tag{1.43}$$

There is something funny happening here: by reformulating the scalar problem in the Lagrangian frame, it is found that the only effect influencing the scalar evolution is the diffusion. Reformulating a scale-dependent Péclet number in Lagrangian coordinates would therefore give a value of zero *at all scales*, independent of the velocity dynamics, since the advection term is not explicitly appearing in the equation. This immediately points out that considering the advection-diffusion equation of the scalar might not be the correct way of studying the multi-scale dynamics of a scalar advected by a velocity field. This seems strange at first sight, but let us think some more about this. A scalar blob of uniform scalar concentration in a velocity field will give birth to smaller scales through the stretching of the blob. Within the blob, the value of the scalar remains constant. Following a fluid particle, the value of the scalar will not change

in the absence of diffusion. The stretching will however directly influence the gradients of the scalar, which is not directly visible in the advection-diffusion equation. It is clearly present if one writes down the equation for the evolution of the *gradient* of the scalar. Defining

$$\gamma_i = \frac{\partial \theta}{\partial x_i}, \tag{1.44}$$

the equation for the advection-stretching-diffusion becomes in the Lagrangian frame:

$$\frac{D\gamma_i}{Dt} = -\frac{\partial u_j}{\partial x_i}\gamma_j + \alpha \frac{\partial^2 \gamma_i}{\partial x_j^2}. \tag{1.45}$$

We can now define a spectrum measuring the strength of the stretching term, the first term on the RHS, compared to the diffusion of scalar the gradient. This will be left for further research, but it is expected that a local Péclet number based on the stretching and the diffusion of the scalar gradient will correctly indicate the Batchelor scale at which the diffusion becomes comparable to the stretching effects.

The problem of scalar advection will be further discussed in chapter 3 and 4. In particular, the non-Gaussianity of the scalar advection will be considered in section 3.4. In Chapter 4, the advection of a passive scalar will be discussed in relation to the dynamics of magnetized plasma and conducting fluids in the presence of a strong magnetic field.

1.4 The multi-scale dynamics of a magnetic field advected by turbulence

The evolution equation for the advection of a vector $\boldsymbol{\chi}$ is

$$\partial_t \boldsymbol{\chi} + \boldsymbol{u} \cdot \nabla \boldsymbol{\chi} = \boldsymbol{\chi} \cdot \nabla \boldsymbol{u} + \eta \Delta \boldsymbol{\chi}. \tag{1.46}$$

This equation governs the advection of the vorticity, $\boldsymbol{\omega} = \nabla \times \boldsymbol{u}$ as well as the advection of a magnetic field $\boldsymbol{b}$. In the first case it corresponds simply to the curl of the Navier-Stokes equations. In the second case the magnetic field is advected by the velocity field, and it retro-acts on the latter by the Lorentz force, $\boldsymbol{F}_L = (\nabla \times \boldsymbol{b}) \times \boldsymbol{b}$, which should be added to the RHS of the Navier-Stokes equations. The interaction of these two-fields, the velocity field and the magnetic field, makes the dynamics of the flow dynamics richer. A new dimensionless parameter is introduced, the magnetic Prandtl number. But even fixing this parameter, the dynamics have gained enormously in free parameters, depending on the boundary conditions, and forcing schemes. Universality does not seem to be easily observed in MHD [33]. The Kolmogorov-Richardson energy cascade, reasonably well established in fluid turbulence, is immediately questionable in MHD, since scale interactions become more nonlocal. Local isotropy is here suppressed by the inherent anisotropy of the magnetic field.

Applications of MHD include the dynamics of accretion-disks, fusion reactors, solar-wind, planetary (and solar) dynamos, the interstellar medium and industrial processes involving liquid metals. In particular we will focus on the application of MHD to the modeling of fusion-plasma devices and more about this will be discussed in chapter 4 and 6.

Chapter 2

The Direct Interaction Approximation

An attempt has been made recently to develop an exact theory of homogeneous turbulence in which all the statistical moments of the velocity field are derived analytically from the Navier-Stokes equation (...) [34].

2.1 Introduction and notation

Statistical theories of turbulence have to deal, one way or another, with the closure problem, which consists in the fact that the averaged Navier-Stokes equations contain more unknowns than equations. This is due to the nonlinear term, which, when averaged, introduces additional unknowns to the system[1]. Analytical closure approaches are an attempt to overcome this problem by relating the unknowns by physical assumptions to the known quantities and hereby reducing the number of unknowns or increasing the number of equations. Early approaches, such as the quasi-normal approach [37, 38, 39], in which the unclosed hierarchy of moments was closed by assuming joint-Gaussian statistics of the fourth order moments of Fourier-modes of the velocity field, did not yield physical results. Negative kinetic energy distributions were observed as a consequence of that closure assumption [40], as was carefully suggested by Kraichnan [41].

A great step forward was the introduction of the Direct Interaction Approximation (DIA) [34]. In the following we will focus on the DIA and consequently on the contributions of Kraichnan to the theoretical description of turbulence. This evidently does not credit all scientists that have contributed to turbulence theory and the present chapter is certainly not an exhaustive review on the subject. It rather discusses contributions that have inspired, and are at the basis of, our own investigations.

[1] A quadratic term is actually not necessary to create a closure problem. Already the product of two stochastic fields leads to the closure problem. This is, for example, the case in the scalar advection equation. This equation is linear, but the advection term leads to a closure problem after averaging, if the velocity field is random. Only in the particular case of a delta-correlated advecting velocity, the scalar equation can be solved exactly [35, 36].

For the sake of readibility, we introduce a symbolic notation in which the Navier-Stokes equations are written in a compact form. First we write the continuous form of the Navier-Stokes equations,

$$[\frac{\partial}{\partial t} + \nu k^2]u_k(\boldsymbol{k},t) = -\frac{i}{2}P_{kpq}(\boldsymbol{k}) \iint \delta_{\boldsymbol{k}-\boldsymbol{p}-\boldsymbol{q}} u_p(\boldsymbol{p},t)u_q(\boldsymbol{q},t)d\boldsymbol{p}d\boldsymbol{q},$$

using the discrete Fourier representation,

$$[\frac{\partial}{\partial t} + \nu k^2]u_k(\boldsymbol{k},t) = -\frac{i}{2}\sum_{\boldsymbol{p},\boldsymbol{q}} \delta_{\boldsymbol{k},\boldsymbol{p}+\boldsymbol{q}} P_{kpq}(\boldsymbol{k})u_p(\boldsymbol{p},t)u_q(\boldsymbol{q},t), \tag{2.1}$$

in which the wave-vectors are a discrete representation of the flow in a cyclic box of size L. In the case in which $L \to \infty$, both representations are equivalent. This system is now written in a more general form [42], which represents also other quadratic systems,

$$(\partial_t + \nu_k)y_k = \sum_{p,q} A_{kpq}y_p y_q. \tag{2.2}$$

The index k of y_k does not indicate a vector index like the index i in $u_i(\boldsymbol{k},t)$, but labels the complete mode $u_i(\boldsymbol{k},t)$. Similarly y_p, y_q indicate the modes $u_p(\boldsymbol{p},t)$ and $u_q(\boldsymbol{q},t)$ and ν_k represents νk^2. This notation is much lighter than the full expression, which is the main reason to introduce it, but it does not explicitly show all the vector indices contained in the Navier-Stokes equation. For this reason we do *not* implicitly sum over repeated indices, as is usual using Einstein's index notation convention. The $\sum_{p,q}$ in the above expression represents the convolution product. Expression (2.2) is more general than the Navier-Stokes system, because it can represent different systems depending on the definition of A_{kpq}, y_k and ν_k. For Navier-Stokes we have the operator

$$A_{kpq} \to -\frac{i}{2}P_{kpq}(\boldsymbol{k}). \tag{2.3}$$

Burgers' equation (1.35) can be represented by the same equation by changing the operator to

$$A_{kpq} \to -\frac{i}{2}\left(q_p\delta_{kp} + p_q\delta_{kp}\right). \tag{2.4}$$

In the following, quantities are evaluated at the present time instant if not further specified. If a quantity is evaluated at a different time, $t = s$, the quantity will be distinguished by adding a dash y'. In section 2.3.2, we will need quantities at two different time-instants in history and the quantities at $t = s$ and $t = s'$ will be indicated by y' and y'' respectively.

The evolution equation for the mode distribution of kinetic energy of $\overline{y_k y_k}/2$, called the Lin equation, can now be written

$$(\partial_t + 2\nu_k)\overline{y_k y_k}/2 = \sum_{p,q} A_{kpq}\overline{y_k y_p y_q}. \tag{2.5}$$

The overline denotes an ensemble average. In order to get a closed expression for the energy transfer, one needs to find an expression for the triple correlation $S_{kpq} \equiv \overline{y_k y_p y_q}$. Such an expression will be derived in section 2.3.1. Recall that

in the previous chapter, to characterize the strength of the nonlinear interaction, we focused on the mean-square nonlinearity, which is the square of the RHS of the last equation (2.2),

$$w_k = \sum_{p,q} \sum_{m,n} A_{kmn} A_{kpq} \overline{y_p y_q y_m y_n}, \tag{2.6}$$

and so one needs an expression for $Q_{pqmn} \equiv \overline{y_p y_q y_m y_n}$. This expression will be derived in section 2.3.2.

2.2 The weak dependence hypothesis and maximum randomness

The DIA is a perturbation method. The influence of the nonlinearity on the dynamics of the flow is treated perturbatively. The obvious problem is that this nonlinearity is not small, and perturbation methods only work adequately in the limit of a small perturbation around a certain equilibrium state[2]. Kraichnan found however a clever way to define an equilibrium state and a small perturbation. In order to explain how he did this, we will first discuss a conventional perturbation method applied to equation (2.2), in order to obtain an expression for $S_{kpq} \equiv \overline{y_k y_p y_q}$.

In a conventional perturbation, one expands about a linear state $y^{(0)}$, which in the case of Navier-Stokes turbulence is given by the solution to the linear problem,

$$(\partial_t + \nu_k) y_k = 0. \tag{2.7}$$

For the case of decaying turbulence from an initial condition $y_k(t = 0)$, this would correspond to purely viscous decay without any mode-coupling induced by the nonlinear term. The solution to this problem, the linear state $y^{(0)}$, is

$$y_k^{(0)} = G_k^{(0)}(t) y_k(t = 0), \tag{2.8}$$

with $G_k^{(0)} = \exp(-\nu_k t)$ the linear Green's function. The quantity $y_k^{(0)}$ is thus a velocity mode decaying solely under the influence of viscosity. If we take nonlinearity into account as a small perturbation, the first order perturbed

[2]We will completely omit the discussion of wave-turbulence or weak-turbulence. In that case a linear term in the governing equations is dominant and waves (such as Rossby waves in rapidly rotating turbulence, or Alfvén waves in the presence of a strong magnetic field) are present. If the frequency of these waves is much larger than the inverse of the nonlinear time-scale, and if the nonlinearity is weak compared to the linear effect, the wave-turbulence closure can be used to close the system. This means that a rigorous perturbation procedure can be carried out, leading to closed expressions for the weak and slow nonlinear interactions between rapidly oscillating wave-packets. We could ask what we can learn from wave-turbulence closures to better understand strong turbulence? The triad interactions are in principle the same, however, the resonance condition on the wave-frequency selects a small fraction of the interactions. The resonance broadening, when the nonlinearity becomes more important, makes the number of interactions tend to the ones that would be important in DIA. However, the applicability conditions for the wave-turbulence closure are not fulfilled anymore. For details on wave-turbulence we refer to a recent treatise on the subject [43].

solution is given by

$$y_k \approx y_k^{(0)} + \underbrace{\int_0^t G_k^{(0)}(s) \sum_{p,q} A_{kpq} y_p'^{(0)} y_q'^{(0)} ds}_{y_k^{(1)}} . \tag{2.9}$$

We recall here that the dash y' indicates evaluation at $t = s$. The superscripts (0) and (1) indicate the order of the perturbation. This expression is obtained by using the linear Green's function $G_k^{(0)} = \exp(-\nu_k t)$ and assuming the non-linearity to be small compared to the viscous effects, which allows to invert the linear operator $(\partial_t + \nu_k)$. We can obtain a solution at second order by perturbing the $y_p'^{(0)}$ and $y_q'^{(0)}$ yielding

$$\begin{aligned} y_k &\approx y_k^{(0)} + \underbrace{\int_0^t G_k^{(0)}(s) \sum_{p,q} A_{kpq} y_p'^{(0)} y_q'^{(0)} ds}_{y_k^{(1)}} \\ &+ \underbrace{2 \int_0^t \int_0^t G_k^{(0)}(s) G_p^{(0)}(s') \sum_{p,q} \sum_{m,n} A_{kpq} A_{pmn} y_q'^{(0)} y_m''^{(0)} y_n''^{(0)} ds' ds + ...}_{y_k^{(2)}}, \end{aligned} \tag{2.10}$$

in which terms of order y^4 are represented by dots. The factor two appears because of p, q symmetry. Substituting this in the triple correlation $S_{kpq} = \overline{y_k y_p y_q}$, we find

$$\begin{aligned} S_{kpq} &\approx \overline{(y_k^{(0)} + y_k^{(1)} + ...)(y_p^{(0)} + y_p^{(1)} + ...)(y_q^{(0)} + y_q^{(1)} + ...)} \\ &\approx \overline{y_k^{(0)} y_p^{(0)} y_q^{(0)}} + \int_0^t G^{(0)}(s) \sum_{m,n} A_{kmn} \overline{y_m'^{(0)} y_n'^{(0)} y_p^{(0)} y_q^{(0)}} ds + ..., \end{aligned} \tag{2.11}$$

In which we showed explicitly only one of the three first order corrections. This expansion should give correct behavior as long as

$$\left| \frac{\sum_{j,k} A_{kpq} y_p y_q}{\nu_k y_k} \right| \ll 1. \tag{2.12}$$

In terms of the Navier-Stokes equation this means

$$\sqrt{\frac{\boldsymbol{N}(\boldsymbol{k}) \cdot \boldsymbol{N}(-\boldsymbol{k})}{\nu k^2 \boldsymbol{u}(\boldsymbol{k}) \cdot \boldsymbol{u}(-\boldsymbol{k}) \nu k^2}} \ll 1, \tag{2.13}$$

which is, apart from the ensemble average, the square root of the scale dependent Reynolds number $R_*(k)$ discussed in the previous chapter. In turbulence $R_*(k)$ is generally not small, in particular in the large scales. As mentioned before, a conventional expansion does therefore not give a useful approximation to high Reynolds number turbulence. Another, relevant, small parameter is needed and we will explain now how we can define one.

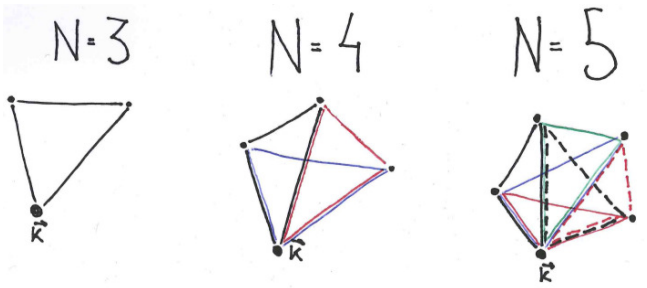

Figure 2.1: The number of possible triad interactions involving mode $\boldsymbol{k}$ increases rapidly with the number of modes present in the domain. We illustrate all possible triad interactions in the case of a system consisting of only $3, 4, 5$ modes respectively. In a system containing a large number of modes N, this number increases roughly proportional to N^2.

As discussed before, the nonlinear term introduces an interaction between all Fourier modes which satisfy $\boldsymbol{k} = \boldsymbol{p} + \boldsymbol{q}$ (or between k and p, q in our model equation). For every mode $\boldsymbol{k}$ in the Navier-Stokes equations,

$$[\frac{\partial}{\partial t} + \nu k^2]u_k(\boldsymbol{k}, t) = -\frac{i}{2}\sum_{\boldsymbol{p},\boldsymbol{q}} \delta_{\boldsymbol{k},\boldsymbol{p}+\boldsymbol{q}} P_{kpq}(\boldsymbol{k}) u_p(\boldsymbol{p}, t) u_q(\boldsymbol{q}, t), \tag{2.14}$$

all possible combinations $\boldsymbol{k} = \boldsymbol{p} + \boldsymbol{q}$ are contained in the convolution. If the number of modes is large, the number of triad-interactions between $\boldsymbol{k}$ and the other modes increases rapidly. If the system consists of only 3 modes, only one triad interaction is possible. If there are four modes present, the number of triads is 3 and when N modes are present, this number is

$$N_i = \sum_{p=1}^{N-2} p = \frac{(N-1)(N-2)}{2} \sim N^2 \text{ (for } N \to \infty). \tag{2.15}$$

These possible interactions are shown in Figure 2.1 for $N = 3, 4, 5$.

Let us now consider one individual triad, and isolate its influence from the rest of all possible triads. If the number of modes is large, the influence of this single triad, compared to the N^2 other modes should become infinitesimally small. It is therefore reasonable to assume that in an infinitely large domain, in which the mode density goes to infinity, the influence of one triad, compared to the cumulative influence of all other triads goes to zero. This ratio is the small parameter, and the fact that this parameter tends to zero is called the weak dependence hypothesis.

We should note here that there is a bound on the validity of this assumption. Consider the case in which our domain, containing a large number of modes, is filled with modes which are all unexcited, except for three excited modes with a very large excitation. In this case the influence of this single triad can not be considered small with respect to the sum of all other triads. Kraichnan excluded such pathological situations from the DIA by invoking the maximum randomness assumption [34]. However, not all situations which violate the weak

dependence assumption are pathological. A typical situation where DIA fails is the very long time behavior of forced, high Reynolds number two-dimensional turbulence. In this case, the energy will start to pile-up in the modes with largest wavelength, as is common in Bose-Einstein condensates. The physical structures related to this state are two counter-rotating vortices (in the case of a periodic domain). The energy spectrum of this state is proportional to k^{-3} (see for example [44]). DIA predicts a condensate, consisting of a single peak in the energy spectrum at the first wavenumber (see figure 3.4). The fact that DIA fails here is probably related to the fact that we cannot ignore the triad-interactions involving this typical scale, since almost all energy is contained in this scale. Intuitively it is clear that the weak dependence assumption might be violated in this case. Having said this, it should be admitted that the weak dependence hypothesis seems very plausible in most other turbulent systems.

Let us now repeat the perturbation series using this weak-dependence assumption. The state that we will perturb about is the velocity field that we would have if all triads were retained except for one. The properties of this system should therefore be very close to the complete system, since one triad should not contribute significantly compared to the sum of all the other. Let us denote this particular triad, which is not acting in the dynamics of the unperturbed velocity field, by (y_k, y_p, y_q). We write again the perturbation approach

$$y_k \approx y_k^{(0)} + \underbrace{2\int_0^t G_k(s) A_{kpq} y_p^{(0)} y_q^{(0)} ds}_{y_k^{(1)}}, \tag{2.16}$$

in which $y_k^{(0)}$ is thus the almost complete system, only independent of modes y_p and y_q, and $y_k^{(1)}$ interacts exclusively with $y_p,\ y_q$. If we compare with (2.9) we observe that $y_k^{(1)}$ does not contain the sum over p, q, which is present in the original equation, but only $y_p,\ y_q$ themselves. This is because only one triad is removed. The factor 2 appears since the model equation is symmetric in p, q so that the single triad appears both as k, p, q and as k, q, p in the nonlinear interaction. G is now the response function which characterizes the response of a velocity mode $y_k \to y_k + \delta y_k$ on an infinitesimal random force f_k applied to the RHS of (2.2). The difference of $G_k(s)$ with $G_k^{(0)}(t)$ in the conventional perturbation is that now the Green's function is not the solution of the linear equation, but of the full system and is an additional unknown. We need therefore an expression for $G_k(s)$ as a function of known quantities and this expression is derived in section 2.3.3.

The velocity is thus decomposed into a part in which $y_k^{(0)}$ is independent of modes $y_p,\ y_q$ plus the direct interaction part, containing only the interaction $y_k,\ y_p,\ y_q$. A peculiarity of this perturbation approach is that we perturb about the actual state that is unknown and not about a known linear solution. The DIA is therefore an implicit approach in some sense. The perturbation should be valid if $|y_k^{(0)}| \gg |y_k^{(1)}|$. Surprisingly enough, investigations that focused on the direct validation of this weak interaction assumption are very scarce [45, 46].

2.3 The DIA procedure applied to triple and quadruple correlation functions

2.3.1 Derivation of the DIA for triple correlations

As mentioned in the beginning of this section, DIA is a perturbation method so that $y_k \to y_k^{(0)} + y_k^{(1)} + y_k^{(2)} + y_k^{(3)} + ...$ The triple correlation S_{kpq} thereby becomes

$$\begin{aligned} S_{kpq}^{DIA} = \overline{y_k^{(0)} y_p^{(0)} y_q^{(0)}} + \Big(\overline{y_k^{(1)} y_p^{(0)} y_q^{(0)}} + \overline{y_k^{(0)} y_p^{(1)} y_q^{(0)}} + \overline{y_k^{(0)} y_p^{(0)} y_q^{(1)}} \Big) \\ + \Big(\overline{y_k^{(1)} y_p^{(1)} y_q^{(0)}} + \overline{y_k^{(1)} y_p^{(0)} y_q^{(1)}} + \overline{y_k^{(0)} y_p^{(1)} y_q^{(1)}} + \\ \overline{y_k^{(2)} y_p^{(0)} y_q^{(0)}} + \overline{y_k^{(0)} y_p^{(2)} y_q^{(0)}} + \overline{y_k^{(0)} y_p^{(0)} y_q^{(2)}} \Big) + \\ \text{higher order contributions.} \end{aligned} \tag{2.17}$$

Subsequently we retain the contribution $\overline{y_k^{(0)} y_p^{(0)} y_q^{(0)}}$ which is determined by the full velocity field from which the influence of the single mode k, p, q is removed, and the first order direct-interaction contributions, the three terms in brackets on the first line of (2.17). For the case of Navier-Stokes turbulence, $\overline{y_k^{(0)} y_p^{(0)} y_q^{(0)}}$ corresponds to $\overline{u_k(-\boldsymbol{k})^{(0)} u_p(\boldsymbol{p})^{(0)} u_q(\boldsymbol{q})^{(0)}}$, from which the interaction of the triad between $-\boldsymbol{k}+\boldsymbol{p}+\boldsymbol{q}$ is removed. When considering the instantaneous field y_k, the contribution of a single triad is small so that the perturbation approach should be valid. However, when considering the correlation involved in the energy transfer, this triad is the only contributing triad. So the non-perturbed triple correlation $\overline{y_k^{(0)} y_p^{(0)} y_q^{(0)}}$ does not contribute to the transfer. The first order terms are evaluated by substituting the DIA contribution for these quantities. Let us consider one of the three of these contributions,

$$\begin{aligned} \overline{y_k^{(1)} y_p^{(0)} y_q^{(0)}} &= 2 \int_0^t G_k(s) A_{kpq} \, \overline{y_p^{(0)} y_q^{(0)} y'^{(0)}_p y'^{(0)}_q} ds \\ &= 2 \int_0^t G_k(s) A_{kpq} \, \overline{y_p^{(0)} y'^{(0)}_p} \; \overline{y_q^{(0)} y'^{(0)}_q} ds, \end{aligned} \tag{2.18}$$

which yields for the Navier-Stokes equations,

$$\begin{aligned} \overline{u_k(-\boldsymbol{k})^{(1)} u_p(\boldsymbol{p}) u_q(\boldsymbol{q})} &= i \int_0^t G(-\boldsymbol{k}, s) P_{kmn}(\boldsymbol{k}) \; \overline{u_p(\boldsymbol{p}) u_q(\boldsymbol{q}) u'_m(-\boldsymbol{p}) u'_n(-\boldsymbol{q})} ds \\ &= i \int_0^t G(-\boldsymbol{k}, s) P_{kmn}(\boldsymbol{k}) \; \overline{u_p(\boldsymbol{p}) u'_m(-\boldsymbol{p})} \; \overline{u_q(\boldsymbol{q}) u'_n(-\boldsymbol{q})} ds, \end{aligned} \tag{2.19}$$

in which the second line follows from the first line using the weak-dependence principle. The weak dependence assumption is here a consequence of spatial homogeneity [34] (see also [47] for a discussion of this property). The same procedure is followed for the quantities $\overline{y_k^{(0)} y_p^{(1)} y_q^{(0)}}$ and $\overline{y_k^{(0)} y_p^{(0)} y_q^{(1)}}$, so that an expression for the evolution of $\overline{y_k y'_k}$ is obtained containing only $\overline{y_k y'_k}$ and G_k. For the moment G_k is an unknown.

2.3.2 DIA for quadruple correlations

Several interesting quantities, characterizing the non-Gaussianity of a turbulent flow are functions of quadruple correlations of the velocity field. Among these quantities are the pressure variance, dissipation rate fluctuations and the variance of the nonlinear term. As stressed in the previous section, the DIA does not assume Gaussianity of the fourth order moments. It is therefore interesting to investigate what it predicts for the non-Gaussianity of these quantities. We therefore focus in this section on the derivation of a closed DIA expression for the quantity $Q_{pqmn} \equiv \overline{y_p y_q y_m y_n}$.

Building on the weak dependence assumption, we again remove one triad from the interaction, the k, p, q triad, so that we obtain as a first order quantity

$$\overline{y_p^{(0)} y_q^{(0)} y_m^{(0)} y_n^{(0)}} + \overline{y_p^{(1)} y_q^{(0)} y_m^{(0)} y_n^{(0)}} + ... \tag{2.20}$$

with the $y_p^{(0)}$ independent of q, k and

$$y_p^{(1)} = 2 \int_0^t G_p(s) A_{pkq} y_k'^{(0)} y_q'^{(0)} ds. \tag{2.21}$$

This does not yield a closed expression, and the DIA perturbation needs to be carried out up to second order. A question is now how to do that. We remove from the original field a second triad, this time the k, m, n triad, so that

$$y_p = y_p^{(0)} + y_p^{(1)} + y_p^{(2)}, \tag{2.22}$$

with $y_p^{(0)}$ independent of k, p, q and of k, m, n.

$$y_p^{(2)} = 4 \int_0^t \int_0^s G_p(s) G_k(s') A_{pkq} A_{kmn} y_m''^{(0)} y_n''^{(0)} y_q'^{(0)} ds' ds. \tag{2.23}$$

Substituting (2.22) in Q_{pqmn}, one obtains

$$\overline{y_p y_q y_m y_n} = \underbrace{\overline{y_p^{(0)} y_q^{(0)} y_m^{(0)} y_n^{(0)}}}_{\text{zeroth order}} + \underbrace{\left(\overline{y_p^{(1)} y_q^{(0)} y_m^{(0)} y_n^{(0)}} + 3 \text{ more} \right)}_{\text{first order}} +$$
$$\underbrace{\left(\overline{y_p^{(1)} y_q^{(1)} y_m^{(0)} y_n^{(0)}} + 5 \text{ more} + \overline{y_p^{(2)} y_q^{(0)} y_m^{(0)} y_n^{(0)}} + 3 \text{ more} \right)}_{\text{second order}} + \text{higher order}. \tag{2.24}$$

Evaluating the different terms we find that the zeroth order correlation does not vanish. As for even moments of independent (Gaussian) Fourier modes we have now a non-zero contribution from the field from which the two triad interactions are removed. The first order contributions contain quintuple correlations, which will vanish according to the weak dependence principle. It is in this case therefore the second order contribution which is the first nonvanishing contribution. Two types of contributions do appear here, 6 contributions with two $y^{(1)}$'s and 4 contributions with one $y^{(2)}$. Of the former six contributions, two are zero,

$$\overline{y_p^{(1)} y_q^{(1)} y_m^{(0)} y_n^{(0)}} = \overline{y_p^{(0)} y_q^{(0)} y_m^{(1)} y_n^{(1)}} = 0. \tag{2.25}$$

This can be seen by substituting the $y_p^{(1)}$'s into these expressions and considering which are the direct interaction triads. The final expression contains thus one

zeroth order contribution and 8 second order contributions. We will explicitly show two of these eight contributions:

$$\begin{aligned}\overline{y_p^{(1)}y_q^{(0)}y_m^{(1)}y_n^{(0)}} &= 4\int_0^t\int_0^t G_p(s)G_m(s')A_{mkn}A_{pkq}\overline{y_k'^{(0)}y_k''^{(0)}}\;\overline{y_q{}^{(0)}y_q'^{(0)}}\;\overline{y_n{}^{(0)}y_n''^{(0)}}ds'ds\\ \overline{y_p^{(2)}y_q^{(0)}y_m^{(0)}y_n^{(0)}} &= 4\int_0^t\int_0^s G_p(s)G_k(s')A_{pkq}A_{kmn}\overline{y_m^{(0)}y_m''^{(0)}}\;\overline{y_n^{(0)}y_n''^{(0)}}\;\overline{y_q'^{(0)}y_q^{(0)}}ds'ds.\end{aligned} \tag{2.26}$$

In principle, we have obtained a closed expression, apart from the response function. In practice, there is still quite some algebra to work out the final expressions to evaluate.

2.3.3 The mean response function

For the linear, viscous problem, the Green's-function is given by

$$G_k = G_k^{(0)} = e^{-\nu k^2(t-t_0)}H(t-t_0), \tag{2.27}$$

with $H(t-t_0)$ the Heaviside function. For convenience we used $t_0 = 0$ in the foregoing. Using this Green-function to describe the time-decorrelation of the nonlinear term leads to the Quasi-Normal approximation. In turbulent flows, the decorrelation is not only due to the viscous diffusion, but also, and dominantly, due to the nonlinear mode coupling, which is not taken into account in the viscous Green's function. If one would therefore use the viscous response function in the derived expressions for triple correlations, the correlations would be overestimated, since the decorrelation is too slow. This yields a transfer which is so strong that the energy is pumped out of large turbulent scales at an unphysically large rate so that the energy spectrum becomes negative at certain wavenumbers. Negative kinetic energy is of course intolerable if one is looking for a correct physical description and therefore one needs to derive a correct form for the Green's function of a turbulent flow. This can be done self-consistently using the DIA.

The correct mean response function which appears in the DIA expressions for the moments of y_k, is the response of the system to an infinitesimal perturbation. Adding an infinitesimally small random forcing term to the right hand side of (2.2),

$$(\partial_t + \nu_k)y_k = \sum_{p,q} A_{kpq}y_p y_q + f_k\delta(t-s), \tag{2.28}$$

we will now define the average response function as

$$G_k(t,s) = \overline{\delta y_k(t)/f_k(s)}, \tag{2.29}$$

in which we show the two time arguments for clarity. The quantity $\delta y_k(t)$ represents the difference induced on y_k through the presence of f_k, not to confuse with the time impulse delta function $\delta(t)$. Retaining only terms linear in $\delta y_k(t)$ (since $|\delta y_k(t)/y_k| \ll 1$, terms involving $(\delta y_k(t))^2$ will be negligible), we obtain for $t > s$,

$$(\partial_t + \nu_k)\overline{\delta y_k} = 2\sum_{p,q} A_{kpq}\overline{\delta y_p y_q}, \tag{2.30}$$

in which p, q symmetry is used. Applying the DIA to this equation, one obtains straightforwardly an equation for $G_k(t,s)$ as a function of $\overline{y_k y_k'}$. A closed system is thereby obtained with an equation for $\overline{y_k y_k'}$ (closed using the expression obtained for the triple correlations S_{kpq}) and an equation for $G_k(t,s)$.

The fact that $\overline{y_k y_k'}$ and G_k are two-time quantities puts certain restrictions on their definition, in particular with respect to the reference frame in which the approximation should be defined. We will discuss this issue in section 2.4.

2.3.4 DIA and Gaussianity

The DIA yields the same expressions as the quasi-normal approximation differing only in the form of the response function. It is therefore often mistakenly assumed that DIA is a variant on the Quasi-normal approach only differing from the latter by the treatment of the response function. However, we did not invoke the assumption of Gaussianity in the whole derivation. The operations that we applied invoking the weak-dependence assumption are clearly valid for a Gaussian quantity, but the fact that it holds does not imply that the quantity is Gaussian (see for example reference [46]). It can be shown that this formal ressemblance between DIA and QN is rather a coincidence for the treatment of triple correlations, and that it does not hold for higher correlations. In particular, QN theory assumes close to Gaussian statistics, whereas DIA can treat systems which are far from Gaussian, as long as the weak-dependence and maximum randomness conditions are fullfilled. We further note that the quasi-normal approach would per definition neglect the fourth order cummulants obtained in the previous section, since the fourth-order correlations are assumed Gaussian. One could propose an adapted version of the quasi-normal approach, in which the fourth-order correlations are not assumed Gaussian, but in which the sixth order correlations are. This would not yield the same expression as obtained by the DIA, and the resulting expression becomes much more elaborate than the above expression.

2.4 A Lagrangian formulation of turbulence theory

As a result of the DIA, Kraichnan determined that the energy distribution should be proportional to $k^{-3/2}$ with k the wavenumber. This is in disagreement with Kolmogorov's phenomenological theory proposed in 1941 [27]. In the 1961 turbulence conference where Kraichnan presented his DIA, the first very high Reynolds number measurements of the energy spectrum were also presented [48]. These measurements convincingly confirmed that the energy spectrum was approximately proportional to $k^{-5/3}$. Kolmogorov's arguments were based on scale-locality, which means that at very high Reynolds numbers, in which the forcing scale is much larger than the dissipative scale, the energy flux $\epsilon_f(k)$ at intermediate scales is only determined by the energy at these scales and the local timescale,

$$\epsilon_f(k) \sim \frac{kE(k)}{\tau(k)}, \tag{2.31}$$

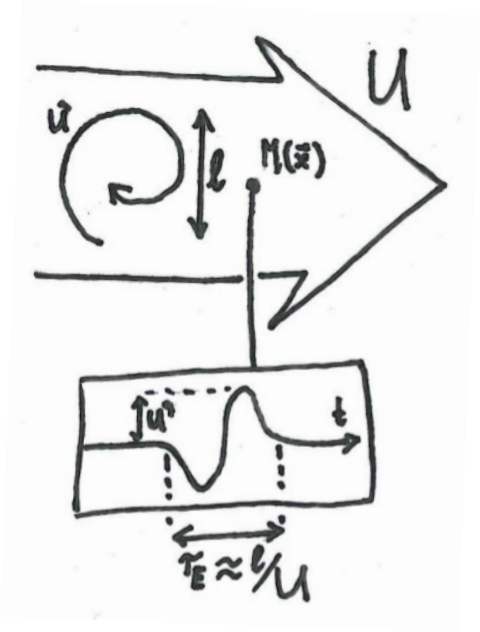

Figure 2.2: Left: an Eulerian observer $M(\vec{x})$ measures a time-correlation of a structure of size l. He deduces the correlation time $\tau = l/U$, with U the large scale (sweeping) velocity that translates the structure.

so that

$$E(k) \sim \frac{\tau(k)\epsilon_f(k)}{k}, \tag{2.32}$$

in which $kE(k)$ represents the energy around k and $\tau(k)$ is the local timescale. If this local timescale is determined by the local eddy turnover-time, $(k\sqrt{kE(k)})^{-1}$, one finds

$$E(k) \sim \epsilon_f(k)^{2/3}k^{-5/3}, \tag{2.33}$$

and a quasi-static evolution of the energy spectrum at large k implies $\epsilon_f(k) \approx \epsilon$. The DIA suggested however

$$E(k) \sim \frac{\tau^E(k)\epsilon_f(k)}{k}, \tag{2.34}$$

in which $\tau^E(k)$ is not a local time, but the time it takes an eddy of size l to be swept a distance of order l by the large scale velocity, roughly given by $\sqrt{\int E(k)dk}$. This sweeping time gives indeed the correlation time associated to an eddy measured by an Eulerian probe. Figure 2.2 illustrates this timescale.

What we would like the time-scale to measure is the correlation-time of an eddy of a certain scale, *i.e.* , the time it takes for this scale to decorrelate and give its energy to other scales. If we now add a uniform velocity U to our flow, the dynamics of the interscale transfer should not change. Clearly, our turbulence should decay exactly the same if we would put our experimental set-up on a train moving with a constant velocity. However, for the observer in

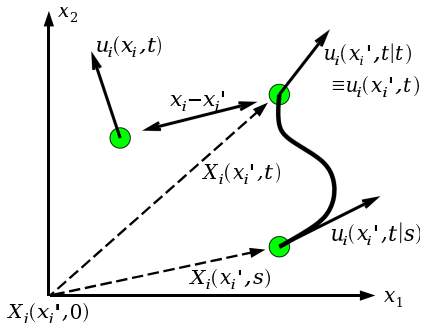

Figure 2.3: The abridged Lagrangian History DIA uses a semi-Lagrangian coordinate system. One point is evaluated along a trajectory and the second one is fixed in space. The second time-argument of the velocities indicates the position on the trajectory that passes through the labeling point at the time indicated by the first time-argument.

the non-moving laboratory frame, the correlation time has changed from

$$\tau^E(k) = \frac{l}{\sqrt{\int E(k)dk}} \rightarrow \tau^E(k) = \frac{l}{\sqrt{\int E(k)dk + U}}. \tag{2.35}$$

This spurious effect is also known as violation of Gallilean invariance. Kraichnan himself pointed out this problem with DIA [49]. Since DIA is a two-time theory, it takes into account the time-history of the correlations of Fourier modes. In the original formulation of DIA, this time-history is computed at a fixed point in the laboratory frame and is therefore sensitive to this sweeping effect. An Eulerian observer can not distinguish the decorrelation of a Fourier mode by nonlinear distortion (such as vortex stretching, straining or other multi-scale processes), from decorrelation by the sweeping of an arbitrary large scale or flow component.

This problem of DIA can be solved by recasting the approximation into a Lagrangian reference frame [28]. The variable that is now considered as the representative is the Lagrangian velocity $\boldsymbol{u}(\boldsymbol{x}, t|t')$ defined as the velocity at time t' of a fluid particle which is at point $\boldsymbol{x}$ at time t. This definition implies that $u(x, t|t)$ is equivalent to the Eulerian velocity $u(x, t)$ (see Figure 2.3 for an illustration of this coordinate frame). By doing so, the dynamics of a Fourier mode at a certain scale becomes insensitive to the sweeping of an arbitrary large flow scale. This shows that the scale-locality assumption of Kolmogorov is directly linked to the Lagrangian character of the time-correlation of the Fourier modes as was illustrated in section 1.2.

The biggest drawback for using the Lagrangian DIA is perhaps its analytical complexity, in particular due to the dependence of the time-history of Fourier modes over Lagrangian trajectories. Indeed, the velocity covariance

$$\overline{\boldsymbol{u}_i(\boldsymbol{x}, t|t')\boldsymbol{u}_j(\boldsymbol{x}', t|t'')}, \tag{2.36}$$

becomes now a function of 4 variables instead of 2. In order to deal with this, approximations have been proposed which model this time history. A first approximation, leading to the abridged Lagrangian-history DIA is to consider

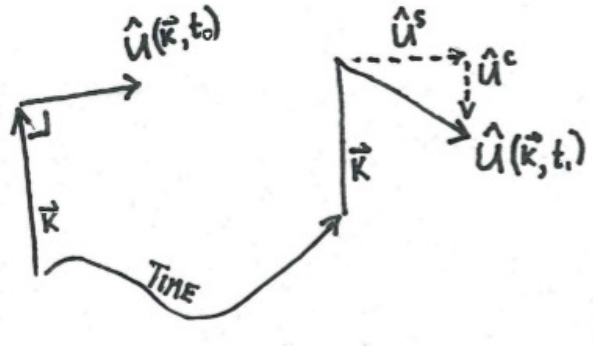

Figure 2.4: An incompressible velocity field is, in Fourier-space, perpendicular to the wave-vector. It is the pressure gradient which removes the divergent part. If we consider a velocity-test-field governed by the Navier-Stokes equations from which the pressure term is removed, in general a potential part u^c, parallel to the wave-vector will be created. By considering simultaneously the dynamics of this test-field and the Navier-Stokes dynamics, one can estimate the influence of the pressure.

the case in which one of the velocities is evaluated at a fixed point. This still yields a rather complicated model and further approximations will be discussed in the following section.

2.5 Markovianization

As noted above, a self-consistent theory with correct inertial range behavior should be dealing with the Lagrangian two-time quantities,

$$\overline{y_k y'_k} \text{ and } G_k(t,s) = \overline{\delta y_k / f'_k}, \tag{2.37}$$

in which the y_i are thus evaluated on particle trajectories, instead of on fixed points, as would be the case in an Eulerian theory. If the two-time quantities are not of direct interest, but one wants to determine single-time statistics like $\overline{y_k y_k}$, one can use a Markovianized approximation of the theory. Markovianization means in this context that to evaluate quantities at time t, we do not use information on times previous to t (but it does not assume zero-correlation between quantities at different time-instants). It should be noted that Markovianization introduces necessarily additional assumptions into the theory. However, Markovianization is a logical thing to do if one wants to evaluate DIA numerically, since the memory requirements to evaluate the dynamics will increase in time because the DIA equations depend on the entire history of the flow. So either truncation of the time-history or Markovianization is helpful in evaluating the long-time dynamics.

Markovianization implies the assumption of a functional time-dependence of the quantities $R_k(t,s)$ and $G_k(t,s)$ with $R_k(t,s)$ defined as

$$\overline{y_k y'_k} = \overline{y_k y_k} R_k(t,s). \tag{2.38}$$

As an example we take the DIA triple correlation defined in expression (2.18) and we rewrite it,

$$\overline{y_k^{(1)} y_p^{(0)} y_q^{(0)}} = 2\int_0^t G_k(t,s) A_{kpq}\ \overline{y_p y_p' y_q y_q'} ds \tag{2.39}$$

$$= 2A_{kpq}\ \Theta_{kpq} \overline{y_p y_p y_q y_q}, \tag{2.40}$$

with

$$\Theta_{kpq} = \int_0^t G_k(t,s) R_p(t,s) R_q(t,s) ds. \tag{2.41}$$

The quantity Θ_{kpq} has the dimension time and corresponds thus to a Lagrangian time-scale, characterizing the simultaneous correlations of the modes k, p, q. The time-correlations $R_k(t,s)$ and $G_k(t,s)$ should be equal to unity at $t = s$ and should tend smoothly to zero at long times. Obvious choices are then exponential time-dependence or Gaussian time-dependence. An exponential time-dependence can actually not be correct, since the time-correlation should be continuous and invariant under the transformation $t \to -t$. Indeed, in the absence of viscosity the complete dynamics should be time-reversible (see section 3.2). A Gaussian time-dependence could be assumed to get correct behavior around zero. It was however shown that the results are relatively insensitive to the exact choice [50] and an exponential time-dependence has the advantage that it simplifies the resulting integrals, which can be evaluated analytically[3]. The fact that the precise form is not so important comes from the fact that we do not use the correlation functions themselves in the resulting model, but only their integral over time. In the following we will assume an exponential time-dependence of the form

$$R_k(t,s) = \exp\left[-\frac{|t-s|}{\tau_k}\right]. \tag{2.42}$$

We can integrate both sides of this expression with respect to s to obtain an expression for τ_k,

$$\tau_k = \int_{t_0}^t R_k(t,s) ds \left(1 - \exp\left[-\frac{|t-t_0|}{\tau_k}\right]\right)^{-1}. \tag{2.43}$$

For the sake of simplicity, we will consider here the case in which the turbulence has been created a time long before we evaluate it, by taking the limit of t_0 tending towards $-\infty$, so that

$$\int_{t_0}^t R_k(t,s) ds \approx \tau_k. \tag{2.44}$$

If we also assume an exponential dependence for the response function, with a correlation time τ_k^G, the triple correlation time becomes now

$$\Theta_{kpq} = \frac{1}{(\tau_k^G)^{-1} + (\tau_p)^{-1} + (\tau_q)^{-1}}. \tag{2.45}$$

[3] In the case of the quantity Θ_{ijk}, a Gaussian time-dependence can also be evaluated analytically. However, the timescales that appear in the second order perturbation terms, needed to evaluate the DIA expression for the quadruple correlations, involve double time-integrals and analytical evaluation of the timescale becomes difficult if the time-correlations are assumed to be Gaussian.

The timescales τ_k^G and τ_k remain to be determined. They should take into account the Galilean invariant character of the time-history. Therefore decorrelation should only be caused by the decorrelation through the effects of pressure and viscous stresses and not through the effect of advection, since it is this advection which is responsible for the violation of Galilean invariance (section 1.2). The decorrelation by viscous stresses does not need modeling, since we can obtain an exact expression for this linear process, but the decorrelation by the pressure, involving scale-interactions is more delicate. Kraichnan proposed an elegant way of modeling the pressure decorrelation by pointing out that the effect of pressure is to remove the energy which is contained in Fourier-modes parallel to the wavevector [51]. By solving an equation for a vector-field, the test-field, which is governed by pressureless dynamics, the time-scale at which energy is transferred towards the parallel modes is taken as the decorrelation time of the Fourier modes. This mechanism is illustrated in figure 2.4. Another way to measure the decorrelation is to write an equation for the displacement vector of a fluid particle, as will be done in section 2.7.

The timescales τ_k^G and τ_k are in principle not equal. They would be equal in a system in thermal equilibrium, since in that case the *Fluctuation-Dissipation theorem* (FDT) holds. The FDT states that the time-correlation of fluctuations of a system in thermal equilibrium is equal to the time-response to infinitesimal perturbations. In turbulence, the response to an infinitesimal perturbation is exactly the response function, $G_k(t,s)$. The perturbations are the velocity fluctuations and their time correlation is given by the normalized two-time velocity correlation. The FDT for a turbulent flow is therefore

$$R_k(t,s) \equiv \overline{y_k y_k'} / \overline{y_k y_k} = G_k(t,s) + G_k(s,t). \tag{2.46}$$

On the right hand side the sum of the two response-functions is needed since the response $G_k(t,s)$ is only non-zero for $t > s$. Evidently, there will be no response to an infinitesimal perturbation before the perturbation is applied. Turbulence is of course far from thermal equilibrium (see also section 3.1), however the FDT seems rather robust and approximately holds for turbulent flows if Eulerian quantities are considered at inertial range scales [52]. This is because both a Fourier mode and the impulse response are mainly decorrelated through the same mechanism, which is the large-scale sweeping of the small scales. However, for Lagrangian quantities, the correlation time of the fluctuations seems to be larger than the correlation time of an infinitesimal perturbation [23, 52], and according to Lagrangian DIA, the correlation time of the velocity-fluctuations is approximately 1.8 times larger than the one associated to the response function. Surprisingly enough, if the Lagrangian velocity is chosen in a slightly different way, as is done in Kaneda's variant of Lagrangian DIA, called Lagrangian Renormalized Approximation (LRA) [53, 54], FDT holds as an exact result. However, this seems to be rather a coincidence, since for higher orders of the LRA the FDT is not exactly satisfied [55]. However, this result shows that the FDT is at least approximately valid. We choose therefore in general the timescales in (2.45) equal.

Most Markovian theories share the structure (2.45) but differ in the way in

which the time-scale Θ_{kpq} is determined. Prescribing

$$G_k(t,s) = \exp\left[-(t-s)\left(\underbrace{\lambda\sqrt{\int_0^k k^2 E(k)dk}}_{\text{eddy damping}} + \nu k^2\right)\right] H(t-s), \qquad (2.47)$$

yields the Eddy-Damped Quasi-Normal Markovian (EDQNM) closure for isotropic turbulence [56], with λ a model parameter determining the Kolmogorov constant (*i.e.* the proportionality factor in expression (1.10)). The particular choice of the eddy-damping determines the precise behavior of the closure[4]. We note here that the EDQNM approximation can also be derived in a less formal manner by adding a damping term to the Quasi-Normal approximation and Markovianizing the resulting expression. In particular in the presence of linear effects such as shear or rotation, a more heuristic approach, starting from a rapid-distortion expression seems to be more convenient [59].

2.6 A Langevin-model for the Direct Interaction Approximation

DIA describes not only the multiscale structure of turbulence but also the non-Markovian (or multi-time) character. An important property of DIA is its realizability. This means that the energy spectrum is non-negative, which was not the case for the Quasi-Normal approximation. This property can be proven because the DIA equations correspond to the dynamics of a generalized Langevin equation for the velocity (*e.g.* reference [60]), which implies that the energy and all other even moments of the velocity field are positive.

Let us outline this in more detail. The classical Langevin equation [61], describing the velocity of a particle in Brownian motion is given by

$$\frac{du}{dt} = -\lambda u + f, \qquad (2.48)$$

in which f is a random forcing term, which is generally chosen white in time, and λ is a friction, the inverse of which corresponds to the time-memory of the velocity dynamics. In the generalized Langevin model, both λ and f are now functions of the response function, the energy spectrum and a Gaussian velocity field with the same energy spectrum as the velocity field.

[4] Orszag, in the original version of EDQNM, simply proposed the dimensionally correct time-scale $\tau(k) \sim \epsilon^{-1/3}k^{-2/3}$, whereas Pouquet *et al.* [57] proposed the now more popular *Heisenberg* straining time-scale used in expression (2.47). This scale represents the straining of the small-scales by the large-scales. If we would also like to take into account the straining of the large-scales by the small scales, we could modify this expression as described in [58] but this modification did not seem to induce significant modifications for three-dimensional turbulence.

The DIA Langevin model is given by [60],

$$(\partial_t + \nu_k)y_k = -\int_0^t \eta_k(t,s)y_k(s)ds + q_k \tag{2.49}$$

$$\eta_k(t,s) = -4\sum_{p,q} A_{kpq}A_{pqk}G_p(t,s)\overline{y_q y_q'} \tag{2.50}$$

$$q_k = \sum_{p,q} A_{kpq}\xi_p(t)\xi_q'(t), \tag{2.51}$$

with $\xi_k(t)$ and $\xi_k'(t)$ independent stochastic processes which have the same time-space covariance as the fluctuating field[5]

$$\overline{\xi_k(t)\xi_k(t')} = \overline{y_k y_k'}. \tag{2.53}$$

Equation (2.49) replaces the original (Navier-Stokes) equations,

$$(\partial_t + \nu_k)y_k = \sum_{p,q} A_{kpq}y_p y_q. \tag{2.54}$$

At first sight the model equation seems more complicated than the original. It has however the advantage that it is only linear dependent on the turbulent fluctuation y_k. To obtain statistics, one could simulate the above equation for a given spectral velocity distribution.

We have now

$$y_k(t') = \int_0^{t'} G_k(t',s)q_k(s)ds. \tag{2.55}$$

In the Direct Interaction Approximation, this is only true for infinitesimal variations of $y_k(t)$. For the above model equations this holds for larger variations since the model equation has become effectively linear in $y_k(t)$. Therefore, what holds for small time variations should also be true for large time-differences. Using this relation, we find that the equation for $\overline{y_k y_k'}$ is the same as obtained by using the DIA. This model equation therefore yields the same statistics as DIA and does so for all moments. Since the moments are directly computed from a velocity field, the even moments are necessarily positive.

With respect to the existence of a Langevin equation for the DIA system we can read Moffatt's comment in the proceedings of the 2011 turbulence conference in Marseille (in a paragraph discussing the realizability of the DIA): *... and this because it was an exact closure for a physically realisable dynamical system, although unfortunately not the Navier-Stokes system ...* Of course we can agree that if the DIA applied to the Navier-Stokes equation could be proven to give identical statistics as the Navier-Stokes equations, we would be very happy. But this is the whole problem with turbulence theory: it has not proven possible to derive solutions of the Navier-Stokes equations for a general turbulent flow. Therefore this critique is not appropriate. Let us assume that it is possible to derive a Langevin equation from the Navier-Stokes equations. The real question

[5]Note that this is a choice, and other formulations of q are possible as long as

$$\overline{q_k(t)q_k(t')} = 2\sum_{p,q} A_{kpq}A_{kpq}\overline{y_p y_p'}\ \overline{y_q y_q'}. \tag{2.52}$$

is then whether the dynamics of Kraichnan's DIA model equation are the same as those of this *perfect* Langevin model.

This generalized Langevin-equation discussed above is given at a fixed point, not moving with the fluid particle as (2.48). In principle, the equation could (and should) be defined in a Lagrangian frame, for the reasons discussed in 2.4. For the Lagrangian DIA, no model equation is known. Realizability has thus not been rigorously proven. For the Markovian variants of the theory a model is known. We mention the Test Field Model (TFM) Langevin equation [51],

$$(\partial_t + \nu_k)y_k = -\eta_k y_k + q_k \tag{2.56}$$

$$\eta_k = -4\sum_{p,q} A_{kpq}A_{pqk}\Theta_{pqk}\overline{y_q y_q'} \tag{2.57}$$

$$q_k = \sum_{p,q} A_{kpq}\Theta_{kpq}^{1/2}\omega(t)\xi_p\xi_q', \tag{2.58}$$

with $\omega(t)$ a white noise process. We observed a problem with this model. It correctly gives the energy transfer (triple correlations) as predicted by the TFM. However, it does not for the mean-square nonlinearity. Computing the quantity

$$\begin{aligned} W_k &= \sum_{p,q}\sum_{m,n} A_{kmn}A_{kpq}\overline{y_p y_q y_m y_n} \\ &= (-\eta_k y_k + q_k)(-\eta_k y_k + q_k), \end{aligned} \tag{2.59}$$

we find that the mean-square nonlinearity becomes proportional to Θ. This can not be correct in general. At short times, if the initial conditions are Gaussian, the mean-square nonlinearity is not zero, but we expect this quantity to have a value of the order of a Gaussian field (zeroth order contribution in equation (2.24)). According to the predictions of the TFM or EDQNM Langevin model we obtain a vanishing mean-square nonlinearity at short times, since Θ is zero at short times, since it measures the effective decorrelation time of the dependent Fourier modes. So the Markovian Langevin model seems to be correct only in predictions of the energy transfer, but not necessarily for higher order quantities in which non-zero Gaussian contributions are present.

2.7 A Lagrangian Markovianized Field Approximation

In general, single-time two-point closures that are derived from the Direct Interaction Approximation by Markovianization yield agreement with Kolmogorov's scaling arguments, if the Lagrangian character of the time-history is properly taken into account. Since the displacement vector of a fluid particle is the time integral of the Lagrangian velocity, it contains information on the Lagrangian correlation-time of a fluid particle. Kaneda's Lagrangian Renormalized Approximation [53] is based on this idea. In our contribution [1], we used the analogy between the dynamics of a passive scalar fluctuation in the presence of a mean, uniform scalar gradient, and the displacement of a fluid particle to attain the same goal: determining the Lagrangian correlation time of a turbulent flow. Let us now discuss this analogy, which was previously suggested by Batchelor [62].

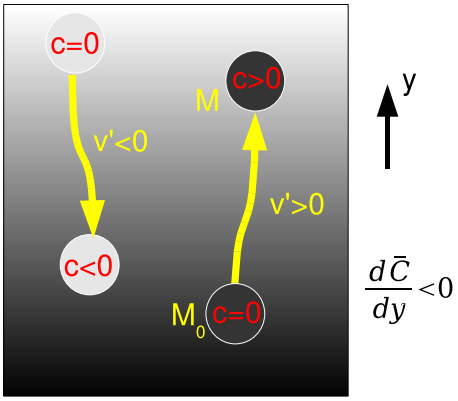

Figure 2.5: In the presence of a mean scalar gradient, the value of scalar fluctuations c is proportional to the displacement distance of a fluid particle parallel with the direction of the mean gradient $d\overline{C}/dy$.

We start with a smooth scalar field with a mean scalar gradient of value Γ, chosen in the y-direction in our example. We have therefore the mean value of the scalar at point x, y given by

$$\bar{\theta}(x, y) = \bar{\theta}(x, 0) + y\Gamma, \tag{2.60}$$

and we will choose $\bar{\theta}(x, 0) = 0$ for convenience. Figure 2.5 shows this situation. Initially we assume that all scalar fluctuations are equal to zero. Let us now consider a fluid particle which is initially at point $M_0 = (x_0, y_0)$ in this scalar field. Its total scalar value (mean plus fluctuation) is then $\theta = \bar{\theta} = y_0\Gamma$, since initially fluctuations are zero. This particle is transported by a velocity fluctuation v' of the fluid to point $M = (x_1, y_1)$. If we neglect the influence of diffusion, the total scalar value of this fluid particle has not changed and is still $\theta = y_0\Gamma$. However, the mean scalar field is a function of y, and at y_1 this value is $\bar{\theta}(y_1) = y_1\Gamma$ so that the value of the fluctuation is

$$\theta' \equiv \theta - \bar{\theta} = y_0\Gamma - y_1\Gamma = -\Delta y\Gamma. \tag{2.61}$$

We see thus directly that the value of the fluctuation of the scalar field is minus the displacement times the value of the mean gradient. Let us go one step further to illustrate how one can determine the correlation time of a turbulent flow using this analogy.

For times as long as the correlation time of the turbulence, we have $\Delta y \approx v'\mathcal{T}$, which shows that

$$\theta' = -\Gamma v'\mathcal{T}. \tag{2.62}$$

Multiplying both sides by v' and averaging, we find

$$\overline{v'\theta'} = -\Gamma\overline{v'v'}\mathcal{T}, \tag{2.63}$$

in which we considered $\mathcal{T}$ to be the average correlation time of the turbulence. To simplify we choose, without loss of generality (since the scalar equation is

linear) the value of $\Gamma = -1$, so that we find for the correlation time of the flow,

$$\mathcal{T} = \frac{\overline{v'\theta'}}{\overline{v'v'}}. \tag{2.64}$$

This is the analogy that we mentioned and that we use to derive the markovian closure model shown in the now following manuscript.

A single-time two-point closure based on fluid particle displacements

W. J. T. Bos[a] and J.-P. Bertoglio
Laboratoire de Mécanique des Fluides et d'Acoustique, UMR CNRS 5509 - Ecole Centrale de Lyon 69134 Ecully, France

(Received 7 December 2005; accepted 1 February 2006; published online 17 March 2006)

A new single-time two-point closure is proposed, in which the equation for the two-point correlation between the displacement of a fluid particle and the velocity allows one to estimate a Lagrangian timescale. This timescale is used to specify the nonlinear damping of triple correlations in the closure. A closed set of equations is obtained without ad hoc constants. Taking advantage of the analogy between particle displacements and scalar fluctuations in isotropic turbulence subjected to a mean scalar gradient, the model is numerically integrated. Results for the energy spectrum are in agreement with classical scaling predictions. An estimate for the Kolmogorov constant is obtained. © *2006 American Institute of Physics*. [DOI: 10.1063/1.2185683]

Two-point single-time closures are efficient and useful tools for studying homogeneous turbulence. Among existing single-time theories, the eddy damped quasi-normal Markovian theory (EDQNM), originally proposed by Orszag[1] (see also Leith[2]) for isotropic turbulence, has been used to investigate a broad range of fundamental problems in turbulence. Examples are: scalar decay in isotropic turbulence,[3,4] rotating turbulence,[5] stratified turbulence,[6] magnetohydrodynamics,[7] relative dispersion,[8] homogeneous shear,[9,10] isotropic turbulence with a mean scalar gradient,[11,12] decay of turbulence in a wall bounded domain,[13] compressible turbulence,[14] two-dimensional turbulence,[15] premixed flame propagation.[16] Without being exhaustive, this list illustrates the variety of problems that have been addressed using this single-time closure. EDQNM was also used to propose subgrid models for large-eddy simulation.[17,18] One common feature of all these works is that they rely on the original heuristic assumption of EDQNM: the presence of an eddy damping term. The eddy damping is an essential ingredient of the EDQNM closure, as it represents the nonlinear damping of the triple correlations, necessary to obtain inertial range spectra in agreement with classical Kolmogorov[19] theory. It should be pointed out that in the case of weakly nonlinear wave-turbulence, only the presence of the damping is mandatory.[5] A convenient specification of its form is of primary importance as soon as strong turbulence is considered. In the case of EDQNM, the eddy damping is specified by dimensional analysis and an ad hoc constant is introduced in the model. For other closures such as the test field model proposed by Kraichnan,[20] in which an auxiliary velocity field that does not respect the incompressibility constraint is introduced, the damping is deduced from a more sophisticated analysis, but an ad hoc constant still has to be introduced (of order unity in the case of the test field model).

More elaborate are the two-point two-time closures proposed by Kraichnan (DIA, for direct interaction approximation[21]), obtained by perturbation techniques applied to the Navier-Stokes equations. The Eulerian formulation of DIA, violating the principle of statistical Galilean invariance and therefore being incompatible with a $K^{-5/3}$ Kolmogorov inertial range, was reformulated in a Lagrangian framework. The Lagrangian history DIA (LHDIA),[22] its abridged versions,[22,23] as well as the version of Kaneda,[24] are known to yield predictions in agreement with Kolmogorov spectra without introducing any ad hoc constant. The price one has to pay is the complexity of the models that depend on the entire Lagrangian history of the flow, in contrast to the single-time theories.

It is known that the EDQNM equations for isotropic turbulence can be obtained from two-time theories by assuming an exponential decay of both the response function and the two-time correlations. The eddy damping then corresponds to the inverse of the correlation time of the turbulent velocity field. In the framework of a Lagrangian formulation of the theories, this correlation time has to be defined along fluid particle trajectories, and indeed, a definition corresponding to LHDIA for isotropic turbulence can be found in Kraichnan:[22]

$$\tau(K,t) = \int_0^t \frac{E(K,t|s)}{E(K,t)} ds \tag{1}$$

with $E(K,t)$ the energy spectrum and $E(K,t|s)$ the Lagrangian two-time energy spectrum (definitions are given below).

In the EDQNM model, this time is modeled as a function of $E(K,t)$ and K, yielding by dimensional analysis:

$$[\tau(K,t)]^{-1} = \eta(K,t) = \alpha\sqrt{K^3 E(K,t)}. \tag{2}$$

Another variant, nonlocal in wave-number space, is the expression proposed in Pouquet *et al.*:[15]

$$[\tau(K,t)]^{-1} = \eta(K,t) = \lambda \sqrt{\int_0^K S^2 E(S,t) dS}. \tag{3}$$

At high Reynolds number, both formulations lead to

$$\tau(K,t) \sim K^{-2/3} \tag{4}$$

in the inertial range of the spectra, mimicking the scaling that the Lagrangian correlation time scale is expected to follow in agreement with Kolmogorov theory. The constant α (or λ) is

[a]Author to whom correspondence should be addressed.

specified to obtain the desired value of the Kolmogorov constant.

The aim of the present letter is to derive a single-time closure that does not contain ad hoc specification of the damping term nor adjustable constant. The eddy damping timescale will be determined within the closure, the key element of the model being the use of Eq. (1).

The Lagrangian two-time spectral tensor is defined by

$$\Phi_{ij}(\boldsymbol{K},t|s) = FT_{\boldsymbol{x}-\boldsymbol{x}'}[\langle u_i(\boldsymbol{x},t)u_j^L(\boldsymbol{x}',t|s)\rangle] \quad (s \leqslant t), \tag{5}$$

in which $FT_{\boldsymbol{x}-\boldsymbol{x}'}$ denotes a Fourier transform with respect to $\boldsymbol{x}-\boldsymbol{x}'$. $u_j^L(\boldsymbol{x}',t|s)$ is defined as the velocity measured at time s within the fluid element that passes through the point $\boldsymbol{x}'$ at time t. In isotropic turbulence, the two-time energy spectrum $E(K,t|s)$ is related to this tensor by the relation

$$P_{ij}(\boldsymbol{K})\frac{E(K,t|s)}{4\pi K^2} = \Phi_{ij}(\boldsymbol{K},t|s) \tag{6}$$

with $P_{ij}(\boldsymbol{K})=(\delta_{ij}-K_iK_j/K^2)$. $E(K,t|s)$ is a key quantity as it appears in Eq. (1) giving the timescale that has to be specified in the closure. It is a two-time Lagrangian quantity and is therefore difficult to evaluate in the framework of a one-time closure. However, only the time integral of $E(K,t|s)$ is required to express $\tau(K,t)$. This integral satisfies

$$\frac{P_{ij}(\boldsymbol{K})}{4\pi K^2}\int_0^t E(K,t|s)ds = FT_{\boldsymbol{x}-\boldsymbol{x}'}\left[\left\langle u_i(\boldsymbol{x},t)\int_0^t u_j^L(\boldsymbol{x}',t|s)ds\right\rangle\right]. \tag{7}$$

The integral of the Lagrangian velocity along the trajectory in (7) is the displacement of a fluid particle. Calling a_j this displacement,

$$a_j(\boldsymbol{x},t) = X_j(\boldsymbol{x},t|t) - X_j(\boldsymbol{x},t|t=0) = \int_0^t u_j^L(\boldsymbol{x},t|s)ds \tag{8}$$

and

$$X_j(\boldsymbol{x},t|t) = x_j, \tag{9}$$

(7) can be written as

$$\frac{P_{ij}(\boldsymbol{K})}{4\pi K^2}\int_0^t E(K,t|s)ds = \mathcal{F}_{u_ia_j}(\boldsymbol{K},t), \tag{10}$$

with

$$\mathcal{F}_{u_ia_j}(\boldsymbol{K},t) = FT_{\boldsymbol{x}-\boldsymbol{x}'}[\langle u_i(\boldsymbol{x},t)a_j(\boldsymbol{x}',t)\rangle]. \tag{11}$$

In isotropic incompressible turbulence, this quantity can be expressed as (Lumley[25])

$$\mathcal{F}_{u_ia_j}(\boldsymbol{K},t) = \frac{P_{ij}(\boldsymbol{K})}{4\pi K^2}F_{ua}(K,t), \tag{12}$$

and therefore expression (1) can be recasted as a function of one-time Eulerian quantities only:

$$\tau(K,t) = \frac{F_{ua}(K,t)}{E(K,t)}. \tag{13}$$

This expression forms the basis of the single-time two-point closure proposed in this paper. In the following, a way to obtain an expression for $F_{ua}(K,t)$ will be proposed that together with the equation for $E(K,t)$ and relation (13) leads to a closed set of equations.

From the Navier-Stokes equations and the equation for the displacement of a fluid particle,

$$\frac{da_j(\boldsymbol{x},t)}{dt} = u_j(\boldsymbol{x},t), \tag{14}$$

a one-time two-point closure for $E(K,t)$ and $F_{ua}(K,t)$ in isotropic turbulence [and alternatively for $\Phi_{ij}(\boldsymbol{K},t)$ and $\mathcal{F}_{u_ia_j}(\boldsymbol{K},t)$ for anisotropic turbulence] can straightforwardly be written, by applying the quasi-normal approximation and Markovian assumption and expressing the relaxation time of the triple correlations using (13). In the present letter, instead of deriving the evolution equation for $F_{ua}(K,t)$, we adopt a simpler approach, taking advantage of the analogy existing between the fluid particle displacement and an advected nondiffusive scalar field. This analogy will permit us to express the closure model using only existing published equations. As pointed out by Batchelor,[26] a nondiffusive passive scalar in isotropic turbulence with a mean scalar gradient obeys the same equation as the displacement of a fluid particle. Considering an isotropic turbulence initially free from passive scalar fluctuations on which, at $t=0$, a mean scalar gradient is imposed in an arbitrary direction, $\partial\bar{\Theta}/\partial x_j$, the interaction of the velocity field with the scalar gradient produces a scalar fluctuation θ governed by

$$\frac{d\theta(\boldsymbol{x},t)}{dt} = -\frac{\partial\bar{\Theta}}{\partial x_j}u_j(\boldsymbol{x},t). \tag{15}$$

Integrating (15) over the Lagrangian trajectory of the fluid particle that arrives at time t at position $\boldsymbol{x}$ yields

$$\theta(\boldsymbol{x},t) = -\frac{\partial\bar{\Theta}}{\partial x_j}[X_j(\boldsymbol{x},t|t) - X_j(\boldsymbol{x},t|t=0)] = -\frac{\partial\bar{\Theta}}{\partial x_j}a_j(\boldsymbol{x},t) \tag{16}$$

and the correlation between $\theta(\boldsymbol{x}',t)$ and $u_i(\boldsymbol{x},t)$ can be expressed as

$$\langle u_i(\boldsymbol{x},t)\theta(\boldsymbol{x}',t)\rangle = -\frac{\partial\bar{\Theta}}{\partial x_j}\langle u_i(\boldsymbol{x},t)a_j(\boldsymbol{x}',t)\rangle. \tag{17}$$

For isotropic turbulence without loss of generality, the direction of the gradient can arbitrarily be specified; for example, x_3. Equation (17) then leads to

$$F_{u_3\theta}(K,t) = -\frac{\partial\bar{\Theta}}{\partial x_3}F_{u_3a_3}(K,t) \tag{18}$$

with $F_{u_3\theta}(K,t)$ defined as the scalar flux spectrum (see, for example, O'Gorman and Pullin[27]), or introducing $F_{ua}(K,t)$ as in Eq. (13):

$$F_{u_3\theta}(K,t) = -\frac{2}{3}\frac{\partial\bar{\Theta}}{\partial x_3}F_{ua}(K,t), \tag{19}$$

since isotropy implies that $F_{u_1a_1}=F_{u_2a_2}=F_{u_3a_3}=\frac{2}{3}F_{ua}$.

One can also arbitrarily specify the value of the gradient, since the scalar equation is linear. Choosing $\partial\bar{\Theta}/\partial x_3=-3/2$ simplifies the formulation. With this particular value of the gradient, Eq. (19) simply expresses the identity between the spectrum of the scalar flux of the nondiffusive scalar and the spectrum of the velocity-displacement correlation. Hence, it is straightforward to use the EDQNM model proposed by Herr *et al.*[11] or Bos *et al.*[12] for the scalar flux spectrum to calculate $F_{u_3\theta}(K,t)=F_{ua}(K,t)$ (in this work we use the formulation of Bos *et al.*). The equations for $E(K,t)$ and $F_{ua}(K,t)$ will be solved simultaneously to calculate the energy spectrum in isotropic turbulence and to evaluate the damping term using (18) that now takes the form

$$\eta(K,t) = [\tau(K,t)]^{-1} = \frac{E(K,t)}{F_{u_3\theta}(K,t)}. \tag{20}$$

The evolution equation for the energy spectrum is

$$\left[\frac{\partial}{\partial t} + 2\nu K^2\right]E(K,t) = T_{\mathrm{NL}}(K,t), \tag{21}$$

in which the expression for the nonlinear transfer T_{NL} is the classical single-time two-point closure expression (Orszag[1]):

$$T_{\mathrm{NL}}(K,t) = \int\int_{\Delta}\Theta(K,P,Q)(xy+z^3)[K^2PE(P,t)E(Q,t) - P^3E(Q,t)E(K,t)]\frac{dPdQ}{PQ}, \tag{22}$$

where Δ is a band in P,Q space so that the three wave vectors $\boldsymbol{K}$, $\boldsymbol{P}$, $\boldsymbol{Q}$ form a triangle. x,y,z are the respective cosines of the angles opposite to the sides K,P,Q of the triangle formed from $\boldsymbol{K},\boldsymbol{P},\boldsymbol{Q}$. The characteristic time $\Theta(K,P,Q)$ is defined as

$$\Theta(K,P,Q) = \frac{1-\exp(-\mu_{KPQ}\times t)}{\mu_{KPQ}} \tag{23}$$

with

$$\mu_{KPQ} = \nu(K^2+P^2+Q^2) + \eta(K,t) + \eta(P,t) + \eta(Q,t). \tag{24}$$

The difference with the EDQNM model[1] is that the eddy damping in the equations is no longer heuristically specified, but is calculated using relation (20).

The equation for $F_{u_3\theta}(K,t)$ is

$$\left[\frac{\partial}{\partial t} + \nu K^2\right]F_{u_3\theta}(K,t) = P(K,t) + T^{\mathrm{NL}}_{u_3\theta}(K,t) + \Pi(K,t), \tag{25}$$

which is the equation of Ref. 12 in the particular case of a nondiffusive scalar. In (25), $P(K,t)$ is a term that in this case can be interpreted as the production of scalar flux by the mean scalar gradient, such that $P(K,t)=-\frac{2}{3}(\partial\bar{\Theta}/\partial x_3)E(K,t)$ $=E(K,t)$. The expressions for the nonlinear terms $T^{\mathrm{NL}}_{u_3\theta}(K,t)$ and $\Pi(K,t)$ are not reproduced here [Eqs. (14) and (15) of Ref. 12]. These closed terms are exactly the same as in the case of the EDQNM model, except that the eddy damping is determined by Eq. (20). More specifically, in relation (16) of Ref. 12,

$$\mu^F_{KPQ} = \mu'(K) + \mu'(P) + \mu''(Q) + \nu(K^2+P^2), \tag{26}$$

μ' is replaced by η, and μ'' is still zero, as in Bos.[12]

The model is applied to the decay of isotropic turbulence by numerically integrating Eqs. (21) and (25). The energy spectrum is initialized by

$$E(K,0) = BK^4e^{-2K^2/K_L^2}, \tag{27}$$

with $K_0=1$, $K_L=10$, and B determined so that the initial kinetic energy is equal to 1. The energy spectrum was evaluated during the period of self-similar decay. Spectra are shown at $R_\lambda=150$, 500, and 1500. The results in Fig. 1 show that a $K^{-5/3}$ inertial range is obtained for the energy spectrum. The value of the Kolmogorov constant is estimated to be 1.73, as can be seen when the spectrum is shown in compensated form. It has to be reminded that in the case of the EDQNM closure this value is not a prediction of the model, but has to be specified by choosing the constant λ. The value of $C_K=1.73$ can be obtained with EDQNM by choosing the value $\lambda=0.49$ in expression (3). A detailed comparison between the EDQNM model and the present closure deserves further attention.

The results in Fig. 1 suggest that the present model yields a reasonable estimate of the Lagrangian timescale in

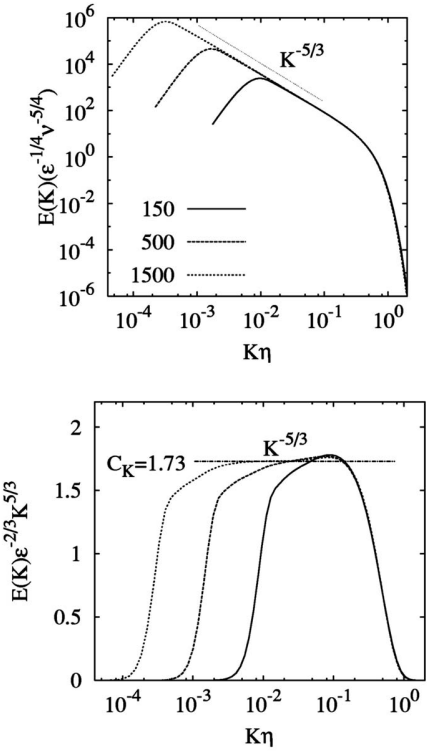

FIG. 1. Top: energy spectrum at $R_\lambda=150$, 500, and 1500; bottom: compensated form.

isotropic turbulence. It would be useful to compare the present results to estimations of the timescale provided by direct numerical simulation using the method proposed in Lee *et al.*[28] (see also Gotoh *et al.*[29]) or to higher Reynolds number data provided by large-eddy simulation.[30]

[1] S. A. Orszag, "Analytical theories of turbulence," J. Fluid Mech. **41**, 363 (1970).
[2] C. E. Leith, "Atmospheric predictability and two-dimensional turbulence," J. Atmos. Sci. **28**, 145 (1971).
[3] J.-M. Vignon and C. Cambon, "Thermal spectral calculation using eddy-damped quasi-normal Markovian theory," Phys. Fluids **23**, 1935 (1980).
[4] J. R. Herring, D. Schertzer, M. Lesieur, G. R. Newman, J. P. Chollet, and M. Larcheveque, "A comparative assessment of spectral closures as applied to passive scalar diffusion," J. Fluid Mech. **124**, 411 (1982).
[5] C. Cambon and L. Jacquin, "Spectral approach to non-isotropic turbulence subjected to rotation," J. Fluid Mech. **202**, 295 (1989).
[6] F. S. Godeferd and C. Cambon, "Detailed investigation of energy transfers in homogeneous stratified turbulence," Phys. Fluids **6**, 2084 (1994).
[7] A. Pouquet, U. Frisch, and J. Leorat, "Strong MHD helical turbulence and the nonlinear dynamo effect," J. Fluid Mech. **77**, 321 (1976).
[8] M. Larcheveque and M. Lesieur, "The application of eddy-damped Markovian closures to the problem of dispersion of particle pairs," J. Mec. **20**, 113 (1981).
[9] C. Cambon, D. Jeandel, and J. Mathieu, "Spectral modelling of homogeneous non-isotropic turbulence," J. Fluid Mech. **104**, 247 (1981).
[10] J. P. Bertoglio, "A model of three-dimensional transfer in non-isotropic homogeneous turbulence," in *Turbulent Shear Flows III* (Springer-Verlag, New York, 1981), p. 253
[11] S. Herr, L. P. Wang, and L. R. Collins, "EDQNM model of a passive scalar with a uniform mean gradient," Phys. Fluids **8**, 1588 (1996).
[12] W. J. T. Bos, H. Touil, and J.-P Bertoglio, "Reynolds number dependency of the scalar flux spectrum in isotropic turbulence with a uniform scalar gradient," Phys. Fluids **17**, 125108 (2005).
[13] H. Touil, L. Shao, and J. P. Bertoglio, "The decay of turbulence in a bounded domain," J. Turbul. **3**, 49 (2002).
[14] J. P. Bertoglio, F. Bataille, and J. D. Marion, "Two-point closures for weakly compressible turbulence," Phys. Fluids **13**, 290 (2001).
[15] A. Pouquet, M. Lesieur, J. C. André, and C. Basdevant, "Evolution of high Reynolds number two-dimensional turbulence," J. Fluid Mech. **72**, 305 (1975).
[16] M. Ulitsky and L. R. Collins, "Application of the eddy-damped quasi-normal Markovian spectral transport theory to premixed turbulent flame propagation," Phys. Fluids **9**, 3410 (1996).
[17] J. P. Chollet and M. Lesieur, "Parameterization for small scales of three-dimensional isotropic turbulence using spectral closures," J. Atmos. Sci. **38**, 2747 (1981).
[18] J.-P. Bertoglio, and J. Mathieu, "Modélisation stochastique des petites échelles de la turbulence: formulation gýnýrale," C. R. Acad. Sci., Ser. II: Mec., Phys., Chim., Sci. Terre Univers **12**, 751 (1984).
[19] A. N. Kolmogorov, "The local structure of turbulence in incompressible viscous fluid for very large Reynolds numbers," Dokl. Akad. Nauk SSSR **30**, 301 (1941).
[20] R. H. Kraichnan, "An almost-Markovian Galilean-invariant turbulence model," J. Fluid Mech. **47**, 513 (1971).
[21] R. H. Kraichnan, "The structure of isotropic turbulence at very high Reynolds numbers," J. Fluid Mech. **5**, 497 (1959).
[22] R. H. Kraichnan, "Lagrangian-history closure approximation for turbulence," Phys. Fluids **8**, 575 (1965).
[23] R. H. Kraichnan and J. R. Herring, "A strain-based Lagrangian-history turbulence theory," J. Fluid Mech. **88**, 355 (1978).
[24] Y. Kaneda, "Renormalized expansions in the theory of turbulence with the use of the Lagrangian position function," J. Fluid Mech. **107**, 131 (1981).
[25] J. L. Lumley, "The spectrum of nearly inertial turbulence in a stably stratified fluid," J. Atmos. Sci. **21**, 99 (1964).
[26] G. K. Batchelor, "Diffusion in a field of homogeneous turbulence. I. Eulerian analysis," Aust. J. Sci. Res., Ser. A **2**, 437 (1949).
[27] P. A. O'Gorman, and D. I. Pullin, "The velocity-scalar cross correlation of stretched spiral vortices," Phys. Fluids **15**, 280 (2003).
[28] C. H. Lee, K. Squires, J.-P. Bertoglio, and J. Ferziger, "Study of Lagrangian characteristic times using direct numerical simulation of turbulence," in *Turbulent Shear Flows VI* (Springer-Verlag, Toulouse, 1987), p. 58
[29] T. Gotoh, R. S. Rogallo, J. R. Herring, and R. H. Kraichnan, "Lagrangian velocity correlations in homogeneous isotropic turbulence," Phys. Fluids A **5**, 2846 (1993).
[30] Guo-Wei He, R. Rubinstein, and Lian-Ping Wang, "Effects of subgrid-scale modeling on time correlations in large eddy simulation," Phys. Fluids **14**, 2186 (2002).

2.8 Perspectives

An a posteriori consistency check of the weak dependence hypothesis

As discussed in section 2.2, the direct interaction approximation is based on the assumption that the influence of an individual triad interaction on a turbulent flow is small compared to the sum of all other interactions. The velocity is thus decomposed into a part in which $y_k^{(0)}$ is independent of modes $y_p,\ y_q$ plus the direct interaction part $y_k^{(1)}$, which is the part of the velocity which directly interacts with modes $y_p,\ y_q$.

This assumption, called weak dependence, seems plausible in the limit of a true homogeneous flow, *i.e.* , a domain with an infinite size. In this case the mode density tends to infinity and the influence of one triad interaction, most probably, tends to zero. Tests of this assumption were carried out by Goto and Kida [45, 46] for well chosen model systems. Their tests focused on the response function and transfer function obtained by applying DIA (or what they called SDIP) to a system for which the exact solution was known.

An alternative approach would be to compute directly the smallness of the single triad velocity compared to the full velocity. This would consist in checking that $|y_k^{(0)}| \gg |y_k^{(1)}|$, or alternatively,

$$\frac{\overline{y_k y_k'}^{(1)}}{\overline{y_k y_k'}^{(0)}} \ll 1, \tag{2.65}$$

with

$$\overline{y_k y_k'}^{(1)} = \int_0^t ds \int_0^t ds' G(t,s) G(t,s') A_{ijk} A_{ijk} y_j' y_k' y_j' y_k'. \tag{2.66}$$

In a discrete Fourier series, the mode density of a Fourier-series is a function of kL, with k the wavenumber and L the box-size. At a fixed k, the mode-density will therefore increase when the box-size is increased. In the dissipation range, the number of active modes decreases rapidly and at very large k the number of excited modes becomes negligible. At fixed L, the mode density will thus decrease as a function of k. The two limits, $k \to \infty$ and $L \to \infty$ are perhaps not exchangeable, so that the weak-dependence assumption might be not valid in the dissipation range. In closure this could be checked *a posteriori*. If the closure gives results invalidating the weak-dependence hypothesis, it gives a hint about the limits of closure theories of the DIA family.

One example where weak dependence seems to break down was discussed in section 2.2. This is the condensation of energy in the largest wavelength in two-dimensional turbulence. Another case where DIA seems to fail is in the prediction of the dissipation rate fluctuations. This small scale intermittency [65] can be explained since in the far dissipation range, *i.e.* at very small scales, the flow becomes relatively smooth and only very sparse energetic fluctuations determine the energy spectrum. The sparseness of the energy fluctuations can be characterized using the flatness of the velocity fluctuations at a certain scale. We investigated the scale-dependent flatness using wavelet-based tools (see Figure 2.6) in both isotropic and anisotropic turbulence. It was observed that this sparseness becomes even stronger in anisotropic turbulence. It is possible that

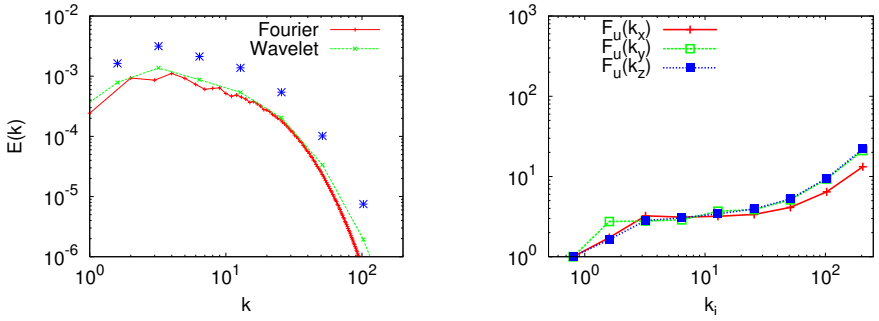

Figure 2.6: Left: The energy spectrum measures the (variance of the) fluctuations of the kinetic energy as a function of scale. The blue stars indicate the standard deviation of the fluctuations of the energy spectrum. These are thus the fluctuations of the variance, related to fourth order velocity statistics. Right: The scale-dependent flatness measures the fluctuations of the fluctuations of kinetic energy at a given scale. The increase of the flatness at the small scales indicates the strong (relative) fluctuations of the energy spectrum in the dissipation range. The analysis was performed on a database of isotropic and anisotropic turbulent flows [63]. Here we show the results for the isotropic flow. More details are given in reference [64].

this sparseness of energetic regions in the very small scales of turbulence might well violate the weak dependence assumption.

Change of representatives

The Abridged Lagrangian History DIA predicts a Kolmogorov constant of the order 1.7. This is the correct order of magnitude but perhaps slightly above the value obtained in experiment and DNS. The value of the Corrsin-Obukhov constant, which is the equivalent of the Kolmogorov constant for the convective-inertial range in three-dimensional passive scalar turbulence, is underestimated by a factor of order two. This underestimation can be traced back to an overestimation of the coherence of the scalar along particle trajectories. A change of representatives might lead to a better prediction of this quantity. In the original case, DIA is applied to the velocity fluctuations, but why not consider other quantities such as the strain or vorticity. Kraichnan and Herring (see also Gotoh and Kaneda) [66, 67, 68] derived the equations for the abridged Lagrangian-history DIA, applied to the strain rate. This improved the predictions for both the Kolmogorov and Corrsin-Obukhov constant. As suggested in section 1.3, it is more natural to consider the scalar gradient. Otherwise the Lagrangian Péclet number will be of order zero. The extension of the LMFA closure (section 2.7) to describe the advection of a scalar gradient seems an interesting perspective.

Theory beyond DIA

In Kraichnan's 1989 paper on non-Gaussian statistics [69], in which DIA was applied to higher order statistics, it became clear that DIA did not correctly predict dissipation rate fluctuations and pressure fluctuations. This inspired him to propose other theoretical approaches to model the fine statistics of turbulence. One of these is the mapping closure [70, 71] another one the constrained decimation scheme [72]. The first one was not completely successful in describing turbulence, but was useful to study mixing. The constrained decimation scheme might be a good approach, but it has not been studied significantly [73]. We will not discuss these approaches here any further but these might be interesting directions for further research.

Chapter 3

Studies on the dynamics of isotropic turbulence

3.1 Gaussianity, statistical mechanics and relaxation to thermal equilibrium

A Gaussian field does not contain structures. It represents a state of pure randomness in which all the modes which constitute the field are statistically independent. If one therefore wants to measure the coherence of a field, which is one of the aims of the present chapter, a logical thing is to compare with a Gaussian field. We will first digress a little from the actual problem of turbulence and discuss some features of a Gaussian field. Subsequently we will describe how turbulence develops from a Gaussian initial state.

We consider the Fourier transform of a three-dimensional field, which in the following will represent the velocity field or the scalar fluctuation field. Let us in this section concentrate on the velocity field. Instead of the coordinate $\boldsymbol{x}$, we now have the wavevector $\boldsymbol{k}$ that indicates the position of a vector or scalar. The Fourier-transformed quantities are complex. Each component of the vector is therefore determined by its norm and its phase (or equivalently by its real and imaginary parts). The important property of a Gaussian field is that this phase is a random variable. This translates the fact that there are no structures. A well localized object in physical space can in the Fourier decomposition be written as the sum of an infinite number of sine functions. To reconstruct the object in physical space it is important to have the correct phases, otherwise the sum of the sine-functions will not describe the object. Therefore, by randomizing the phases all knowledge about the shape and location of the object is lost.

It is possible to construct random Gaussian fields with different variance distributions with respect to the lengthscale. In the case of white noise the variance of the velocity fluctuations of a particular mode is independent of its wavelength. But since in three dimensions the number of modes with a given length is proportional to k^2 (see equation (1.8)), the cumulative energy of all modes with the same length will lead to an energy spectrum proportional to k^2. In Figure 3.1 we sketch the energy distribution of a three-dimensional field consisting of Gaussian white noise, compared to a typical energy distribution of a

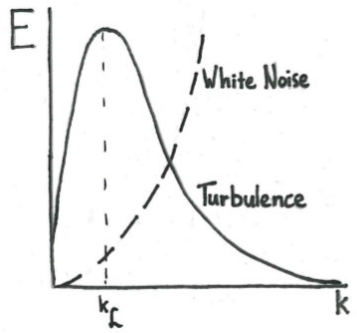

Figure 3.1: White noise is characterized by a statistical equipartition of energy over all modes. For a three-dimensional vector-field, this yields an energy-spectrum proportional to the wavenumber squared, since the energy-spectrum is defined as the integral over a spherical surface of radius k of the three-dimensional energy distribution in Fourier-space. A typical developed turbulent flow has a different distribution, with a peak around the integral scale-wavenumber and a rapid fall-off at large wavenumbers.

turbulent flow. Modes in thermal equilibrium will have such a white noise energy distribution. One can argue that this type of distribution is irrelevant for the description of turbulence, in which the energy is generally dominant in the large scales so that the distribution is far from thermal equilibrium. It can however be shown that the Euler equations will relax to a state displaying such a behavior if a Galerkin trunctation is applied to the system [74], and the nonlinearity of the Euler equations is identical to the nonlinearity of the Navier-Stokes equations.[1] Scrutinizing the behavior of the Euler equations might therefore, perhaps, help to understand the nonlinear behavior of the Navier-Stokes equations.

In order to study the non-Gaussianity induced by the nonlinear term in the Navier-Stokes or Euler equations, one can perform the following (numerical) experiment: we start with an initial Gaussian energy distribution confined to the large scales, *i.e.*, the small wavenumbers, of a Galerkin truncated set of modes. This system is not in thermal equilibrium since the energy is not equally distributed over the different wavemodes. However, a Gaussian vector field will, on average, not transfer energy to modes of another wavenumber shell. This can easily be seen by the fact that the mean transfer between modes is directly related to the skewness of the distribution, or rather the skewness of its gradients, and this skewness is on average zero in a Gaussian field. Some non-Gaussianity needs to be developed from the initial Gaussian state to relax to equilibrium, since the initial conditions are not in statistical equilibrium. This

[1] Formally, a Galerkin truncation is the application of a linear, low-pass filtering operator on the velocity field and its evolution equation, which sets all Fourier harmonics with $k > k_f$ to zero. A Galerkin truncation thus simply means that we consider a fixed range of wavemodes, limited by a cut-off wavenumber k_f and modes with $k \leq k_f$ do not interact with modes $k > k_f$ (and a similar cut-off is considered at the infrared end of the spectrum). All pseudo-spectral direct numerical simulations use a Galerkin truncation since the available computer power is not infinite. A turbulent flow is then discretized on a finite number of modes and the parameters are chosen such that the energy at the largest available wavenumbers is sufficiently small such that the truncation does not influence the scales of interest.

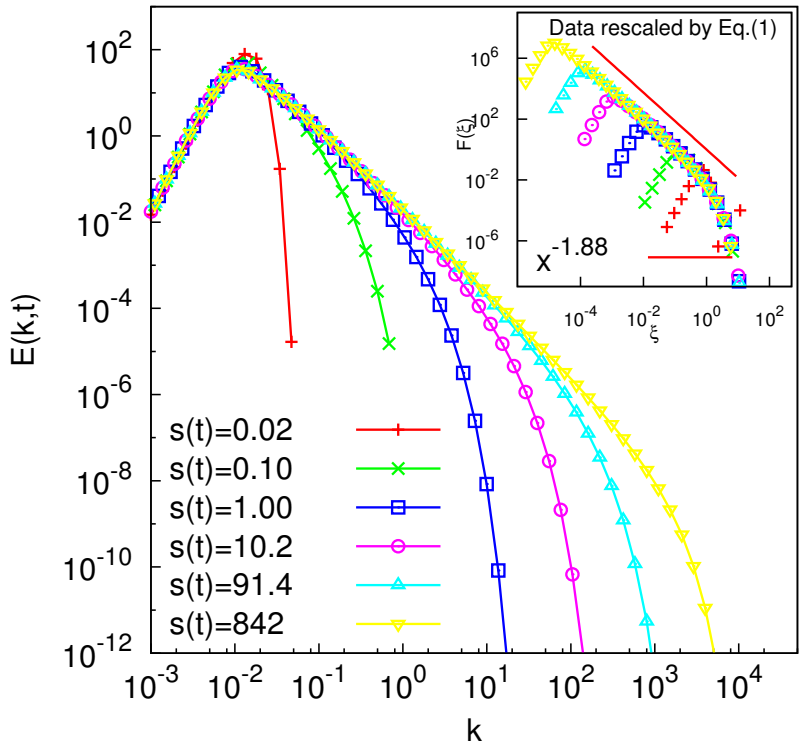

Figure 3.2: The development of the nonlinear cascade of energy governed by the Euler or Navier-Stokes equations displays a scaling which is not the same as proposed by Kolmogorov for constant flux cascades. The steeper slope, with a power-law exponent of order 1.89, has not yet been described by a simple dimensional analysis [3].

non-Gaussianity needs to be due to the quadratic term in the Euler-equations, since the pressure term only ensures incompressibility and will be zero if the nonlinear term is zero (at least in isotropic flow in a periodic domain this is the case). The way in which this system will relax to this equilibrium-state is perhaps one of the cleanest situations to study the non-Gaussianity of turbulence, since no non-Gaussian forcing or initial condition is imposed, so that all non-Gaussian features stem directly from the nonlinear dynamics of the Euler equations. The end-state, which is the thermal equilibrium state, is Gaussian again. The ensemble of Fourier-modes will thus only transiently be non-Gaussian. This non-Gaussian transient, in which energy is transferred from an initial Gaussian state with non-equipartitioned energy to a thermal equilibrium follows a two-stage procedure, which will now be described.

Self-similarity of the second kind. In the initial stage the scales will pass their energy to smaller and smaller scales in a completely inertial way, mean-

ing that no viscous damping is experienced by the modes. This stage should be identical for both Navier-Stokes dynamics at very high Reynolds number and Euler-dynamics, since the viscous term is neglibible if the initially excited modes are confined to a sufficiently small wavenumber range[2]. It was recently shown for MHD turbulence in the weak wave turbulence limit [76] that in this stage the energy distribution displays a power-law behaviour with an exponent which is not simply deducable from dimensional analysis. We showed that the same behavior was observed in closures for the Navier-Stokes equations with a powerlaw scaling of the energy spectrum with an exponent between $-5/3$ and -2. In Figure 3.2 (from [3]) we illustrate this behavior in an EDQNM computation. We note here that in this particular simulation not the Euler equations are considered but the Navier-Stokes equations at very high Reynolds number. As stated before, it is expected that during the initial stage this difference will not be important for the dynamics. Currently, no dimensional analysis is known to predict or explain the value of the power-law exponent, like the one proposed by Kolmogorov for the inertial range energy spectrum of a high-Reynolds number turbulent flow. Its value is numerically close to the fraction $-17/9 \approx -1.89$, but it is for the moment not even clear if a dimensional analysis predicting this exponent and corresponding to the physical mechanism should exist. It could be a typical example of self-similarity of the second kind [77].

If the system were not truncated, the cascade would continue indefinitely to small scales. The typical timescale of the smaller scales that are created is increasingly small so that, if the cascade would proceed in a self-similar way, an infinite wavenumber would be reached in a finite time. This singular behavior, the finite time singularity, is related to the blow-up of the Euler equations, and is still an issue of debate, and the question whether this blow-up exists in high-Reynolds number turbulence is far from settled. Numerical simulations have to deal with enormous amounts of computational power, combined with efficient mesh-refinement schemes in the hope to capture fine enough scales in which the singular behavior will take place or, on the contrary, where the cascade will be arrested. A mechanism which arrests the cascade, should necessarily suppress the nonlinearity of the Euler equations (at least locally in physical space). Only if the nonlinearity is suppressed sufficiently the Euler equations can be saved from blow-up. The suppression of nonlinearity will be the subject of section 3.4. In the present section we consider a Galerkin truncated system so that the smallest scale is limited by the largest wavenumber of the Fourier domain and the question of blow-up is not directly relevant.

Truncated Euler and effective viscosity. In the second stage of the evolution, the smallest scales of the system have received energy and the energy piles up at these modes, filling up a *reservoir* of thermalized modes, displaying a k^2 spectrum. At this point the modes transferring energy will experience a damping. Indeed, the thermalized modes will act, through non-local interaction, as an effective viscosity on the active modes and the latter will behave as in a constant flux energy cascade, obeying approximately the Kolmogorov 1941 inertial range phenomenology. This transient behavior is illustrated in Figure 3.3. We

[2] An interesting study on this subject is reported in reference [75], where is evaluated, for 2D magnetohydrodynamic turbulence, until what time the evolution of the viscous and the ideal equations yield the same results.

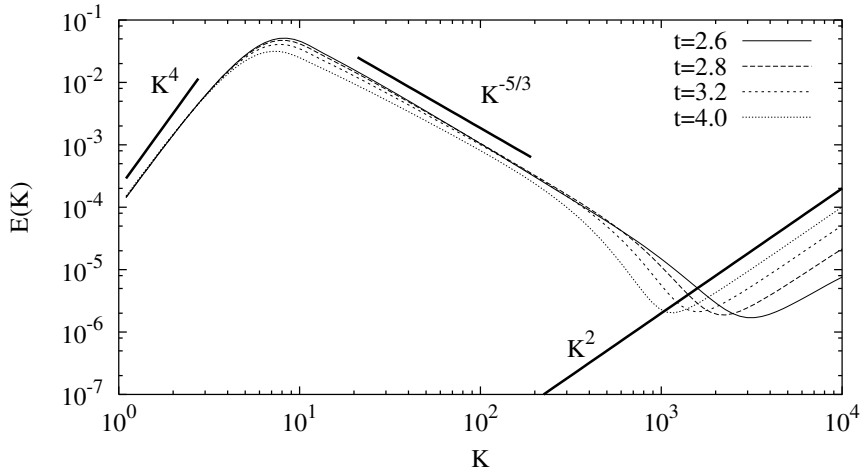

Figure 3.3: When the truncated Euler equations are solved starting from an initial condition in which the energy is confined to the large scales, the dynamics will tend to relax the system to a state in thermal equilibrium. In this final state the energy spectrum is proportional to k^2. During the transient a Kolmogorov inertial range can coexist with modes in thermal equilibrium at the smallest wave-lengths. These thermalized modes act as an effective viscosity on the modes out of equilibrium [2].

note that this behavior was predicted by Kraichnan in 1975 [78]. A numerical study was carried out and reported in reference [79]. In a first version of this manuscript, the authors proposed two different estimates for the local minimum of the energy-spectrum between the inertial range and the thermalized range. In reference [2] we showed which estimate adequately describes this minimum.

Bottlenecks, hyperviscosity and hypofriction. The final state of the truncated system will consist of statistically stationary Fourier modes, displaying an energy spectrum proportional to k^2. The transient nonlinear and non-Gaussian phase shares the essential feature of nonlinear mode-coupling with real Navier-Stokes turbulence. Another, indirect, link between the thermalization observed in the truncated Euler equations and Navier-Stokes turbulence was proposed by Uriel Frisch and coworkers [80]. They started from the observation that if the Laplacian in the viscous term of the Navier-Stokes equations was replaced by a power of the Laplacian (as is usual in hyper-viscous approaches[3]), the dynamics of the system will tend asymptotically to the truncated dynamics if the power of the Laplacian tends to infinity. For a power unity, *i.e.* the normal viscous operator, the dynamics will already very slightly mimic the thermalization at large scales, and a small pile up of energy will be observed in the dissipation range. This interpretation of the so-called bottleneck effect as an incomplete thermalization links the dynamics of the Navier-Stokes equations to the truncated Euler equation. We showed that the same game can be played in

[3]Hyperviscosity [81] is generally used to concentrate the influence of the viscous dissipation to a small range of wavenumbers, in order to enlarge the inertial range, which is defined as the range in which viscosity and forcing are negligible.

two-dimensional turbulence, in which a pile-up of energy at large scales can be expected if one uses a hypo-friction [4]. This friction consists of adding a term to the RHS of the Navier-Stokes equations,

$$\left(\partial_t + \nu k^2\right) u_i(\boldsymbol{k}) = -\frac{i}{2} P_{ijm}(\boldsymbol{k}) \iint u_j(\boldsymbol{p}) u_m(\boldsymbol{q}) \delta(\boldsymbol{k}-\boldsymbol{p}-\boldsymbol{q}) d\boldsymbol{p} d\boldsymbol{q} - k^{-2\alpha} u_i(\boldsymbol{k}). \tag{3.1}$$

The parameter α determines the locality of this friction in wavenumber space. The value $\alpha = 0$ corresponds to linear Ekman friction. High values lead to bottlenecks at the large scales of the flow due to a mechanism similar to the one discovered by Frisch and coworkers. Results are illustrated in Figure 3.4).

3.2 Third-order moments and inertial range energy flux

We still did not answer the question how non-Gaussian the transient from Gaussian initial conditions to a final, thermalized state is. To characterize non-Gaussianity, one can compare statistics of a flow to those obtained from a Gaussian field. We will consider two quantities, the skewness, which is related to triple velocity correlations and the mean-square nonlinearity, a quantity which contains quadruple velocity correlations. In a Gaussian field all odd moments of the field-variable are zero. Hereby it can be shown that no net energy transfer can take place, since this is related to the third-order moment of the velocity field. Therefore the energy transfer in a turbulent flow is a direct measure of the non-Gaussianity. In the present section we will discuss the energy transfer in more detail, in particular focusing on its scale dependence in physical space, its symmetry and on the difference between the energy flux and the viscous dissipation rate.

Reversibility of the nonlinear interaction. The nonlinear terms of the Euler equations and the Navier-Stokes equations are identical. If the Reynolds number of a flow is very large, the large scales are negligibly influenced by the viscosity and should thus obey the same symmetries as the Euler equations. The Euler equations are invariant under the simultaneous change $t \to -t$ and $\boldsymbol{u} \to -\boldsymbol{u}$. This implies that if in an Euler flow we change the sign of the velocity at every point of space, the flow will evolve backwards to its initial condition. This symmetry is not retained by the Navier-Stokes equations in the dissipation range since the viscous term does not share the same symmetry. But for scales approximately free from dissipative effects this should hold and this property is discussed in Figure 3.5. In the development of Large Eddy Simulation techniques, this property is often used to defend or attack subgrid-models. In our recent investigation [5] we argue that the use of this criterion in the judgment of subgrid-models is incompatible with the fundamental idea behind Large Eddy Simulation. Indeed, if we want to model the small scales, assumptions are needed, and these assumptions determine the reversibility (or irreversibility) of the subgrid dynamics.

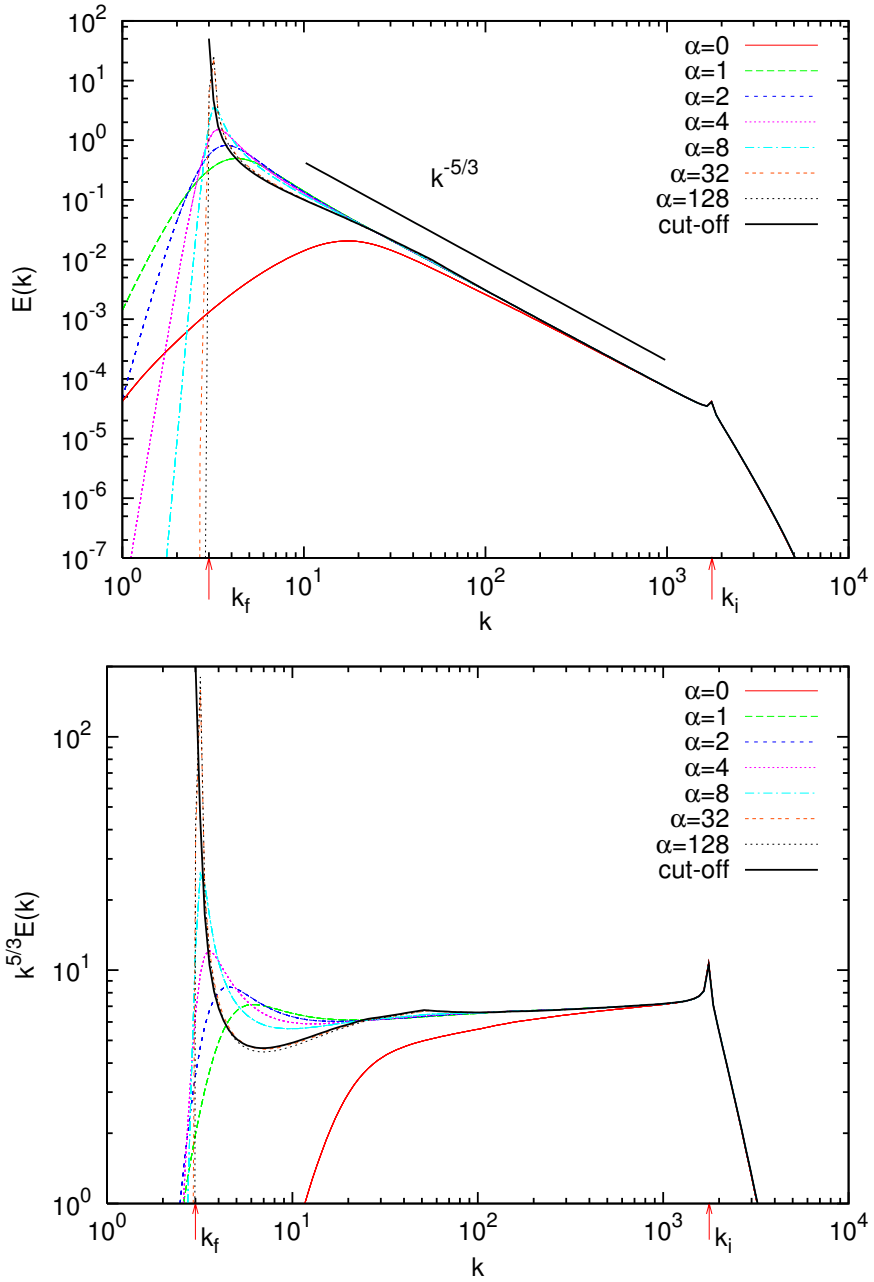

Figure 3.4: The existence of a large-scale bottleneck in 2D turbulence is directly related to the process of energy condensation, the pile up of energy at wavenumbers corresponding to the domain size. In two-dimensional turbulence a friction is often used to either model a physical process, or to simply avoid the pile up of energy at the large scales. The parameter α corresponds to the order of the friction term in equation (3.1). The careless use of hypo-friction ($\alpha > 0$) might reduce the inertial range of the energy spectrum through the appearance of bottlenecks due to the friction term [4].

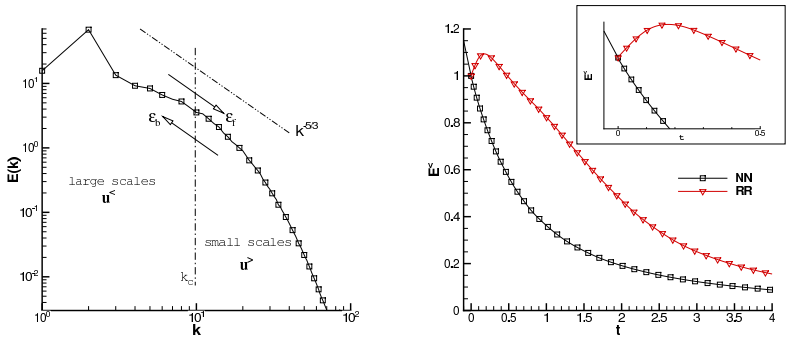

Figure 3.5: The Euler-equations are time-reversible. The Navier-stokes equations are not. At high Reynolds numbers the influence of the viscosity is small on the large-scales. The dynamics of these scales should thus be approximately time-reversible. On the left we show an arbitrary division of the flow-scales into large and small scales. On the right we show the evolution of the energy contained in the large scales. At $t = 0$ the velocity is reversed, $\boldsymbol{u} \rightarrow -\boldsymbol{u}$, and it is observed that for this case (called RR; NN is the unmodified flow) at short times the energy flows back to the large-scales as would be expected in the case of Euler-dynamics. At longer times the energy flow reverses a second time and is directed towards the small scales. The details of this study can be found in reference [5].

Third order structure functions. The nonlinear transfer can be related to the third-order structure function in physical space[4]. Both wavenumber spectra and structure functions measure scale distributions of moments of the velocity field. An exact correspondence between the two types of quantities exists. Well known examples of the relations between second- and third-order structure functions on the one hand and energy and transfer spectra on the other can be found in reference [7]. Even though the relations exist, the transformations are not always bijective. For example, if an energy distribution in wavenumber-space is steeper than k^{-3}, the corresponding second order structure function will become insensitive to the exponent and will show a scale-distribution following a power-law proportional to r^2, corresponding to a perfectly smooth velocity distribution. With respect to this aspect, wavenumber spectra (or wavelets with a sufficiently number of vanishing moments) are more sensitive tools, since they can probe the wavenumber distribution of these steep energy distributions.

When it comes to higher order statistics, δu_n for $n > 2$, most investiga-

[4]The longitudinal structure function of order n, is defined by

$$\delta u_n = \overline{[(\boldsymbol{u}(\boldsymbol{x}) - \boldsymbol{u}(\boldsymbol{x}+\boldsymbol{r})) \cdot (\boldsymbol{r}/r)]^n}. \tag{3.2}$$

The relation to the energy transfer is

$$D_{LLL}(r) = r \int_0^\infty T(k) g(kr) dk, \tag{3.3}$$

with

$$g(x) = 12 \frac{3(\sin x - x \cos x) - x^2 \sin x}{x^5}. \tag{3.4}$$

The complete derivation of this expression is given in reference [7].

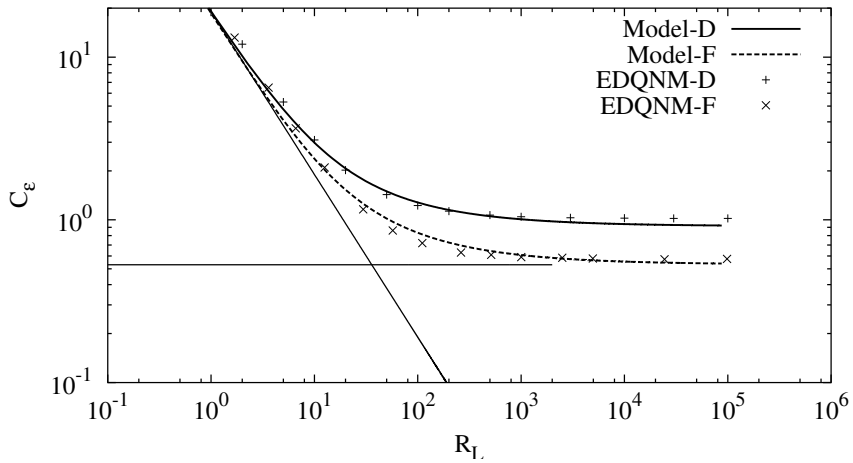

Figure 3.6: The normalized dissipation rate is defined as $C_\epsilon = \epsilon\mathcal{L}/\mathcal{U}^3$ in which ϵ is the viscous dissipation rate and $\mathcal{L}$ and $\mathcal{U}$ correspond to the integral length and velocity scales, respectively. $\mathcal{U}^3/\mathcal{L}$ corresponds roughly to the rate at which the large scales loose their energy through nonlinear interaction. This energy will cascade to the small scales and will there be dissipated. In a steady state the energy flux and dissipation are statistically identical at high enough Reynolds number (at low Reynolds numbers the energy-flux is smaller since the large scales are directly dissipated by viscous dissipation). In unsteady turbulence, the cascade-time, or time it takes for the energy to reach the smallest scales, introduces an imbalance which is characterized by a variation of C_ϵ. In the figure this is illustrated by comparing stationary, forced turbulence (indicated by **F**) with a canonical case of unsteady turbulence: freely decaying turbulence (indicated by **D**). The curves correspond to a simplified model prediction of the Reynolds number behaviour based on this idea of a cascade time. From [6].

tions have focused on structure functions rather than wavenumber spectra, in particular to measure the deviations from Kolmogorov's 1941 proposition for inertial range scaling. This issue, addressing so-called anomalous scaling, has received a disproportionate amount of attention[5]. The original work suggesting a possible correction to Kolmogorov's prediction for the energy spectrum (or structure function), was due to Kolmogorov himself [82] and presented at a famous conference in Marseille 50 years ago. Kolmogorov's self-criticism was motivated by the observation that scale-dependent fluctuations of the energy dissipation rate introduce an additional possible parameter in the dynamics of the inertial range, so that the scale dependence of the energy spectrum cannot be determined by dimensional analysis only, as was the case for the 1941 theory. These scale dependent fluctuations of the dissipation rate were indeed observed. As correctly pointed out by Kraichnan [83], however, the relevant quantity determining the inertial range is not the energy dissipation, but the energy flux through scales. Even though these quantities have the same mean value in a statistically stationary state, they are not necessarily the same, since they reflect different physical mechanisms. The energy flux represents the nonlinear interaction between modes, whereas the energy dissipation corresponds to the diffusion of momentum fluctuations through the action of viscous stresses. Note that for the same reason the normalized dissipation rate $epsilon\mathcal{L}/\mathcal{U}^3$, a quantity which in numerous engineering turbulence models is taken to be constant, is a function of the type of flow considered (see the discussion in the caption of Figure 3.6).

From first principles, *i.e.*, starting from the Navier-Stokes equations, it has not been possible yet to prove or disprove the existence of anomalous scaling. In favour of the partisans of anomalous scaling we can mention that it is possible to show deviations from normal, dimensional scaling, for structure functions of a passive scalar advected by a model velocity field [36]. Similarly, anomalous scaling can be shown to exist for the Burgers' equation. Both examples differ from the Navier-Stokes equation by the absence of a pressure term. Experiments seem to indicate anomalous scaling [84]. However, it is not evident to disentangle anomalous effects from effects which reduce the extent of the inertial range, such as the finiteness of the Reynolds number and the energy input in the large scales by some forcing mechanism. This issue is addressed in [7], in which it is shown that for Reynolds numbers currently available in simulations and experiments the deviations from Kolmogorov scaling as described by formalisms describing anomalous scaling are of the same order of magnitude as finite Reynolds number effects for second order structure functions (Figure 3.7).

3.3 Periodically forced turbulence

In many engineering applications, controlling the turbulent motions of a fluid flow is a major issue. Control can be either passive or active. In both cases a turbulent flow is perturbed in such a way that the turbulence is either damped

[5]Perhaps this tremendous amount of attention for anomalous scaling was due to the fact that in between 1941 and 1961 the $k^{-5/3}$ scaling of the energy spectrum was one of the only robust universal features of high Reynolds number turbulence. Its questioning (however small the correction is) removed one of the only solid corner-stones from the description of turbulent flows.

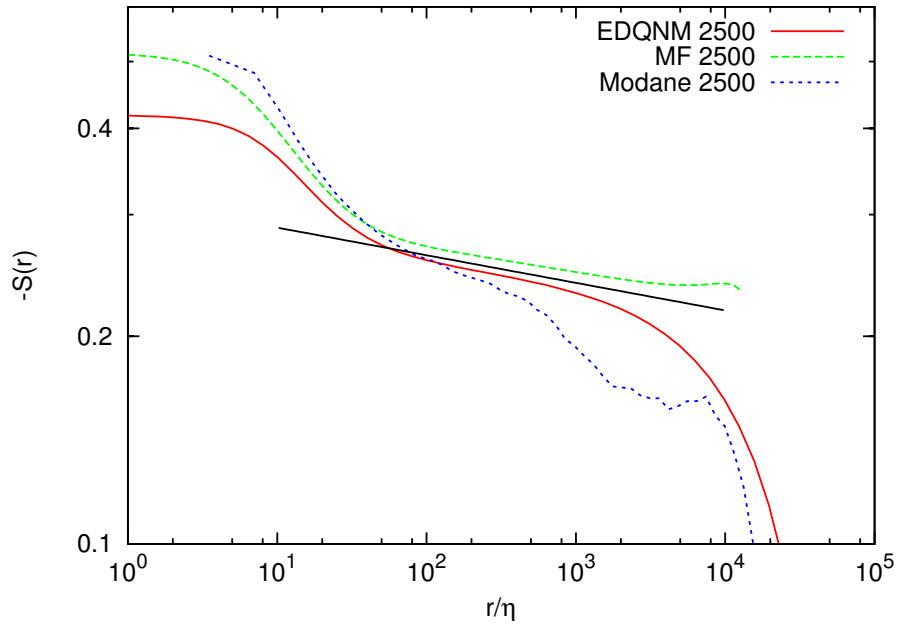

Figure 3.7: In the framework of Kolmogorov's 1941 theory, the skewness of the velocity increments should display a scale-independent plateau at very high Reynolds numbers. In his 1962 theory this was not any longer the case and a power-law was predicted with a small power-law coefficient. Formalisms such as multifractality were applied to hydrodynamic turbulence to describe these effects, which are absent in two-point closure theories. However, at least at the level of the velocity increment skewness, this power-law coefficient is of the same order of magnitude as finite Reynolds number corrections for Reynolds numbers up to roughly 10^4. This is a very high value which has not yet been obtained in controlled experiments. In the figure results of an EDQNM simulation, the multifractal formalism and a wind-tunnel experience for the velocity increment skewness are compared at a Taylor-scale Reynolds number of 2500. From [7].

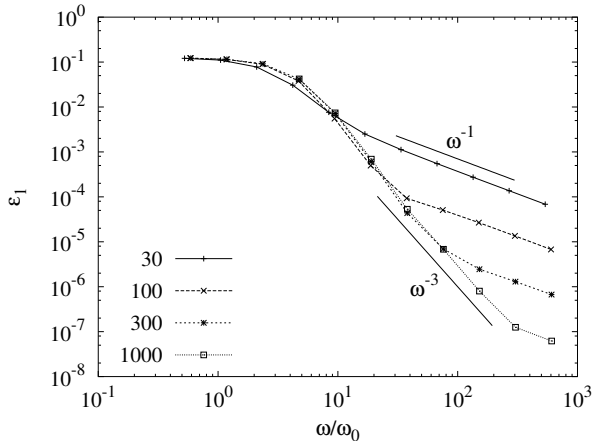

Figure 3.8: In reference [8] we characterized the filter properties of the turbulent energy cascade. The energy cascade acts as a low-pass filter with a characteristic frequency dependence proportional to ω^{-3}, with ω the frequency. The periodic part of the dissipation ϵ_1 is denoted by $\tilde{\epsilon}$ in the text.

or enhanced. At which lengthscale and with which frequency can we control the turbulent flow in the most efficient way? We carried out an analytical study, completed by two-point closure simulations to determine the response of a turbulent flow to a periodic forcing.

Isotropic turbulence is considered, forced by a forcing P in a narrow band of wavenumbers. The kinetic energy budget can be written as

$$\dot{\kappa} = P - \epsilon. \tag{3.5}$$

The forcing consists of a steady part plus a small periodic sinusoidal contribution. The smallness of the periodic part allowed to consider the response of the flow on the perturbation in a linear manner, which implies that both the kinetic energy κ and dissipation ϵ can be decomposed in a steady part plus a sinusoidal contribution,

$$\begin{aligned} P(t) &= \bar{P} + \tilde{P}\cos(\omega t) && (3.6)\\ \kappa(t) &= \bar{\kappa} + \tilde{\kappa}\cos(\omega t + \phi_\kappa) && (3.7)\\ \epsilon(t) &= \bar{\epsilon} + \tilde{\epsilon}\cos(\omega t + \phi_\epsilon). && (3.8) \end{aligned}$$

The whole problem is now to determine the amplitudes $\tilde{\kappa}$, $\tilde{\epsilon}$, the phase-shifts ϕ_κ and ϕ_ϵ as a function of the forcing frequency. It is straightforward to show that the steady part of the flow obeys $\bar{P} = \bar{\epsilon}$, which gives for the fluctuations,

$$-\omega\tilde{\kappa}\sin(\omega t + \phi_\kappa) = \tilde{P}\cos(\omega t) + \tilde{\epsilon}\cos(\omega t + \phi_\epsilon). \tag{3.9}$$

From this relation the limits $\omega \to 0$ and $\omega \to \infty$ can be determined. In the very slow, quasi-static limit, the left hand side of the last expression vanishes and $\tilde{P} \approx \tilde{\epsilon}$. For very high frequencies the turbulence has no time to respond and only the forcing scale is perturbed. In this case, the perturbed dissipation is very small, at high enough Reynolds number, and the perturbed kinetic energy will be

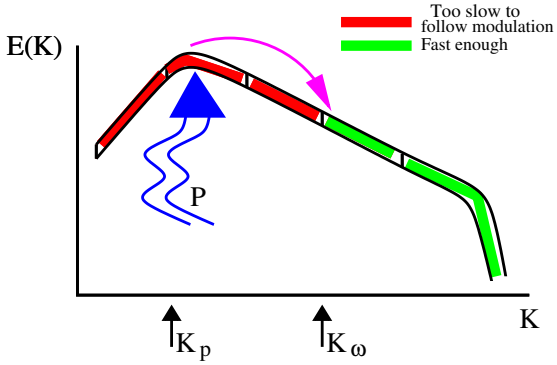

Figure 3.9: A periodic forcing can only influence scales with an intrinsic frequency that is larger than or of the same order as the forcing frequency. This can be seen as the locality of interaction principle in the frequency domain. The frequency of scales increases with wavenumber, so that at high forcing frequencies only the smallest scales are modulated.

proportional to $\tilde{P}/\omega$. The frequency dependence of the dissipation and kinetic energy in both these limits is trivial and the investigation of this dependence will not contribute to a better understanding of the response of a turbulent flow to external forcing. The true challenge in the current setting is to understand how the nonlinear interaction between the different lengthscales is influenced by the forcing. We therefore focused on the response of the modulated dissipation $\tilde{\epsilon}(\omega)$. This quantity will translate how the energy cascade transmits information from the large to the small scales. It is tempting to describe the energy cascade as a low pass-filter and we will try to characterize how the large frequencies are filtered out. The frequency response is shown in figure 3.8.

The constant value for $\omega \to 0$ and the ω^{-1} behavior for $\omega \to \infty$ correspond to the trivial limits we just mentioned. The truly interesting part of the frequency response is the decay between these two limits. For high Reynolds numbers this fall-off of the frequency response is proportional to ω^{-3}. This behavior will be explained phenomenologically in the following.

If we accept that a scale cannot adapt to a perturbation if the perturbation is at a higher temporal frequency than its intrinsic frequency (the inverse of the eddy turnover time $\tau(k)$) then we can identify a length-scale k_ω^{-1} which separates a region of scale-space with small scales that can adapt to the frequency and a region with large scales, too slow to adapt to the frequency

$$\tau(k_\omega) \approx \omega^{-1}. \tag{3.10}$$

This situation is sketched in Figure 3.9.

Let us consider the case that we are interested in, where this frequency corresponds to an eddy frequency somewhere in the inertial range and typically the frequency is determined by the local energy flux and wavenumber. We find

$$\tau(k_\omega) \sim \bar{\epsilon}^{-1/3} k_\omega^{-2/3} \approx \omega^{-1}. \tag{3.11}$$

The question now is how energy can be transferred from the forcing scale towards the region with $k > k_\omega$ which can respond fast enough to respond to the forcing.

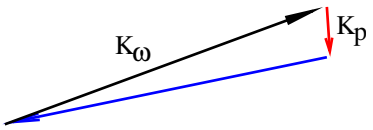

Figure 3.10: A typical non-local triad with the large forcing scale, corresponding to wavevector $\boldsymbol{K}_f$ interacting with a smaller scale with wavevector $\boldsymbol{K}_\omega$.

Since the scales $k_F < k < k_\omega$ cannot transmit the information, a stepwise cascade cannot succeed this task. The only mechanism is by a direct interaction between the forcing scale and the scales $k > k_\omega$. In other words, by means of non-local interactions.

To what extent are these non-local interactions efficient enough to transfer directly the energy? It was shown by Kraichnan [50] (see also [85]) that the amount of energy transfer by nonlinear interactions, compared to the total transfer, is a function of the disparity parameter, defined by the ratio of the wavenumbers of the triad involved in the transfer:

$$s = \frac{\text{Longest Leg}}{\text{Shortest Leg}} \tag{3.12}$$

which in our case corresponds to $s \approx k_\omega/k_p$. Such a triad of wavenumbers is sketched in Figure 3.10. The transfer is then given by

$$\frac{\epsilon_f(K,s)}{\epsilon_f^{Total}(K)} \sim s^{-4/3}. \tag{3.13}$$

since the total flux of energy is approximately given by the relation

$$\epsilon_f^{Total} \sim \frac{\tilde{k}}{\mathcal{T}}, \tag{3.14}$$

with $\mathcal{T}$ the eddy turnover time of the forcing scales, and since $\tilde{k} \sim P/\omega$, one finds that

$$\epsilon_f(K,s) \sim \omega^{-3}. \tag{3.15}$$

The filter characteristics of the energy cascade are thus determined by non-local interactions between modes at the forcing scale and inertial range modes with a typical frequency larger than ω. In a follow-up contribution we showed how one can construct a multiple scale turbulence model which takes into account these non-local interactions. The manuscript reporting on this investigation is attached at the end of this chapter.

3.4 Depletion of nonlinearity in turbulent flows

Written in Fourier-Space the Navier-Stokes equations (1.4) consist of three contributions: the time-derivative, the dissipation and the complete nonlinear term (RHS of equation (1.4)). The time-derivative and dissipation are local quantities in scale space whereas, as mentioned above, the nonlinear term couples

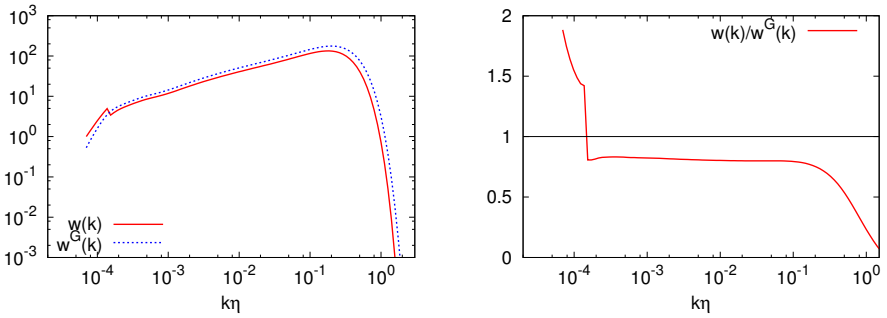

Figure 3.11: Left: spectrum of the nonlinear term (as in figure 1.3) and the same spectrum computed assuming the velocity-field to consist of independent (Gaussian) Fourier modes. Right: the ratio of the two spectra.

all different lengthscales. This nonlinearity is responsible for the net energy cascade between scales. An important feature of turbulence is that the different (Fourier) modes are not independent. This dependence is hidden in the phase correlations in a Fourier-transformed turbulent field. If these phases are random, we have noise. It should however be noted that the nonlinear term is not zero in noise. At every point in a Gaussian field one can evaluate the nonlinearity

$$\boldsymbol{N} = \boldsymbol{u} \cdot \nabla \boldsymbol{u} + \nabla p \tag{3.16}$$

and its value is generally nonzero. On average its value is zero, but this is also the case in turbulence. The norm of the nonlinear term can also be evaluated in both noise and turbulence. What can we expect if we compare these quantities?

It is observed that turbulence displays the perhaps surprising property, that it locally tends to a state in which the strength of the nonlinear term is reduced, compared to a random ensemble of independent Fourier modes with the same kinetic energy. This depletion of nonlinearity seems to be a quite general property of systems containing a quadratic nonlinearity as was suggested by Kraichnan and Panda [86].

In order to better understand the multi-scale dynamics underlying this property, it is interesting to consider the scale distribution of the strength of the nonlinear term, which was already discussed in section 1.2,

$$\int_0^\infty w(k)dk = \overline{N_i N_i}. \tag{3.17}$$

The mean-square nonlinearity is not a conserved quantity (of the Euler equations) in contrast to the kinetic energy, and its inertial range behavior is therefore not determined by a flux argument such as the kinetic energy spectrum. The spectral distribution of nonlinearity $w(k)$, computed by closure[6], is given

[6]In one of the original papers introducing DIA [34], it was already mentioned that the theory was applicable to describe statistical moments of arbitrary order. It was however not until thirty years later that it was shown by Kraichnan and coworkers [69] how this could be done in practice. In that investigation it was outlined how arbitrary order cumulants (the non-Gaussian contributions) can be computed by DIA. In particular, the spectrum of the nonlinear term was shown to be predicted correctly.

by (Figure 3.11),

$$w(k) \sim \overline{u_i u_i} \epsilon^{2/3} k^{1/3}. \tag{3.18}$$

This is indeed observed both in a Gaussian field and in a turbulent field. However, deviations from the Gaussian distribution of nonlinearity are observed at all scales. The strength of the nonlinearity seems to be reduced through the dependence of the Fourier modes in both the inertial range and the dissipation range. Only in the forced scales the nonlinearity is super-Gaussian.[7] It is tempting to relate the observed results to structures. Since a field consisting of independent Fourier modes is completely structureless, or incoherent, the current results are not inconsistent with the presence of structures in the dissipation range.

The manifestation of depletion of nonlinearity is quite dramatic in two-dimensional turbulence. If we consider the rather academic case of freely evolving two-dimensional turbulence in a periodic domain, the end state, long before all energy is dissipated, consists of a longliving counter-rotating vortex pair. This *final state*, in which nonlinear interaction is almost completely absent can be predicted by statistical mechanics, as was first suggested by Onsager [88]. A first, successful approach, based on the dynamics of point-vortices, was carried out by Joyce and Montgomery [89, 90]. They showed that an entropy could be defined based on the vorticity. By optimizing this vorticity under constraints they succeeded to describe the most probable final state. Numerical simulations of the two-dimensional Navier-Stokes equations in a periodic domain showed that the theory was very successful in describing the dynamics [91]. Robert and Sommeria [92] and Miller [93] formalized this approach mathematically for a continuous distribution of vorticity. In axisymmetric three-dimensional turbulence progress has recently be made to apply statistical mechanics in a predictive way [94, 95]. For non-axisymmetric three-dimensional turbulence no fully successful attempts can be reported. However, the fact that an important depletion of nonlinearity is observed in both two- and three-dimensional turbulence, gives some hope that some features can be predicted in three dimensions by similar approaches. This constitutes an exciting challenge in turbulence theory research.

In a recent investigation, which is included at the end of this chapter, we tested the concept of depletion of nonlinearity for the case of a passive scalar advected by turbulence. The scalar equation is linear, but the advection term plays for the scalar a similar role as the nonlinearity of the Navier-Stokes equations with respect of the coupling of different modes. Indeed all products of fields correspond to convolution products in Fourier space, which couple all different length scales. It was found that also the dynamics of the scalar tend to a state depleted of advection. In particular in the small scales of the scalar it was observed that the strength of the advection term was reduced substantially compared to its Gaussian estimate. In the case of the scalar this phenomenon might be related to the appearance of fronts, since fronts are stabilized when the scalar gradient is perpendicular to the velocity field, as is the case when the advection term is reduced. This hypothesis should however be carefully checked since fronts are insensitive to the sweeping of very large scales whereas the depletion of advection is directly influenced by sweeping (as was discussed

[7] This effect of non-Gaussianity in the inertial range might be related to the parameter α modeled in the tetrad model for the evolution of velocity gradient dynamics [87].

in section 1.3).

In both the case of the turbulent velocity field and the mixing of a passive scalar, the statistical imprint of coherence can thus be probed by computing the depletion of nonlinearity. It is for the moment, however, far from clear what the relation is between the generation of scalar fronts and coherent structures on the one hand and depletion of nonlinearity and advection on the other. It is our opinion that such a relation must not be excluded. It might seem surprising that, if the depression of nonlinearity is linked to coherent structures, it could be captured by statistical closures. Indeed it is often mistakenly assumed that these statistical approaches cannot predict anything on structure related issues since all phase-information is averaged out. The apparent contradiction disappears if one admits that that structures are a dynamical consequence of the underlying equations and the statistical theories are derived from these equations. It is therefore not completely surprising that, if the assumptions used in deriving the closures are physically sound, the statistics observed from closures can be related to the structures observed in experiments and simulations.

On the unsteady behavior of turbulence models

R. Rubinstein[1] and W. J. T. Bos[2]
[1]*Newport News, Virginia 23601, USA*
[2]*LMFA-CNRS, Université de Lyon, Ecole Centrale de Lyon, UCBL, INSA Lyon, 69134 Ecully, France*

(Received 16 January 2009; accepted 20 March 2009; published online 22 April 2009)

Periodically forced turbulence is used as a test case to evaluate the predictions of two-equation and multiple-scale turbulence models in unsteady flows. The limitations of the two-equation model are shown to originate in the basic assumption of spectral equilibrium. A multiple-scale model based on a picture of stepwise energy cascade overcomes some of these limitations, but the absence of nonlocal interactions proves to lead to poor predictions of the time variation of the dissipation rate. A new multiple-scale model that includes nonlocal interactions is proposed and shown to reproduce the main features of the frequency response correctly. © *2009 American Institute of Physics*.
[DOI: 10.1063/1.3121303]

A basic premise of one point closures such as the k-ϵ model is the hypothesis of "spectral equilibrium," which justifies two distinct roles of the dissipation rate ϵ: On the one hand, it appears in the energy balance, defined as a correlation of velocity gradients, hence a small-scale quantity; on the other hand, it is used phenomenologically to describe large-scale transport properties. The most basic formulation of the latter is Kolmogorov's hypothesis $\epsilon \propto k^{3/2}/L$, where k is the turbulent kinetic energy and L is a length scale characteristic of the largest scales of motion; equivalent formulations include $\nu_t \propto k^2/\epsilon$, the formula for turbulent viscosity, or $\tau \propto k/\epsilon$, the formula for the turbulent time scale. The Kolmogorov theory, or more general assumptions of self-similarity of all scales of motion, justifies all of these proportionalities,[1] although the constants of proportionality need not coincide in all self-similar flows.[2]

However, turbulence models are not needed to describe self-similar flows, which merely serve as calibration cases; models are needed to describe departure from self-similarity, when spectral equilibrium becomes a strong constraint on turbulence evolution. In a study of a flow in which turbulence evolves from a steady state to a self-similar time-dependent state,[3] the implications of the departure from spectral equilibrium were investigated. This departure was connected to transient failure of the Tennekes–Lumley balance[4] and to the consequent relevance of small-scale dynamics for the large scales. The breakdown of spectral equilibrium has also been observed in engineering flows including turbulent diffusers and wakes.[5]

The limitations of the spectral equilibrium hypothesis are very well known in the modeling literature and have led to proposals for *multiple-scale models*[6] that more realistically address the complexity of the nonlinear interactions in turbulent flows. This letter reports on some investigations of multiple-scale models applied to an especially simple and attractive test case for transient turbulence: *periodically forced turbulence*.[7–9] This problem arises when isotropic incompressible turbulence, maintained in a steady state by a large-scale isotropic forcing with total amplitude $\bar{p}$, is subjected to a small time-dependent periodic perturbation with amplitude $\tilde{p}$: $p(t)=\bar{p}+\tilde{p}\cos(\omega t)$, such that the ratio $\tilde{p}/\bar{p} \ll 1$ and such that the forcing length scale does not depend on time. The phase-averaged kinetic energy k can then be decomposed into a mean $\bar{k}$ and a periodic part $\tilde{k}(\omega)\cos[\omega t+\phi_k(\omega)]$, with ϕ_k the phase shift between the forcing and the kinetic energy. Similarly, the viscous dissipation rate can be written as $\epsilon=\bar{\epsilon}+\tilde{\epsilon}(\omega)\cos[\omega t+\phi_\epsilon(\omega)]$; $\bar{k}$ and $\bar{\epsilon}$ are related to the time-independent forcing length scale $\bar{L}$ by $\bar{L} \propto \bar{k}^{3/2}/\bar{\epsilon}$. The periodic parts of k and ϵ are sinusoidal, such as the forcing because $\tilde{p}/\bar{p} \ll 1$. The functions $\tilde{k}(\omega)$, $\tilde{\epsilon}(\omega)$, $\phi_k(\omega)$, and $\phi_\epsilon(\omega)$, which characterize the linearized response of steady state turbulence to periodic perturbation of the forcing, can be called the *linear response functions*.

We will use periodically forced turbulence as a test case to evaluate the ability of multiple-scale models to predict the dynamics of time-dependent turbulence. It will first be shown that the unsteady predictions of multiple-scale models are significantly better than the predictions of a two-equation model. However, an elementary multiple-scale model based on the heuristic picture of stepwise energy cascade is found to have limitations in predicting the unsteady dissipation rate. A multiple-scale model that includes the possibility of nonlocal interactions is proposed; it is shown that this model can capture some fine features of the unsteady energy dissipation.

The linear response functions were determined in recent work[10] using the eddy-damped quasi-normal Markovian (EDQNM) closure theory, which was shown to compare very well to available low Reynolds number experimental, and direct numerical simulation (DNS) data. Comparison with high Reynolds number data for linear response functions would be desirable, but such data is not yet available. Briefly summarizing the major conclusions, the two-equation model is satisfactory both in the *static* limit $\omega \to 0$, in which the phase shifts ϕ_k, ϕ_ϵ vanish, and in the *frozen* limit $\omega \to \infty$, in which $\tilde{k} \sim \omega^{-1}$ and $\phi_k \sim \pi/2$. However, this agreement is trivial; only the results at intermediate frequencies provide a real test of the model. The two-equation model reproduces

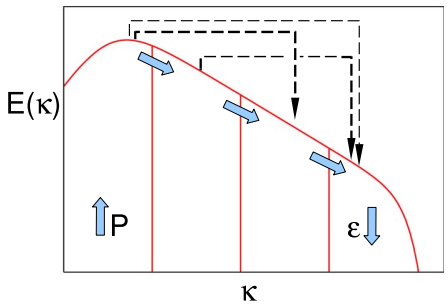

FIG. 1. (Color online) Schematic of a discretized energy cascade. The solid arrows indicate the energy fluxes between neighboring wavenumber shells. The dashed lines indicate the nonlocal fluxes between spectrally remote shells. Note that a similar picture can be found in a paper by Lumley (Ref. 11).

the function $\tilde{k}(\omega)$ reasonably well, but the transition from the static limit $\phi_k \approx 0$ to the frozen limit $\phi_k \approx \pi/2$ occurs over a frequency range that is much too wide. The amplitude $\tilde{\epsilon}(\omega)$ is not satisfactory: a range in which $\tilde{\epsilon} \sim \omega^{-3}$ at high Reynolds numbers is absent. We note that since observations of the modulated dissipation rate are very difficult, and relevant high Reynolds number data are not yet available, the EDQNM results for this quantity remain theoretical predictions; they are nevertheless supported by arguments[10] based on the well-established role of distant interactions in turbulence. Finally, the two-equation model also makes the incorrect prediction that $\phi_k = \phi_\epsilon$ regardless of ω.

We investigate whether these predictions can be improved using multiple-scale modeling following the ideas of Schiestel.[6] Multiple-scale models can be considered numerical methods for spectral closures, with significant modifications designed to permit reasonable accuracy at a very low order of discretization. Thus, whereas a numerical implementation of a spectral closure would solve for the energy spectrum at perhaps hundreds of discrete wavenumbers κ_i, in Schiestel's formulation, the energy spectrum is divided into a relatively small number of wavenumber shells $\kappa_{i-1} \le \kappa \le \kappa_i$; for each shell, equations are written for two scalar descriptors: the fluctuation energy contained in the shell and the net energy flux into it. To enhance the accuracy possible with a relatively small number of shells, Schiestel allowed the partition wavenumbers κ_i to be functions of time. A schematic picture of the resulting discretized energy cascade is given in Fig. 1, following Lumley.[11]

The starting point for the analytical formulation is the Lin equation governing the energy spectrum $E(\kappa,t)$,

$$\left(\frac{\partial}{\partial t} + \nu\kappa^2\right)E(\kappa,t) = P(\kappa,t) - \frac{\partial F(\kappa,t)}{\partial \kappa}. \tag{1}$$

In this equation ν is the viscosity, $P(\kappa,t)$ the forcing term, and $F(\kappa,t)$ is the energy flux across wavenumber κ. Schiestel applied the Kovaznay model[12]

$$F(\kappa,t) = C\kappa^{5/2}E(\kappa,t)^{3/2}, \tag{2}$$

with C a parameter which determines the Kolmogorov constant. This model represents a stepwise cascade of energy in spectral space from small to large κ and reproduces a $\kappa^{-5/3}$ inertial range. Figure 1 would correspond to a stepwise cascade if the dashed lines were absent.

To obtain a multiple-scale model, write the equation for the time derivative of the spectral energy flux $F(\kappa,t)$,

$$\dot{F}(\kappa,t) = \frac{3}{2}\frac{F(\kappa,t)}{E(\kappa,t)}\dot{E}(\kappa,t). \tag{3}$$

From the viewpoint of Schiestel's analysis, we have assumed that the partition wavenumbers are constant in time. This assumption seems appropriate for this problem, in which the forcing wavenumber is fixed. The production scales are assumed to be confined to low κ, and the dissipation to high κ (a more general description including finite-Reynolds number effects or broadband forcing will not be attempted here). For κ in the inertial range, Eq. (1) becomes

$$\dot{E}(\kappa,t) = -\frac{\partial F(\kappa,t)}{\partial \kappa}. \tag{4}$$

We combine this with Eqs. (2) and (3) to obtain

$$\dot{F}(\kappa,t) = -\frac{3}{2}\frac{F(\kappa,t)}{E(\kappa,t)}\frac{\partial F(\kappa,t)}{\partial \kappa}. \tag{5}$$

A discrete model is obtained by splitting the spectral domain into n shells as illustrated in Fig. 1. The energy in shell i is $e_i \approx E(\kappa_i)\Delta\kappa_i$. The spectral flux $f_i \approx F(\kappa_i)$ and the time derivative is $\partial F(\kappa_i,t)/\partial k \approx (f_i - f_{i-1})/\Delta\kappa_i$ so that we obtain

$$\dot{f}_i = -\frac{3}{2}\frac{f_i}{e_i}(f_i - f_{i-1}), \quad 1 \le i \le n. \tag{6}$$

Integrating Eq. (4) over each shell gives the partial energy balance equations

$$\dot{e}_i = -(f_i - f_{i-1}), \quad 1 \le i \le n, \tag{7}$$

in which all f_i and e_i are functions only of time. The oscillating production term $\tilde{p}$, assumed to act at the small wavenumbers, is identified with f_0, the flux entering shell 1. Furthermore, the high Reynolds numbers case is considered in which we assume that the viscous dissipation takes place at the last wavenumber shell: $\epsilon = f_n$. This assumption makes it unnecessary to introduce partial dissipation rates for each shell and corresponding equations of motion. A special feature of the Kovaznay model is that the partition wavenumbers do not appear in the model.

By choosing $n=1$, one obtains a two-equation model; the equation for f_1 becomes the dissipation rate equation $\dot{\epsilon} = (3/2)(\epsilon/k)(P-\epsilon)$. Note that the two model constants, generally called $C_{\epsilon 1}$ and $C_{\epsilon 2}$ in literature, are equal, which allows the study of statistically stationary isotropic turbulence. Consistency with homogeneous shear flow, or with any problem in which the forcing length scale increases as a power law or exponential in time,[13] requires $C_{\epsilon 1} < C_{\epsilon 2}$.

Choosing $n \ge 2$ should improve the predictions by introducing the possibility of spectral imbalance, a necessary requirement if the same model is to be applied to both forced and decaying turbulence;[2] imbalance is possible because the partial fluxes f_i with $1 \le i \le n-1$ and the dissipation $\epsilon = f_n$ are independent.

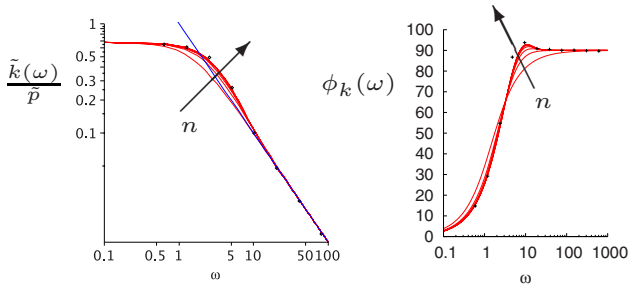

FIG. 2. (Color online) Linear response functions $\tilde{k}(\omega)$ (left) and $\phi_k(\omega)$ (right) for the multiple-scale model based on the Kovaznay spectral closure (6). The 7 curves in each graph correspond to models with $n=1,2,\ldots,7$ spectral shells and n increases in the direction of the arrow. The theoretical amplitude prediction ω^{-1} is indicated by a straight line. Also shown are the results of EDQNM simulations (symbols). The frequency ω is normalized by the large-scale frequency $\bar{\epsilon}/\bar{k}$.

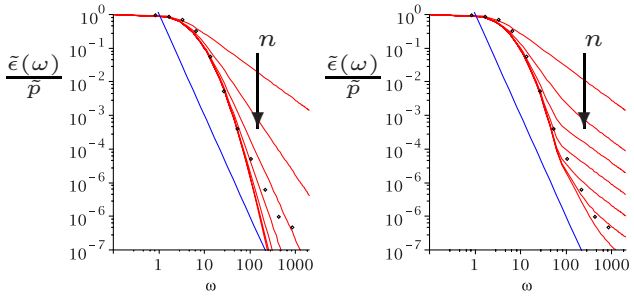

FIG. 3. (Color online) Frequency response function $\tilde{\epsilon}(\omega)$ for the model based on the Kovaznay closure (8) (left) and for the model based on the Ellison closure (11) (right). The 7 curves in each graph correspond to $n=1,2,\ldots,7$ and n increases in the direction of the arrow. The theoretical prediction ω^{-3} is indicated by the straight lines. Also shown are the results of EDQNM simulations (symbols).

The unsteady behavior of this model is now assessed as follows. Beginning with a steady state with shell energies $\bar{e}_i$ such that $\bar{p}=\bar{f}_i=\bar{\epsilon}$, the periodic perturbation $\tilde{p}\cos(\omega t)$ is added to the forcing. Describing the periodic response in terms of complex amplitudes $\hat{k}(\omega)$ and $\hat{\epsilon}(\omega)$ so that $\tilde{k}(\omega)=|\hat{k}(\omega)|$ and $\tan\phi_k(\omega)=\Im\hat{k}(\omega)/\Re\hat{k}(\omega)$ with the obvious analogs for ϵ, the equations for the periodic part of the partial kinetic energies and local fluxes become

$$i\omega\hat{e}_i=-(\hat{f}_i-\hat{f}_{i-1}),\quad i\omega\hat{f}_i=-\frac{3}{2}\frac{\bar{f}_i}{\bar{e}_i}(\hat{f}_i-\hat{f}_{i-1}). \tag{8}$$

The resulting linear system is easily solved analytically for $\hat{e}_i(\omega)$ and $\hat{f}_i(\omega)$ in terms of the periodic forcing perturbation $\tilde{p}$ and the parameters $\bar{e}_i$ and $\bar{f}_i$.

Figure 2 compares the results for the amplitude $\tilde{k}(\omega)$ and phase shift $\phi_k(\omega)$ for models with $n=1$ to $n=7$ wavenumber shells. Also shown are results obtained in EDQNM computations[10] at Reynolds number $R_\lambda=1000$, with $R_\lambda\approx 15R_L^{1/2}$ and $R_L=(2\bar{k}/3)^{1/2}\bar{L}/\nu$. It has been shown[10] that at low ω, $\tilde{k}(\omega)$ should tend to a plateau and that at large ω, $\tilde{k}(\omega)$ follows a power-law proportional to ω^{-1}. Confirming the conclusion of Bos *et al.*,[10] $\tilde{k}(\omega)$ is in reasonable agreement with EDQNM even for the two-equation model $n=1$, although this agreement improves significantly as the number of wavenumber partitions n increases.

The error in the two-equation model prediction of $\tilde{k}(\omega)$ is a too gradual transition from the plateau to the ω^{-1} region. This defect appears more prominently in the phase $\phi_k(\omega)$: Although all models give the correct static and frozen limits, the two-equation model transitions much too gradually, and only the models with $n\geq 2$ are in close agreement with EDQNM. The relatively rapid transition in the energy phase shift therefore appears as a typical multiple-scale effect. Evidently, in this problem, the small scales are not simply "slaved" to the large scales through a constant dissipation rate as is assumed in a two-equation model; instead, they are dynamically independent and have a strong effect on what is apparently a purely large-scale property.

It has also been demonstrated[10] that the response function $\tilde{\epsilon}(\omega)$ follows at high ω a power-law proportional to ω^{-3} up to the Kolmogorov frequency $\omega_\eta\sim\bar{\epsilon}/\nu$. For $\omega>\omega_\eta$, $\tilde{\epsilon}(\omega)$ becomes proportional to ω^{-1}. These results are shown for comparison in the graph on the left side of Fig. 3 (the phase shift ϕ_ϵ proves difficult to compute with any confidence because of the extremely small amplitudes involved, therefore comparisons are omitted).

The agreement of $\tilde{\epsilon}(\omega)$ given by the multiple-scale model Eq. (8) with the EDQNM results is very good down to values $\tilde{\epsilon}/\tilde{p}=10^{-3}$ for $n>3$ [note that $\tilde{k}(\omega)$ and $\tilde{\epsilon}(\omega)$ are proportional to $\tilde{p}$, and $\tilde{p}$ is chosen unity without loss of generality]. However for smaller values of $\tilde{\epsilon}/\tilde{p}$, the discrete model starts to diverge from the EDQNM results, especially for large n. It is easily shown that for this model, the leading order contributions at high ω are proportional to ω^{-n}: Indeed, recursive solution of the equations for $\hat{f}_i$ in Eq. (8) shows that $\tilde{f}_i\sim\omega^{-i}\tilde{p}$. Thus, only if $n=3$ can we obtain $\tilde{\epsilon}(\omega)\sim\omega^{-3}$, but this is the result of a coincidence, which disappears if the number of partition wavenumbers is increased. This difficulty reflects a limitation of the multiple-scale model: Eq. (5) implies a linear first-order partial differential equation for $\hat{F}$ in which disturbances in F propagate along characteristics; this property is probably significantly compromised by a finite dimensional approximate model.

It has been shown[10] that nonlocal interactions are responsible for the ω^{-3} range. Nonlocal interactions are represented in Fig. 1 by dashed lines. Such interactions do not occur in the model Eqs. (6) and (7) because quantities in shell i depend only on its nearest neighbor, shell $i-1$. The absence of nonlocal interactions will be even more significant in problems in which the role of nonlocality is greater, as in the Batchelor regime of the passive scalar[14] and in magnetohydrodynamics (MHD).[15]

To address this problem, a new multiple-scale model will now be derived including the effect of nonlocal interactions. We start from a simple spectral model containing nonlocal interactions due to Ellison,[12]

$$F(\kappa,t) = C\left(\int_0^\kappa \kappa^2 E(\kappa,t)d\kappa\right)^{1/2} \kappa E(\kappa,t). \tag{9}$$

Applying the same procedure as to the Kovaznay model, the partial energy balance Eq. (7) is unchanged, but Eq. (6) is replaced by

$$\dot{f}_i = -\frac{f_i}{e_i}(f_i - f_{i-1}) - \frac{f_i}{2}\frac{\sum_{p=1}^{i}\kappa_p^2(f_p - f_{p-1})}{\sum_{p=1}^{i}\kappa_p^2 e_p}. \tag{10}$$

This expression contains the wavenumbers κ_i because nonlocal interactions, which depend on the spacing between the wave-number partitions, have been retained. The specification of the κ_i becomes part of the model. We will use a logarithmic discretization with $\kappa_i = \kappa_1 r^{i-1}$ in which r is a model parameter which determines the logarithmic grid size. Using this discretization, the ratio $\kappa_n/\kappa_1 = r^{n-1}$ so that a large range of scales can be considered by increasing r. Note that if a linear discretization is used, $\kappa_n/\kappa_1 = (n\Delta\kappa/1\Delta\kappa) = n$ so that the number of partitions for high Reynolds numbers becomes prohibitively large. Using the logarithmic discretization, the model for periodic forcing becomes

$$\dot{\hat{f}}_i = -\frac{\bar{f}_i}{\bar{e}_i}(\hat{f}_i - \hat{f}_{i-1}) - \frac{\bar{f}_i}{2}\frac{\sum_{p=1}^{i} r^{2(p-1)}(\hat{f}_p - \hat{f}_{p-1})}{\sum_{p=1}^{i} r^{2(p-1)}\bar{e}_p}, \tag{11}$$

with the same partial energy equations as in Eq. (8). Again, when $n=1$ the model reduces to a two-equation model. For $n>1$ the model differs from the previous model through the interaction term which couples wave-number shell i with all wavenumber shells $p=1,\ldots,i$. The response functions depend on both n and r, which will be chosen through a compromise between computational cost and precision.

The results for $\tilde{\epsilon}(\omega)$ obtained from Eq. (11) with $r=3$ and $1\le n\le 7$ wavenumber partitions are shown in the graph on the right side of Fig. 3. In the same figure, EDQNM results[10] at $R_\lambda = 1000$ are shown. The agreement with EDQNM is very good down to values $\tilde{\epsilon}/\tilde{p} = 10^{-3}$ for $3<n<7$, and for $n=7$, agreement is good down to $\tilde{\epsilon}/\tilde{p} = 10^{-6}$. We conclude that the model including nonlocal interactions Eq. (11) makes better predictions of $\tilde{\epsilon}$ than the model Eq. (8), in which nonlocal interactions are absent. The predictions of Eq. (11) (not shown) for $\tilde{k}(\omega)$ and $\phi_k(\omega)$ very nearly coincide with the results obtained using Eq. (8).

To conclude, we have found that in the problem of periodically forced turbulence, a two-equation model only gives satisfactory predictions for $\tilde{k}(\omega)$ and $\phi_k(\omega)$ at asymptotically high and low frequencies. The predictions at intermediate frequencies are improved by using a multiple-scale model based on the heuristic picture of stepwise energy cascade, the Kovaznay model. In particular, this model correctly predicts the rapid jump of the phase shift $\phi_k(\omega)$ between the static and frozen limits. The multiple-scale model based on the Ellison closure includes nonlocal effects, and leads to better agreement with EDQNM, including the high Reynolds number ω^{-3} scaling range for $\tilde{\epsilon}(\omega)$.[10] Both models give practically indistinguishable results for the amplitude and phase of the oscillating kinetic energy, which is not strongly influenced by nonlocal interactions. Our approach suggests how one might construct reduced order models for phenomena dominated by significant nonlocal interactions, such as the Batchelor range of the passive scalar and some cases of MHD.

We would like to acknowledge the interesting and thoughtful comments of the referees, which led to significant modifications of the paper.

[1] M. Oberlack, "Similarity in non-rotating and rotating turbulent pipe flows," J. Fluid Mech. **379**, 1 (1999).
[2] W. J. T. Bos, L. Shao, and J.-P. Bertoglio, "Spectral imbalance and the normalized dissipation rate of turbulence," Phys. Fluids **19**, 045101 (2007).
[3] R. Rubinstein, T. Clark, D. Livescu, and L. Luo, "Time-dependent isotropic turbulence," J. Turbul. **5**, 011 (2004).
[4] H. Tennekes and J. L. Lumley, *A First Course in Turbulence* (MIT Press, Cambridge, MA, 1972).
[5] H. Touil, J. P. Bertoglio, and S. Parpais, "A spectral closure applied to anisotropic inhomogeneous turbulence," in *Advances in Turbulence 8*, edited by C. Dopazo (CIMNE, Barcelona, 2000).
[6] R. Schiestel, "Multiple-time-scale modeling of turbulent flows in one-point closures," Phys. Fluids **30**, 722 (1987).
[7] D. Lohse, "Periodically kicked turbulence," Phys. Rev. E **62**, 4946 (2000).
[8] O. Cadot, J. H. Titon, and D. Bonn, "Observation of resonances in modulated turbulence," J. Fluid Mech. **485**, 161 (2003).
[9] A. K. Kuczaj, B. J. Geurts, D. Lohse, and W. van de Water, "Turbulence modification by periodically modulated scale-dependent forcing," Comput. Fluids **37**, 816 (2008).
[10] W. J. T. Bos, T. T. Clark, and R. Rubinstein, "Small scale response and modeling of periodically forced turbulence," Phys. Fluids **19**, 055107 (2007).
[11] J. L. Lumley, "Some comments on turbulence," Phys. Fluids A **4**, 203 (1992).
[12] A. S. Monin and A. M. Yaglom, *Statistical Fluid Mechanics* (MIT Press, Cambridge, MA, 1975).
[13] R. Rubinstein and T. Clark, "Self-similar turbulence evolution and the dissipation rate transport equation," Phys. Fluids **17**, 095104 (2005).
[14] G. K. Batchelor, "Small-scale variation of convected quantities in turbulent fluid," J. Fluid Mech. **5**, 113 (1959).
[15] A. Pouquet, U. Frisch, and J. Léorat, "Strong MHD helical turbulence and nonlinear dynamo effect," J. Fluid Mech. **77**, 321 (1976).

PHYSICS OF FLUIDS **24**, 075104 (2012)

Reduction of mean-square advection in turbulent passive scalar mixing

Wouter J. T. Bos,[1] Robert Rubinstein,[2] and Le Fang[1,3]
[1]*LMFA, CNRS, Ecole Centrale de Lyon - Université de Lyon, Ecully, France*
[2]*Newport News, Virginia 23601, USA*
[3]*Ecole Centrale de Pékin, Laboratoire International Associé, Beihang University, Beijing 100191, China*

(Received 18 October 2011; accepted 11 June 2012; published online 2 July 2012)

Direct numerical simulation data show that the variance of the coupling term in passive scalar advection by a random velocity field is smaller than it would be if the velocity and scalar fields were statistically independent. This effect is analogous to the "depression of nonlinearity" in hydrodynamic turbulence. We show that the trends observed in the numerical data are qualitatively consistent with the predictions of closure theories related to Kraichnan's direct interaction approximation. The phenomenon is demonstrated over a range of Prandtl numbers. In the inertial-convective range the depletion is approximately constant with respect to wavenumber. The effect is weaker in the Batchelor range. © *2012 American Institute of Physics*. [http://dx.doi.org/10.1063/1.4731302]

I. INTRODUCTION

The modal amplitudes in the Fourier decomposition of any homogeneous random field are uncorrelated. In a Gaussian random field, they are also statistically independent; but in homogeneous turbulence, nonlinearity produces statistical dependence among the amplitudes. The simplest consequence is that the third-order correlations representing energy transfer, which would vanish in a Gaussian random field, do not vanish in homogeneous turbulence.

Some further consequences of statistical dependence of Fourier amplitudes in homogeneous turbulence were considered in an important paper by Chen *et al.*,[1] which compared various fourth-order moments with the corresponding moments in a Gaussian random field with the same second-order properties as the turbulent velocity field (the construction of such Gaussian surrogates is sometimes called "kinematic simulation"[2,3]). Among the quantities investigated by Chen *et al.* was the variance of the fluctuating nonlinear term in the Navier-Stokes equations,

$$\langle |\boldsymbol{u}(\boldsymbol{x},t)\cdot\nabla\boldsymbol{u}(\boldsymbol{x},t)+\nabla p(\boldsymbol{x},t)|^2\rangle. \tag{1}$$

It had been observed[4] that this quantity is significantly smaller in a turbulent velocity field than in its Gaussian counterpart; that is, there is a significant (negative) cumulant contribution to the fourth order moment defined by Eq. (1). One of the mechanisms which can lead to this *depression of nonlinearity* is the preferential alignment of velocity and vorticity, also called *Beltramization*.[5] However, this preferential alignment is not the only non-trivial mechanism which is consistent with the depression of nonlinearity; we will return to this issue in Sec. V.

From the viewpoint of a Fourier analysis of the spectrum of the correlation in Eq. (1), the depression of nonlinearity is a consequence of statistical dependence of the uncorrelated Fourier amplitudes that enter the expression for this spectrum. One finding of Chen *et al.* was that this phenomenon appears to be well predicted by Kraichnan's[6] direct interaction approximation (DIA). The successful prediction of a nonzero fourth-order cumulant by a closure theory might seem unexpected or even surprising, since from the very beginning, closure theories have been associated with cumulant discard hypotheses;[7] the debate between Kraichnan and Proudman at the famous 1961 Marseille conference[8] centered on this issue.[24] The computation of a nonzero cumulant and

the favorable comparison with data perhaps vindicate, somewhat after the fact, Kraichnan's assertion at that time,[9] that DIA *does not assume (or imply) the vanishing of fourth order cumulants.*

In the present work, we will show that an effect of statistical dependence of Fourier amplitudes analogous to depression of nonlinearity also appears in the advection of a passive scalar θ. Thus, we consider the scalar analog of the moment in Eq. (1): the variance of fluctuations of the bilinear scalar-velocity coupling

$$\langle (\boldsymbol{u}(\boldsymbol{x},t)\cdot\nabla\theta(\boldsymbol{x},t))^2\rangle. \tag{2}$$

Herring and Métais[10] have shown that this quantity is smaller in passive scalar advection than it would be if the Fourier amplitudes of velocity and scalar were statistically independent, even at the more refined level of Fourier spectra. We confirm their conclusions using higher resolution DNS data, and following Chen *et al.*, show that closures related to the DIA predict trends consistent with the data.

A different perspective on non-Gaussian properties of turbulence is provided by recent detailed studies of the properties of realizations of turbulent velocity fields. Such studies, made possible by high resolution direct numerical simulations,[11] reveal the existence of flow structures such as vortex tubes and sheets, and spotty regions of very high dissipation; in comparison, since a Gaussian random field is simply space- and time-filtered white noise, it is expected to be essentially "featureless." This viewpoint makes the existence of such structures the most significant effect of non-Gaussianity in turbulence. In the present paper, we focus on a statistical characterization of non-Gaussian features in turbulence and do not investigate features of the instantaneous flow realizations. We suggest, however, that investigating the connections between this physical space perspective and the viewpoint of dependence among Fourier modes can be a useful direction for future research.

The paper is organized as follows: in Sec. II the theoretical considerations leading to closure expressions for the mean-square advection term are given. Section III presents details of the numerical evaluation of cumulant corrections. Section IV presents comparisons between closure computations and direct numerical simulation data. Section V contains a discussion of the results. Conclusions are drawn in Sec. VI.

II. ANALYSIS

We consider the advection of a passive scalar in homogeneous turbulence. The governing equation is

$$\left[\partial_t+\alpha k^2\right]\theta(\boldsymbol{k},t)=-ik_i\int d\boldsymbol{p}d\boldsymbol{q}\;\delta(\boldsymbol{k}-\boldsymbol{p}-\boldsymbol{q})\theta(\boldsymbol{p},t)u_i(\boldsymbol{q},t)+f_\theta(\boldsymbol{k},t), \tag{3}$$

where α denotes the scalar diffusivity and $f_\theta(\boldsymbol{k},t)$ is a source of scalar fluctuations that we will assume confined to the large scales. By analogy to Chen *et al.*, we consider the contribution of each Fourier mode to the variance of the velocity-scalar coupling term. It is defined by

$$W_\theta(\boldsymbol{k},t)=k_ik_j\int d\boldsymbol{p}\;d\boldsymbol{q}\;\int d\boldsymbol{p}'\;d\boldsymbol{q}'\;\delta(\boldsymbol{k}-\boldsymbol{p}-\boldsymbol{q})\delta(\boldsymbol{k}+\boldsymbol{p}'+\boldsymbol{q}')\langle\theta(\boldsymbol{p},t)u_i(\boldsymbol{q},t)\theta(\boldsymbol{p}',t)u_j(\boldsymbol{q}',t)\rangle. \tag{4}$$

The integral of $W_\theta(\boldsymbol{k},t)$ over all wavevectors is equal to the moment in Eq. (2),

$$\int d\boldsymbol{k}\;W_\theta(\boldsymbol{k},t)=\langle[\boldsymbol{u}(\boldsymbol{x},t)\cdot\nabla\theta(\boldsymbol{x},t)]^2\rangle. \tag{5}$$

Without introducing any assumptions, we can write

$$W_\theta(\boldsymbol{k},t)=W_\theta^G(\boldsymbol{k},t)+W_\theta^C(\boldsymbol{k},t), \tag{6}$$

where $W_\theta^G(\boldsymbol{k},t)$ is evaluated assuming the independence of the Fourier amplitudes in Eq. (4) and $W_\theta^C(\boldsymbol{k},t)$ is a cumulant correction. In the following we will consider the isotropic case. In that case

the velocity and scalar are uncorrelated. Then

$$W_\theta^G(\boldsymbol{k},t) = k_i k_j \int d\boldsymbol{p}\, d\boldsymbol{q}\ \delta(\boldsymbol{k}-\boldsymbol{p}-\boldsymbol{q})\, U_\theta(\boldsymbol{p},t) U_{ij}(\boldsymbol{q},t), \tag{7}$$

where

$$U_{ij}(\boldsymbol{k},t) = \langle u_i(\boldsymbol{k},t) u_j(-\boldsymbol{k},t)\rangle \tag{8}$$

is the single-time velocity autocorrelation and

$$U_\theta(\boldsymbol{k},t) = \langle \theta(\boldsymbol{k},t)\theta(-\boldsymbol{k},t)\rangle \tag{9}$$

is the single-time scalar autocorrelation.

We now analyze W_θ using Kraichnan's DIA theory. There are many equivalent formulations of this theory, but for this analysis, the Langevin model formulation[12] is the most convenient. The DIA Langevin model for passive scalar advection replaces the exact governing equation Eq. (3) by

$$\left[\partial_t + \alpha k^2\right]\theta(\boldsymbol{k},t) + \int_0^t ds\ \eta_\theta(\boldsymbol{k};t,s)\theta(\boldsymbol{k},s) = -ik_i \int d\boldsymbol{p} d\boldsymbol{q}\ \delta(\boldsymbol{k}-\boldsymbol{p}-\boldsymbol{q})\xi_\theta(\boldsymbol{p},t)\xi_i(\boldsymbol{q},t) + f_\theta(\boldsymbol{k},t), \tag{10}$$

where ξ_θ and ξ_i are independent Gaussian random variables with the same *two-time* correlation functions as θ and u_i,

$$\langle \xi_\theta(\boldsymbol{k},t)\xi_\theta(-\boldsymbol{k},t')\rangle = \langle \theta(\boldsymbol{k},t)\theta(-\boldsymbol{k},t')\rangle = U_\theta(\boldsymbol{k};t,t'), \tag{11}$$

$$\langle \xi_i(\boldsymbol{k},t)\xi_j(-\boldsymbol{k},t')\rangle = \langle u_i(\boldsymbol{k},t)u_j(-\boldsymbol{k},t')\rangle = U_{ij}(\boldsymbol{k};t,t'), \tag{12}$$

and the damping function η_θ is defined as

$$\eta_\theta(\boldsymbol{k};t,t') = k_i k_j \int d\boldsymbol{p}\, d\boldsymbol{q}\ \delta(\boldsymbol{k}-\boldsymbol{p}-\boldsymbol{q})\, G_\theta(\boldsymbol{p};t,t') U_{ij}(\boldsymbol{q};t,t'). \tag{13}$$

Here, G_θ is the *response function*, defined as the inverse of the (formally) linear operator on the left side of Eq. (10). This linearity allows us to write, ignoring the contribution of the scalar source term,

$$\theta(\boldsymbol{k},t) = -ik_i \int_0^t ds\ G_\theta(\boldsymbol{k};t,s) \int d\boldsymbol{p} d\boldsymbol{q}\ \delta(\boldsymbol{k}-\boldsymbol{p}-\boldsymbol{q})\xi_\theta(\boldsymbol{p},s)\xi_i(\boldsymbol{q},s). \tag{14}$$

This brings up an important feature of DIA, namely that it is not closed in terms of the correlation function alone. The introduction of the response function is one major contribution of DIA to turbulence theory.[25] DIA provides equations of motion for both G_θ and the correlation function U_θ related to the model Eq. (10). We refer to Ref. 13 for details.

Paraphrasing Kraichnan's own description of DIA, we see that it first replaces the nonlinear coupling by a random forcing by surrogate statistically independent random fields with the same second-order properties as the actual fields; this step suppresses any statistical dependence among Fourier modes that develops under the exact evolution. These dependences are then *modeled* by the damping provided by η_θ; then the transfer of scalar fluctuations between modes is treated in DIA as the result of this damping acting against the forcing. Perhaps the most important qualitative feature to note is that the theory requires two-time statistics: this complication is inevitable given that DIA attempts to describe complex bilinear interactions by means of second-order statistics alone.

Thus, DIA can be described as the replacement

$$-ik_i \int d\boldsymbol{p} d\boldsymbol{q}\ \delta(\boldsymbol{k}-\boldsymbol{p}-\boldsymbol{q})\theta(\boldsymbol{p},t)u_i(\boldsymbol{q},t) \to -\left[\int_0^t ds\ \eta_\theta(\boldsymbol{k};t,s)\theta(\boldsymbol{k},s) + ik_i \int d\boldsymbol{p} d\boldsymbol{q}\ \delta(\boldsymbol{k}-\boldsymbol{p}-\boldsymbol{q})\xi_\theta(\boldsymbol{p},t)\xi_i(\boldsymbol{q},t)\right], \tag{15}$$

where the arrow simply indicates modeling; at this point, there is no assertion about an "approximation." Then the DIA model for the variance of the advection term is the variance of the right side of

Eq. (15):

$$\left\langle \left| \int_0^t ds\ \eta_\theta(\boldsymbol{k};t,s)\theta(\boldsymbol{k},s) + ik_i \int d\boldsymbol{p}d\boldsymbol{q}\ \delta(\boldsymbol{k}-\boldsymbol{p}-\boldsymbol{q})\xi_\theta(\boldsymbol{p},t)\xi_i(\boldsymbol{q},t) \right|^2 \right\rangle$$

$$= \int_0^t ds \int_0^t ds'\ \eta_\theta(\boldsymbol{k};t,s)\eta_\theta(\boldsymbol{k};t,s')\langle\theta(\boldsymbol{k},s)\theta(-\boldsymbol{k},s')\rangle \tag{16}$$

$$-2ik_i \int d\boldsymbol{p}d\boldsymbol{q}\ \delta(\boldsymbol{k}-\boldsymbol{p}-\boldsymbol{q}) \int_0^t ds\ \eta_\theta(\boldsymbol{k};t,s)\ \langle\xi_\theta(-\boldsymbol{p},t)\xi_i(-\boldsymbol{q},t)\theta(\boldsymbol{k},s)\rangle \tag{17}$$

$$+k_ik_j \int d\boldsymbol{p}d\boldsymbol{q}\ \int d\boldsymbol{p}'d\boldsymbol{q}'\ \delta(\boldsymbol{k}-\boldsymbol{p}-\boldsymbol{q})\delta(\boldsymbol{k}-\boldsymbol{p}'-\boldsymbol{q}')\langle\xi_\theta(\boldsymbol{p},t)\xi_i(\boldsymbol{q},t)\xi_\theta(-\boldsymbol{p}',t)\xi_j(-\boldsymbol{q}',t)\rangle. \tag{18}$$

The rules for correlations of Gaussian variables, and the relations Eqs. (11) and (12) give for the term in Eq. (18),

$$k_ik_j \int d\boldsymbol{p}d\boldsymbol{q}\ \int d\boldsymbol{p}'d\boldsymbol{q}'\ \delta(\boldsymbol{k}-\boldsymbol{p}-\boldsymbol{q})\delta(-\boldsymbol{k}-\boldsymbol{p}'-\boldsymbol{q}')\langle\xi_\theta(\boldsymbol{p},t)\xi_i(\boldsymbol{q},t)\xi_\theta(\boldsymbol{p}',t)\xi_i(\boldsymbol{q}',t)\rangle$$

$$= k_ik_j \int d\boldsymbol{p}d\boldsymbol{q}\ \delta(\boldsymbol{k}-\boldsymbol{p}-\boldsymbol{q})U_\theta(\boldsymbol{p},t)U_{ij}(\boldsymbol{q},t) = W_\theta^G(\boldsymbol{k},t), \tag{19}$$

so that, as was evident from its definition, this term simply reproduces the Gaussian contribution Eq. (7). The remaining terms are cumulant corrections. Obviously, the term in Eq. (16) is simply

$$\int_0^t ds \int_0^t ds'\ \eta_\theta(\boldsymbol{k};t,s)\eta_\theta(\boldsymbol{k};t,s')\langle\theta(\boldsymbol{k},s)\theta(-\boldsymbol{k},s')\rangle$$

$$= k_ik_jk_mk_n \int_0^t ds \int_0^t ds'\ \int d\boldsymbol{p}\,d\boldsymbol{q}\ \delta(\boldsymbol{k}-\boldsymbol{p}-\boldsymbol{q})\ \int d\boldsymbol{p}'\,d\boldsymbol{q}'\ \delta(\boldsymbol{k}-\boldsymbol{p}'-\boldsymbol{q}')$$

$$\times G_\theta(\boldsymbol{p};t,s)U_{ij}(\boldsymbol{q};t,s)G_\theta(\boldsymbol{p}';t,s')U_{mn}(\boldsymbol{q}';t,s')U_\theta(\boldsymbol{k};s,s'), \tag{20}$$

where we have used the definition Eq. (13) of η_θ.

The term in Eq. (17) is evaluated by expressing θ in terms of the ξ_θ and ξ_i using Eq. (14), so that

$$-2ik_i \int d\boldsymbol{p}d\boldsymbol{q}\ \delta(\boldsymbol{k}-\boldsymbol{p}-\boldsymbol{q}) \int_0^t ds\ \eta_\theta(\boldsymbol{k};t,s)\ \langle\xi_\theta(-\boldsymbol{p},t)\xi_i(-\boldsymbol{q},t)\theta(\boldsymbol{k},s)\rangle$$

$$= -2ik_i(-ik_j) \int d\boldsymbol{p}d\boldsymbol{q}\ \int d\boldsymbol{p}''d\boldsymbol{q}''\ \delta(\boldsymbol{k}-\boldsymbol{p}-\boldsymbol{q})\delta(\boldsymbol{k}-\boldsymbol{p}''-\boldsymbol{q}'') \int_0^t ds$$

$$\times \int_0^s ds'\ \eta_\theta(\boldsymbol{k};t,s)G_\theta(\boldsymbol{k};s,s')$$

$$\times \left\langle\xi_\theta(-\boldsymbol{p},t)\xi_i(-\boldsymbol{q},t)\xi_\theta(\boldsymbol{p}'',s')\xi_j(\boldsymbol{q}'',s')\right\rangle$$

$$= -2k_ik_jk_mk_n \int d\boldsymbol{p}d\boldsymbol{q}\ \int d\boldsymbol{p}'d\boldsymbol{q}'\ \delta(\boldsymbol{k}-\boldsymbol{p}-\boldsymbol{q})\delta(\boldsymbol{k}-\boldsymbol{p}'-\boldsymbol{q}') \int_0^t ds\ \int_0^s ds'$$

$$\times G_\theta(\boldsymbol{p}';t,s)U_{mn}(\boldsymbol{q}';t,s)G_\theta(\boldsymbol{k};s,s')U_\theta(\boldsymbol{p};t,s')U_{ij}(\boldsymbol{q};t,s'). \tag{21}$$

The cumulant contribution W_θ^C is the sum of the results of Eqs. (20) and (21). But to express the result in the most transparent form, it will be useful to reformulate Eq. (20) somewhat: abbreviating

the integrand for simplicity,

$$\int_0^t ds \int_0^t ds'\, \mathcal{I}(\boldsymbol{p},\boldsymbol{q},\boldsymbol{p}',\boldsymbol{q}';t,s,s') = \left(\int_0^t ds \int_0^s ds' + \int_0^t ds \int_s^t ds'\right) \mathcal{I}(\boldsymbol{p},\boldsymbol{q},\boldsymbol{p}',\boldsymbol{q}';t,s,s')$$
$$= \left(\int_0^t ds \int_0^s ds' + \int_0^t ds' \int_0^{s'} ds\right) \mathcal{I}(\boldsymbol{p},\boldsymbol{q},\boldsymbol{p}',\boldsymbol{q}';t,s,s'), \tag{22}$$

where the order of integration has been interchanged in the second term. Since the integrand is invariant under the simultaneous interchanges of s, s' and $\boldsymbol{p}$, $\boldsymbol{p}'$, we obviously have

$$\int_0^t ds \int_0^t ds'\, \mathcal{I}(\boldsymbol{p},\boldsymbol{q},\boldsymbol{p}',\boldsymbol{q}';t,s,s') = 2\int_0^t ds \int_0^s ds'\, \mathcal{I}(\boldsymbol{p},\boldsymbol{q},\boldsymbol{p}',\boldsymbol{q}';t,s,s'), \tag{23}$$

so we can write

$$\int_0^t ds \int_0^t ds'\, \eta_\theta(\boldsymbol{k};t,s)\eta_\theta(\boldsymbol{k};t,s')\langle\theta(\boldsymbol{k},s)\theta(-\boldsymbol{k},s')\rangle$$
$$= 2k_ik_jk_mk_n \int_0^t ds \int_0^s ds' \int d\boldsymbol{p}\, d\boldsymbol{q}\, \delta(\boldsymbol{k}-\boldsymbol{p}-\boldsymbol{q}) \int d\boldsymbol{p}'\, d\boldsymbol{q}'\, \delta(\boldsymbol{k}-\boldsymbol{p}'-\boldsymbol{q}')$$
$$\times G_\theta(\boldsymbol{p};t,s)U_{ij}(\boldsymbol{q};t,s)G_\theta(\boldsymbol{p}';t,s')U_{mn}(\boldsymbol{q}';t,s')U_\theta(\boldsymbol{k};s,s'). \tag{24}$$

Interchanging indices (ij) and (mn) and the wavevector arguments $(\boldsymbol{p},\boldsymbol{q})$ and $(\boldsymbol{p}',\boldsymbol{q}')$ and adding the result of Eq. (21), we obtain

$$W_\theta^C(\boldsymbol{k},t) = -2k_ik_jk_mk_n \int d\boldsymbol{p}\, d\boldsymbol{q} \int d\boldsymbol{p}'\, d\boldsymbol{q}'\, \delta(\boldsymbol{k}-\boldsymbol{p}-\boldsymbol{q})\delta(\boldsymbol{k}-\boldsymbol{p}'-\boldsymbol{q}')$$
$$\times \int_0^t ds \int_0^s ds'\, U_{ij}(\boldsymbol{q};t,s)U_{mn}(\boldsymbol{q}';t,s')$$
$$\times \left[G_\theta(\boldsymbol{p};t,s)G_\theta(\boldsymbol{p}';t,s')U_\theta(\boldsymbol{k};s,s') - G_\theta(\boldsymbol{p}';t,s)G_\theta(\boldsymbol{k};s,s')U_\theta(\boldsymbol{p};t,s')\right]. \tag{25}$$

This expression makes clear an important property of the DIA cumulant correction, namely that it vanishes identically, independently of the velocity field, in the scalar *non-diffusive truncated ensemble* when diffusivity $\alpha = 0$ and a maximum wavenumber is imposed on the scalar fluctuations. This equilibrium ensemble is Gaussian, therefore all cumulants vanish. The proof follows from the properties of this system, that the scalar field is in steady-state equipartition, so that $U_\theta(\boldsymbol{k},t)$ is a constant, and the fluctuation-dissipation relation

$$U_\theta(\boldsymbol{k};t,t') = U_\theta(\boldsymbol{k})[G_\theta(\boldsymbol{k};t,t') + G_\theta(\boldsymbol{k};t',t)] \tag{26}$$

holds. (Note that the response function is *causal*: $G_\theta(\boldsymbol{k};t,t') = 0$ for $t' > t$.) Substituting these relations in Eq. (25) shows at once that $W_\theta^C \equiv 0$ independently of the velocity field, as required. We remark that this conclusion is a non-trivial check of the DIA calculation, since DIA only treats moments, and the multipoint probability density functions play no explicit role.

It is easily verified that the same result holds for the cumulant corrections to the mean-square nonlinearity in the analysis of the velocity field.

III. NUMERICAL EVALUATION OF THE DIA CUMULANT CORRECTIONS

At this point, we introduce the assumption that the velocity field is time stationary and that the scalar field is maintained in a steady state by a scalar source term. Then numerical evaluation is greatly simplified by expressing the results in terms of spectra rather than correlations. If $W_\theta(\boldsymbol{k})$ depends only on $k = |\boldsymbol{k}|$, then the corresponding spectrum is

$$w_\theta(k) = \oint dS(\boldsymbol{k})\, W_\theta(\boldsymbol{k}) = 4\pi k^2 W_\theta(k) \tag{27}$$

and, corresponding to Eq. (6), we have

$$w_\theta(k) = w_\theta^G(k) + w_\theta^C(k). \tag{28}$$

We introduce the usual energy and scalar fluctuation spectra by

$$U_{ij}(\boldsymbol{k}) = \frac{1}{4\pi k^2} E(k)(\delta_{ij} - k^{-2}k_i k_j) \quad U_\theta(\boldsymbol{k}) = \frac{1}{2\pi k^2} E_\theta(k). \tag{29}$$

With these simplifications, Eq. (7) can be reformulated, following procedures that are standard in the closure literature, as

$$w_\theta^G(k) = k^3 \int_\Delta (1 - z^2) E(p) E_\theta(q) \frac{dp}{p} \frac{dq}{q}, \tag{30}$$

where, as usual, the integration region Δ indicates that the wavenumbers k, p, q are the sides of a triangle and z is the cosine of the angle between the sides of lengths k and p. The time integrations in Eq. (25) are evaluated by replacing the two-time quantities by functions of time difference only, then passing to the steady state limit $t \to \infty$. Since we wanted to be able to compute the cumulants under a variety of conditions, we found it expedient to make the double time integrations of Eq. (25) analytically computable by assuming simple exponential time-dependence

$$\begin{aligned} G_\theta(\boldsymbol{k}; t - t') &= e^{-\eta_\theta(k)(t-t')} H(t - t'), \quad U_\theta(\boldsymbol{k}; t - t') = U_\theta(\boldsymbol{k}) e^{-\eta_\theta(k)|t-t'|}, \\ U_{ij}(\boldsymbol{k}; t - t') &= U_{ij}(\boldsymbol{k}) e^{-\eta_\theta(k)|t-t'|}. \end{aligned} \tag{31}$$

As usual, $H(s)$ is the "Heaviside function" equal to one for $s > 0$ and zero otherwise; we have also introduced a "fluctuation-dissipation" relation in which the damping function η_θ is the same in the scalar response function G_θ and two-time correlation function U_θ. The very commonly introduced exponential *ansatz* for the two-time dependence is also made by Herring and Métais;[10] we emphasize that we use it entirely in the interest of analytical simplicity, and no assertion is made that it approximates the two-time response that would actually be predicted by DIA. But since two-time statistics enter our results only after integration over all time-differences, any resulting errors are unlikely to be qualitatively important.

After making all of these simplifications, the cumulant spectrum is evaluated as

$$\begin{aligned} w_\theta^C(k) = \frac{1}{2} \int_\Delta \frac{dp}{p} \frac{dq}{q} \int_{\Delta'} \frac{dp'}{p'} \frac{dq'}{q'} (1 - z^2) k q^2 E(p) (1 - z'^2) k q'^2 E(p') \\ \times \left[\left(\Xi_{kpqp'q'} + \Xi_{kp'q'pq} \right) E_\theta(k) - 2 \Xi_{kpqp'q'} (k/q)^2 E_\theta(q) \right], \end{aligned} \tag{32}$$

where Δ' indicates that the wavenumbers k, p', q' are the sides of a triangle, z' is the cosine of the angle between the sides of lengths k and p', and the time integrals yield

$$\Xi_{kpqp'q'} = \frac{1}{\eta_\theta(k) + \eta(p') + \eta_\theta(q')} \frac{1}{\eta(p) + \eta_\theta(q) + \eta(p') + \eta_\theta(q')}. \tag{33}$$

The spectra $E(k)$ and $E_\theta(k)$ are evaluated using EDQNM (Eddy-Damped Quasi-Normal Markovian) closures[14,15]

$$\left[\frac{\partial}{\partial t} + 2\nu k^2 \right] E(k) = \int_\Delta \Theta(k, p, q)[xy + z^3] p E(q) \left[k^2 E(p) - p^2 E(k) \right] \frac{dpdq}{pq} + F(k), \tag{34}$$

$$\left[\frac{\partial}{\partial t} + 2\alpha k^2 \right] E_\theta(k) = \int_\Delta \Theta^\theta(k, p, q)[1 - y^2] k E(q) \left[k^2 E_\theta(p) - p^2 E_\theta(k) \right] \frac{dpdq}{pq} + F_\theta(k), \tag{35}$$

in which $F(k)$ and $F_\theta(k)$ are external forcing terms confined to the smallest wavenumbers (both $F(k)$ and $F_\theta(k)$ are unity for $k \leq 2$ and zero elsewhere), x is the cosine of the angle between the sides of lengths p and q, and y is the cosine of the angle between the sides of lengths k and q. The triad

relaxation times $\Theta(k, p, q)$ and $\Theta^\theta(k, p, q)$ are

$$\Theta = \frac{1}{\eta(k) + \eta(p) + \eta(q)}, \qquad \Theta^\theta = \frac{1}{\eta_\theta(k) + \eta(p) + \eta_\theta(q)}. \tag{36}$$

We use the (inverse) time-scales

$$\eta(k) = \lambda\sqrt{\int_0^k E(r)dr} + \nu k^2, \qquad \eta_\theta(k) = \lambda_\theta\sqrt{\int_0^k E(r)dr} + \alpha k^2 \tag{37}$$

and we set the constants $\lambda = \lambda_\theta = 0.5$. Note that η and η_θ are the same quantities that appear in Eq. (31). An interesting perspective for future work would be the use of a Lagrangian two-time theory[16,17] or a self-consistent Markovian closure[18,19] to evaluate the cumulants, which would avoid the introduction of adjustable constants and *ad hoc* formulation of damping time-scales. Computations are carried out on a logarithmically spaced grid with 36 gridpoints per octave and results are evaluated when a steady state is reached.

IV. NUMERICAL COMPARISONS

In this section, we confirm the reduction of mean-square advection in DNS data,[10] and compare the results with closure predictions. We have computed the scalar spectrum and energy spectrum by closure theory as described in Sec. III and the parameters have been chosen to match the DNS as closely as possible. The DNS database used is from high resolution (1024^3 gridpoint) pseudospectral direct numerical simulations of a passive scalar advected by isotropic turbulence.[20] The force terms for the velocity and scalar fluctuations are random-Gaussian and delta-correlated in time (and solenoidal for the velocity forcing), acting in the wave-number range $1 \le k \le 2$. In these simulations the Reynolds number based on the Taylor microscale is equal to 427 and the Prandtl number $\mathcal{P}r = \nu/\alpha = 1$. The resolution is higher than that used in the simulations of both Herring and Métais[10] and Chen *et al.*[1]

Using DNS data, $w_\theta(k)$ can be determined from Eqs. (4) and (27). The contribution $w_\theta^G(k)$ is obtained by randomizing the phases of the Fourier amplitudes of $\theta(\boldsymbol{x}, t)$; this randomization will yield scalar fields with statistically independent Fourier amplitudes without changing the wavenumber spectra. This independence, not the probability density function itself, is the key property for us. The fields are therefore random-phase fields and the amplitude statistics are not necessarily Gaussian.

Figure 1 compares the scalar variance spectra in DNS and the closure computations at $R_\lambda = 427$ and $\mathcal{P}r = 1$. The inset shows the energy spectra. The wavenumber of these results is normalized by the Kolmogorov scale, which is equal to the Batchelor scale for unit Prandtl number. Good agreement is observed between the DNS results and the EDQNM results. A Corrsin-Obukhov inertial range for the scalar spectrum and a Kolmogorov inertial range for the energy spectrum, both approximately proportional to $k^{-5/3}$ are clearly observed.

In Figure 2, left, the spectrum of the advection term $w_\theta(k)$ is shown, as well as its Gaussian estimate. These spectra, for both closure and DNS, display an increasing trend in the inertial range and peak around the Batchelor scale. The peak of $w_\theta(k)$ is smaller than the Gaussian value, which indicates a reduction of mean-square advection. This reduction is more clearly observed in Figure 2, right, in which we display the measure of the departure from Gaussianity, the ratio $w_\theta(k)/w_\theta^G(k)$;[10] the analogous quantity for the velocity field was introduced by Kraichnan and Panda.[4] The ratio departs noticeably from the Gaussian values over the entire wavenumber range, and a significant depression of the $w_\theta(k)$ compared to the Gaussian value is observed at scales larger than the forcing scales. The region where $w_\theta(k)/w_\theta^G(k) < 1$ extends over the entire inertial-convective range. These general trends, including the observation that $w_\theta(k)/w_\theta^G(k) > 1$ at large scales, are consistent with previous observations.[1,10] The results in Figures 1 and 2 show that the closure yields results in good agreement with the DNS.

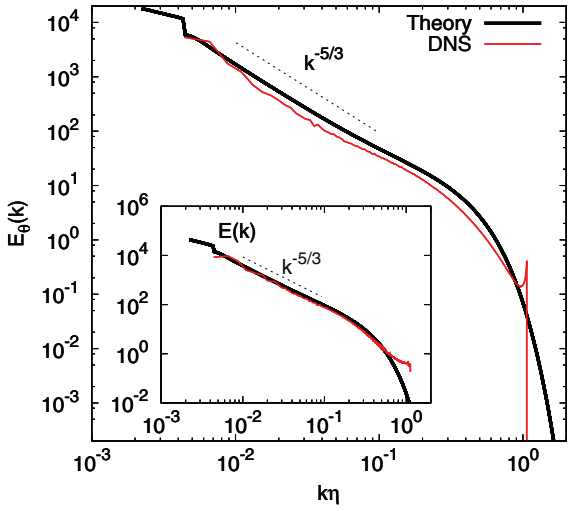

FIG. 1. DNS and theoretical results for the scalar spectra in isotropic turbulence at a Taylor-scale Reynolds number of 427 and $\mathcal{P}r = 1$. In the inset the energy spectra are shown.

The ratio of the measured variance to the value assuming independence of the Fourier amplitudes,

$$\rho_\theta = \frac{\langle (\boldsymbol{u} \cdot \nabla\theta)^2 \rangle}{\langle |\boldsymbol{u}|^2 \rangle \langle |\nabla\theta|^2 \rangle} = \frac{\int_0^\infty w_\theta(k) dk}{\int_0^\infty w_\theta^G(k) dk} \tag{38}$$

is also of interest. Figure 2 (left) shows that the spectrum $w_\theta(k)$ is an increasing function of the wavenumber, consequently its integral is dominated by the small scales, where the variance is reduced. The DNS value for ρ_θ is 0.41 and the closure value is 0.54. These values are consistent with the previous reported results: Herring and Métais[10] quotes a value for ρ_θ of about 0.5 in the scalar case, and Kraichnan and Panda[4] reported the value 0.57 for the comparable ratio of the mean-square nonlinearity. We conclude that the effect we investigate is observed in DNS and closure and is of comparable magnitude in both.

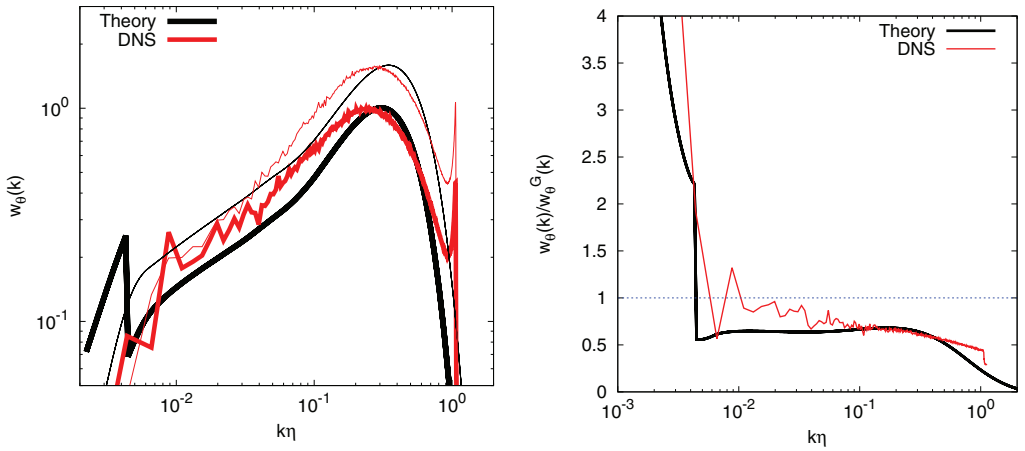

FIG. 2. DNS and theoretical results in isotropic turbulence at a Taylor-scale Reynolds number of 427 and $\mathcal{P}r = 1$. Left: Spectrum of the mean square advection term of the scalar equation in isotropic turbulence. Also shown are the Gaussian spectra (thin lines). Right: Ratio of the spectra to the Gaussian spectra.

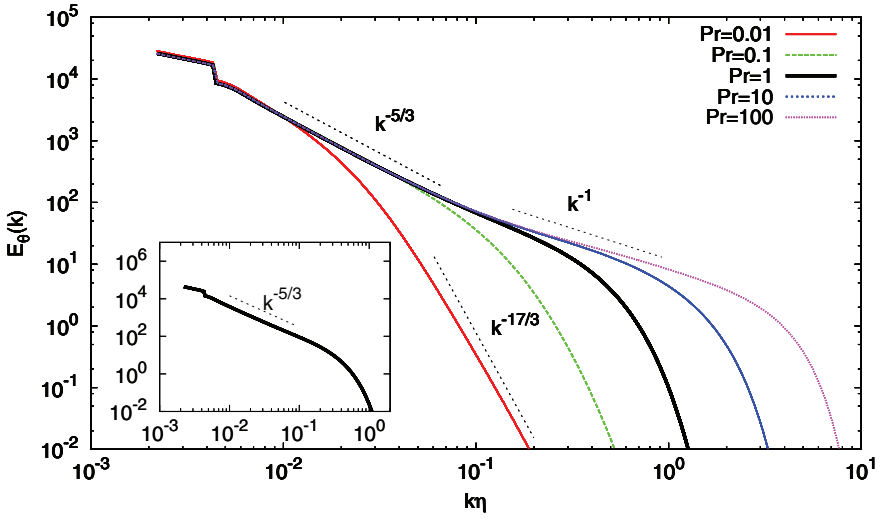

FIG. 3. Closure results for the spectrum of the scalar variance at a Taylor-scale Reynolds number of 427 and $\mathcal{P}r = 0.01, \ldots, 100$. Inset: Energy spectrum.

In problems involving passive scalars, the dependence on Prandtl number is always of interest. We investigate the effect of the Prandtl number on the reduction of mean-square advection by varying the Prandtl number from 0.01 to 100 at a fixed Reynolds number $R_\lambda = 427$. There is no DNS data available for these cases, in particular for the high Prandtl number cases, so we limit the discussion to closure predictions. Figures 3 and 4 show the closure results. In Figure 3 we show the scalar spectrum for five different Prandtl numbers. At low Prandtl numbers the $k^{-17/3}$ spectrum is observed and at large $\mathcal{P}r$ we observe a k^{-1} spectrum.[21,22]

Figure 4 (left) shows the spectrum of the advection term. For all $\mathcal{P}r$, this spectrum is an increasing function of the wavenumber. At the highest value of $\mathcal{P}r$, the spectrum seems to approach its Gaussian estimate. Figure 4 (right) shows $w_\theta(k)/w_\theta^G(k)$. It is clearly observed that the spectrum is under its Gaussian value for all scales, except the forced scales, but the precise behavior seems to depend strongly on the Prandtl number. In the inertial-convective range the depletion is approximately constant with respect to wavenumber. The effect is weaker in the Batchelor range.

The numerical values of ρ_θ are displayed in Figure 5. The value ranges from a minimum of $\rho_\theta = 0.38$ at $\mathcal{P}r = 0.1$ to a maximum of $\rho_\theta = 0.8$ at $\mathcal{P}r = 100$. This change is non-negligible, but the trend is rather weak if we consider that $\mathcal{P}r$ changes over four orders of magnitude in our simulations. The reduction of advection seems thus an effect which is persistent, but becomes weaker

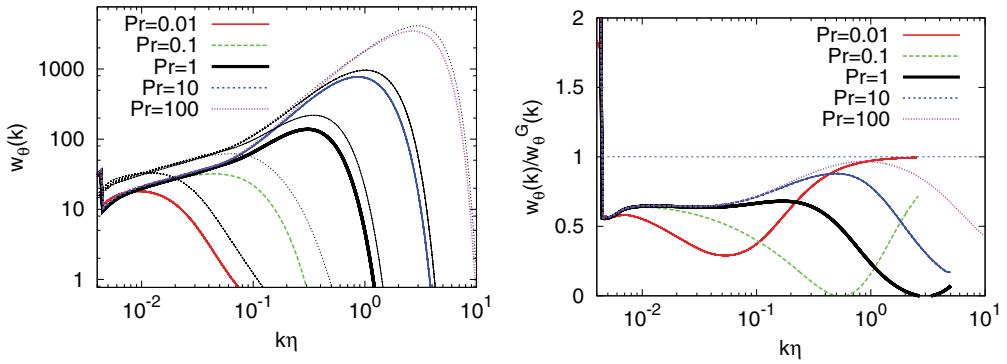

FIG. 4. Closure results for the spectrum of the mean square advection term at a Taylor-scale Reynolds number of 427 and $\mathcal{P}r = 0.01, \ldots, 100$. Also shown are the Gaussian spectra (thin lines). Right: Ratio of the spectra to the Gaussian spectra.

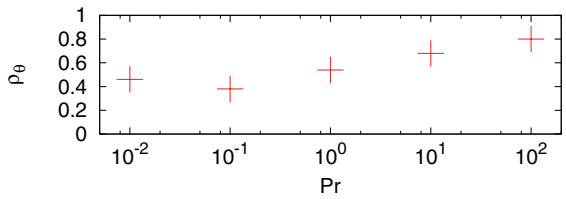

FIG. 5. The mean square advection term of the scalar equation in isotropic turbulence compared to its Gaussian value as a function of the Prandtl number at a Taylor-scale Reynolds number of 427.

for high values of the Prandtl number. Its amount is mainly determined by the precise behavior of the cumulant-spectrum around the scale where the spectrum $w_\theta(k)$ peaks.

V. DISCUSSION: MECHANISMS OF THE SUPPRESSION OF ADVECTION

The analysis of the variance of the nonlinear term in the Navier-Stokes equations by Chen *et al.*[1] was motivated in part by the suggestion of Levich and Tsinober[23] of the possibility of *Beltramization*, the preferential alignment of velocity and vorticity in turbulence. Since the nonlinear term can be written as

$$\nabla^{-2}\nabla \times \nabla \times (\boldsymbol{\omega}(\boldsymbol{x}) \times \boldsymbol{u}(\boldsymbol{x})), \tag{39}$$

with $\boldsymbol{\omega} = \nabla \times \boldsymbol{u}$ the vorticity, this alignment will obviously reduce the magnitude of the nonlinear term, and hence will also reduce the intensity of its fluctuations, which is consistent with the observed depression of nonlinearity.

Another mechanism consistent with depression of nonlinearity was identified by Kraichnan and Panda,[4] who noted that the nonlinearity also vanishes if the Lamb vector $\boldsymbol{\lambda}(\boldsymbol{x}) \equiv \boldsymbol{\omega}(\boldsymbol{x}) \times \boldsymbol{u}(\boldsymbol{x})$ is a potential field ($\boldsymbol{\lambda}(\boldsymbol{x}) = \nabla\Phi(\boldsymbol{x})$), so that it lies in the null-space of the double curl operator in Eq. (39). These two possibilities are illustrated in Figure 6 (left). Both possibilities can contribute to the depression of nonlinearity in turbulent flows.

The situation is much simpler for scalar advection. For the passive scalar, the equivalent of Beltramization would be the identical vanishing of the scalar flux vector $\boldsymbol{\gamma} = \boldsymbol{u}\theta$; this trivial case can be ignored. The only non-trivial way to reduce the advection term is for the scalar flux vector to

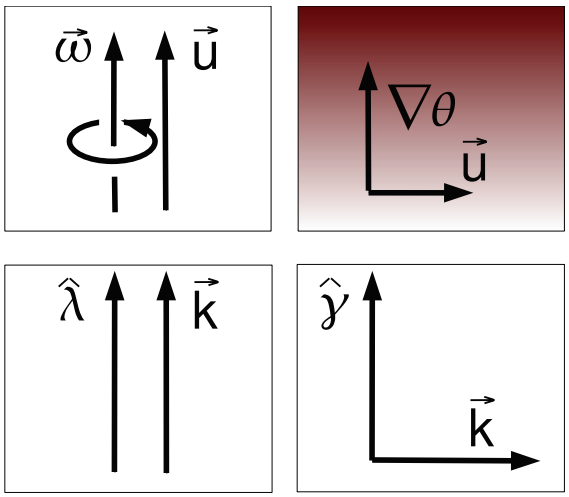

FIG. 6. Left, top: Velocity Beltramization and bottom: depression of nonlinearity through alignment of the Lamb-vector and the wavevector. Right: Depletion of advection in physical and Fourier space. The scalar flux vector is defined as $\boldsymbol{\gamma} = \boldsymbol{u}\theta$.

be divergence-free, so that

$$\nabla \cdot \boldsymbol{\gamma} = \boldsymbol{u} \cdot \nabla\theta \approx 0. \tag{40}$$

This corresponds to the case in which the velocity is perpendicular to the scalar gradient, as illustrated in Figure 6 (right). It is evident that if the variance of the advection term is smaller in passive scalar advection than in a jointly Gaussian random field, then $\boldsymbol{u}$ and $\nabla\theta$ *must* be more likely to be orthogonal in passive scalar advection than in a jointly Gaussian random field.

VI. CONCLUSIONS

We have shown that the closure computation of the fourth order cumulant that enters in the depression of nonlinearity in hydrodynamic turbulence[1] can be applied to passive scalar advection. Corresponding to depression of nonlinearity is a reduction of the variance of the advection term, which is connected to a tendency of the velocity vector to align perpendicular to the scalar gradient. Study at the level of Fourier spectra shows that the reduction of advection is approximately constant in the inertial-convective range and becomes weaker in the viscous-convective (Batchelor) range. Closure related to the DIA gives satisfactory predictions in comparison to DNS data. Closure predicts that the phenomenon persists at both low and high Prandtl numbers although there is a weak but noticeable tendency for the mean-square advection to return to the Gaussian value as the Prandtl number increases.

ACKNOWLEDGMENTS

The authors are indebted to Toshiyuki Gotoh for discussions and for making the DNS data available. Part of the DNS data was downloaded from the CINECA database.

[1] H. Chen, J. Herring, R. Kerr, and R. Kraichnan, "Non-Gaussian statistics in isotropic turbulence," Phys. Fluids A **1**, 1844 (1989).
[2] J. Fung, J. Hunt, N. Malik, and R. Perkins, "Kinematic simulation of homogeneous turbulence by unsteady random Fourier modes," J. Fluid Mech. **236**, 281 (1992).
[3] R. Kraichnan, "Diffusion by a random velocity field," Phys. Fluids **13**, 22 (1970).
[4] R. Kraichnan and R. Panda, "Depression of nonlinearity in decaying isotropic turbulence," Phys. Fluids **31**, 2395 (1988).
[5] H. Moffatt and A. Tsinober, "Helicity in laminar and turbulent flow," Annu. Rev. Fluid Mech. **24**, 281 (1992).
[6] R. Kraichnan, "The structure of isotropic turbulence at very high Reynolds numbers," J. Fluid Mech. **5**, 497–543 (1959).
[7] T. Tatsumi, "The theory of decay process of incompressible isotropic turbulence," Proc. R. Soc. London, Ser. A **239**, 16 (1957).
[8] I. Proudman, "On Kraichnan's theory of turbulence," in *Mécanique de la Turbulence, Coll. Internationale du CNRS à Marseille* (CNRS, Paris, 1962), pp. 107–112.
[9] R. Kraichnan, "Relations among some deductive theories of turbulence," in *Mécanique de la Turbulence, Coll. Internationale du CNRS à Marseille* (CNRS, Paris, 1962), pp. 99–106.
[10] J. Herring and O. Métais, "Spectral transfer and bispectra for turbulence with passive scalars," J. Fluid Mech. **235**, 103 (1992).
[11] T. Ishihara, T. Gotoh, and Y. Kaneda, "Study of high Reynolds number isotropic turbulence by direct numerical simulation," Annu. Rev. Fluid Mech. **41**, 65 (2009).
[12] R. Kraichnan, "Convergents to turbulence functions," J. Fluid Mech. **41**, 189 (1970).
[13] G. R. Newman and J. Herring, "A test field model of a passive scalar in isotropic turbulence," J. Fluid Mech. **94**, 163 (1979).
[14] S. Orszag, "Analytical theories of turbulence," J. Fluid Mech. **41**, 363 (1970).
[15] J. Herring, D. Schertzer, M. Lesieur, G. Newman, J. Chollet, and M. Larcheveque, "A comparative assessment of spectral closures as applied to passive scalar diffusion," J. Fluid Mech. **124**, 411 (1982).
[16] R. Kraichnan, "Lagrangian-history closure approximation for turbulence," Phys. Fluids **8**, 575 (1965).
[17] Y. Kaneda, "Renormalized expansions in the theory of turbulence with the use of the Lagrangian position function," J. Fluid. Mech. **107**, 131–145 (1981).
[18] R. Kraichnan, "An almost-Markovian Galilean-invariant turbulence model," J. Fluid Mech. **47**, 513 (1971).
[19] W. Bos and J.-P. Bertoglio, "A single-time two-point closure based on fluid particle displacements," Phys. Fluids **18**, 031706 (2006).
[20] T. Watanabe and T. Gotoh, "Statistics of a passive scalar in homogeneous turbulence," New J. Phys. **6**, 40 (2004).
[21] G. Batchelor, I. D. Howells, and A. A. Townsend, "Small-scale variation of convected quantities like temperature in turbulent fluid Part 2. The case of large conductivity," J. Fluid Mech. **5**, 134 (1959).
[22] G. Batchelor, "Small-scale variation of convected quantities like temperature in turbulent fluid. Part 1. General discussion and the case of small conductivity," J. Fluid Mech. **5**, 113 (1959).

[23] E. Levich and A. Tsinober, "On the role of helical structures in three-dimensional turbulent flow," Phys. Lett. A **93**, 293 (1983).

[24] Proudman observed that the quasinormality hypothesis selects precisely the "direct interactions" retained in the analysis of the equations for third order moments by Kraichnan in DIA; in Proudman's own words,"[T]he zero-fourth-cumulant theory implies that the triple moment is non-zero only on account of interaction between its own three wavenumbers. Such a theory may be termed *a* 'direct interaction theory'. Kraichnan's theory is of this kind, and down at this conceptual level, therefore, it is closely related to zero-fourth-cumulant theories. Indeed both theories tend to have the same very general properties and to stand or fall by similar criteria." (emphasis added).

[25] Proudman's very favorable assessment of this idea is noteworthy, since otherwise, his assessment of DIA was sharply critical and even dismissive.

3.5 Perspectives

Is the observed state an extremum predictable by variational methods?

We investigate whether the observed state in which the advection is reduced is the *minimum* advection state given a fixed variance (or another fixed quantity). We therefore use a standard variational method. We define the Lagrangian,

$$\Lambda = \int (\boldsymbol{u} \cdot \nabla\theta)^2 - \beta\theta^2 dV, \tag{3.19}$$

in which β is a Lagrange multiplier. We will consider an imposed velocity field so that only the scalar and the scalar gradients can evolve in time. In order to have an extremum, the variation of Λ needs to be zero. This implies (in two dimensions)

$$\delta\Lambda = \int \frac{\partial\Lambda}{\partial\theta} - \frac{d}{dx}\frac{\partial\Lambda}{\partial(\partial\theta/\partial x)} - \frac{d}{dy}\frac{\partial\Lambda}{\partial(\partial\theta/\partial y)} dx\ dy = 0, \tag{3.20}$$

which gives,

$$\theta = -\frac{1}{\beta}\nabla \cdot [(\boldsymbol{u} \cdot \nabla\theta)\boldsymbol{u}]\,. \tag{3.21}$$

If a scatterplot of the results of a simulation or experiment of scalar mixing will yield a linear relation between θ and $\nabla \cdot [(\boldsymbol{u} \cdot \nabla\theta)\boldsymbol{u}]$, then we will have shown that the mixing process minimizes the advection term for a given value of the scalar variance. This would have important implications, in particular for the interpretation of the depletion of nonlinearity in Navier-Stokes turbulence. This remains to be done.

The origin of non-vanishing anisotropy of the passive scalar field, forced by a mean gradient

In three-dimensional isotropic turbulence, the gradients of the scalar field and velocity field are determined by the smallest scales. One of Kolmogorov's assumptions on turbulent flows, is that at high enough Reynolds numbers the velocity field should be approximately isotropic at the small scales, even when the large scales are not so. This assumption of local isotropy of the small scales is approximately valid in most high Reynolds numbers turbulent flows. A well known counter-example is the small scale structure of the scalar field in the presence of a uniform imposed gradient. In this case, the skewness of the scalar-gradients aligned with the mean gradient,

$$S_\theta = \frac{\langle(\partial\theta/\partial x_3)^3\rangle}{\langle(\partial\theta/\partial x_3)^2\rangle^{3/2}}, \tag{3.22}$$

is of order unity, and does not seem to decrease with Reynolds number [96]. In an isotropic passive scalar field this quantity should be zero. Arguments have been presented to explain this puzzling observation [97]. But in my opinion no satisfactory explanation is given. In section 2.7, we exploited the analogy between a passive scalar field generated by a uniform imposed gradient on an

isotropic turbulence and the displacement of fluid particles. We will try to give an explanation of the non-vanishing skewness S_θ, using this analogy.

The rationale is as follows: the scalar field possesses an anisotropy, due to the direction of the mean gradient. However, the displacement field is isotropic, and the scalar is obtained by projecting the displacement on a typical direction. The displacement field is given by the equation,

$$\frac{\partial X_i}{\partial t} + u_j \frac{\partial X_i}{\partial x_j} = u_i \tag{3.23}$$

and the general displacement variance tensor can be defined by

$$\Phi^X_{ij}(\boldsymbol{k}) = \overline{X_i(\boldsymbol{k}) X_j(\boldsymbol{k})^*}. \tag{3.24}$$

In an isotropic field, this tensor can be decomposed into a solenoidal part and a potential part,

$$\Phi^X_{ij}(\boldsymbol{k}) = F_s(k) P_{ij}(\boldsymbol{k}) + F_p(k) \Pi_{ij}(\boldsymbol{k}), \tag{3.25}$$

with $\Pi_{ij}(\boldsymbol{k}) = k_i k_j / k^2$.

The passive scalar spectrum is now obtained by considering one component of the trace, for example, if the mean gradient is imposed in the x_3 direction,

$$\Phi_\theta(\boldsymbol{k}) = \Phi^X_{33}(\boldsymbol{k}) = (1-\mu^2) F_s(k) + \mu^2 F_p(k) = F_s(k) + \mu^2 (F_p(k) - F_s(k)), \tag{3.26}$$

where $\mu = k_3/k$, the cosine of the angle between the wavevector and the direction of the gradient. It is directly seen that this quantity is inherently anisotropic if $F_p(k) \neq F_s(k)$. Small scale isotropy will only be retrieved if

$$\lim_{k\to\infty} \frac{F_p(k) - F_s(k)}{F_s(k)} \to 0. \tag{3.27}$$

This does however not imply that the skewness S_θ of the scalar gradients vanishes at small scales. As a counter example we can consider the case of an isotropic velocity field. The skewness of the gradients of such a field is not zero at small scales. I will derive the closure expressions for $F_p(k)$, $F_s(k)$, analyze their inertial range behavior, and compute the prediction for S_θ.

Depletion of nonlinearity in inhomogeneous turbulence

In the framework of the PhD project of Andrey Pushkarev, we investigate the depletion of nonlinearity in wall-bounded flow by means of Direct Numerical Simulation. In Figure 3.12 we show preliminary results on the turbulent flow decaying between two parallel walls. It is observed that the mean-square nonlinearity, normalized by the product of enstrophy and energy, is unaffected in the center of the domain, but that strongly super-Gaussian values are observed near the boundaries. The interpretation of these results and the investigation of the case of stationary channel flow are currently in progress.

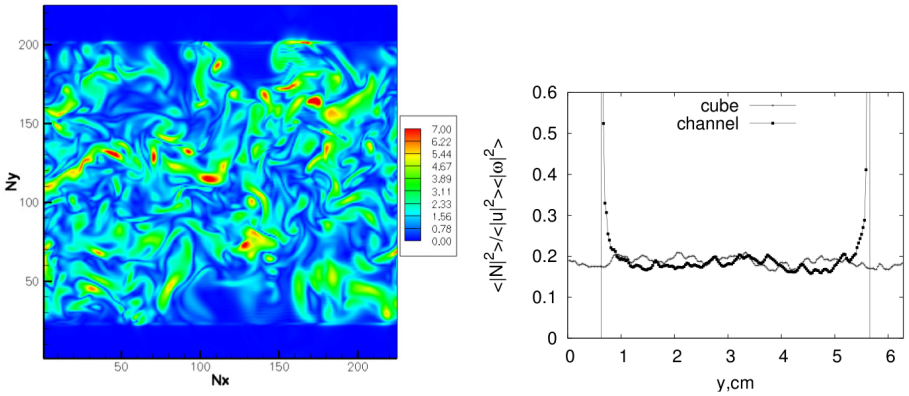

Figure 3.12: Left: isovalues of the enstrophy in decaying wall bounded turbulence. Right: the normalized value of the mean-square nonlinearity compared to observations in freely decaying turbulence in a periodic domain.

Chapter 4

Magnetized plasmas and two-dimensional turbulence

4.1 Introduction: the fluid mechanics of fusion plasmas

Most of the existing magnetically confined fusion plasmas move and are turbulent, which is sometimes quite a problem. Indeed, in order to get a nuclear fusion reaction started, and to keep it going, one needs to obtain high temperatures and the hot plasma is supposed to be kept in place by the magnetic field. The amount of energy created by a fusion reaction is measured by the triple-product $nT\tau$, in which n is the plasma density, T the temperature and τ the confinement time. If the plasma deviates too far from its equilibrium position, and if convective plasma movements transport heat from the center to the edge of the plasma, the temperature can drop so that the fusion reaction stops, and wall components can be damaged after contact with the plasma. Intuitively it is quite understandable that keeping the plasma in place is not an obvious task, since the plasma core is ideally at a temperature of several hundreds of thousands of degrees (hotter than the sun), while the outside, at only a meter distance or so, is at room temperature. Extremely large temperature, pressure and density gradients are thus present, which combined with the curvature of the magnetic field lead to an uncountable number of instabilities.

To understand the origin and dynamics of the turbulent movements of fusion plasmas, it is important to first briefly describe the magnetic geometry of these plasmas. At the high temperatures at which fusion-reactions can be sustained, gases will get ionized, which means that electrons get decoupled from the ions. A magnetic field can then be used for confinement of this gas of charged particles. Charged particles will describe a helical motion around magnetic field lines, due to the Lorentz force, which exerts a force on the particles both perpendicular to their velocity and perpendicular to the magnetic field. If we neglect all other forces on the particle, the velocity will evolve according to

$$m\dot{\boldsymbol{v}} = q\boldsymbol{v} \times \boldsymbol{b}, \tag{4.1}$$

with m the mass, q the charge and $\boldsymbol{v}$ the velocity of the particle. $\boldsymbol{b}$ is the magnetic field, that we will choose homogeneous in this example. For a finite

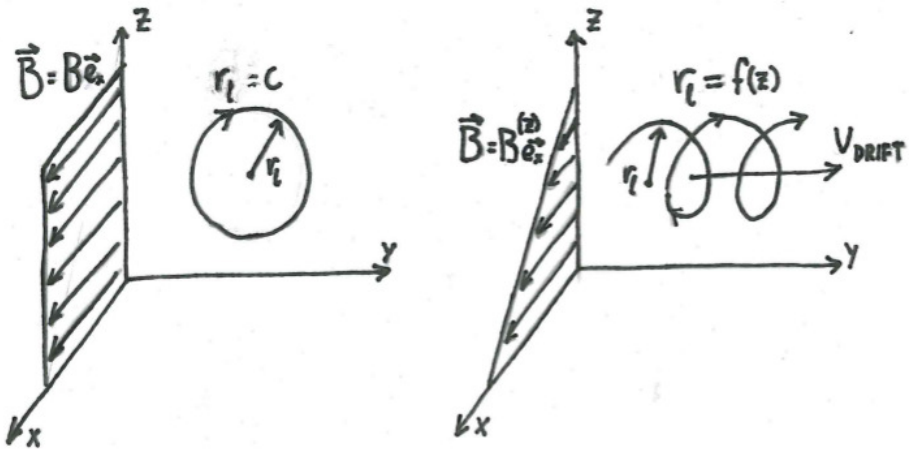

Figure 4.1: Left: in a uniform magnetic field particles will describe a helical motion around the field lines. In the plane perpendicular to the magnetic field the trajectory is circular with a fixed radius r_l. Right: as soon as the magnetic field is non-uniform, r_l will become a function of position. The particle will therefore drift in a direction perpendicular to the gradient of the magnetic field.

initial velocity of the ion or electron, this will lead to a circular motion around a magnetic field line with (Larmor or gyro)-radius

$$r_l = \frac{m v_\perp}{|q| b}, \tag{4.2}$$

with b the strength of the magnetic field and $v_\perp$ the norm of the velocity of the particle in the plane perpendicular to the magnetic field. The movement of the plasma in the direction perpendicular to the magnetic field is thus constrained. Since the Lorentz force only acts in the plane perpendicular to the magnetic field, the particles can freely move in the direction of the magnetic field. By closing the magnetic field on itself in a torus, the ions and electrons will at least not escape at the ends of the magnetic field lines. However, when bending the magnetic field, necessarily inhomogeneities in the magnetic field strength will be induced, and due to this inhomogeneity the particles will drift and escape from the magnetic field. Let us describe this drift.

If, in a plane perpendicular to the magnetic field, the magnetic field is not homogeneous, the Lorentz force on the particles will vary during one circular orbit of the particle. On one side of the orbit the magnetic field is stronger than on the other. Thereby the circular motion will be deformed since the radius of the orbit-radius is inversely proportional to the magnetic field strength [equation (4.2)]. Since the orbits are no longer circular, a net velocity will result, also called drift velocity. The mechanism is sketched in Figure 4.1.

To solve this problem, the magnetic field is not only bended, but also twisted, so that the magnetic field is helically twisted on the torus. This twist is generated by superposing a poloidal magnetic field on the toroidal magnetic field (the definition of the poloidal and toroidal direction are shown in Figure 4.2).

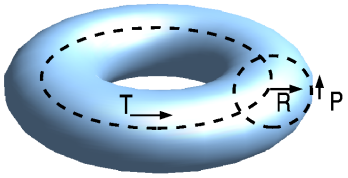

Figure 4.2: In most magnetic fusion devices the magnetic field contains a toroidal (T) and poloidal (P) magnetic component. The radial direction is indicated by (R).

The pitch at which it is twisted is called the safety-factor (number of toroidal turns for one poloidal turn) since it is directly related to an MHD instability which is dangerous in the sense that it will make the magnetic field escape from its initial position, leading to a loss of the plasma, also called a disruption. The most promising fusion reactor designs are toroidally shaped with a helically twisted magnetic field. We can mention in this context tokamaks, stellarators and reversed field pinches (RFPs), which differ only in the generation and precise geometry of the poloidal magnetic field. In stellarators both the toroidal and poloidal magnetic field are externally imposed. In the other two-geometries, tokamaks and RFPs, the toroidal magnetic field is imposed by external coils, but the poloidal field is generated by a toroidal current which is induced. In tokamaks the so-generated poloidal field is several times weaker than the toroidal field. In the RFP the current is relatively strong, corresponding to several poloidal windings of the magnetic field for one toroidal winding. This magnetic geometry is unstable and the plasma self-organizes strongly into a magnetic field which reverses near the edges with respect to what would be expected from considering the magnetic field induced by the toroidal current without self-organization. Until relatively recently this process was explained by the tendency of a system to minimize its energy under constraints [98]. It is now understood that the relaxation mechanism is rather related to a fundamental plasma-instability, the tearing mode, which leads to a relaxed, but dynamically active *quasi-single-helicity* state [99].

Even without considering the MHD instabilities, the confinement of the plasma is problematic. If MHD instabilities are controlled, the confinement would in principle be good enough such that room-size tokamaks would be a viable energy source. The coulomb interactions (electrostatic interactions between the individual charged particles) degrade the plasma confinement, but this degradation is not large enough to prevent a small tokamak from producing energy. However, the coulomb interactions are not the only source of transport. There are also turbulent plasma movements.

In fusion plasmas a certain class of electrostatic instabilities (which means that the instability is not caused by the dynamics of the magnetic field) is almost impossible to avoid, leading to small scale turbulent behavior. In particular in the edge of the plasma, turbulent motion is almost always present. It is this turbulence which is one of the main problems that are responsible for the fact that fusion is not yet a generally used energy source. Chapter 5 will be partly dedicated to the investigation of this micro-turbulence.

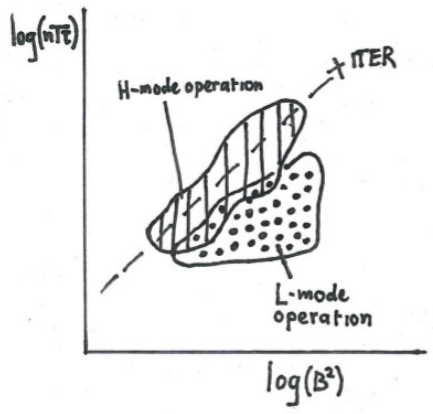

Figure 4.3: A rough sketch of the magnetic energy needed to obtain a triple-product value for both Low-confinement (L) mode experiments and High-confinement (H) mode experiments. The predicted value of H-mode operation of ITER is based on an extrapolation of roughly one order of magnitude in magnetic energy. The magnetic energy is approximately proportional to the size of the machine.

It was found that, increasing the machine-size, the overall confinement time increased and, extrapolating, the goal of energy production could in principle be attained if large enough machines could be constructed. In these larger machines the influence of the edge turbulence seems to become of a lesser relative importance. Plotting triple product $nT\tau$ against machine-size it was however concluded that, in order to reach the value for ignition, the machines should be so large that the technical difficulties would make their construction sheer impossible. Fortunately, in the 1980's it was observed that some kind of transition takes place for certain plasma parameters, which reduces the level of turbulence [101]. This transition from a low to a high confinement state (LH-transition), showed that, according to an extrapolation, the construction of igniting fusion reactors would be feasible and the construction of ITER is based on this belief. Figure 4.3 illustrates this extrapolation.

The precise origin of the LH-transition is today still not clarified. Experimentalists know how to produce such a state in their machine by pushing the right buttons, but the physics-picture is still far from complete. It seems that there is a strong link with plasma rotation. A plasma can be spun-up by injecting beams of neutral particles, thereby directly increasing the angular momentum. But even in the absence of external momentum sources, a tokamak seems to rotate in the toroidal direction. The first systematic studies of this phenomenon can be attributed to Rice and coworkers (see [102] for an overview). There still is a lot of speculation on the origin of spontaneous rotation and a number of mechanisms has been proposed (See for example reference [103] for a review). Chapter 6 will be dedicated to the investigation of large-scale plasma flow, and the spontaneous generation of angular momentum, within the MHD framework.

Before discussing micro-turbulence and self-organization, we will first give

an outline of the physical models used to study these plasma phenomena and we will point out the importance of the imposed magnetic field for the dynamics.

4.2 A fluid description of plasma dynamics

A plasma is a gas in which the electrons and ions are detached from one another. This separation called ionization takes normally place at high temperatures. Since the molecules are not charge neutral any more, the plasma will interact with magnetic fields. The same happens in metals, in which electrons are also detached. The dynamics of plasmas and liquid metals therefore share some dynamical properties.

Let us recall the Maxwell equations, which describe the dynamics of the electromagnetic fields $\boldsymbol{E}$ and $\boldsymbol{b}$.

$$\nabla \cdot \boldsymbol{b} = 0 \tag{4.3}$$

$$\frac{\partial \boldsymbol{b}}{\partial t} = -\nabla \times \boldsymbol{E} \tag{4.4}$$

$$\nabla \cdot \boldsymbol{E} = \frac{q}{\epsilon_0} \tag{4.5}$$

$$\nabla \times \boldsymbol{b} = \mu_0 \boldsymbol{j} + \mu_0 \epsilon_0 \frac{\partial \boldsymbol{E}}{\partial t}, \tag{4.6}$$

in which ϵ_0 is the permettivity and μ_0 the permeability of vacuum. These quantities are related to the speed of light by $c = 1/\sqrt{\epsilon_0 \mu_0}$. $\boldsymbol{j}$ is the current density. A charged particle with charge q and mass m in such a field will experience two forces, one due to the electric field, the other due to the magnetic field. Its velocity will then evolve according to

$$m\dot{\boldsymbol{v}} = q\left(\boldsymbol{E} + \boldsymbol{v} \times \boldsymbol{b}\right). \tag{4.7}$$

If one would track all ions and electrons and compute the changes that their movements induce on the electromagnetic fields, one obtains a complete description of the plasma. This is the most fundamental description of a plasma. Every particle is described by its position and its velocity. The complete description at time t is thus given by the six dimensional function $f(\boldsymbol{x}_n, \boldsymbol{v}_n, t)$ in which n labels a particular particle. The evolution of f is given by the kinetic equation,

$$\partial_t f + \boldsymbol{v} \cdot \nabla_{\boldsymbol{x}} f + \dot{\boldsymbol{v}} \cdot \nabla_{\boldsymbol{v}} f = 0, \tag{4.8}$$

in which $\nabla_{\boldsymbol{x}}$ and $\nabla_{\boldsymbol{v}}$ indicate partial derivatives with respect to position and velocity respectively. In general, one is interested in the average behavior and not in individual particles, so that one averages over a large ensemble of equivalent particle distributions,

$$\partial_t \overline{f} + \overline{\boldsymbol{v}} \cdot \nabla_{\boldsymbol{x}} \overline{f} + \overline{\dot{\boldsymbol{v}}} \cdot \nabla_{\boldsymbol{v}} \overline{f} = R. \tag{4.9}$$

$\dot{\boldsymbol{v}}$ is given by expression (4.7). The term R appears since $\overline{\boldsymbol{v} \cdot \nabla_{\boldsymbol{x}} f} \neq \overline{\boldsymbol{v}} \cdot \nabla_{\boldsymbol{x}} \overline{f}$, just like in the turbulence closure problem, where the average introduces the Reynolds stress. This term is called the interaction term since it corresponds to the interaction of the different particles, and no precise form for R exists for most cases. One model is to take into account purely elastic collisions between the different particles.

For most practical purposes one is interested in the collective behavior of the plasma at scales much larger than the mean-free path. In these cases a fluid description is most useful.[1] Braginskii [105] derived fluid equations starting from the above kinetic description for the case of a plasma consisting of electrons and a single type of ions. Using the relations,

$$n_a = \int f_a d\boldsymbol{v}, \quad u_a = n_a^{-1} \int f_a v_a d\boldsymbol{v}, \tag{4.10}$$

one obtains continuum equations for the collective behavior of the plasma, with u_a the velocity and n_a the particle density of species a, a being here i for the ion fluid or e for the electron fluid. The resulting equations are

$$\partial_t n_a + \nabla \cdot (n_a \boldsymbol{u}_a) = 0 \tag{4.11}$$

$$m_a n_a \left(\partial_t \boldsymbol{u}_a + \boldsymbol{u}_a \cdot \nabla \boldsymbol{u}_a\right) = \nabla \cdot \bar{\bar{P}}_a + q_a n_a \left(\boldsymbol{E} + \boldsymbol{u}_a \times \boldsymbol{B}\right) + \boldsymbol{R}_a. \tag{4.12}$$

The tensor $\bar{\bar{P}}$ is given by

$$P_{ij} = p\delta_{ij} + \pi_{ij} \quad \text{with}$$
$$\pi_{ij} = -\eta \left[\frac{\partial u_i}{\partial x_j} + \frac{\partial u_j}{\partial x_i}\right] + \frac{2}{3}\delta_{ij}\frac{\partial u_p}{\partial x_p}. \tag{4.13}$$

This expression, with η a viscosity, depending on temperature and density, does not hold in the presence of a strong magnetic field. In that case, different viscosities act depending on the orientation of the strain tensor with respect to the magnetic field. Expressions for this more complicated case can be found in Braginskii [105]. Analogously, an equation can be derived for $T_a = (3n_a)^{-1} \int f_a m_a (v_a - u_a)^2 d\boldsymbol{v}$. This set of equations, together with the Maxwell equations forms a closed set, if the viscous stress $\bar{\bar{\pi}}_a$, the interaction term R_a and similar terms in the equation for T_a are specified.

In the following we will consider two sets of approximations leading to different fluid descriptions. The first description is electrostatic and considers two fluids, an ion and an electron fluid, which have distinct features. The second is the magnetohydrodynamic description, in which the electrons and ions in each fluid particle move together, so that only one fluid has to be considered.

4.3 Electrostatic drift-wave turbulence: the Hasegawa-Wakatani model

To illustrate some features of the two-fluid description, we will consider one particular set of model-equations, which is due to Hasegawa and Wakatani [106, 107]. We will first describe the approximations which lead to this model. To start with, this approach is electrostatic, which means that the magnetic

[1] We will not discuss Gyrokinetics here. In that approach the individual dynamics of electrons and ions in the presence of a magnetic field is considered, but the fast circular movement of the ions and electrons around the magnetic fieldlines (charged particles will describe a circular motion perpendicular to the magnetic field) is averaged out and hereby the smallest relevant time-scales increase by a considerable number of orders of magnitude. The resolution of the so-obtained dynamics is still time-consuming but modern super computers can currently compute some tokamak-relevant plasma flows within a reasonable amount of time. See [104] for a recent review on the topic.

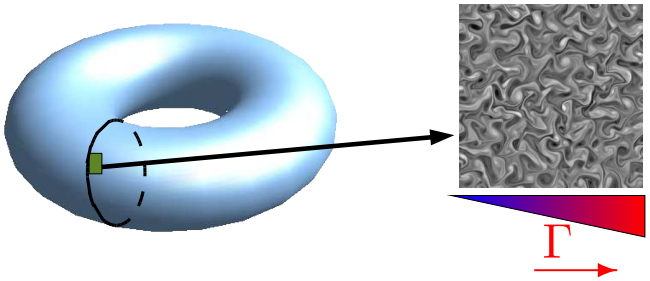

Figure 4.4: In our studies of drift-wave turbulence we consider a square domain. This domain represents a small slab near the edge of a tokamak, perpendicular to the magnetic field. The x-direction of our slab then corresponds roughly to the radial direction, and the y-coordinate represents the poloidal direction. The combination of turbulent velocity fluctuations and a strong density gradient Γ lead then to a turbulent flux of plasma in the radial direction. Figure taken from reference [12].

field is fixed. Since in the edge of fusion plasmas the electrostatic turbulence evolves on a small time-scale compared to the time-scale of the magnetic field, this approximation is useful to study the dynamics of the micro-turbulence disentangled from the large-scale dynamics. In particular in the edge of fusion plasmas, this micro-turbulence is an unavoidable feature. In the edge the plasma density rapidly falls off. In the present model, the equilibrium plasma density profile is considered to be given, with a radial dependence, $n_0(r)$. The magnetic field is not only considered constant, but also spatially uniform. These two approximations hold approximately in the plasma edge, and in Figure 4.4, we show the geometry which is considered in our investigations of electrostatic drift-wave turbulence.

We start by writing the four equations, which form the starting point of our model. These are the Braginskii fluid equations (4.11) for the ions and the electrons

$$\partial_t n_i + \nabla \cdot (n_i \boldsymbol{u}_i) = 0 \tag{4.14}$$

$$m_i n_i \left(\partial_t \boldsymbol{u}_i + \boldsymbol{u}_i \cdot \nabla \boldsymbol{u}_i\right) = \nabla \cdot \bar{\bar{P}}_a + e n_i \left(\boldsymbol{E} + \boldsymbol{u}_i \times \boldsymbol{B}\right) + \boldsymbol{R}_i \tag{4.15}$$

$$\partial_t n_e + \nabla \cdot (n_e \boldsymbol{u}_e) = 0 \tag{4.16}$$

$$m_e n_e \left(\partial_t \boldsymbol{u}_e + \boldsymbol{u}_e \cdot \nabla \boldsymbol{u}_e\right) = \nabla \cdot \bar{\bar{P}}_e - e n_e \left(\boldsymbol{E} + \boldsymbol{u}_e \times \boldsymbol{B}\right) - \boldsymbol{R}_i, \tag{4.17}$$

in which we used that $R_i = -R_e$, as will be explained later. These eight equations contain 10 variables: the three components of the ion-fluid-velocity, the three components of the electron-fluid-velocity, the plasma densities n_e and n_i and the two pressures. We assume here that the viscosities involved in $\bar{\bar{P}}_a$ are known. We will consider the equation of state $p_a = n_a T_a$, and neglect temperature gradients, so that we have a closed system. The set of approximations that we will introduce below will lead to a final model containing only two equations, one for the plasma density fluctuations and one for the ion fluid vorticity.

The first step in deriving this model is to consider the ion-momentum equation. In the strong magnetic field approximation, we introduce the small pa-

rameter

$$\frac{1}{\omega_{ci}}\frac{\partial}{\partial t} \ll 1. \tag{4.18}$$

This means that the typical time-scales of the fluid movement are much larger than the plasma-oscillations, with $\omega_{ci} = eb/m_i$. It can then directly be seen by an order of magnitude analysis that the leading order terms in the ion-momentum equation (4.15) are the ones proportional to e, so that

$$\boldsymbol{u}_i \times \boldsymbol{b} = -\boldsymbol{E}. \tag{4.19}$$

Taking the vector product with $\boldsymbol{b}$ at each side, we obtain for the leading-order ion velocity

$$\boldsymbol{u}^{E\times b} = \frac{\boldsymbol{E}\times\boldsymbol{b}}{b^2}. \tag{4.20}$$

This is the $E\times b$ velocity, which is two-dimensional in a uni-directional magnetic field. Furthermore, it can be easily checked that this velocity is incompressible in the present case. An important feature of this velocity is that it is identical for ions and electrons since it does not depend on the mass and charge of the particles. In the present case we will also be interested in the sub-dominant contribution. For that we pose $\boldsymbol{u}_i = \boldsymbol{u}^{E\times b} + \boldsymbol{u}^p$ and substitute this into equation (4.15). To next order the ion-moment equation reads then,

$$m_i n_i (d_t + \mu\Delta)\boldsymbol{u}^{E\times b} = -\nabla p_i + n_i e \boldsymbol{u}^p \times \boldsymbol{b}. \tag{4.21}$$

We used expression (4.13) to explicit the stress term. The interaction term $\boldsymbol{R}$ is neglected in this equation, since, due to the large mass ratio, ion-electron collisions do not influence the ion-dynamics much[2]. Let us consider the case in which the $E\times b$ velocity is zero. In this case we obtain an expression for u^p by taking again the vector product with $\boldsymbol{b}$ on the RHS. This yields,

$$\boldsymbol{u}_p = (n_i e B^2)^{-1}\nabla p_i \times \boldsymbol{b}. \tag{4.22}$$

It was assumed that temperature gradients were negligible, so that, using the equation of state $p = nT$, we obtain

$$\boldsymbol{u}_p = \frac{T}{n_i e B^2}\nabla n_i \times \boldsymbol{b}. \tag{4.23}$$

The presence of a radial gradient of plasma density gives thus rise to a poloidal velocity. If the $E\times b$ is not zero, we have that the inertia of the ion-fluid directly influences this velocity, $\boldsymbol{u}_p$ which is called the polarization velocity. Like the $E\times b$ velocity, it is also perpendicular to the magnetic field, but unlike it, it is not divergence free. Taking the curl of equation (4.21), we find for the $E\times b$ -vorticity ($\omega^{E\times b} = \boldsymbol{e}_z\cdot(\nabla\times\boldsymbol{u}^{E\times b})$)

$$m_i n_i (d_t + \mu\Delta)\omega^{E\times b} \quad = \quad n_i e(-b\nabla\cdot\boldsymbol{u}^p), \tag{4.24}$$

so that

$$\frac{1}{\omega_{ci}}(d_t + \mu\Delta)\omega^{E\times b} \quad = \quad -\nabla\cdot\boldsymbol{u}^p. \tag{4.25}$$

[2]The ratio of the masses of the ions and the electrons is comparable to the ratio of the mass of a football to a fly.

This shows that the divergence of the polarization-velocity acts as a source (or sink) term in the equation for the $E \times b$ -vorticity. Since its value is proportional to the particle mass, it is much larger for the ions. The ion-continuity equation will link this divergence to the plasma density fluctuations. This equation is

$$\partial_t n + \nabla \cdot (\boldsymbol{u}_i n) = 0. \tag{4.26}$$

We assume adiabatic electrons so that the ion density is equal to the electron density. Here and in the following we drop therefore the indices on n. Substituting the total velocity ($E \times b$ plus polarization) and using the fact that the $E \times b$ -velocity is divergence free, we write,

$$\partial_t n + \boldsymbol{u} \cdot \nabla n = -n \nabla \cdot \boldsymbol{u}^p \rightarrow \nabla \cdot \boldsymbol{u}^p = -d_t \ln n. \tag{4.27}$$

The electron continuity equation is

$$\partial_t n + \nabla \cdot (\boldsymbol{u}_e n) = 0. \tag{4.28}$$

The polarization velocity is small for the electrons, since it is related to the inertia and the electron mass is small. We therefore neglect it in the plane, compared to the $E \times b$-velocity,

$$\partial_t n + \boldsymbol{u}^{E\times b} \cdot \nabla_\perp n = -\nabla_{||}(u_{e||} n) = \nabla_{||}(J_{||}/e), \tag{4.29}$$

in which the last equality follows from the fact that the parallel ion-velocity is approximately negligible compared to the parallel electron velocity.[3] The final expression, which closes the system should express $J_{||}$ as a function of n, ω. This relation is derived from the electron momentum equation,

$$m_e n (d_t + \mu\Delta)\boldsymbol{u}_e = -\nabla p_e - ne(\boldsymbol{E} + \boldsymbol{u}_e \times \boldsymbol{b}) + \boldsymbol{R}_e. \tag{4.30}$$

In this equation the interaction term can not be neglected, but the inertia can, as well as the parallel viscous drag. The interaction term is given by $\boldsymbol{R} = \eta(n_i \boldsymbol{u}_i - n_e \boldsymbol{u}_e) = \eta \boldsymbol{J}/e$.[4] We write the equation for the parallel component, $J_{||}$,

$$0 = -\nabla_{||} p_e - neE_z + \eta J_{||}/e. \tag{4.32}$$

Using the equation of state $p = nT$ and neglecting temperature gradients, we obtain

$$J_{||}/e = \frac{T_e n_0}{\eta} \nabla_{||} \left(\frac{n}{n_0} - \frac{\phi e}{T_e} \right). \tag{4.33}$$

At this point we have obtained a closed set of equations. We can combine (4.25), (4.27), (4.29), (4.33), which yields

$$\frac{1}{\omega_{ci}}(d_t + \mu\Delta)\omega^{E\times b} = \frac{T_e n_0}{\eta} \nabla_{||}^2 \left(\frac{n}{n_0} - \frac{\phi e}{T_e} \right) \tag{4.34}$$

$$\partial_t n + \boldsymbol{u}^{E\times b} \cdot \nabla_\perp n = \frac{T_e n_0}{\eta} \nabla_{||}^2 \left(\frac{n}{n_0} - \frac{\phi e}{T_e} \right). \tag{4.35}$$

[3] The ion velocity dynamics are two-dimensional to first and second order. The electron dynamics are however three-dimensional. Since the mass ratio is so large, the plasma seems to behave as a two-dimensional fluid. However, the parallel electron dynamics are essential to trigger the drift-wave instability.

[4] The interaction term is given by

$$\boldsymbol{R} = -n m_e (\boldsymbol{v}_e - \boldsymbol{v}_i) \nu_{ei}. \tag{4.31}$$

where ν_{ei} is the frequency of coulomb-collisions between ions and electrons. We have $\boldsymbol{R}_i = -\boldsymbol{R}_e$ since elastic collisions are considered.

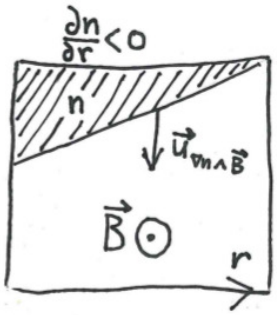

Figure 4.5: A diamagnetic drift is present in magnetized plasmas, both perpendicular to the magnetic field and to the density gradient.

The density is assumed to fluctuate around an imposed equilibrium distribution, with small fluctuations $\tilde{n}$, so that $\ln(n) \approx \ln(n_0)+\tilde{n}/n_0$. Also, assuming that the parallel dynamics are dominated by modes with a narrow frequency distribution, $\nabla^2_{||}$ can be chosen constant and equal to $-k^2_{||}$.

In the case of adiabatic electrons (electrons that move rapidly and without friction along the field lines), the electron density distribution is given by $n = n_0 \exp(\phi e/T_e)$. In this case, we find

$$\frac{\tilde{n}}{n_0} = \frac{\tilde{\phi} e}{T_e}. \tag{4.36}$$

In this case the system reduces to the Hasegawa-Mima system [108], a system of equations equivalent to the Charney-geostrophic equations, describing the dynamics of a thin layer of fluid on a rotating sphere (an obvious simplification of the atmosphere). Both the Hasegawa-Wakatani model and the Charney-Hasegawa-Mima (CHM) model allow wave-like solutions. In the present configuration, these drift-waves are perpendicular to both the magnetic field and the density gradient, and they propagate with the polarization velocity. In the HW model, these waves are unstable and a saturated turbulent state results, an instability which is absent in the CHM model. The HW system does therefore contain an internal forcing, where the energy is coming from the imposed density gradient. The essential feature leading to this instability is the finite time it takes for the electrons to restore charge neutrality.

In the case in which the friction of the electrons is large, the time it takes to restore charge-neutrality becomes large and the effective coupling between the density fluctuations and the electrostatic potential becomes weak. In this case the HW model behaves as a two-dimensional Navier-Stokes flow with a large-scale forcing term, advecting a passive scalar which is fed through the presence of a uniform scalar gradient. A more detailed description of this fluid analogy is given in reference [12]. In Figure 4.6 the vorticity field in the saturated nonlinear state is shown for different values of the electron-adiabaticity.

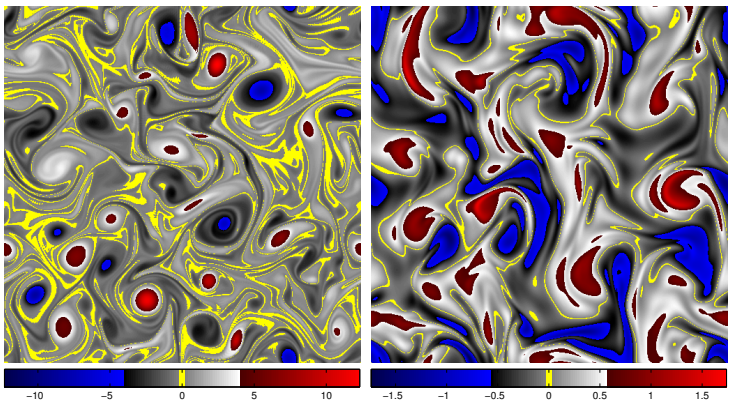

Figure 4.6: Vorticity field in the fully nonlinear saturated state of the HW model in slab-geometry. Left: when the electrons move slowly in the parallel direction (perpendicular to the plane of the figure), the resulting perpendicular flow (in the plane of the figure) ressembles two-dimensional Navier-Stokes turbulence forced at the large scales. Right: the electrons are nearly adiabatic and the behavior in the plane is close to shallow water dynamics. From reference [12].

4.4 The MHD approximation

In the special case in which every fluid particle is charge neutral ($n_i = n_e \equiv n$), one can derive an equation for the fluid particles by summing equations (4.14). This yields the MagnetoHydroDynamic (MHD) approximation. Neglecting the electron inertia we have

$$m_i n \left(\frac{\partial}{\partial t} + \boldsymbol{v}_i \cdot \nabla \right) \boldsymbol{v}_i = -\nabla p + \boldsymbol{J} \times \boldsymbol{B}, \tag{4.37}$$

in which $p = p_i + p_e$ is the total pressure and $\boldsymbol{v}_i \approx \boldsymbol{u}$ is the plasma velocity. The evolution equation of the magnetic field is described by the Faraday-Maxwell equation,

$$\frac{\partial \boldsymbol{B}}{\partial t} = -\nabla \times \boldsymbol{E}, \tag{4.38}$$

and the relation between the electric field $\boldsymbol{E}$ and the magnetic and velocity field is given by Ohm's law,

$$\boldsymbol{E} = \boldsymbol{J}/\sigma - \boldsymbol{u} \times \boldsymbol{B}, \tag{4.39}$$

with σ the electric conductivity. Finally, the relation between the magnetic field and the current density is

$$\mu_0 \boldsymbol{J} = \nabla \times \boldsymbol{B}, \tag{4.40}$$

in which the displacement current has been neglected (which is a good approximation for typical velocities which are small compared to the speed of light), and in which μ_0 is the magnetic permeability of vacuum. In the incompressible and isothermal case the above set of equations is closed if we add the continuity equation for the velocity $\nabla \cdot \boldsymbol{u} = 0$. The density of a fluid element is equal to

$$\rho = (m_i + m_e)n. \tag{4.41}$$

We normalize the magnetic fluctuations $\boldsymbol{b} \to (\mu_0\rho)\boldsymbol{b}$, which allows to simplify the above equations to

$$\left(\frac{\partial}{\partial t} + \boldsymbol{u}\cdot\nabla\right)\boldsymbol{u} = -\frac{1}{\rho}\nabla p + \nabla\times\boldsymbol{B}\times\boldsymbol{B} \tag{4.42}$$

$$\frac{\partial \boldsymbol{B}}{\partial t} = \nabla\times\boldsymbol{u}\times\boldsymbol{B} + \eta\Delta\boldsymbol{B}, \tag{4.43}$$

with the magnetic diffusivity $\eta = (\sigma\mu_0)^{-1}$.

The MHD approximation is very good for the description of the dynamics of liquid metals, which are encountered in industrial applications (*e.g.* reference [109]) or in the description of the dynamo problem [110]. Typical plasma applications in which the MHD approximation gives good results are the solar wind [111] and the reversed field pinch fusion device [98]. That the latter application seems to be well described by MHD is actually rather surprising. Charge neutrality is normally rather well verified in plasmas with a high collision rate, since a large number of collisions improves the Maxwellianity of the charge distribution. In fusion plasmas the mean free path is however of the same order of magnitude as the machine dimensions. Fortunately, the helical motion of the particles around the imposed magnetic field prevents the particles from escaping and collisions happen every once in a while, enough for charge neutrality to be approximately restored.

4.5 A strong magnetic field and two-dimensionalization

As explained before, in a magnetic field, a moving charged particle experiences the Lorentz force, perpendicular to both the magnetic field and the direction of movement. Moving parallel to the field, this force vanishes. This immediately shows the intrinsic anisotropic character of MHD turbulence. Whereas a uniform velocity does not influence the dynamics of a turbulent flow, since one can define a reference frame moving with the velocity, there is no such transformation to get rid of the influence of the magnetic field on the velocity. Fundamentally MHD flows are therefore anisotropic. Even if only isotropically distributed magnetic field fluctuations are present in a flow, the influence of these on velocity scales much smaller than the typical lengthscale of the isotropic magnetic fluctuations, is equivalent to the presence of a large-scale magnetic field.

Let us now focus on the case in which a strong uniform magnetic field is present. This case was theoretically addressed by Montgomery and Turner [112] and first simulated in two dimensions in [113]. In [112] it was suggested that the dynamics of the system in this case would rapidly evolve towards a case in which the system consists of two parts. First a two-dimensional system, perpendicular to the magnetic field, second an Alfvén wave contribution. In the case of low magnetic Prandtl number, *i.e.* a magnetic diffusivity compared to the kinematic viscosity, the Alfvén-wave part of the dynamics is rapidly damped out. Indeed, these waves exist only since magnetic field lines are frozen into the fluid if the magnetic diffusivity tends to zero.

This case of quasistatic MHD turbulence, in which a uniform magnetic field is

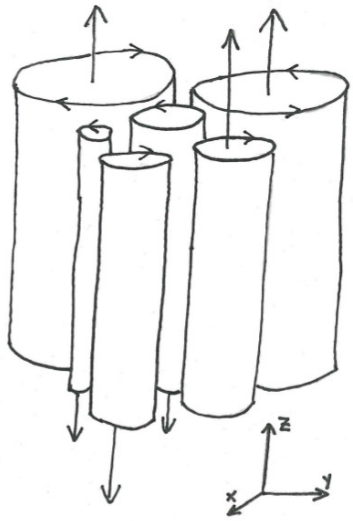

Figure 4.7: Two and a half dimensional turbulence

present and the magnetic Prandtl number is small[5], was investigated in Favier *et al.* [114, 10]. In particular it was observed and explained how the results from linear analysis disagreed with results from Direct Numerical Simulations and EDQNM simulations. Linear analysis [115] predicts that at long times the ratio of parallel kinetic energy to perpendicular kinetic energy tends to a value of two. We explained that this is not observed due to fairly simple nonlinear effect. Indeed, the system perpendicular to the magnetic field tends to a two-dimensional behavior, and two-dimensional turbulence at high enough Reynolds number tends to conserve the kinetic energy. The parallel dynamics are at long times similar to the behavior of a passive scalar, advected by the two-dimensional perpendicular motions. This state of a velocity field in which the two perpendicular velocity components mix the third component, without feedback of this third component on the perpendicular dynamics was baptized two-and-a-half dimensional turbulence by Montgomery and Turner [116], a terminology which can be used more generally for situations in which three components of the fluctuation field are considered, but only two components of the wave-vector. Since the mixing of a passive scalar (in the present case the parallel velocity component) is characterized by a direct cascade toward the small, dissipative scales, the parallel kinetic energy is more rapidly dissipated than the perpendicular kinetic energy, which explains why the linear analysis (which does not take into account the rapid nonlinear cascade of the parallel kinetic energy) fails.

In Figure 4.8, results are shown from DNS and EDQNM during the regime

[5]The quasistatic description is in particular useful in the description of liquid metals. However, the tendency toward two-dimensionalization is generally observed in all systems of conducting fluids and plasmas in which a strong magnetic field is present. The precise form of the anisotropy and the mechanisms involved in the two-dimensionalization may differ from case to case.

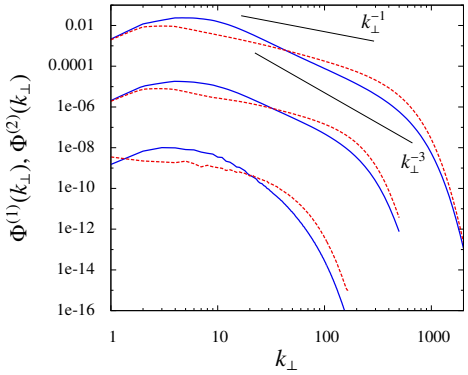

Figure 4.8: Quasi-static MHD turbulence behaves as two-and-a-half-dimensional turbulence. The perpendicular velocity advects the parallel velocity as were it a passive scalar. This behavior is illustrated by considering the energy spectra. The energy spectra of the perpendicular velocity (solid lines) display a steep inertial range behavior with a spectral exponent of the order three or four, as is usual for two-dimensional turbulence. The spectrum of the third velocity component (dotted lines) displays a Batchelor-type behavior, as is expected in the case of advection by a velocity field with a steep energy distribution. The lower two curves are obtained using DNS, the upper four curves are EDQNM results. From reference [10].

in which the parallel kinetic energy is advected as were it a passive scalar by the quasi-two-dimensional motion of velocity fluctuations perpendicular to the magnetic field. In this case, of freely evolving two-dimensional turbulence advecting a passive scalar, the inertial range scaling of the parallel velocity is expected to be close to Batchelor scaling [117], whereas the parallel kinetic energy is expected to be characterized by a k^{-3} enstrophy cascade type of spectrum (as will be explained in more detail in the next section).

4.6 Mixing in two-dimensional turbulence

In the following manuscript the behavior of a passive scalar, advected by two-dimensional turbulence, is addressed in more detail. At first sight it might seem unappropiate to present these two-dimensional Navier-Stokes turbulence results in this chapter. As we discussed however in section 4.3, the drift-wave turbulence dynamics in the limit of a small adiabaticity are equivalent to two-dimensional turbulence advecting a passive scalar. The only difference is that in the latter case an external forcing is needed to study statistically stationary flows, whereas the HW system contains an internal instability. We also observed in the previous section that quasi-static MHD turbulence tends to a two-dimensional fluid turbulence limit, advecting the parallel velocity as a passive scalar.

In the now presented investigation we study therefore a flow which is relevant for both charge-neutral plasma dynamics and two-fluid descriptions. In particular we will focus on the turbulent flux of scalar in the down-gradient direction. This is the relevant quantity for radial turbulent transport in fu-

sion plasmas. The transported quantity can be the concentration of impurities, or can be heat or toroidal momentum. In the following manuscript, the self-similarity of the spectral distribution is characterized by quantifying the scaling exponents in the inertial range of the scalar flux spectrum. Both phenomenological arguments and DNS are used for this characterization. Related studies for three-dimensional turbulence both in isotropic and sheared turbulence can be found in references [118, 119].

Inertial range scaling of the scalar flux spectrum in two-dimensional turbulence

W. J. T. Bos,[1] B. Kadoch,[2] K. Schneider,[2] and J.-P. Bertoglio[1]
[1]*LMFA-CNRS, Université de Lyon, Ecole Centrale de Lyon, Université Lyon 1, INSA Lyon, Ecully 69134, France*
[2]*M2P2, CNRS and CMI, Universités d'Aix-Marseille, Marseille 13453, France*

(Received 10 July 2009; accepted 7 October 2009; published online 18 November 2009)

Two-dimensional statistically stationary isotropic turbulence with an imposed uniform scalar gradient is investigated. Dimensional arguments are presented to predict the inertial range scaling of the turbulent scalar flux spectrum in both the inverse cascade range and the enstrophy cascade range for small and unity Schmidt numbers. The scaling predictions are checked by direct numerical simulations and good agreement is observed. © *2009 American Institute of Physics*.
[doi:10.1063/1.3263703]

I. INTRODUCTION

In the present work we consider the spectral distribution of the passive scalar flux in two-dimensional incompressible Navier–Stokes turbulence. The scalar flux appears as the unclosed quantity in the Reynolds averaged equation for the mean scalar field: separating the velocity and passive scalar field into mean and fluctuations, $\boldsymbol{u}=\overline{\boldsymbol{u}}+\boldsymbol{u}'$ and $\theta=\overline{\theta}+\theta'$, the equation for the mean scalar field reads

$$\frac{\partial \overline{\theta}}{\partial t}+\overline{u}_j\frac{\partial \overline{\theta}}{\partial x_j}=\kappa\frac{\partial^2\overline{\theta}}{\partial x_j^2}-\frac{\partial \overline{u_j'\theta'}}{\partial x_j}, \tag{1}$$

where κ is the diffusivity of the scalar and the overbar denotes an ensemble average. The last term of this equation contains the correlation $\overline{u_j'\theta'}$, which is called the scalar flux. It is the term which represents the influence of the turbulent fluctuations on the mean scalar profile. Since it is the unclosed term in the Reynolds averaged equations, it needs to be modeled, e.g., by means of an eddy diffusivity. To propose correct models for the scalar flux, understanding of the physics of the turbulent flux is needed. For an overview of models for the scalar flux, we refer to the book by Schiestel,[1] the work by Rogers *et al.*,[2] or more recently the model derived by Wikström *et al.*[3] For the more complicated case of the scalar flux in the presence of shear and rotation, see the work by Brethouwer.[4] These studies focus on three-dimensional turbulence.

We consider statistically homogeneous velocity and scalar fields so that we can investigate the scale distribution of the turbulent scalar flux by means of Fourier spectra. The Fourier spectrum related to the scalar flux is defined as

$$F_{u_j\theta}(k)=\int_{\Sigma(k)}\mathcal{F}|_{\boldsymbol{x}-\boldsymbol{x}'}[\overline{u_j'(\boldsymbol{x},t)\theta'(\boldsymbol{x}',t)}]d\Sigma(k), \tag{2}$$

in which $\Sigma(k)$ is a circular wavenumber shell with radius k, the wavenumber, and $\mathcal{F}|_{\boldsymbol{x}-\boldsymbol{x}'}[\cdots]$ denotes the Fourier transform with respect to the separation vector $\boldsymbol{x}-\boldsymbol{x}'$. This definition is such that by construction we have

$$\int_0^\infty F_{u_j\theta}(k)dk=\overline{u_j'\theta'}, \tag{3}$$

which illustrates that the scalar flux spectrum characterizes the contribution of different lengthscales (or wavenumbers) to the scalar flux. This spectrum is also called the scalar-velocity cospectrum since it is defined as the real part of the scalar-velocity correlation in Fourier space. The imaginary part is called the quadrature spectrum. The quadrature spectrum does not contribute to the scalar flux in physical space and we therefore concentrate on the cospectrum.

Academically the least complicated case to study the turbulent scalar flux is, as proposed by Corrsin,[5] isotropic turbulence on which we impose a stationary uniform mean scalar gradient $\partial\overline{\theta}/\partial x_1\equiv\Gamma$, arbitrarily chosen in the x_1-direction. In this case there exists one nonzero component of the scalar flux, aligned with the gradient. The other component is zero. We consider this case and in particular, we focus on the inertial range scaling of the scalar flux spectrum. We will in the following drop the subscripts and denote the cospectrum by $F(k)$. We will also drop the primes and denote the fluctuations of velocity and scalar by $\boldsymbol{u}$ and θ, respectively. Before starting the study of the scaling in two-dimensional turbulence, we briefly discuss the results obtained in the related case of three-dimensional turbulence. Lumley[6,7] predicted that at high Reynolds numbers the inertial range should fall off as $k^{-7/3}$. Indeed he predicted the inertial range to be given by

$$F(k)\sim\Gamma\epsilon^{1/3}k^{-7/3}, \tag{4}$$

with ϵ the dissipation of kinetic energy, or more precisely the energy flux at scale k. This scaling was investigated experimentally in the atmospheric boundary layer[8] and in decaying grid turbulence at Taylor-scale Reynolds numbers up to $R_\lambda=600$.[9,10] In these grid-turbulence experiments it was found that the $-7/3$ scaling was not observed at this Reynolds number. It was subsequently proposed[11] that the inertial range exponent might be -2 instead of $-7/3$. However, in closure calculations, it was shown that the -2 scaling was a

low-Reynolds number effect and that the $-7/3$ scaling should be observed at higher Reynolds numbers.[12,13] This was confirmed by the work of O'Gorman and Pullin[14] and recent direct numerical simulations (DNSs).[15]

In the case of two-dimensional turbulence only few studies address the problem of the scaling of the scalar flux spectrum. Let us recall that in two-dimensional turbulence, in which the energy is injected at a wavenumber k_i, two cascades can be observed: first an energy cascade toward the large scales and, second, an enstrophy cascade to the small scales. If the injection scale is much smaller than the domain size and much larger than the range in which the viscous stresses become important, both cascades are characterized by power-law scaling.[16–18] We focus on these inertial ranges, which we will denote by IC for the inverse energy cascade and FC for the forward enstrophy cascade range. In particular we investigate the wavenumber dependence of the scalar flux spectrum in these ranges.

One of the few works investigating the scaling of the scalar flux spectrum in two-dimensional turbulence is Ref. 19, which mentions that the scalar flux spectrum can be roughly estimated by

$$F(k) \approx E(k)^{1/2} E_\theta(k)^{1/2}, \tag{5}$$

in which the scalar variance spectrum is defined as

$$E_\theta(k,t) = \frac{1}{2}\int_{\Sigma(k)} \mathcal{F}|_{x-x'}[\overline{\theta(\boldsymbol{x},t)\theta(\boldsymbol{x}',t)}]d\Sigma(k). \tag{6}$$

In the inverse cascade (IC) range, where both the energy spectrum $E(k)$ and the scalar variance spectrum $E_\theta(k)$ are known to obey the Kolmogorov–Obukhov scaling,[20,21] this would lead to a $k^{-5/3}$ inertial range. Close observation of the numerical results in Ref. 19 shows that this is not the case.

In the present paper we show that this $k^{-5/3}$ inertial range prediction does not correspond to the physics of the problem. Phenomenological scalings for the inertial ranges in both the IC and the forward enstrophy cascade will be proposed for the scalar flux spectrum $F(k)$ and the scalar variance spectrum $E_\theta(k)$ for the cases of unity and small Schmidt number (the Schmidt number is defined as the ratio of the diffusivity of momentum to that of the scalar, $Sc=\nu/\kappa$, and is identical to the Prandtl number when the passive scalar is temperature). DNSs are carried out to verify the validity of the predictions.

Note that since the scalar fluctuations are produced by a mean gradient, the scalar fluctuations are in principle not isotropic, but axisymmetric around the direction of the gradient. It was shown[22,23] that in the case of three-dimensional isotropic turbulence the spectral distribution of scalar flux can be described by a single scalar function. The distribution of scalar variance can be described by two scalar functions. In the present work, by integrating over wavenumber shells [Eqs. (2) and (6)], we eliminate the angle dependence. A detailed study of the anisotropy of the scalar field will not be performed in the present work.

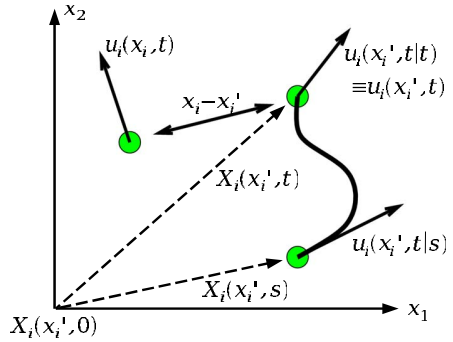

FIG. 1. (Color online) Representation of the Lagrangian two-point velocity correlation.

II. LINK BETWEEN THE LAGRANGIAN TIMESCALE AND SCALAR FLUX SPECTRUM

The phenomenological scaling for the scalar flux proposed in the present work is based on the direct relation which exists between the scalar field and the Lagrangian dynamics of the turbulent velocity field. We therefore first discuss this link. Kraichnan proposed in the framework of the Lagrangian history direct interaction approximation[24] that the dominant spectral timescale characterizing the inertial range dynamics can be estimated by

$$\tau(k,t) = \int_0^t \frac{E(k,t|s)}{E(k,t)}ds = \frac{1}{E(k,t)}\int_0^t E(k,t|s)ds. \tag{7}$$

This quantity was investigated numerically in Ref. 25. The energy spectrum is the spherically averaged Fourier transform of the two-point velocity correlation,

$$E(k,t) = \frac{1}{2}\int_{\Sigma(k)} \mathcal{F}|_{x-x'}[\overline{u_i(\boldsymbol{x},t)u_i(\boldsymbol{x}',t)}]d\Sigma(k). \tag{8}$$

$E(k,t|s)$ is the equivalent spectrum in which the Eulerian velocity $u_i(\boldsymbol{x}',t)$ is replaced by $u_i(\boldsymbol{x}',t|s)$, which is defined as the velocity at time s of a fluid particle which arrives at point $\boldsymbol{x}'$ at time t. The definition of $u_i(x',t|s)$ is illustrated in Fig. 1. The definition of $E(k,t|s)$ is thus

$$E(k,t|s) = \frac{1}{2}\int_{\Sigma(k)} \mathcal{F}|_{x-x'}[\overline{u_i(\boldsymbol{x},t)u_i(\boldsymbol{x}',t|s)}]d\Sigma(k). \tag{9}$$

By definition $E(k,t|t)$ coincides with the Eulerian spectrum $E(k,t)$. An interesting property of Eq. (7) is that the integral can be explicited by integrating $u_i(x,t|s)$ along its trajectory.

$$\int_0^t E(k,t|s)ds = \frac{1}{2}\int_{\Sigma(k)} \mathcal{F}|_{x-x'}\left[\overline{u_i(\boldsymbol{x},t)\int_0^t u_i(\boldsymbol{x}',t|s)ds}\right]d\Sigma(k)$$

$$= \frac{1}{2}\int_{\Sigma(k)} \mathcal{F}|_{x-x'}[\overline{u_i(\boldsymbol{x},t)X_i(\boldsymbol{x}',t)}]d\Sigma(k). \tag{10}$$

Instead of the two-time quantity $u_i(\boldsymbol{x}',t|s)$, the expression now contains the single-time displacement vector of the fluid particle, $X_i(\boldsymbol{x}',t)$, corresponding to the vector pointing from its position at $t=0$ to its position at t, $\boldsymbol{x}'$, or, in other words, the trajectory. The link between the scalar flux spectrum and the integral of $E(k,t|s)$ becomes evident if we compare the

evolution equation of a nondiffusive passive scalar fluctuation θ in the presence of a mean scalar gradient,

$$\frac{\partial \theta}{\partial t} + u_j \frac{\partial \theta}{\partial x_j} = -\Gamma u_1, \tag{11}$$

with the equation of the x_1-component of the Lagrangian position vector $X_i(\boldsymbol{x},t)$:

$$\frac{dX_1}{dt} = \frac{\partial X_1}{\partial t} + u_j \frac{\partial X_1}{\partial x_j} = u_1. \tag{12}$$

Indeed, both equations are identical, only differing by a factor $-\Gamma$. As was already stated in Ref. 26, the scalar fluctuation is therefore proportional to the displacement of a fluid particle in the direction of the gradient. In the limit of vanishing diffusivity, relation (7) can thus be recasted, using Eqs. (2) and (10) as in Ref. 27:

$$\tau(k) = \frac{\Gamma^{-1} F(k)}{E(k)}. \tag{13}$$

If the energy spectrum and the Lagrangian timescale are known, the scalar flux spectrum is given by relation (13).

A. Prediction of the scaling of the scalar flux spectrum at large and unity Schmidt number

Dimensional analysis and phenomenological reasoning[24,28] give that at a scale $l \sim k^{-1}$ the Lagrangian timescale should be approximately given by $l/u(l)$ in which the typical velocity $u(l)$ can be estimated to be of the order of $\sqrt{kE(k)}$. This yields an estimation for the timescale $\tau(k)$,

$$\tau(k) \sim [k^3 E(k)]^{-1/2}. \tag{14}$$

Combining this relation with Eq. (13) yields an estimation for the scalar flux inertial range scaling,

$$F(k) \sim \Gamma \sqrt{\frac{E(k)}{k^3}}, \tag{15}$$

which is a direct relation between inertial range scaling of the scalar flux spectrum and the energy spectrum. In three-dimensional turbulence, using Kolmogorov scaling for the energy spectrum,

$$E(k) \sim \epsilon^{2/3} k^{-5/3}, \tag{16}$$

leads to classical scaling for the scalar flux spectrum,

$$F(k) \sim \Gamma \epsilon^{1/3} k^{-7/3}. \tag{17}$$

In two-dimensional turbulence this scaling should hold in the IC range where Kolmogorov scaling is expected. In the forward enstrophy cascade range, the energy spectrum is predicted to scale as[16–18]

$$E(k) \sim \beta^{2/3} k^{-3}, \tag{18}$$

with β as the flux of enstrophy in the direct cascade. This scaling was later refined introducing logarithmic corrections,[29,30]

$$E(k) \sim \beta^{2/3} k^{-3} / \ln(k/k_i)^{1/3}, \tag{19}$$

with k_i as the wavenumber corresponding to the energy injection. We neglect this correction as a first approach. For this forward entrophy cascade range (15) yields the scaling

$$F(k) \sim \Gamma \beta^{1/3} k^{-3}. \tag{20}$$

It should be noted that the preceding analysis supposes a high Schmidt number. Indeed, the analogy between the position of a fluid particle and a scalar fluctuation [Eqs. (11) and (12)] is exact for infinite Schmidt number. However, the effect of the Schmidt number for Sc larger than one is small.[22,31] O'Gorman and Pullin[14] showed that when changing the Schmidt number from 1 to 10^4, the shape of the scalar flux spectrum was only little affected. We now explain this.

The equation for the cospectrum can be derived directly from the scalar advection-diffusion equation combined with the Navier–Stokes equation (e.g., Refs. 12 and 22). It reads

$$\left[\frac{\partial}{\partial t} + (\nu + \kappa) k^2\right] F(k) = -\frac{2}{3}\Gamma E(k) + T_{u\theta}^{\mathrm{NL}}(k). \tag{21}$$

The left hand side contains the time derivative and the influence of viscosity ν and scalar diffusivity κ. We consider the statistically stationary state in which the time-derivative term drops. The first term on the right hand side is the production of scalar flux by interaction of the velocity field with the mean scalar gradient Γ. The last term is the nonlinear interaction which contains two contributions: a purely conservative nonlinear interaction which sums to zero by integration over wavenumbers and a purely destructive pressure scrambling term which annihilates the correlation between scalar and velocity fluctuations. The viscous-diffusive term can be written as

$$(\nu + \kappa) k^2 F(k) = \nu(1 + Sc^{-1}) k^2 F(k). \tag{22}$$

This term changes only by a factor of 2 when the Schmidt number goes from 1 to ∞. The influence of the Schmidt number for Sc larger than one is therefore small.

B. Prediction of the scaling of the scalar flux spectrum at small Schmidt number

In the case of $Sc \to 0$ we do expect the above reasoning to change. We now discuss this case of small Schmidt number.

When the diffusivity becomes very large (keeping ν constant to retain an inertial range for the energy spectrum), the influence of the nonlinear terms in Eq. (21) will become small, since the diffusive timescale becomes smaller than the nonlinear timescale (such as the eddy turnover time). The production term is then directly balanced by the diffusive term. In this case Eq. (21) reduces to the equilibrium

$$\kappa k^2 F(k) = -\tfrac{2}{3}\Gamma E(k), \tag{23}$$

which yields

$$F(k) = -\frac{2\Gamma E(k)}{3\kappa k^2}. \tag{24}$$

O'Gorman and Pullin[14] obtained the same expression in three dimensions. In the IC range this should yield a $k^{-11/3}$ scaling and in the FC range a k^{-5} scaling.

In Sec. IV results of DNSs of isotropic 2D turbulence with an imposed mean scalar gradient are presented to check the relations:

$$\Gamma^{-1}F(k) \sim \begin{cases} \epsilon^{1/3}k^{-7/3} & \text{IC for } Sc \geq 1, \\ \beta^{1/3}k^{-3} & \text{FC for } Sc \geq 1, \\ \kappa^{-1}\epsilon^{2/3}k^{-11/3} & \text{IC for } Sc \ll 1, \\ \kappa^{-1}\beta^{2/3}k^{-5} & \text{FC for } Sc \ll 1. \end{cases} \tag{25}$$

III. PREDICTIONS FOR THE SPECTRUM OF THE PASSIVE SCALAR VARIANCE

It is expected that the scalar variance spectrum displays Batchelor scaling[32] in the forward enstrophy cascade as was experimentally demonstrated by[33]

$$E_\theta(k) \sim \epsilon_\theta \beta^{-1/3}k^{-1}, \tag{26}$$

with ϵ_θ the (diffusive) destruction rate of passive scalar fluctuations. In the IC, Corrsin–Obukhov scaling is expected.

$$E_\theta(k) \sim \epsilon_\theta \epsilon^{-1/3}k^{-5/3}. \tag{27}$$

The equation for the scalar variance spectrum reads

$$\left[\frac{\partial}{\partial t} + 2\kappa k^2\right] E_\theta(k) = -F(k)\Gamma + T_\theta^{\mathrm{NL}}(k), \tag{28}$$

with $T_\theta^{\mathrm{NL}}(k)$ being the nonlinear transfer term. For very small Schmidt number this equation can again be linearized, yielding for the statistically stationary state

$$E_\theta(k) = \frac{-F(k)\Gamma}{2\kappa k^2}. \tag{29}$$

This gives, using Eq. (24),

$$E_\theta(k) = \frac{E(k)\Gamma^2}{3\kappa^2 k^4}. \tag{30}$$

For the scalar variance, our predictions are therefore

$$E_\theta(k) \sim \begin{cases} \epsilon_\theta \epsilon^{-1/3}k^{-5/3} & \text{IC for } Sc \geq 1, \\ \epsilon_\theta \beta^{-1/3}k^{-1} & \text{FC for } Sc \geq 1, \\ \Gamma^2\kappa^{-2}\epsilon^{2/3}k^{-17/3} & \text{IC for } Sc \ll 1, \\ \Gamma^2\kappa^{-2}\beta^{2/3}k^{-7} & \text{FC for } Sc \ll 1. \end{cases} \tag{31}$$

IV. NUMERICAL VERIFICATION OF THE PROPOSED INERTIAL RANGE SCALINGS

A. Numerical method

Simulations are performed using a standard pseudospectral method.[34] The simulations are fully dealiased and the resolution is 1024^2 gridpoints for a square periodic domain of size 2π. The time is advanced using a second order Adams–Bashforth time-stepping scheme.

The equations for the vorticity field and scalar field are

$$\frac{\partial \omega}{\partial t} + u_j\frac{\partial \omega}{\partial x_j} = (-1)^{\alpha+1}\nu_\alpha\frac{\partial^{2\alpha}\omega}{\partial x_j^{2\alpha}} + f - \gamma\frac{\partial^{-2}\omega}{\partial x_j^{-2}}, \tag{32}$$

$$\frac{\partial \theta}{\partial t} + u_j\frac{\partial \theta}{\partial x_j} = (-1)^{\alpha'+1}\kappa_{\alpha'}\frac{\partial^{2\alpha'}\theta}{\partial x_j^{2\alpha'}} - \Gamma u_1, \tag{33}$$

with the vorticity $\omega = \boldsymbol{e}_z \cdot (\nabla \times \boldsymbol{u})$, f a random-phase isotropic forcing localized in a band in wavenumber-space with a time-correlation equal to the timestep. The parameters α and α' are integers equal to one in the case of Newtonian viscosity and diffusivity and equal to 8 in the case of hyperviscosity or hyperdiffusivity. The mean gradient Γ is in all cases taken equal to 1 so that the scalar flux, and its spectrum, is dominantly negative.

In all cases, hyperviscosity is used to concentrate the influence of the viscous term at the highest wavenumbers. This allows to increase the extent of the inertial range, which is the main subject in the present work. Equivalently the scalar variance is removed at the largest wavenumbers by a hyperdiffusive term except in the case of small Schmidt number. Since in that case the diffusive term becomes the dominant mechanism, the scaling is directly affected by the type of diffusion, as can be seen in expressions (23) and (29). In that case we therefore use a "normal" Laplacian diffusive term ($\alpha' = 1$). In two-dimensional turbulence the energy shows a tendency to cascade to smaller wavenumbers, i.e., to larger scales. To avoid a pile-up of energy at the smallest wavenumber linear Rayleigh friction [the last term in Eq. (32)] is used, with γ equal to unity.

Two different fully developed turbulent flows are investigated. First the IC range, in which the forcing is localized in a wavenumber shell around $k_i = 210$. In this case the forward enstrophy range is reduced to less than an octave and a full decade of IC inertial range is observed in the simulations. Second the forward enstrophy range. In this case the forcing is localized around $k_i = 8$, and the IC range is absent since the friction acts strongly in the region $k < k_i$. Parameters used in the simulations are summarized in Table I. Also shown are some average values of some typical turbulence quantities.

In both velocity fields two different cases are considered for the passive scalar. One at $Sc = 1$, with hyperdiffusivity ($\alpha' = 8$) and one at small Schmidt number and $\alpha' = 1$. It is not straightforward to define Schmidt numbers for these cases. The precise definition of the Schmidt numbers is however not important for the present study, but what is important is the location of the inertial ranges and the ranges where diffusivity becomes important. These ranges can be determined as follows. We define a wavenumber k_* at which the nonlinear timescale $\tau(k)$ becomes of the order of the diffusive timescale $(\kappa k^2)^{-1}$. If k_* is in the inertial range, we can estimate its value by using expression (14) and the inertial range scalings (16) and (18). This yields $k_* \sim (\epsilon/\kappa^3)^{1/4}$ in the IC and $k_* \sim (\beta/\kappa^3)^{1/6}$ in the forward cascade. The wavenumber k_* marks the crossover between an inertial-convective range and an inertial-diffusive range. We will call unity Schmidt number cases, these cases in which both viscosity and diffusivity mainly act in the last two octaves of the energy and

TABLE I. Details of the simulations. Parameters used in the simulations and average values of some typical turbulence quantities. These quantities are averaged over space and time during a time interval of approximately 300 time units. The correlation coefficient $\rho_{u\theta}$ is defined as $\rho_{u\theta}=\overline{u\theta}/\sqrt{\overline{u^2}\,\overline{\theta^2}}$ and analogous for $\rho_{v\theta}$.

	IC, $Sc=1$	FC, $Sc=1$	IC, $Sc\ll 1$	FC, $Sc\ll 1$
k_i	210	8	210	8
k_e	9	4	9	4
α	8	8	8	8
α'	8	8	1	1
ν_α	1×10^{-38}	1×10^{-35}	1×10^{-38}	1×10^{-35}
$\kappa_{\alpha'}$	1×10^{-35}	1×10^{-32}	10	10
Δt	5×10^{-4}	10^{-4}	5×10^{-4}	10^{-4}
$\overline{u^2}$	1×10^{-2}	0.2	1×10^{-2}	0.2
$\overline{v^2}$	1×10^{-2}	0.2	1×10^{-2}	0.2
$\overline{\theta^2}$	0.1	0.9	5×10^{-8}	1.4×10^{-5}
$\overline{u\theta}$	-1.5×10^{-2}	-0.1	-1.5×10^{-5}	-1.2×10^{-3}
$\overline{v\theta}$	4×10^{-4}	2.4×10^{-3}	-4×10^{-8}	9×10^{-7}
$\rho_{u\theta}$	-0.45	-0.3	-0.6	-0.7
$\rho_{v\theta}$	1×10^{-2}	6×10^{-3}	-2×10^{-3}	5×10^{-4}

scalar spectra, i.e., k_* is of the order of the viscous wavenumber, $(\epsilon/\nu^3)^{1/4}$. The direct influence of the viscosity and diffusivity is then small for wavenumbers smaller than approximately 100. In the case of small Sc, a normal diffusive term is used since the scaling depends directly on the Laplacian. The diffusivity is here taken large enough for it to act at all scales, including the large scales, i.e., k_* is of the order of, or smaller than k_e, the wavenumber at which the energy spectrum peaks.

Simulations are performed until a statistically stationary flow is obtained. The spectra are subsequently obtained by averaging over a time interval of approximately 300 time units, until a relatively smooth spectrum is obtained. This corresponds to 270 T_e for the IC-range and 540 T_e for the FC-range. The large-scale turnover time T_e is here defined as $T_e=1/[k_e(\overline{u'^2})^{1/2}]$.

B. Results

In Fig. 2 visualizations of various quantities are shown at an arbitrary time. It is observed that the vorticity field contains clear vortical structures in the forward cascade. In the IC the vorticity field seems almost structureless. However, closer inspection shows small vortical structures. Visualization of the stream function shows more clearly that these structures are present. The scalar field shows how fluctuations of passive scalar are created by interaction of the flow with the mean scalar gradient. In the IC case this scalar field is almost structureless, but shows patches of scalar fluctuation. We also displayed the instantaneous scalar flux, which is the product of the x_1-component of the velocity with the scalar field. Both positive and negative values of the flux are observed. The mean value is however smaller than zero (since the mean gradient is positive), so that the net flux is nonzero.

In Fig. 3 visualizations are shown for the scalar field and

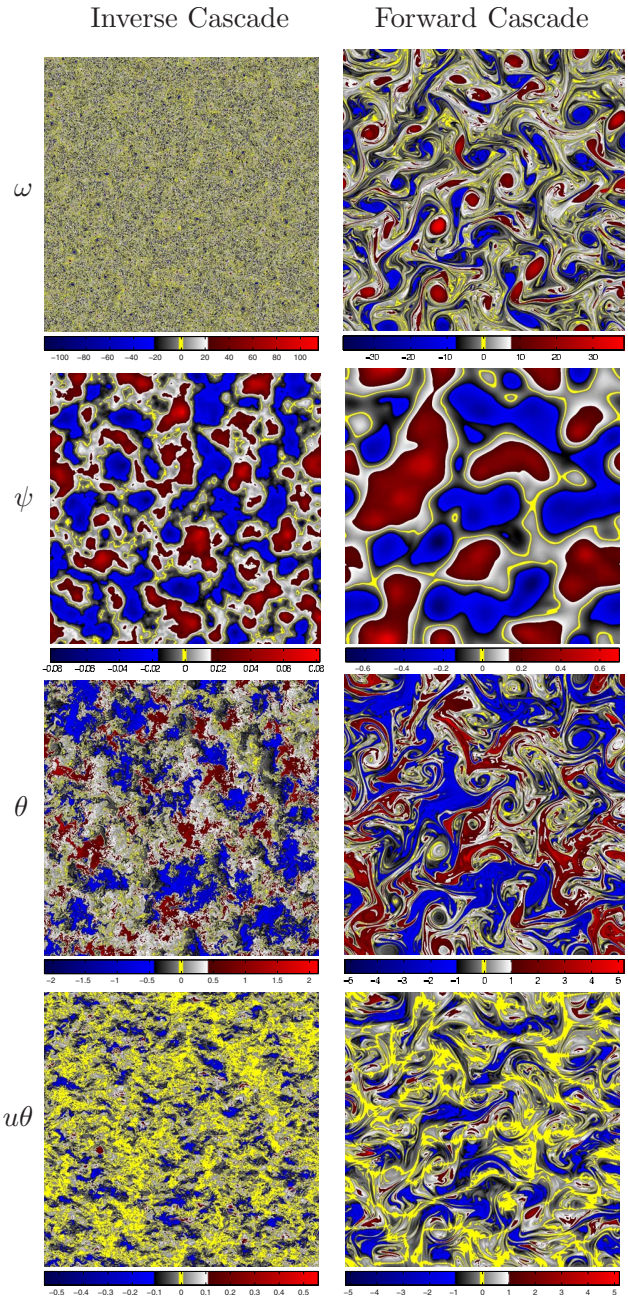

FIG. 2. (Color online) Visualizations of (from top to bottom) vorticity, streamfunction, scalar fluctuations, scalar flux. Left: IC. Right: forward cascade. The Schmidt number is unity. The mean scalar gradient is in the horizontal direction.

the scalar flux for the small Schmidt number case. Vorticity fields and stream function are not shown, since they are qualitatively the same as in Fig. 2. Due to the large diffusivity, all scalar gradients are rapidly smoothed out, so that in both the IC and FC case the scalar field consists of large blobs. The scalar flux fields are characterized by a finer structure.

In Fig. 4 wavenumber spectra are shown for the energy, scalar variance, and scalar flux. In the IC case, classical Kolmogorov scaling proportional to $k^{-5/3}$ holds for $E(k)$ in the inertial range. The scalar variance spectrum $E_\theta(k)$ is also

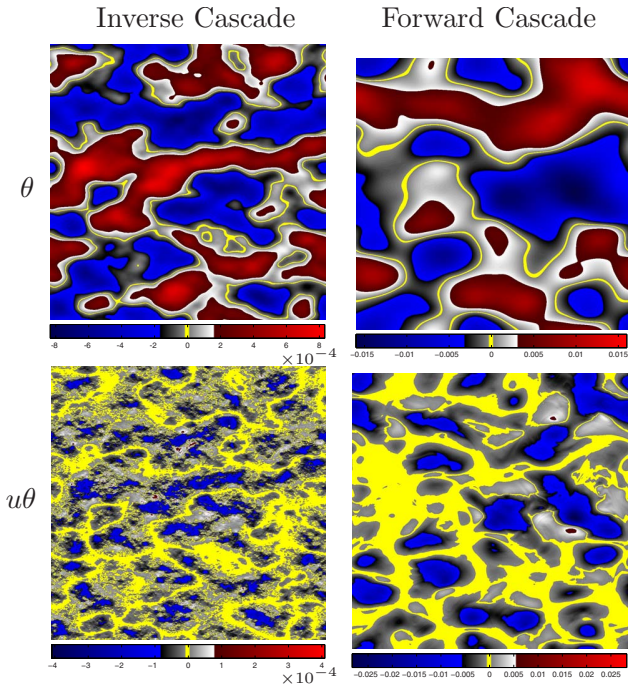

FIG. 3. (Color online) Visualizations of scalar fluctuations (top), scalar flux (bottom), in the IC (left) and in the forward cascade (right) for the case of small Schmidt number.

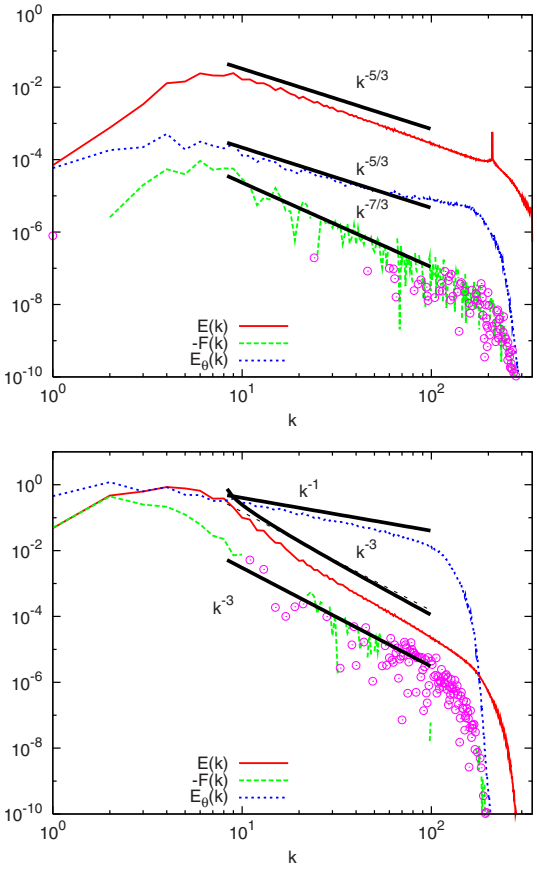

FIG. 4. (Color online) The energy spectrum, scalar flux spectrum and scalar variance spectrum for $Sc=1$. Top: the case of large wavenumber forcing (inverse energy cascade). Bottom: the case of small wavenumber forcing (forward entrophy cascade). The solid lines are dimensional predictions given by Eqs. (25) and (31). In the FC case also the log-corrected k^{-3} scaling is shown for the energy spectrum, which almost superposes the normal k^{-3} scaling. Dots indicate positive values of the scalar flux spectrum.

proportional to $k^{-5/3}$ as can be expected from Corrsin–Obukhov arguments, but showing an important prediffusive bump. This bump is frequently observed in spectra of the scalar variance, e.g., Refs. 9 and 35. The scalar flux spectrum is proportional to $k^{-7/3}$, which is in disagreement with expression (5) proposed as a rough estimate by Smith *et al.*,[19] and in perfect agreement with expression (25), which corresponds to classical Lumley scaling. Zero crossings are observed so that not the whole spectrum has the same sign.

In the FC range, the energy spectrum is approximately proportional to k^{-3}, but slightly steeper for the wavenumbers close to the injection scale k_i. Taking into account the logarithmic correction, the agreement with the prediction improves even more. The scalar variance spectrum $E_\theta(k)$ shows a Batchelor regime[32] proportional to k^{-1}. The scalar flux spectrum does show a scaling close to the scaling of the energy spectrum, especially for the absolute value of the spectrum. It is observed that the spectrum changes sign at several wavenumbers. These sign changes were also observed in the investigation of the scalar flux by the stretched spiral vortex model for three-dimensional turbulence.[23] The spectrum of the planar contribution of the Lundgren vortex to the scalar flux showed equivalent negative excursions. We therefore relate this behavior to the roll-up of the scalar field by large coherent vortices. Indeed, a fluid particle which remains for a long time trapped in a vortical structure will contribute both positively and negatively to the scalar flux.

As can be observed in Fig. 5, at small Schmidt number, excellent agreement is observed with the predictions. In the IC range, $F(k)$ is proportional to $k^{-11/3}$ and $E_\theta(k)$ to $k^{-17/3}$. In the FC range, $F(k)$ is proportional to k^{-5} and $E_\theta(k)$ to k^{-7}.

V. CONCLUSION

In this work the scaling of the scalar flux spectrum in two-dimensional isotropic turbulence was addressed. Phenomenological arguments based on Lagrangian dynamics were proposed leading to the following predictions for the inertial range scaling of the scalar flux spectrum:

$$\Gamma^{-1}F(k) \sim \begin{cases} \epsilon^{1/3}k^{-7/3} & \text{IC for } Sc \geq 1, \\ \beta^{1/3}k^{-3} & \text{FC for } Sc \geq 1, \\ \kappa^{-1}\epsilon^{2/3}k^{-11/3} & \text{IC for } Sc \ll 1, \\ \kappa^{-1}\beta^{2/3}k^{-5} & \text{FC for } Sc \ll 1, \end{cases} \tag{34}$$

and for the scalar variance spectrum,

$$E_\theta(k) \sim \begin{cases} \epsilon_\theta\epsilon^{-1/3}k^{-5/3} & \text{IC for } Sc \geq 1, \\ \epsilon_\theta\beta^{-1/3}k^{-1} & \text{FC for } Sc \geq 1, \\ \Gamma^2\kappa^{-2}\epsilon^{2/3}k^{-17/3} & \text{IC for } Sc \ll 1, \\ \Gamma^2\kappa^{-2}\beta^{2/3}k^{-7} & \text{FC for } Sc \ll 1. \end{cases} \tag{35}$$

It was shown by DNS that in the IC the scalar flux spectrum

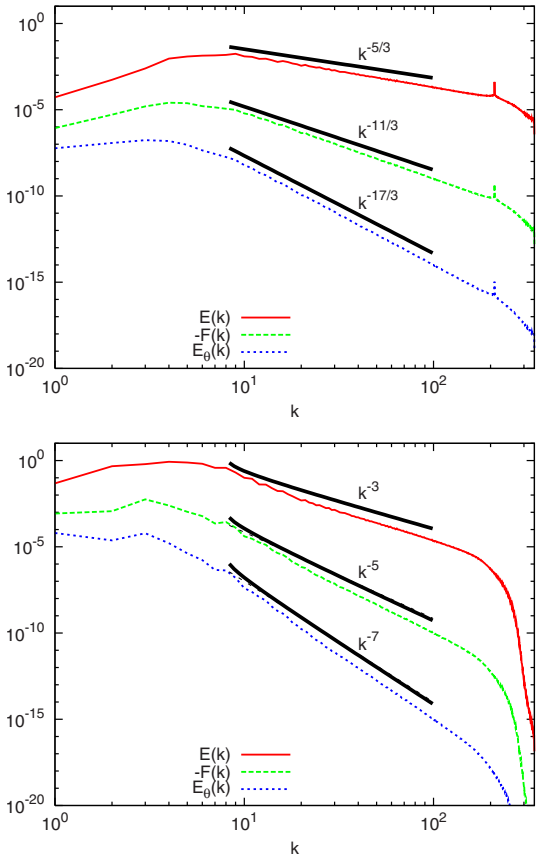

FIG. 5. (Color online) The energy spectrum, scalar flux spectrum, and scalar variance spectrum for $Sc \ll 1$. Top: the case of large wavenumber forcing (inverse energy cascade). Bottom: the case of small wavenumber forcing (direct entrophy cascade). The solid lines are dimensional predictions given by Eqs. (25) and (31). In the FC case all predictions are also shown with logarithmic corrections, which almost superpose on the uncorrected scalings.

is proportional to $k^{-7/3}$, in perfect agreement with the scaling arguments. The scalar variance shows Corrsin–Obukhov scaling, proportional to $k^{-5/3}$. In the direct enstrophy cascade the energy spectrum obeys a log-corrected k^{-3} scaling and the scalar spectrum displays Batchelor scaling proportional to k^{-1}. The scalar flux spectrum shows important positive and negative contributions, probably related to the presence of long-living coherent structures. The absolute value of the spectrum shows a scaling close to k^{-3}. At small Schmidt number, excellent agreement is observed with the predictions. The scalar flux spectrum scales here as $k^{-11/3}$ in the IC case and k^{-5} in the FC case. The scalar spectrum is proportional to $k^{-17/3}$ (IC) and k^{-7} (FC).

ACKNOWLEDGMENTS

We thankfully acknowledge financial support from the Agence Nationale de la Recherche, project "M2TFP."

[1] R. Schiestel, *Modélisation et Simulation des Écoulements Turbulents* (Hermes, Paris, 1993).
[2] M. M. Rogers, P. Moin, and W. C. Reynolds, "The structure and modeling of the hydrodynamic and passive scalar fields in homogeneous turbulent shear flow," Stanford University, Department of Mechanical Engineering Technical Report No. TF-25, 1986.
[3] P. M. Wikström, S. Wallin, and A. V. Johansson, "Derivation and investigation of a new explicit algebraic model for the passive scalar flux," Phys. Fluids **12**, 688 (2000).
[4] G. Brethouwer, "The effect of rotation on rapidly sheared homogeneous turbulence and passive scalar transport: Linear theory and direct numerical simulations," J. Fluid Mech. **542**, 305 (2005).
[5] S. Corrsin, "On the spectrum of isotropic temperature fluctuations in an isotropic turbulence," J. Appl. Phys. **22**, 469 (1951).
[6] J. Lumley, "Similarity and the turbulent energy spectrum," Phys. Fluids **10**, 855 (1967).
[7] J. Lumley, "The spectrum of nearly inertial turbulence in a stably stratified fluid," J. Atmos. Sci. **21**, 99 (1964).
[8] J. Wyngaard and O. Coté, "Cospectral similarity in the atmospheric surface layer," Q. J. R. Met. Soc. **98**, 590 (1972).
[9] L. Mydlarski and Z. Warhaft, "Passive scalar statistics in high-Péclet-number grid turbulence," J. Fluid Mech. **358**, 135 (1998).
[10] L. Mydlarski, "Mixed velocity-passive scalar statistics in high-Reynolds-number turbulence," J. Fluid Mech. **475**, 173 (2003).
[11] W. Bos, H. Touil, L. Shao, and J.-P. Bertoglio, "On the behaviour of the velocity-scalar cross correlation spectrum in the inertial range," Phys. Fluids **16**, 3818 (2004).
[12] W. Bos, H. Touil, and J.-P. Bertoglio, "Reynolds number dependency of the scalar flux spectrum in isotropic turbulence with a uniform scalar gradient," Phys. Fluids **17**, 125108 (2005).
[13] W. Bos and J.-P. Bertoglio, "Inertial range scaling of scalar flux spectra in uniformly sheared turbulence," Phys. Fluids **19**, 025104 (2007).
[14] P. A. O'Gorman and D. I. Pullin, "Effect of Schmidt number on the velocity-scalar cospectrum in isotropic turbulence with a mean scalar gradient," J. Fluid Mech. **532**, 111 (2005).
[15] T. Watanabe and T. Gotoh, "Scalar flux spectrum in isotropic steady turbulence with a uniform mean gradient," Phys. Fluids **19**, 121701 (2007).
[16] G. K. Batchelor, "Computation of the energy spectrum in homogeneous two-dimensional turbulence," Phys. Fluids Suppl. II **12**, II–233 (1969).
[17] R. Kraichnan, "Inertial ranges in two-dimensional turbulence," Phys. Fluids **10**, 1417 (1967).
[18] C. Leith, "Diffusion approximation for two-dimensional turbulence," Phys. Fluids **11**, 671 (1968).
[19] K. Smith, G. Boccaletti, C. Henning, I. Marinov, C. Tam, I. Held, and G. Vallis, "Turbulent diffusion in the geostrophic inverse cascade," J. Fluid Mech. **469**, 13 (2002).
[20] A. Kolmogorov, "The local structure of turbulence in incompressible viscous fluid for very large Reynolds numbers," Dokl. Akad. Nauk SSSR **30**, 301 (1941).
[21] A. Oboukhov, "Structure of the temperature field in turbulent flows," Izv. Akad. Nauk. SSSR, Geogr. Geofiz. **13**, 58 (1949).
[22] S. Herr, L. Wang, and L. Collins, "EDQNM model of a passive scalar with a uniform mean gradient," Phys. Fluids **8**, 1588 (1996).
[23] P. O'Gorman and D. Pullin, "The velocity-scalar cross correlation of stretched spiral vortices," Phys. Fluids **15**, 280 (2003).
[24] R. Kraichnan, "Lagrangian-history closure approximation for turbulence," Phys. Fluids **8**, 575 (1965).
[25] H. Lee, K. Squires, J. P. Bertoglio, and J. F. Ferziger, "Study of Lagrangian characteristic times using direct numerical simulation of turbulence," in *Turbulent Shear Flows 6*, edited by J. C. Andre, J. Cousteix, F. Durst, and B. E. Launder (Springer-Verlag, Berlin, 1989), p. 58.
[26] G. Batchelor, "Diffusion in a field of homogeneous turbulence. I. Eulerian analysis," Aust. J. Sci. Res., Ser. A **2**, 437 (1949).
[27] W. Bos and J.-P. Bertoglio, "A single-time two-point closure based on fluid particle displacements," Phys. Fluids **18**, 031706 (2006).
[28] H. Tennekes and J. Lumley, *A First Course in Turbulence* (The MIT Press, Cambridge, 1972).
[29] R. Kraichnan, "Inertial-range transfer in a two- and a three-dimensional turbulence," J. Fluid Mech. **47**, 525 (1971).
[30] C. Leith and R. Kraichnan, "Predictability of turbulent flows," J. Atmos. Sci. **29**, 1041 (1972).
[31] H. Zhou, G. Cui, Z. Zhang, and L. Shao, "Dependence of turbulent scalar flux on molecular Prandtl number," Phys. Fluids **14**, 2388 (2002).
[32] G. Batchelor, "Small-scale variation of convected quantities like temperature in turbulent fluid. Part 1. General discussion and the case of small

conductivity," J. Fluid Mech. **5**, 113 (1959).
[33]M.-C. Jullien, P. Castiglione, and P. Tabeling, "Experimental observation of Batchelor dispersion of passive tracers," Phys. Rev. Lett. **85**, 3636 (2000).
[34]K. Schneider, "Numerical simulation of the transient flow behaviour in chemical reactors using a penalization method," Comput. Fluids **34**, 1223 (2005).
[35]J. R. Herring, D. Schertzer, M. Lesieur, G. Newman, J.-P. Chollet, and M. Larcheveque, "A comparative assessment of spectral closures as applied to passive scalar diffusion," J. Fluid Mech. **124**, 411 (1982).

Chapter 5

Lagrangian statistics in 2D fluid and plasma turbulence

5.1 Time-correlations and intermittency of the Lagrangian acceleration in turbulence

It was already mentioned in the beginning of this manuscript that the nonlinear term of the Navier-Stokes equations couples different lengthscales. This was illustrated by noticing that a multiplication of two fields becomes a convolution when we consider the Fourier transform. A convolution involves an integral over all wavenumbers and thereby the scales are coupled. The multi-scale character is the most challenging feature for the theoretical description of a turbulent flow. In order to get an insight into the variety of scales and their importance, multiple point statistics were considered. The most straightforward statistic is the energy spectrum or second-order structure function. These quantities contain the information on the energy distribution of the different scales. The small scale limits of these quantities are directly linked to the velocity gradients in the flow and thereby to the energy dissipation. Third order spectra or structure functions are related to the energy transfer mechanism and fourth order velocity statistics are directly linked to the fluctuations around an energy distribution, the fluctuations of the fluctuations. Higher orders are related to even finer statistics. Probability density functions contain the entire hierarchy of moments. The probability density function of the velocity fluctuations is close to a Gaussian in three dimensional turbulence. This does however not mean that the velocity is a close to Gaussian variable. Indeed, the small scale multi-point statistics of the velocity are highly non-Gaussian, which can be seen by considering the PDF of the velocity gradients, and this would not be the case if the velocity were Gaussian. If the velocity modes were independent, the velocity gradients would also be Gaussian. The multi-scale information can be obtained by considering PDFs of velocity increments, or their Fourier transforms[1].

[1]Note that the PDF of the Fourier transform of the velocity is Gaussian. To observe the non-Gaussianity in Fourier space a possibility is to consider the PDF of the Fourier transform

Turbulence is not only a multiple-lengthscale phenomenon but also a multiple time-scale phenomenon. The study of time-correlations deserves therefore, in principle, as much attention as the space-correlations do. Hot-wire measurements in wind-tunnel turbulence give time series. However, these time series generally give information on the lengthscale correlations of a flow. By using Taylor's frozen turbulence assumption [120], the time-series are transformed into space-series. Indeed, if the mean velocity of the flow in a wind-tunnel is large compared to the characteristic velocity of the turbulent fluctuations, the time-series ressemble an instantaneous cut through a homogeneous decaying turbulent flow at a given time instant. So not much information about the time-scales is obtained in this way. One could hope that if we measure the time-correlations in a non-moving isotropic turbulent flow (*e.g.* generated by synthetic jets [121]), one would have a better chance. In fact this hardly improves the situation and will only give insight in the time-correlation of the largest eddies. Indeed, even in the absence of a mean flow, a small turbulent structure will be swept along the measurement point on a time-scale small compared to its intrinsic correlation time. So again we recover the measurement of a frozen Eulerian small scale turbulence, in which the largest flow structures of our turbulence are now playing the same role as the mean flow in the windtunnel experiments [21]. This is the same effect discussed in section 1.2.

How can we then measure the time correlations associated to scales smaller than the integral flow scales? To get rid of the influence of the sweeping of the large scales, one can try to follow a scale while it is swept around. In other words, our measuring probe will now move with the velocity. This is the Lagrangian reference frame. Measurements in the Lagrangian reference frame can thus unravel the temporal structure of turbulence. The velocity space increments, related to the spatial structure of turbulence in the Eulerian frame, have their Lagrangian counterpart, the velocity-time increments in the Lagrangian frame (but their relationship is not trivial [122]). In homogenous and stationary turbulence, the statistical distribution of the Lagrangian velocity can be shown to be identical to the statistical distribution of the Eulerian velocity. This is simply due to the fact that a fluid particle will have an equal probability to sample any position in space. Single-time statistics are thereby equal to the single-point statistics, a property called ergodicity. The PDF of the Lagrangian velocity is therefore, like the Eulerian, close to Gaussian. Other quantities in a turbulent flow are not necessarily Gaussian. A good example of this is the pressure. Imagine the velocity field is random and the modes independent. Its statistics are then Gaussian. One can now determine the pressure field by solving a Poisson-equation. The pressure is given by

$$p(\boldsymbol{x}) = FT^{-1}\left[-\rho\frac{k_i k_j}{k^2}\hat{u}_i(\boldsymbol{k}) \otimes \hat{u}_j(\boldsymbol{k})\right]. \tag{5.1}$$

The important point is here that the convolution on the right hand involves products of the Gaussian field. And the pdf of the product of two Gaussian variables is not Gaussian. More precisely, it was shown analytically in reference [123] that expression (5.2) yields pdfs with exponential tails for the pressure and for the pressure gradient, if the velocity is Gaussian. We also checked this numerically and confirmed this observation (see also reference [124]). This has

of the velocity increments, $\delta\hat{u}_L(\boldsymbol{k}) = \boldsymbol{e}_r \cdot \hat{\boldsymbol{u}}(\boldsymbol{k})\left[1 - e^{i\boldsymbol{k}\cdot\boldsymbol{r}}\right]$.

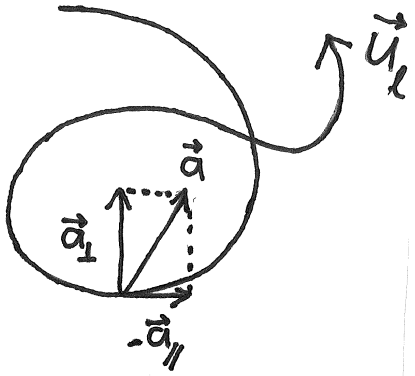

Figure 5.1: The acceleration of a fluid particle can always be decomposed into a component parallel to the trajectory and a component which is perpendicular. These two components of the Lagrangian acceleration are correlated over a much larger time-scale than the acceleration in arbitrary directions.

implications for the interpretation of results for the Lagrangian acceleration, which is the right hand side of the Navier Stokes equations, evaluated on a trajectory $\boldsymbol{X}(\boldsymbol{x}, t)$,

$$\boldsymbol{a}(\boldsymbol{X}, t) = -\frac{1}{\rho}\nabla p(\boldsymbol{X}, t) + \nu\Delta\boldsymbol{u}(\boldsymbol{X}, t) + \boldsymbol{f}(\boldsymbol{X}, t). \tag{5.2}$$

The dominant contribution to the acceleration is the pressure gradient [125]. The pdf of the acceleration will therefore closely ressemble the pdf of the pressure gradient. Even in a Gaussian velocity field the acceleration is therefore not Gaussian. Intermittency can thus not straightforwardly be measured by the non-Gaussianity of the velocity-time increments or the Lagrangian acceleration. A more precise definition is needed if one wants to employ the term intermittency to denote the anomalous features of turbulence. Again, as in section 3.4, one should compare to the case in which the flow-field is Gaussian. This need to compare with the statistics obtained in a flow consisting of independent modes is one of the messages in the following paper.

It was observed in simulations [126] that the PDF of the Lagrangian acceleration was indeed non Gaussian (as can be expected) and the tails of the PDF were shallower than exponential. This was confirmed in experiments [127, 128]. A phenomenological explanation was given in [129], arguing that long temporal correlations of the acceleration-field in the Lagrangian frame were responsible for the flaring tails of the acceleration PDF. In particular it is the norm of the accelation that is correlated over long time-intervals. A fluid particle in vortical motion changes direction on a very short time-scale such that the components of the acceleration in a Eulerian reference frame are decorrelated very rapidly. If the reference frame is aligned and moving with the trajectory, such as in Figure 5.1, the correlations are correlated over a much longer time. In such a frame, the time-correlation of the acceleration is related to the life-time of a flow structure or the time a fluid particle remains trapped in a flow structure. This

seems plausible, but the relation between the shape of the PDF and the time-correlations is not clearly proven hereby. It would be nice if we could vary the correlation time of the acceleration (or its norm), and check what the influence is on the shape of the PDF. This is of course not straightforward in Navier-Stokes turbulence. However, in the two-fluid plasma model of Hasegawa and Wakatani (as derived in section 4.3), the adiabaticity parameter exactly plays this role. The parallel electron dynamics tends to neutralize electric field fluctuations and the adiabaticity parameter regulates the rate at which this is happening. Very slow electron movement along the perpendicular magnetic field will allow the flow structures to have a long correlation time, whereas quasi-adiabatic electron behavior limits strongly the lifetime of the structures. By acting on the adiabaticity parameter we therefore have a way to modify the correlation time of the Lagrangian dynamics. Subsequently we can investigate how this changes the shape of the PDFs. This study has been carried out and is reported in the following manuscript.

Origin of Lagrangian Intermittency in Drift-Wave Turbulence

B. Kadoch,[1] W. J. T. Bos,[2] and K. Schneider[1]
[1]M2P2, CNRS UMR 6181 & CMI, Ecole Centrale de Marseille, Universités d'Aix-Marseille, Marseille, France
[2]LMFA, CNRS UMR 5509, Ecole Centrale de Lyon - Université de Lyon, Ecully, France
(Received 26 February 2010; published 27 September 2010)

The Lagrangian velocity statistics of dissipative drift-wave turbulence are investigated. For large values of the adiabaticity (or small collisionality), the probability density function of the Lagrangian acceleration shows exponential tails, as opposed to the stretched exponential or algebraic tails, generally observed for the highly intermittent acceleration of Navier-Stokes turbulence. This exponential distribution is shown to be a robust feature independent of the Reynolds number. For small adiabaticity, algebraic tails are observed, suggesting the strong influence of point-vortex-like dynamics on the acceleration. A causal connection is found between the shape of the probability density function and the autocorrelation of the norm of the acceleration.

DOI: 10.1103/PhysRevLett.105.145001 PACS numbers: 52.25.Fi, 52.35.Ra, 52.55.Fa

Turbulence is one of the main actors in degrading the confinement quality of magnetically confined fusion plasmas. This so-called micro-turbulence in the edge of plasma fusion devices, such as tokamaks, is commonly admitted to be of electrostatic nature [1,2]. A typical instability leading to this turbulent motion is the drift-wave instability, present in plasmas with a strong magnetic field and a temperature or pressure gradient. Turbulence leads to an enhanced diffusivity and its average influence can be characterized by transport coefficients which represent the mean influence of turbulent motion as an enhanced fluid property [3]. Reviews on the use of transport coefficients in fusion devices are given in [4,5]. Transport coefficients allow us to describe the mean transport on the level of second order moments such as the variance of the impurity density, kinetic energy, and fluxes. The spatial and temporal fluctuations around these variances are however not described by such an approach, since they are directly related to fourth-order moments. These fourth-order moments will give a rough description of the intermittent properties of the turbulence: is the transport bursty, corresponding to non-Gaussian fluctuations or diffusive so that it could be modeled by a Gaussian process? Indeed, if the turbulent transport is dominated by rare but strong events, the impact on the confinement quality will be different from the case where a Gaussian process governs the transport. In three-dimensional fluid turbulence it is now well established that the velocity displays near Gaussian statistics but that the velocity gradients and acceleration are characterized by probability density functions (PDFs) with strongly non-Gaussian tails [6,7]. In two dimensions it was shown that Lagrangian statistics can be strongly non-Gaussian even when the Eulerian statistics are perfectly Gaussian [8]. The present investigation is dedicated to the characterization of Lagrangian intermittency in the close-to-two-dimensional dynamics of electrostatic plasma turbulence.

Intermittency can be investigated through the statistical properties of velocity increments $\delta \boldsymbol{u}$, which can be defined both in an Eulerian and in a Lagrangian reference frame. Lagrangian velocity increments are defined as $\delta \boldsymbol{u}(t, \tau) = \boldsymbol{u}(t + \tau) - \boldsymbol{u}(t)$, where $\boldsymbol{u}(t)$ is the Lagrangian velocity, i.e., the velocity of a passive tracer monitored on its trajectory as a function of time. When the shape of the PDF of the velocity increments varies as a function of τ, the statistics are usually said to be intermittent, even though this definition can be criticized [9]. At smallest τ, the PDFs approach the shape of the acceleration PDF, which is generally non-Gaussian in turbulent flows.

The study of the Lagrangian dynamics of fluid turbulence is now possible in controlled turbulence experiments in which small solid tracer particles are followed in the flow (e.g., [10–12]) and numerical simulations of the Navier-Stokes equations [6]. Whereas the experimental tracing of particles in fusion reactors introduces problems related to the extreme conditions in controlled fusion, tracing of particles in numerical simulations of drift-wave turbulence is perfectly possible. In a recent study [9], we presented detailed results on the Lagrangian statistics obtained in simulations of drift-wave turbulence, within the context of the Hasegawa-Wakatani model [13,14]. In the present Letter we will focus on the non-Gaussianity of the acceleration statistics. In particular, we will investigate the influence of the Reynolds number and the collisionality on the statistics and we will propose explanations for the observed behavior.

The Hasegawa-Wakatani model can be derived from the Braginskii two-fluid description [15], considering an ion fluid and an electron fluid in the presence of a fixed magnetic field, assuming isothermal inertialess electrons and cold ions. For details on the derivation of the 2D slab version of Hasegawa-Wakatani equation, we refer, e.g., to [16]. The model assumptions yield eventually a closed set of equations, describing the vorticity $\omega = \nabla^2 \phi$ of the

$E \times B$ motion (with ϕ the electrostatic potential) and the advection of the plasma density fluctuations n:

$$\left(\frac{\partial}{\partial t} - \nu\nabla^2\right)\nabla^2\phi = [\nabla^2\phi, \phi] + c(\phi - n), \quad (1)$$

$$\left(\frac{\partial}{\partial t} - D\nabla^2\right)n = [n, \phi] - \boldsymbol{u}\cdot\nabla\ln(\langle n\rangle) + c(\phi - n), \quad (2)$$

in which all quantities are suitably normalized as in [17]. The model equations closely resemble the two-dimensional Navier-Stokes equations combined with the advection equation for a scalar n, representing here the fluctuations of the plasma density around a mean profile. Small-scale damping is introduced through the Laplacians, with ν and D denoting viscosity and diffusivity, respectively. Nonlinearities are written as Poisson brackets $[a, b] = \frac{\partial a}{\partial x}\frac{\partial b}{\partial y} - \frac{\partial a}{\partial y}\frac{\partial b}{\partial x}$. The source term in the above equation is the mean plasma-density profile $\langle n\rangle$, which is assumed to be exponentially decaying in the x direction and homogeneous in the y direction, so that Eq. (2) reduces to the advection of a scalar fluctuation with respect to an imposed uniform mean scalar gradient. The electrostatic potential ϕ plays for the $E \times B$ velocity the role of a stream-function, $\boldsymbol{u} = \nabla_\perp\phi$, i.e., $u_x = -\partial\phi/\partial y$ and $u_y = \partial\phi/\partial x$. The Lagrangian acceleration of tracer particles, advected by the $E \times B$ velocity is then

$$\begin{aligned}\boldsymbol{a}_L &= \frac{\partial\nabla_\perp\phi}{\partial t} + [\phi, \nabla_\perp\phi] \\ &= -\nabla p + \nu\nabla^2\boldsymbol{u} - \frac{\nabla_\perp}{\nabla^2}[c(n - \phi)], \end{aligned} \quad (3)$$

where p is the pressure. The adiabaticity c is given by

$$c = \frac{T_e k_z^2}{e^2 n_0 \eta \omega_{ci}}, \quad (4)$$

with T_e the electron-temperature, k_z the effective parallel wave number, e the electron charge, n_0 the reference plasma density, η the electron resistivity and ω_{ci} the ion-gyro-frequency. The adiabaticity is therefore determined by the electron resistivity, which is strongest in the edge of fusion devices, where the temperature drops. The proportionality to k_z^2, the square of the dominant wave number in the parallel direction, is a simplification which allows us to reduce the model towards a two-dimensional system. Since the strong magnetic field homogenizes the parallel dynamics, the perpendicular $E \times B$ velocity field is close to two-dimensional. This, in combination with the incompressibility of the $E \times B$ velocity and the assumption that the parallel dynamics is governed by a narrow spectrum peaked around a constant value k_z, allows us to use the above set of equations for the scalars ω and n.

The coupling term $c(\phi - n)$ permits the system to access a saturated turbulent state even in the absence of external forcing. This is the main difference with the equations describing the two-dimensional mixing of a scalar in fluid turbulence. It is related to the presence of the parallel current density, which couples the two equations and gives rise to an electrostatic plasma instability leading to a saturated turbulent state in which the energy is drawn from the imposed mean plasma-density profile. The collisionality of the ions and electrons plays a key role in the model. If the collisionality tends to a large value, hence c becomes small, the equations tend to a hydrodynamic 2D limit in which long-living vortices are observed. It was found in [9] that the Lagrangian acceleration in this case showed a very intermittent behavior, reflected by probability density functions with heavy tails. For intermediate values of c the flow is called quasiadiabatic. The PDFs of the acceleration in this regime tend to exponential distributions.

One remaining open question is whether this intermittent behavior is a Reynolds number effect. Indeed in three-dimensional Navier-Stokes turbulence [12,18] the flatness of the acceleration PDF increases as a function of the Reynolds number for the Reynolds numbers currently available. In the present investigation this Reynolds-number dependence is analyzed by exploiting the results of a set of direct numerical simulations of the Hasegawa-Wakatani model for varying Reynolds number.

Another issue is the relation between the time-correlation of the norm of the acceleration and the manifestation of intermittency as proposed by Mordant *et al.* [19]. The present study will allow us to assess this relation for the different regimes.

Equations (1) and (2) were solved in a double-periodic domain of size 64^2 using a fully dealiased pseudospectral method at a resolution of 1024^2 gridpoints, starting from Gaussian random initial conditions. In the saturated, fully developed turbulent flow 10^4 particles were injected, equally spaced, and their velocity and acceleration were monitored during a large number of large-scale turnover times ($\sim 400T_e$). The eddy turnover time T_e obtained in the different regimes, defined as $1/\sqrt{\mathcal{W}}$ where $\mathcal{W}$ is the rms vorticity, is of the same order of magnitude, $\sim$0.4. Details on the simulations of Eqs. (1) and (2) can be found in [9] and on the Lagrangian part of the study in [20] in which a similar investigation was performed for Navier-Stokes turbulence. The adiabaticity is varied between $c = 0.01$ and $c = 2$, to obtain different flow regimes. Visualizations of the vorticity field for two flow regimes are shown in Fig. 1.

In Fig. 2, the PDFs of the Lagrangian acceleration are shown for different values of c. It is observed that the PDF evolves from a close to exponential shape for large c to an algebraic shape for $c = 0.01$. To check if this is merely an effect of the Reynolds number, we performed simulations at different Reynolds numbers, which is here defined as $R_\lambda = \lambda\mathcal{U}/\nu$, with $\mathcal{U}$ the rms velocity and $\lambda = \mathcal{U}/\mathcal{W}$, an intrinsic scale of the turbulence. This Reynolds number was varied by a factor 6. The Prandtl number was chosen equal to one for all simulations. The results are shown in Fig. 3, where it is observed that the Reynolds number only slightly influences the shape of the PDFs. Therefore we need to find an alternative explanation for the difference in shapes of the

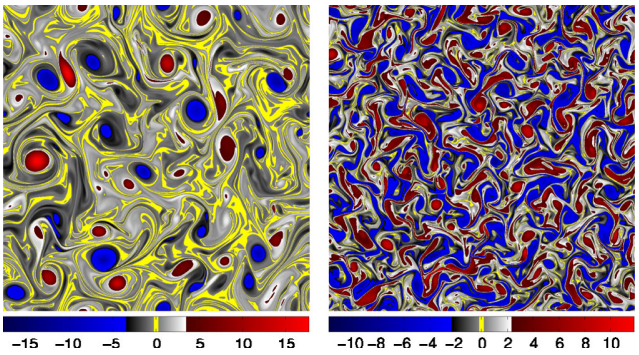

FIG. 1 (color online). Visualizations of the vorticity field for two different values of the adiabaticity. Left: $c = 0.01$, right: $c = 0.7$.

accelerations for the two different flow regimes. The exponential distributions can be explained as follows: it was argued in [21] that an exponential distribution for the pressure gradient PDF can be obtained from random Gaussian (nonintermittent) velocity fields by simply solving a Poisson-equation to obtain the pressure and subsequently computing the gradient, without considering the nonlinear dynamics of the Navier-Stokes equations. It can be seen from Eq. (3) that the pressure gradient is directly related to the Lagrangian acceleration. The shape of the PDFs for the cases for moderate and large c simply shows that the flow is not intermittent from a Lagrangian point of view, but governed by a Gaussian-like diffusion process.

More puzzling are the algebraic tails, found for small c. In the inset of Fig. 3 we show that the tails show a close to algebraic behavior of the form $p(a) \sim 1/a^{\beta}$ with β of the order 2. It is interesting to note that the shape of the PDFs obtained in the hydrodynamic case closely resembles the results obtained for point-vortices. Indeed, in Ref. [22] the point-vortex model, introduced by Onsager [23] and Townsend [24], was used to study the influence of point vortices on the Lagrangian acceleration of passive tracers. In their work, the acceleration PDF was to leading order given by $p(a) \sim 1/a^{5/3}$. In this light the results for the quasihydrodynamic flow seem to be at least partially explained by the presence of vortical structures as observed in Fig. 1. The exponent of the power-law tails of the acceleration PDF is close to the value $-5/3$ as in the point-vortex study. Even better agreement might be obtained by comparing with vortex-interaction models using vortices with a finite extension [25] (such as the Burger's vortex).

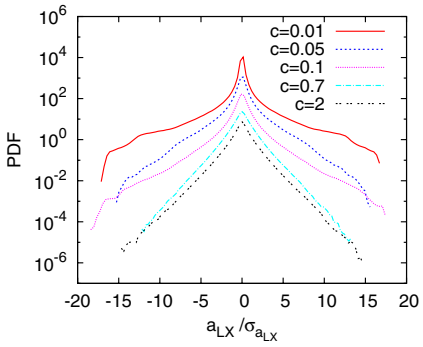

FIG. 2 (color online). PDFs of the Lagrangian acceleration (x component) for different values of c. PDFs are normalized by $\sigma_{a_{LX}}$, the rms value of the acceleration. Graphs for different c are shifted vertically for clarity.

It remains to be explained why this is not the case for the quasiadiabatic case. As observed in Fig. 1, in this case the drift-waves also seem to organize into vortical structures. However the lifetime of these structures is shorter [26]. The parallel dynamics are thus responsible for the change in lifetime of the vortices. For higher adiabaticity, electrostatic fluctuations are rapidly smoothed out through the parallel current. Vortices do then not exist long enough to influence the acceleration statistics intermittently. In this sense the long-time correlations seem to be essential to obtain the algebraic tails in the acceleration PDF. The centripetal component of the acceleration is constant in a purely circular orbit, and this is captured by the autocorrelation of the norm of the acceleration, which can therefore be directly related to the lifetime of the vortical structures. This is checked in Fig. 4. For all curves, time is normalized by the time at which the autocorrelation of the x component of the acceleration is minimum. This timescale can be qualitatively related to the timescale of the average circular motion of fluid particles. The autocorrelation of the acceleration components displays a behavior similar to what is observed in three-dimensional Navier-Stokes turbulence, with a rapid decrease and a negative dip. This dip becomes less pronounced for lower values of c. It is observed that in the cases in which a closer to exponential decay of the acceleration PDFs is observed, the autocorrelation of the norm decorrelates faster than in the cases in which

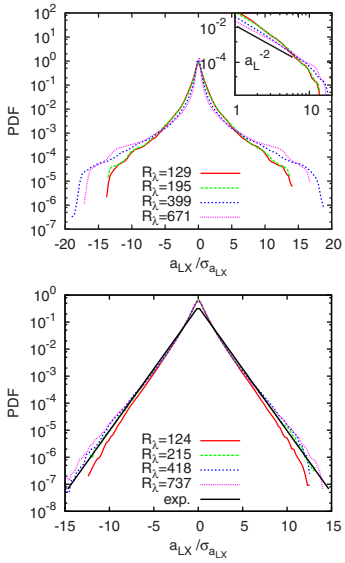

FIG. 3 (color online). PDFs of Lagrangian acceleration at different Reynolds numbers for $c = 0.01$ (top panel) and $c = 0.7$ (bottom panel). In the inset of the top panel, the power-law behavior of the tails of the PDF is demonstrated in double-logarithmic representation.

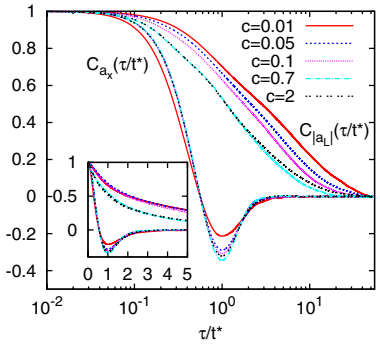

FIG. 4 (color online). Autocorrelations of the acceleration $C_{a_{Lx}}$ and autocorrelation of the norm of the acceleration $C_{|a_L|}$ for the five cases. Inset: Autocorrelations of the acceleration in lin-lin. For each curve, time is normalized by t^*, the time at which the correlation component reaches its minimum value.

the PDFs are algebraically decaying. Indeed the time correlations of the norm become longer for small adiabaticities. This constitutes a proof of the direct relation between the time-correlation of the norm of the acceleration and Lagrangian intermittency as proposed in [19]. A way to numerically check the assumption of the role played by time correlations of the norm of the acceleration within a point-vortex model would be to vary the lifetime of the vortices. If short enough lifetimes are imposed, exponential tails are probably obtained.

The main conclusion of the present work is that the electrostatic turbulence studied here is not intermittent once the adiabaticity is large enough. This corresponds to the case in which the parallel structures have a short enough wavelength (or high parallel wave number) or small collisionality. Intermittency due to electrostatic vortex structures is therefore expected to be stronger near the edge of fusion plasmas, where the collisionality becomes more important.

In the present Letter, the transition between long-living structures and short-lived wavy structures takes place somewhere in between $c = 0.1$ and $c = 0.7$. In reality the parallel spectrum is broadband and we assumed its peak around a certain frequency to obtain the simplified two-dimensional model. If the full three-dimensional model is considered, the dynamics will probably be a mixture between the different cases, dominated by a certain peak-wave number. Also the conclusions of this Letter relate to the dynamics captured within the present model, i.e., homogeneous electrostatic turbulence fed by a strong plasma-density gradient.

For larger adiabaticity ($c > 0.7$), which is expected to correspond to a situation further away from the edge or for colder plasmas, the statistics of this kind of turbulence are close to what would be expected from a Gaussian system. This study suggests that with respect to transport coefficients, microturbulence can be modeled by a Gaussian diffusion process with some additional rare point vortices if the adiabaticity is small enough ($c < 0.7$). This does not imply that plasma turbulence is not intermittent, only that its origin is not due to the mechanism contained in the present slab geometry if the adiabaticity is large enough. It could be interesting to carry out a similar study in a more complete geometry, such as in the study by Holland *et al.* [27]. In their work, dynamic regimes containing long-living vortices were observed, directly related to the large-scale zonal flows. However, no fully developed turbulent state was considered. Studying the turbulent Lagrangian dynamics in such a geometry constitutes an interesting perspective.

Salah Neffaa is acknowledged for the validation of the numerical code, and Diego del-Castillo-Negrete, Sadruddin Benkadda, and Shimpei Futatani for stimulating interaction.

[1] B. D. Scott, New J. Phys. **4**, 52 (2002).
[2] W. Horton, Phys. Rep. **192**, 1 (1990).
[3] J. Boussinesq, *Memoires Presentes par Divers Savants* Vol. 23, pp. 46-50 (Academie des Sciences Institut de France, Paris, 1877).
[4] X. Garbet, Plasma Phys. Controlled Fusion **43**, A251 (2001).
[5] X. Garbet, C.R. Physique **7**, 573 (2006).
[6] P. K. Yeung and S. B. Pope, J. Fluid Mech. **207**, 531 (1989).
[7] F. Toschi and E. Bodenschatz, Annu. Rev. Fluid Mech. **41**, 375 (2009).
[8] O. Kamps and R. Friedrich, Phys. Rev. E **78**, 036321 (2008).
[9] W. J. T. Bos, B. Kadoch, S. Neffaa, and K. Schneider, Physica D (Amsterdam) **239**, 1269 (2010).
[10] S. Ott and J. Mann, J. Fluid Mech. **422**, 207 (2000).
[11] N. Mordant, P. Metz, O. Michel, and J.-F. Pinton, Phys. Rev. Lett. **87**, 214501 (2001).
[12] G. Voth, A. L. Porta, A. Crawford, J. Alexander, and E. Bodenschatz, J. Fluid Mech. **469**, 121 (2002).
[13] A. Hasegawa and M. Wakatani, Phys. Rev. Lett. **50**, 682 (1983).
[14] M. Wakatani and A. Hasegawa, Phys. Fluids **27**, 611 (1984).
[15] S. Braginskii, in *Reviews of Plasma Physics*, edited by E. M. A. Leontovich (Consultants Bureau, New York, 1965), Vol. 1, p. 205.
[16] W. Horton and Y-H. Ichikawa, *Chaos and Structures in Nonlinear Plasmas* (World Scientific, Singapore, 1996).
[17] W. J. T. Bos, S. Futatani, S. Benkadda, M. Farge, and K. Schneider, Phys. Plasmas **15**, 072305 (2008).
[18] P. Vedula and P. K. Yeung, Phys. Fluids **11**, 1208 (1999).
[19] N. Mordant, J. Delour, E. Leveque, A. Arneodo, and J.-F. Pinton, Phys. Rev. Lett. **89**, 254502 (2002).
[20] B. Kadoch, W. J. T. Bos, and K. Schneider, Phys. Rev. Lett. **100**, 184503 (2008).
[21] M. Holzer and E. Siggia, Phys. Fluids A **5**, 2525 (1993).
[22] M. P. Rast and J.-F. Pinton, Phys. Rev. E **79**, 046314 (2009).
[23] L. Onsager, Nuovo Cimento **6**, 279 (1949).
[24] A. Townsend, Proc. R. Soc. A **208**, 534 (1951).
[25] M. Wilczek, F. Jenko, and R. Friedrich, Phys. Rev. E **77**, 056301 (2008).
[26] A. E. Koniges, J. A. Crotinger, and P. H. Diamond, Phys. Fluids B **4**, 2785 (1992).
[27] C. Holland, G. R. Tynan, J. H. Yu, A. James, D. Nishijima, M. Shimada, and N. Taheri, Plasma Phys. Controlled Fusion **49**, A109 (2007).

5.2 The influence of walls on Lagrangian statistics

The non-Gaussianity of the Lagrangian acceleration is thus not a direct measure for the statistical dependence of the modes of a turbulent flow. Its deviations from an exponential distribution are, however. In three dimensional turbulence the PDF of the acceleration presents, at high Reynolds numbers, tails which are significantly wider than exponential. These flaring tails imply that fluid particles experience very strong accelerations, but that these extreme events are relatively rare (but more frequent than in a Gaussian velocity field). The PDFs measured in different experimental set-ups show often universal features but also persistent differences. The question as to what extent the flow geometry influences the shape of the statistics deserved therefore attention. We addressed this question by performing simulations of decaying two-dimensional turbulence in which we compared the statistics of a flow in a periodic domain with the statistics of a flow in a wall bounded domain. It was observed that the pdfs of the acceleration in the wall-bounded domain showed algebraic tails, whereas in the periodic domain the pdfs were closer to exponential. Qualitative insights were obtained about where the strong values of the acceleration originated [14]. These results are illustrated in Figure 5.2.

However, two-dimensional turbulence has the peculiarity that the enstrophy is dissipated much more rapidly than the energy. Since the entrophy is directly proportional to the energy dissipation, the system rapidly evolves to a state with almost constant energy, unless enstrophy is produced somewhere. In a periodic domain the enstrophy production is zero. However, in a wall bounded domain the walls act as an enstrophy source. This means that in the presence of walls the energy will be dissipated more rapidly. It is therefore hard to compare the statistics of the flows obtained in the two-different geometries. In order to improve the comparability of the statistics, we normalized the velocity field by the rms velocity before computing the statistics. This corrects for the different decay-rate of the flows. It does however not correct for the different decrease in the intrinsic Reynolds number, which is related to the range of interacting lengthscales. This Reynolds number decays faster in the wall-bounded case, and normalizing the velocity does not correct for this.

We therefore carried out a study in which we added a large-scale forcing to the flows. This would allow us to avoid the problem of the energy decay. However, the presence of a forcing in two-dimensional turbulence also needs the introduction of a damping term, in particular in periodic geometry, since the inverse cascade of energy will lead to a pile-up of energy in the smallest allowed wave-mode, eventually leading to an unphysically large energy in the largest flow scale. This means that the system contains a large number of parameters: the friction wave-length, the friction strength, the forcing-wavelength, time-correlation and strength, and the viscosity. Despite this large number of parameters we managed to create flows that seemed to be comparable with respect to the amount of energy and Reynolds number in the two different geometries. As a result the differences in shape in the PDFs became much smaller then in the decaying case. However, the influence of the walls remained measurable and in particular the enstrophy level seemed to influence the statistics [15].

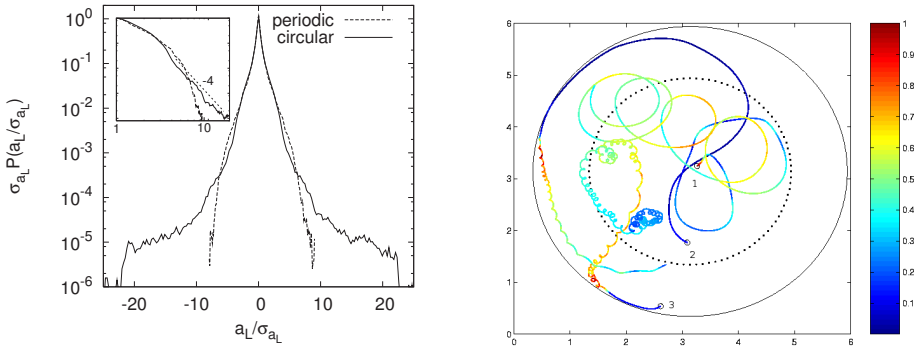

Figure 5.2: The influence of solid (no-slip) boundaries on the Lagrangian statistics in two-dimensional turbulence are investigated by comparing two-dimensional flow with and without walls. The PDF of the acceleration significantly changes its shape (left) when boundaries are present. An illustration of a trajectory, coloured by the value of the norm of the acceleration is shown in the right figure.

5.3 The influence of flow topology

It is very tempting to link the non-Gaussian features observed in the Lagrangian dynamics of turbulent flows to flow structures. However, a long-lasting problem is to identify the effect of a coherent structure on a flow, since one then needs to define the coherent structure, and this is often a matter of taste and/or vigorous debate. It can be asked whether the quest for a definition of a coherent structure, isolated from the incoherent flow-field even makes sense.

For example, a great idea was the apophatic definition proposed in [130]: a coherent structure is what remains if the incoherent part of a flow is removed. The incoherent part was then defined by the fully independent modes, in other words the noise. The resulting coherent flow possessed a number of degrees of freedom which was greatly reduced, compared to the total number of degrees of freedom needed to simulate the entire flow. Roughly, about only one percent of the total number of degrees of freedom is needed to capture all energetically important features of a statistically stationary turbulent flow and almost all dissipative features. In particular, the conclusion of this definition of a coherent structure implies that the coherent structures contain almost all the energy and enstrophy of the system. If the coherent structures are removed, almost nothing is left and if one wants to consider the coherent structures alone, almost the full flow is retained, so that this approach does not yield a tractable system amenable to a simple statistical description[2].

It is possible to avoid this issue by considering the influence of the flow topology, without trying to define a coherent structure. We can for example reformulate the question and ask whether regions of strong vorticity lead to

[2]Since the original flow in the cited reference corresponds to a Direct Numerical Simulation (DNS) of three-dimensional isotropic turbulence projected on 256^3 Fourier modes, 1% still corresponds to 5.10^5 degrees of freedom. So whereas the the reduction is impressive, and the technique certainly deserves to be exploited to propose efficient numerical computation of turbulence, we cannot consider the resulting set of modes a low-dimensional system.

extreme events, or strong shear layers. The link between flow topology and acceleration was studied in reference [16]. In order to separate the flow in topologically distinct regions the Okubo-Weiss criterion was used. This criterion is defined by [131]:

$$\begin{aligned} Q &= s^2 - \omega^2 \\ &= 2\Delta p \end{aligned} \tag{5.3}$$

With $s^2 = s_1^2 + s_2^2$ and $s_1 = \partial_x u - \partial_y v$ and $s_2 = \partial_x v + \partial_y u$. In elliptic regions the vorticity dominates and $\omega^2 > s^2$ so that Q is negative. In hyperbolic regions the strain dominates, $\omega^2 < s^2$, and Q is positive. This criterion is not necessarily adapted to define coherent structures, since the definition of coherent structures is vague. However, we can objectively separate a flow into elliptic and hyperbolic regions by using the above criterion.

We used the above criterion to analyze the influence of the flow topology on Lagrangian statistics. Forced two-dimensional turbulence was considered and at each time, the value of Q was computed for the flow-field. In Figure 5.3 (top right) the probability density function of the Weiss field is shown, indicating how much the different values of Q appear in the flow. It is observed that the PDF is strongly skewed, showing a non-negligible chance of occurences of strong negative values of Q, smaller than several standard deviations σ_Q (the Lagrangian and Eulerian PDFs coincide due to ergodicity). Subsequently, we arbitrarily separate the flow-field into three subspaces, the part of the flow with Q smaller then $-\sigma_Q$, the part with $Q > \sigma_Q$ and the remaining intermediate Q-valued part of the flow. We then determine statistics within the three subspaces. In 5.3 (top left) we show a particle trajectory, in which the color of the trajectory changes when it changes its local value of Q, according to the above defined limit-values. In 5.3 (bottom left) we show the PDFs of the Lagrangian acceleration, corresponding to these different topological regions. In particular, it is observed that in the elliptic and hyperbolic regions the tails of the PDFs are not "flaring" significantly, but are close to exponential. The typical shape of the PDFs is rather caused by a large peak in the PDFs around zero for the intermediate Q values. To some extent, the origin of the characteristic shape of the PDFs can be attributed to the intermittency of the flow topology. A large part of the flow is topologically quiescent, and the Lagrangian acceleration in this part is strongly peaked around zero. The contributions of the topologically more extreme regions leads to tails that are raised. Considering these topologically more active regions by themselves, the PDFs are close to exponential, as would be expected for Gaussian velocity fields.

In a related study [132], we investigated the flow-topology of drift wave turbulence. In Figure 5.4 we show the probability density function of the Q-parameter for two distinct values of the adiabaticity. As discussed in the previous section, this parameter controls the time-correlations of the velocity field. In the case of strong adiabaticity, vortical structures do not have a long lifetime and very strong vorticity fluctuations are very rare. However in the case in which the adiabaticity is small, strong and extreme vortical regions persist and the PDF of the Q parameter is much closer to what is observed in Navier-Stokes turbulence.

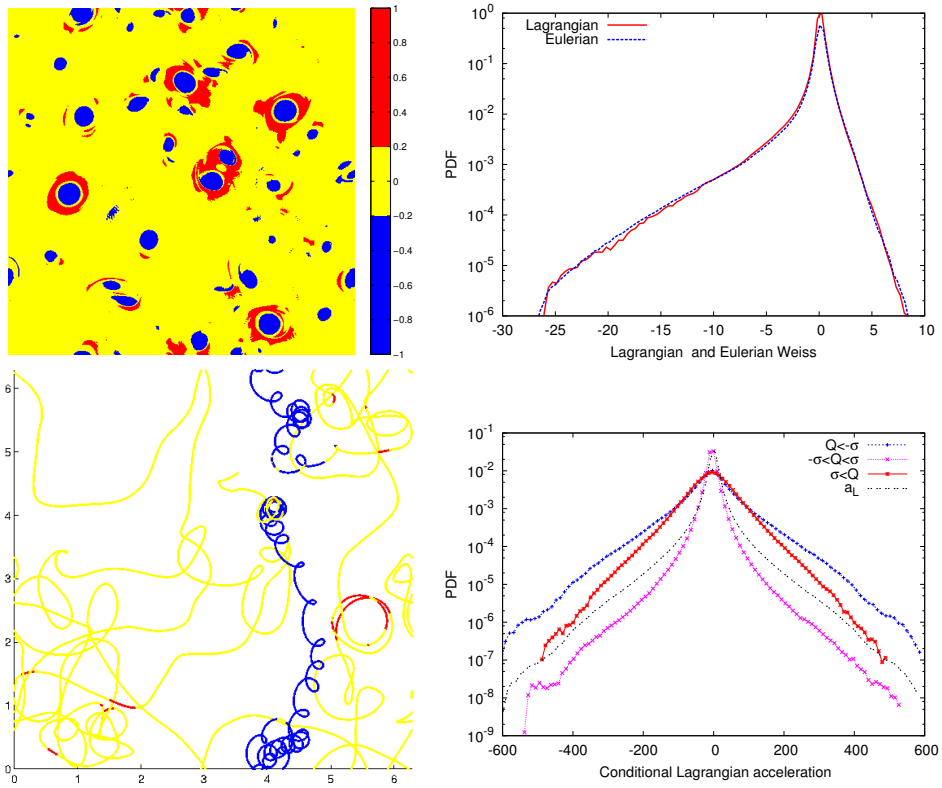

Figure 5.3: The influence of the flow-topology on Lagrangian statistics in two-dimensional turbulence is studied. Top left: the flow field is divided into strongly elliptic, strongly hyperbolic and intermediate strain regions. Top right: the PDF of the Q-criterion indicates the distribution of space over these different regions. Roughly, the values on the LHS of the peak correspond to the highly elliptic regions and on the RHS of the peak to the highly hyperbolic regions. The peak itself corresponds to the intermediate valued regions. Bottom left: a trajectory of a fluid particle coloured at each time by its Q-value. Bottom right: Lagrangian acceleration PDFs for the different subregions. From reference [15].

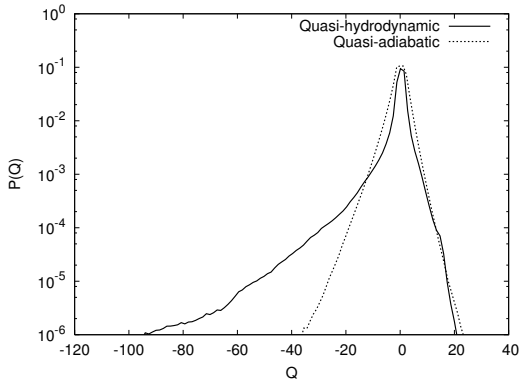

Figure 5.4: Probability density function of the Q-criterion in drift-wave turbulence. In the case of quasi-adiabatic electrons the PDF is almost symmetric and no extreme vorticity concentrations appear as is the case in hydro-dynamic or quasi-hydrodynamic flows. From reference [132].

5.4 Perspectives

Lagrangian spectra in two and three dimensions computed from markovian closures

In principle, all the Galilean invariant closures discussed in chapter 2 contain information on the Lagrangian correlation times of the turbulent velocity field. Some results are obtained using closure to study Lagrangian quantities [23, 133], but a large number of quantities is unexplored. This seems a promising direction in order to study the asymptotic behavior of Lagrangian statistics. Indeed, the Reynolds numbers needed to observe clear scaling ranges are even larger for Lagrangian than for Eulerian quantities. Closure can help to study the Reynolds number dependence of the scaling of Lagrangian spectra to bridge the gap between low Reynolds number observations and asymptotic scaling predictions.

The dynamics of drift-wave turbulence in wall bounded geometry

The self-organization of drift-wave turbulence in a plasma column was studied both experimentally and numerically in the group of George Tynan [134]. It was observed that a poloidally spinning plasma resulted from the drift-wave turbulence zonal flow interaction (see reference [135] for a review on zonal flows and [136] for a review on experimental studies of the subject). The numerical methods we use to study wall bounded flows (6.3) allow to easily change flow geometry and flow-parameters. The influence of the shape of the geometry on the generation of zonal flows in drift-wave turbulence deserves further study.

Chapter 6

Self-organization in magnetohydrodynamic turbulence

6.1 Decay and final states

Inviscid invariants, defined as quantities that are conserved by a system in the absence of viscosity, determine to a large extent the dynamics of a system. An important example is the kinetic energy of a three-dimensional turbulent flow. Since this quantity cannot be dissipated if the viscosity is zero, the nonlinear interactions can only redistribute the quantity over different modes. From a statistical mechanics point of view, one expects that this redistribution will act in such a way as to increase some kind of entropy of the system. Since the truncated Euler-system admits a solution in thermal equilibrium (corresponding to a maximum entropy state), it is tempting to expect that the nonlinear interactions will on average redistribute the energy in such a way as to approach this equilibrium. The equilibrium for the three-dimensional, mirror invariant, Euler-equations corresponds to an equipartition of energy between the different modes (see section 3.1). In most turbulent flows in nature, instabilities inject energy in large scales so that the initial condition is far from this equipartitioned state. In order to approach the equilibrium, the system will transfer, on average, its energy towards smaller scales. If the energy input into the system is statistically steady, a constant flux of energy through scale-space is expected, better known as the cascade. Phenomenological arguments about scale-interaction-locality then lead to predictions for the energy spectrum.

In two-dimensional turbulence, more than one invariant exist. The kinetic energy is one of them. All squared functions of the vorticity are also invariants. The only variants that survive a Galerkin truncation are the enstrophy and the energy. We therefore give more importance to these two quantities. A simple argument due to Fjørtoft shows that the nonlinear interaction of modes cannot transfer both energy and enstrophy in the same direction. The enstrophy

spectrum is related to the energy spectrum by the relation[1],

$$Z(k) = k^2 E(k), \tag{6.4}$$

in which

$$\int Z(k)dk = \frac{1}{2}\overline{\omega_i \omega_i}. \tag{6.5}$$

The (truncated inviscid) equilibrium energy distribution of two-dimensional turbulence is of the form

$$E(k) \sim \frac{k}{\beta + \alpha k^2}, \tag{6.6}$$

in which α and β are constants for a given flow-geometry. For large k this spectrum is proportional to k^{-1}. The enstrophy spectrum is thus proportional to k. For large k this corresponds to an equipartition of the enstrophy[2]. Kraichnan suggested [137] that if the system is to evolve towards such a distribution, the enstrophy will on average be transferred to the small scales, which implies that energy will tend to transfer to the large scales. This is indeed observed in two-dimensional turbulence. This clearly shows the importance of the invariants for the evolution of turbulent flows.

In the case of MHD, even more invariants can be identified. In the two-dimensional case we can mention the total energy E, which is the sum of the kinetic and magnetic energy, the mean-square vector potential A and the cross-helicity H_c. Again these inviscid invariants determine the dynamics of the system as was shown in an investigation by Ting, Matthaeus and Montgomery [138]. They studied, using low resolution DNS, the dynamics of 2D MHD for a large variety of initial conditions, and they determined towards which state the system evolves. It was observed that the results were well predicted by a variational computation in which the energy was minimized subject to constraints on the quantities A and H_c. In total, four qualitatively different dynamical behaviors were identified. These behaviors were: the *Navier-Stokes* behavior (for very small initial magnetic field), *magnetically dominated* behavior, (for initial magnetic field comparable or larger than the velocity field and small cross-helicity), *dynamic alignment* (for substantial initial cross-helicity) and a kind of *transition*

[1] This relation can be shown as follows. The vorticity is given in Fourier space by the relation

$$\omega_i(\boldsymbol{k}) = i\epsilon_{ijk}k_j u_k(\boldsymbol{k}). \tag{6.1}$$

Since the vorticity is solenoidal, the spectral correlation tensor of the vorticity has the form

$$\overline{\omega_i(\boldsymbol{k})\omega_j(-\boldsymbol{k})} = P_{ij}(\boldsymbol{k})\frac{Z(k)}{4\pi k^2}. \tag{6.2}$$

The enstrophy spectrum is thus given by

$$\begin{aligned} Z(k) &= 2\pi k^2 \overline{\omega_i(\boldsymbol{k})\omega_i(-\boldsymbol{k})} \\ &= 2\pi k^2 \left[\epsilon_{ijk}\epsilon_{imn}k_j k_m \overline{u_k(\boldsymbol{k})u_n(-\boldsymbol{k})}\right] \\ &= 2\pi k^2 \left[(\delta_{jm}\delta_{kn} - \delta_{jn}\delta_{km})k_j k_m \overline{u_k(\boldsymbol{k})u_n(-\boldsymbol{k})}\right] \\ &= 2\pi k^4 \left[\overline{u_i(\boldsymbol{k})u_i(-\boldsymbol{k})}\right] = k^2 E(k). \end{aligned} \tag{6.3}$$

[2] In two dimensions, equipartition distributions over wave-vectors yield a power-spectrum proportional to k. This comes from the fact that we now do not integrate a constant function (the energy per mode) over a spherical shell $4\pi k^2 dk$, as in three dimensions, but over a circular shell $2\pi k dk$.

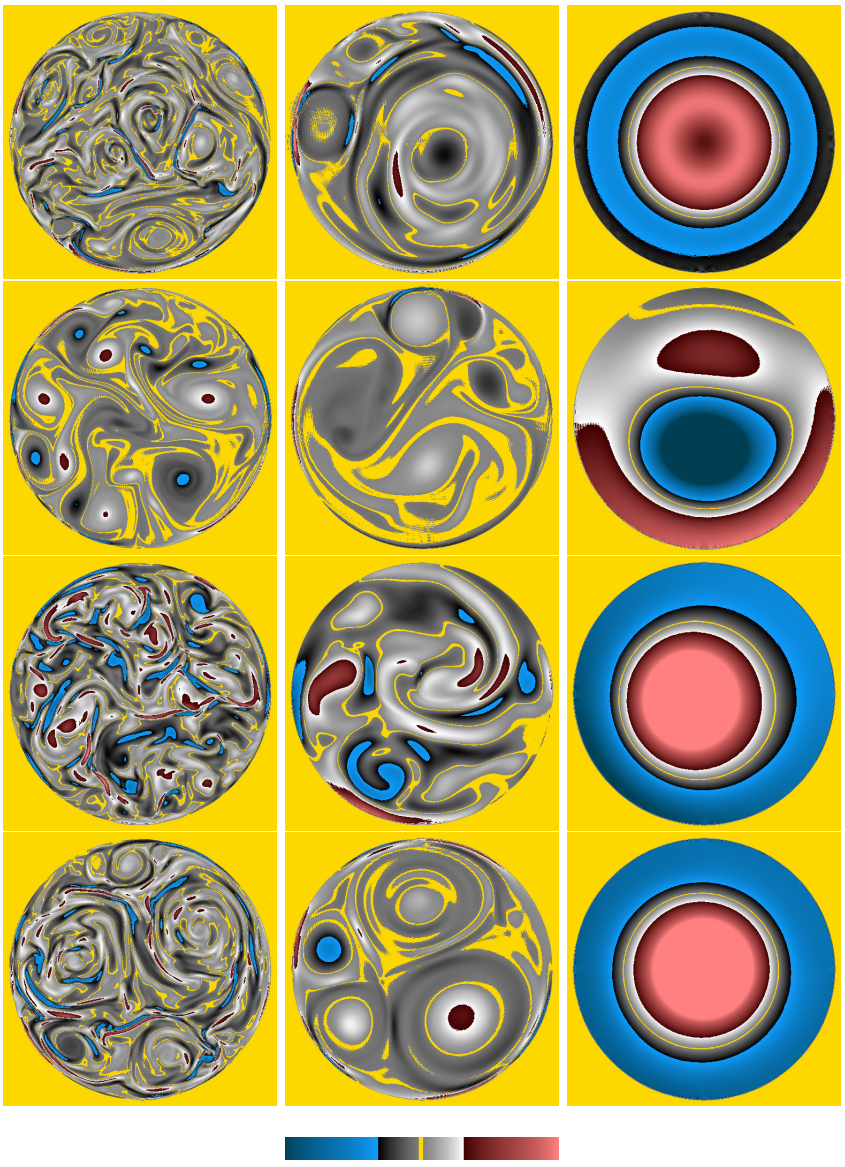

Figure 6.1: Vorticity at different instants. From top to bottom: regime I, regime II, regime III and regime IV; from left to right: $t = 5$, $t = 40$ and in the last column the time coresponds to $t = 250$ for regime I and $t = 1250$ for regimes II, III and IV. From reference [17].

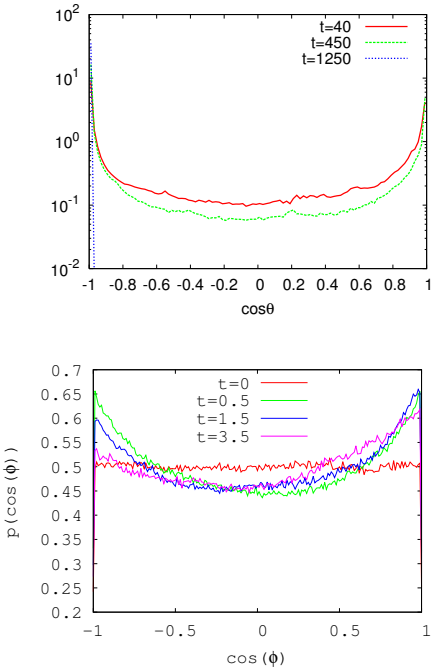

Figure 6.2: Top: Alignment of the velocity and magnetic field in the 'transition'-regime. The average alignment is small, but locally very strong alignment and anti-alignment of the two vector-fields is observed. This is a clear manifestation of depletion of nonlinearity in 2D MHD. Bottom: alignment of velocity and vorticity in decaying isotropic turbulence (preliminary results by Andrey Pushkarev).

state, sometimes tending to the magnetically dominated regime, sometimes to the the dynamic alignment regime.

In a recent study [17], we investigated how the dynamics change when the system is confined by isolating boundaries. Flow visualizations are shown in Figure 6.1. The boundary conditions were chosen such that the normal component of the magnetic field vanishes at the wall. The presence of these boundaries did not show the appearance of qualitatively different regimes, i.e., the four identified regimes survived. However, our simulations, at higher resolution than the study by Ting *et al.* showed that the Navier-Stokes regime does not survive at arbitrarily high Reynolds number, unless the magnetic field is chosen vanishingly small in the beginning. The small-scale dynamo effect, with its ability to (transiently) amplify a seed magnetic field will lead to a state in which the Lorentz force is not negligible if the initial Reynolds number is strong enough and the magnetic field is not too small (See also the study by Biskamp and Welter [139]).

In our investigation we observed that the transition state corresponds to a state in which locally the magnetic field and the velocity field are strongly aligned (Figure 6.2). If only a subregion were considered, the cross-helicity would be strong. The sum of the different subregions leads however to a van-

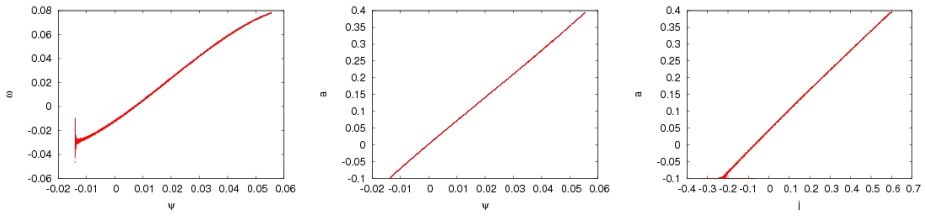

Figure 6.3: Scatter plots of (from left to right) ω vs ψ, a vs ψ and a vs j for the magnetically dominated regime, at the latest time instant $t = 250$.

ishing cross-helicity for the total field. This phenomenology can be compared to a 3D flow in which the velocity and the vorticity locally align, leading to local helicity fluctuations, summing up to zero for the total flow (Figure 6.2, bottom). In both cases this leads to a reduction of the strength of the nonlinear term[3]. Again this is thus a manifestation of the phenomenon of depletion of nonlinearity (as discussed in section 3.4). In other investigations in the same year, the same dynamics were reported [140, 141].

It was shown by Joyce and Montgomery [89] that in hydrodynamic periodic two-dimensional flows a long lasting final state is reached, depleted from nonlinearity. This state is characterized by a functional relation between the vorticity and the streamfunction of the form $\omega \sim \sinh(\psi)$. That a functional relation leads to a state, depleted from nonlinearity is easily shown from the equation for the vorticity:

$$(\partial_t - \nu\Delta)\omega = [\omega, \psi], \tag{6.7}$$

with the Poisson bracket defined as $[a, b] = (\partial a/\partial x)(\partial b/\partial y) - (\partial a/\partial y)(\partial b/\partial x)$. A functional relation $\omega = F(\psi)$ leads to a vanishing Poisson bracket,

$$[\omega, \psi] = \frac{\partial \omega}{\partial x}\frac{\partial \psi(\omega)}{\partial y} - \frac{\partial \omega}{\partial y}\frac{\partial \psi(\omega)}{\partial x} \tag{6.8}$$

$$= \frac{\partial \omega}{\partial x}\frac{\partial \psi(\omega)}{\partial \omega}\frac{\partial \omega}{\partial y} - \frac{\partial \omega}{\partial y}\frac{\partial \psi(\omega)}{\partial \omega}\frac{\partial \omega}{\partial x} = 0. \tag{6.9}$$

If we consider now the equations for incompressible MHD:

$$(\partial_t - \nu\Delta)\omega = [\omega, \psi] - [a, j] \tag{6.10}$$

$$(\partial_t - \eta\Delta)a = [a, \psi], \tag{6.11}$$

we see that two nonlinearities play a role: $[\omega, \psi]$ and $[a, j]$. The term $[a, \psi]$ can be considered as a pseudo-nonlinearity if ψ is regarded as given (see also our discussion on depletion of advection 3.4). Although important theoretical progress has been made in the comprehension of final states [142, 143] no analytical nontrivial solution is presently known for the case of decaying MHD turbulence. It was however shown in Kinney *et al.* [144] that close to functional

[3]That alignment of the magnetic field with the velocity field leads to a depletion of the nonlinear interaction can be seen by rewriting the equations for $\boldsymbol{u}$ and $\boldsymbol{b}$ as equations for $\boldsymbol{z}^+ \equiv \boldsymbol{u} + \boldsymbol{b}$ and $\boldsymbol{z}^- \equiv \boldsymbol{u} - \boldsymbol{b}$. In these equations the nonlinear term appears in the form $\boldsymbol{z}^+ \cdot \nabla \boldsymbol{z}^-$. This term is minimized when $\boldsymbol{u} \approx \pm \boldsymbol{b}$.

relations do exist in homogeneous two-dimensional MHD turbulence. In figure 6.3 we show for the magnetically dominated regime scatter plots corresponding to the three nonlinearities.

We observe a well defined nonlinear functional relation $\omega(\psi)$. Clearly, we have a non trivial final state. The plot a vs. j shows a straight line, which corresponds to a vanishing Lorentz-force: the magnetic field does not interact with the velocity field during this final period of decay.

6.2 Spin-up

A new quantity which appears as soon as boundaries are added to the flow (in contrast to periodic geometry) is the angular momentum, defined by

$$\int \boldsymbol{r} \times \boldsymbol{u} \; dS. \tag{6.12}$$

The angular momentum quantifies to what extent the flow contains a preferential large-scale swirling structure. The generation of angular momentum from initial conditions free from angular momentum is thus an example of symmetry breaking. The transport of angular momentum is important in the dynamics of planetary accretion disks. The mechanism in which angular momentum is transported in these disks has recently aroused the interest of the astronomical community. Indeed, in these disks, in Keplerian motion, angular motion is transported in the radial direction at a rate which can only be explained by turbulent motion, since their dynamics are essentially inviscid. However the flows are linearly stable according to hydrodynamic stability criteria. A possible mechanism to trigger turbulence is then the magneto-rotational instability *e.g.* [145]. Experimental studies in this area use the Taylor-Couette set-up which represents certain features of accretion disks *e.g.* [146, 147]. For the moment the mechanism remains poorly understood, in particular since the dimensionless numbers characterizing accretion disks are difficultly attainable in experimental set-ups and since the boundary conditions seem to play an important role [148].

Another major manifestation of angular momentum transport and generation is the intrinsic rotation of fusion plasmas which we will discuss in the following section.

Academically, one of the most simple settings in which we can study the generation and transport of angular momentum is the case of two-dimensional Navier-Stokes turbulence. It was discovered in [149] that angular momentum was spontaneously created from random initial conditions as soon as the confining boundaries are not axisymmetric. We investigated this phenomenon, called spin-up, in two-dimensional MHD and the results are presented in the following article.

Rapid Generation of Angular Momentum in Bounded Magnetized Plasma

Wouter J. T. Bos,[1,2] Salah Neffaa,[2] and Kai Schneider[2]
[1]*LMFA, UMR CNRS 5509, Ecole Centrale de Lyon–Université de Lyon, Ecully, France*
[2]*M2P2, UMR 6181 CNRS & CMI, Universités d'Aix-Marseille, Marseille, France*
(Received 17 July 2008; published 2 December 2008)

Direct numerical simulations of two-dimensional decaying MHD turbulence in bounded domains show the rapid generation of angular momentum in nonaxisymmetric geometries. It is found that magnetic fluctuations enhance this mechanism. On a larger time scale, the generation of a magnetic angular momentum, or angular field, is observed. For axisymmetric geometries, the generation of angular momentum is absent; nevertheless, a weak magnetic field can be observed. The derived evolution equations for both the angular momentum and angular field yield possible explanations for the observed behavior.

DOI: 10.1103/PhysRevLett.101.235003 PACS numbers: 52.30.Cv, 47.65.−d, 52.65.Kj

The generation of large coherent structures of the size of the flow domain is a generic feature of two-dimensional (2D) turbulence. Indeed, due to the inverse energy cascade, 2D flows show a tendency to create space filling structures. The nature of these structures and the way they are produced vary from flow to flow. In the context of Navier-Stokes turbulence, the generation of a large-scale domain-filling structure was predicted by Kraichnan [1] and observed in the case of forced turbulence in a periodic domain in which energy condenses at the smallest possible wave number modes [2,3]. In forced wall-bounded flows, this was reproduced numerically [4] and experimentally [5], and it was shown that a large-scale rotating structure emerges, which dramatically reduces the level of the turbulent fluctuations [6].

A similar observation can be made in fusion plasmas, in which the dynamics share many features with 2D flows due to the imposed magnetic field. It is often assumed that in these plasmas, large-scale poloidal structures, called zonal flows, are beneficial for the confinement as they suppress turbulence and shear apart radially extended structures, which are largely responsible for anomalous transport [7–9]. The hereby created transport barriers might play a key role in the transition to an improved confinement state (H mode) [10]. In the case of MHD turbulence, the role of rotation was shown to have a similar effect on the flow, reducing the velocity fluctuations and hereby stabilizing the magnetic field [11]. In the present Letter, we will continue the investigation of wall-bounded nonideal MHD. The generation of zonal flows through the absence of charge neutrality will not be addressed (charge neutrality being implied by the one-field MHD approximation). However, MHD allows for an affordable global description of nonuniform magnetoplasmas [12]. The present work could be related to the L-H transition through the beneficial effects of large-scale poloidal rotation (which is observed in the present work) on the confinement of the plasma. The present study is also motivated by the observation that MHD-equilibria in toroidal geometry imply finite flow-fields due to the presence of nonzero viscosity and resistivity [12–14]. In these works, nonideal MHD steady states were investigated in both the limit of small and large viscosity. In each case, it was shown that the steady state contains nonvanishing velocity fields, at odds with classical static equilibria, on which decades of confinement research are based. In the present work, we will not consider steady states, but we will investigate the full nonlinear relaxation of nonideal MHD with nontrivial boundary conditions in two space dimensions. The resistivity and viscosity are nonzero but small, allowing for a turbulent flow. This approach cannot take into account toroidal velocities and nonuniform toroidal magnetic fields and the extension of the present approach to three dimensions constitutes therefore an important direction for further research.

In the case of decaying Navier-Stokes turbulence, it is shown that the self-organization in a periodic domain will lead to a final state, consisting of two, noninteracting, counterrotating vortices [15]. This picture changes however in the presence of no-slip walls. In this case, the flow relaxes to a state with or without angular momentum, depending on the shape of the domain [16–18]. Indeed, in circular domains without initial angular momentum the flow generally relaxes to a state free from angular momentum [19], whereas as soon as the axisymmetry is broken the flow relaxes to a state containing a domain filling structure, containing significant angular momentum [20]. Theoretical progress has been made to explain the phenomenon in the inviscid case, based on a model of interacting vortices [21–23].

In the case of bounded two-dimensional MHD, it is not known, up to now, to which kind of state the flow relaxes, and this will be addressed in the present Letter. We investigate the case in which both the magnetic field and the velocity field cannot penetrate into the walls. The velocity field obeys the no-slip condition at the wall, whereas the

tangential component of the magnetic field can freely evolve, allowing a net current through the domain. We will focus however in the present study on the case in which no net current is initially present.

We start by writing the governing equations. In the present case, we define two angular momenta: a kinetic and a magnetic one,

$$L_u = \int_\Omega \boldsymbol{e}_z \cdot (\boldsymbol{r} \times \boldsymbol{u}) dA, \qquad L_B = \int_\Omega \boldsymbol{e}_z \cdot (\boldsymbol{r} \times \boldsymbol{B}) dA \tag{1}$$

in which Ω is the flow domain, $\boldsymbol{r}$ the position vector with respect to the center of the domain, and $\boldsymbol{u}$ and $\boldsymbol{B}$ the velocity and magnetic-field vector, respectively. Through integration by parts, these quantities can also be expressed as a function of the stream function $\psi = \nabla^{-2}\omega$ and vector potential $a = \nabla^{-2} j$, respectively, with $\boldsymbol{j} = j\boldsymbol{e}_z = \nabla \times \boldsymbol{B}$ the current density and $\boldsymbol{\omega} = \omega \boldsymbol{e}_z = \nabla \times \boldsymbol{u}$, the vorticity

$$L_u = -2\int_\Omega \psi dA, \qquad L_B = -2\int_\Omega a dA, \tag{2}$$

in which a and ψ are chosen to be zero at the wall.

A large value of the angular momentum can generally be associated with the presence of a large-scale vortical structure. By analogy, we can anticipate that a large value of L_B corresponds to a large-scale current density structure, and we baptize the quantity L_B *angular field*. The evolution equations for L_u and L_B can be derived following the procedure described in Maassen [24], by time deriving Eqs. (1) and using the MHD equations

$$\frac{\partial \boldsymbol{u}}{\partial t} + (\boldsymbol{u} \cdot \nabla)\boldsymbol{u} = -\nabla p + \boldsymbol{j} \times \boldsymbol{B} + \nu \nabla^2 \boldsymbol{u} \tag{3}$$

$$\frac{\partial \boldsymbol{B}}{\partial t} = \nabla \times (\boldsymbol{u} \times \boldsymbol{B}) + \eta \nabla^2 \boldsymbol{B} \tag{4}$$

together with $\nabla \cdot \boldsymbol{u} = 0$ and $\nabla \cdot \boldsymbol{B} = 0$. The pressure is denoted by p, and ν and η are the kinematic viscosity and magnetic diffusivity, respectively. If we write the Lorentz force in the form

$$\boldsymbol{j} \times \boldsymbol{B} = -\frac{1}{2}\nabla B^2 + (\boldsymbol{B} \cdot \nabla)\boldsymbol{B}, \tag{5}$$

we can absorb the first term into the pressure term of the Navier-Stokes equations by introducing the modified pressure $p^* = p + B^2/2$. The $(\boldsymbol{B} \cdot \nabla)\boldsymbol{B}$ term does not induce new terms in the equation for L_u. It vanishes in a similar way as the nonlinear term $(\boldsymbol{u} \cdot \nabla)\boldsymbol{u}$ does, using $\nabla \cdot \boldsymbol{B} = 0$ and $\boldsymbol{B} \cdot \boldsymbol{n}|_{\partial\Omega} = 0$. The equation for L_u becomes

$$\frac{dL_u}{dt} = \nu \oint_{\partial\Omega} \omega(\boldsymbol{r} \cdot \boldsymbol{n}) ds + \oint_{\partial\Omega} p^* \boldsymbol{r} \cdot d\boldsymbol{s}. \tag{6}$$

The only difference with respect to the hydrodynamic case [18] is the pressure which is now replaced by the modified pressure p^*. In most fusion plasmas, the quantity $\beta = p/B^2 \ll 1$ to insure confinement, which means that the magnetic part of the pressure dominates. It is important to note that the pressure term in Eq. (6) vanishes in axisymmetric domains. In this work, we therefore consider both a circular and a square domain to analyze the influence of this term.

The derivation of the equation for L_B is analogous to the derivation for L_u. The resulting equation is

$$\frac{dL_B}{dt} = \eta \oint_{\partial\Omega} j(\boldsymbol{r} \cdot \boldsymbol{n}) ds - 2\eta I. \tag{7}$$

We observe that there is a term involving the net current I through the domain defined by $I = \int_\Omega j\boldsymbol{e}_z dA$. This term is the equivalent of the circulation in the hydrodynamic case, which is zero due to the no-slip walls. The net current is however not imperatively zero as the tangential magnetic field does not vanish at the wall. Nevertheless, a net current will not be generated if it is initially zero, which is the case in the present work.

We performed computations in two different geometries: a square of size $D = 2$ and a circular geometry with a diameter $D = 2.24$. A description of the generation of the initial conditions and the numerical scheme, a spectral method with volume penalization, are given in [25]. The initial velocity and magnetic field consist of correlated Gaussian noise with vanishing cross-helicity $\int_\Omega \boldsymbol{u} \cdot \boldsymbol{B} dA$. The magnetic Prandtl number, ν/η is equal to one. The initial Reynolds number, based on the domain size, is $\sqrt{2E_u}D/\nu$ and yields 1960. The ratio of the magnetic and kinetic energy $E_B/E_u = 2.3$, with $E_u = \frac{1}{2}\int_\Omega |\mathbf{u}|^2 dA$ and $E_B = \frac{1}{2}\int_\Omega |\mathbf{B}|^2 dA$. The resolution of the simulations is 512^2 Fourier modes. In each geometry, 10 runs were performed starting from different statistical realizations with the same initial parameters. The numerical value of a and ψ is not automatically zero at the domain boundary. This is accomplished *a posteriori* by substracting a constant value at each point in the domain.

In Fig. 1, snapshots of the stream function and vector potential are shown at $t^* = 0.75$, 3, 12 with $t^* = t\sqrt{2E_u(t=0)}/D$. It can be inferred from (2) that these quantities should give a good visual interpretation of the presence of angular momentum and field. At time-instant $t^* = 0.75$, in which inertial effects are dominant over viscous effects, it is well visible that the velocity field self-organizes into a large domain-filling structure in the square geometry, whereas in the circular geometry, several structures are observed. At $t^* = 3$, a large structure appears also in the magnetic field in the square geometry. At $t^* = 12$, the large-scale velocity and magnetic structures in the square domain are (anti-)aligned. In the circular domain, the tendency to create domain-filling structures is weaker, even though the magnetic field in the circular domain shows some evidence of the formation of a large current structure at $t^* = 12$. To characterize the relaxation of the flows in both geometries, we also show in Fig. 1 the decay of the kinetic and magnetic energy in both domains, as well as the absolute value of the cosine of the alignment angle.

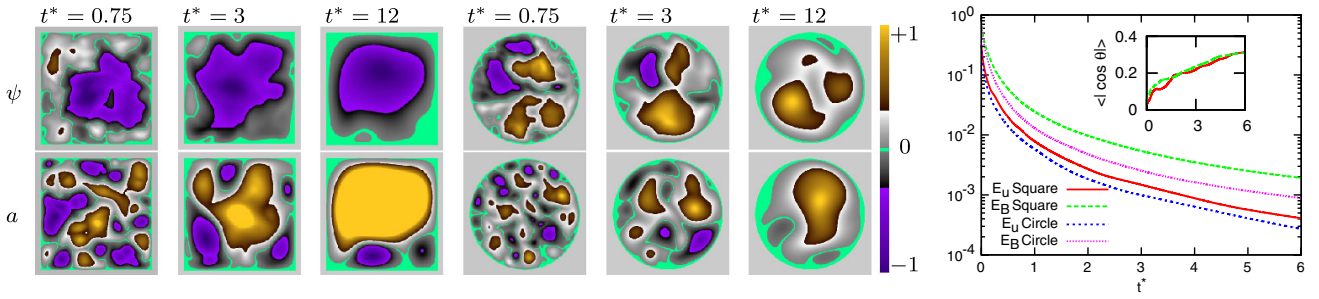

FIG. 1 (color online). Visualizations of the stream-function ψ and the vector-potential a for both geometries. Figures for ψ are normalized by the maximum of $|\psi|$ (and $\max(|a|)$ for a). The values of $\max(|\psi|)$ are from left to right 0.1, 0.05, 0.03; 0.06, 0.03, 0.01; and for $\max(|a|)$ 0.08, 0.06, 0.04; 0.04, 0.03, 0.01. Right: time evolution of the kinetic and magnetic energy in both geometries. In the inset, the evolution of the absolute value of the relative cross helicity $\langle|\cos(\theta)|\rangle$, illustrates the global alignment of the velocity and magnetic field in both geometries. Solid (red) line: square geometry; dashed (green) line: circular geometry.

A continuous decrease of kinetic and magnetic energy is observed and a continuous increase of global alignment.

At this moderate Reynolds number, spin-up, i.e., spontaneous generation of angular momentum, does not occur in every flow realization. Also, the criterion what is strong or weak spin-up is rather arbitrary. We therefore focus first on mean quantities to illustrate the general tendency to spin-up. In Fig. 2, we show the absolute value of the angular momentum, averaged over 10 runs. We take the absolute value because there is no preferential direction of the spin-up so that an average of the angular momentum would yield values close to zero for all cases. The time evolution of $\langle|L_u|\rangle$ and $\langle|L_B|\rangle$ is shown for both the square and the circular geometry. $\langle\cdot\rangle$ denotes the average over 10 realizations. The quantities are normalized by $\mathcal{L}_u(0) = \|r\|_2\sqrt{2\langle E_u(t=0)\rangle}$ and $\mathcal{L}_B(0) = \|r\|_2\sqrt{\langle 2E_B(t=0)\rangle}$, with $\|r\|_2$ the Euclidean norm of $\boldsymbol{r}$. The quantity $\mathcal{L}_u(t)$ corresponds to the value of the angular momentum of a flow in solid-body rotation with kinetic energy $\langle E_u(t)\rangle$, which is the flow which optimizes the value of the angular momentum for a given kinetic energy. By analogy, $\mathcal{L}_B(t)$ is used to normalize the angular field. The following is observed: at short times L_u rapidly increases in the square, but does not increase in the circular geometry. The value of L_B also increases in the square, but delayed with respect to L_u. In the circular geometry, an increase of L_B is also observed. In the inset, the values of $\langle|L_u|\rangle$ and $\langle|L_B|\rangle$ are plotted normalized by $\mathcal{L}_u(t)$ and $\mathcal{L}_B(t)$. This normalization has the advantage to correct for the decay of the kinetic and magnetic energy but has the disadvantage that it is sensitive to selective decay [26] so that at long times, we observe generation of angular momentum in each case even if its absolute value might be small. In the following, we will give, where possible, an explanation for the 4 curves in Fig. 2.

First, in the square geometry, a strong spin-up of the velocity field is observed. In the hydrodynamic case, it was argued in [18,20] that the pressure term triggers the spin-up in the square geometry. The magnetic field enhances the pressure term through the magnetic pressure ($p^* = p + B^2/2$). If in the present case it is also the pressure term in (6) which triggers the spin-up, the effect could be enhanced by increasing the magnetic fluctuation strength B^2. This is illustrated in Fig. 2 (bottom). For one run in which spin-up was observed, the initial magnetic fluctuations are in-

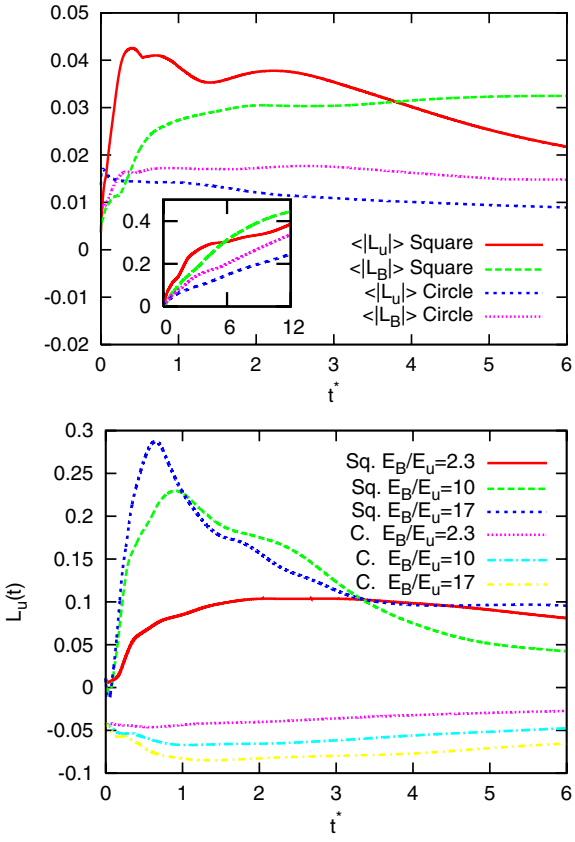

FIG. 2 (color online). Top: Time evolution of the absolute value of the angular momentum and angular field, averaged over all realizations, normalized by $\mathcal{L}_u(0)$ and $\mathcal{L}_B(0)$, respectively. In the inset, the same quantities are given, normalized by $\mathcal{L}_u(t)$ and $\mathcal{L}_B(t)$ (defined in the text). Bottom: time dependence of the angular momentum L_u in the square and circular geometry, normalized by $\mathcal{L}_u(0)$. The influence of the magnetic pressure on the spin-up in the square container is illustrated by changing the ratio E_B/E_u, while keeping E_u fixed.

creased from $E_B/E_u = 2.3$ up to $E_B/E_u = 10$ and 16.7, while keeping the initial E_u fixed. The resulting spin-up is significantly stronger.

Second, for L_u in the circular geometry, like in the hydrodynamic case [19], no spontaneous spin-up is observed. Increasing the magnetic-field strength does only weakly influence this result (Fig. 2, bottom).

Third, the interpretation of the generation of the angular field in the square geometry is less straightforward, as Eq. (7) does not contain a pressure term. The tendency to create large-scale magnetic structures can be attributed to the selective decay mechanism [27], which was recently shown to persist in bounded geometries [25]. This does however not explain the symmetry breaking or angular momentum generation, which is the main issue of the present work. A possible trigger for the spin-up could be alignment. It is well known that the magnetic field and the velocity field tend to align so that the nonlinear term in the equation for j (or $\boldsymbol{B}$) vanishes. Hence, the magnetic field tends to an alignment with the velocity field which acquired angular momentum through the modified pressure term. It is therefore expected that the magnetic spin-up follows the hydrodynamic spin-up after a time scale corresponding to the alignment. Indeed, L_B spins-up shortly after L_u. The cosine of the angle between $\boldsymbol{u}$ and $\boldsymbol{B}$, measuring the global alignment, is plotted in the inset of Fig. 1 (right). A tendency towards global alignment is observed for long times.

Fourth, in the circular geometry, the weak spin-up of the magnetic field is surprising. Higher resolution simulations are needed to clarify whether this is a viscous effect and/or a statistically more probable (maximum entropy) state. In this context we can refer to [23], where, based on point-vortices, it was shown that two types of most probable states exist in a circular domain: a double vortex, free from angular momentum and an axisymmetric flow, with finite angular momentum. This work neglected the influence of viscosity so that it is not clear how the angular momentum is acquired in the circular geometry.

We now resume our findings. Rapid generation of angular momentum takes place in bounded MHD turbulence, as long as the geometry is nonaxisymmetric. The effect is enhanced by the magnetic pressure. On a slower time scale also, magnetic spin-up is observed in both geometries. It is not clear how this angular field is created. Both alignment and selective decay could be possible explanations.

We want to stress the implications of the present study for confinement research. Fusion plasmas are wall bounded and not axisymmetric so that even in the case of charge neutrality the plasma might have a tendency to create zonal flows and zonal fields, depending on the geometry of the cross-section of the plasma and the strength of the magnetic fluctuations. The present work opens several perspectives for future research, such as the influence of Pr_m, Re, and, in particular, the extension to three dimensions in which the effects of imposed magnetic fields, currents, and toroidal velocities can be taken into account.

We acknowledge valuable discussions with Herman Clercx, David Montgomery, and Geert Keetels. This work was supported by the ANR under Contract No. M2TFP.

[1] R. H. Kraichnan, Phys. Fluids **10**, 1417 (1967).
[2] D. K. Lilly, Phys. Fluids, Suppl. II **12**, 240 (1969).
[3] M. Hossain, W. H. Matthaeus, and D. C. Montgomery, J. Plasma Phys. **30**, 479 (1983).
[4] G. J. F. van Heijst, H. J. H. Clercx, and D. Molenaar, J. Fluid Mech. **554**, 411 (2006).
[5] J. Sommeria, J. Fluid Mech. **170**, 139 (1986).
[6] M. G. Shats, H. Xia, H. Punzmann, and G. Falkovich, Phys. Rev. Lett. **99**, 164502 (2007).
[7] H. Biglari, P. H. Diamond, and P. W. Terry, Phys. Fluids B **2**, 1 (1990).
[8] P. W. Terry, Rev. Mod. Phys. **72**, 109 (2000).
[9] P. H. Diamond, S.-I. Itoh, K. Itoh, and T. S. Hahm, Plasma Phys. Controlled Fusion **47**, R35 (2005).
[10] F. Wagner *et al.*, Phys. Rev. Lett. **49**, 1408 (1982).
[11] X. Shan and D. C. Montgomery, Phys. Rev. Lett. **73**, 1624 (1994).
[12] D. C. Montgomery, J. W. Bates, and L. P. Kamp, Plasma Phys. Controlled Fusion **41**, A507 (1999).
[13] J. W. Bates and D. C. Montgomery, Phys. Plasmas **5**, 2649 (1998).
[14] L. P. Kamp and D. C. Montgomery, Phys. Plasmas **10**, 157 (2003).
[15] G. Joyce and D. C. Montgomery, J. Plasma Phys. **10**, 107 (1973).
[16] S. Li, D. C. Montgomery, and W. B. Jones, Theor. Comput. Fluid Dyn. **9**, 167 (1997).
[17] H. J. H. Clercx, S. R. Maassen, and G. J. F. van Heijst, Phys. Rev. Lett. **80**, 5129 (1998).
[18] H. J. H. Clercx, A. H. Nielsen, D. J. Torres, and E. A. Coutsias, Eur. J. Mech. B, Fluids **20**, 557 (2001).
[19] K. Schneider and M. Farge, Phys. Rev. Lett. **95**, 244502 (2005).
[20] G. H. Keetels, H. J. H. Clercx, and G. J. F. van Heijst, Phys. Rev. E **78**, 036301 (2008).
[21] Y. B. Pointin and T. S. Lundgren, Phys. Fluids **19**, 1459 (1976).
[22] P. H. Chavanis and J. Sommeria, J. Fluid Mech. **314**, 267 (1996).
[23] J. B. Taylor, M. Borchardt, and P. Helander, Interacting vortices and spin-up in 2-d turbulence (to be published).
[24] S. Maassen, Ph.D. thesis, Technische Universiteit Eindhoven, 2000.
[25] S. Neffaa, W. J. T. Bos, and K. Schneider, Phys. Plasmas **15**, 092304 (2008).
[26] G. H. Keetels, Ph.D. thesis, Technische Universiteit Eindhoven, 2008.
[27] W. H. Matthaeus and D. C. Montgomery, Ann. N.Y. Acad. Sci. **357**, 203 (1980).

6.3 Work in progress and perspectives: 3 Dimensional self-organization of fusion plasmas

In the foregoing two sections, large-scale self-organization was considered in two-dimensional MHD turbulence. In the present section we will discuss two manifestations of this phenomenon in three-dimensional plasmas in toroidal geometry. The investigation of these phenomena is work in progress within the PhD project of Jorge Morales. The first phenomenon is the intrinsic rotation observed in fusion plasmas. The second is the quasi-single helicity state which improves the confinement in reversed field pinches. Our feeling is that both effects might be strongly related. Let us first explain the context and then our approach.

6.3.1 Plasma movement in tokamaks and RFPs

Intrinsic rotation of tokamaks. The intrinsic rotation of fusion plasmas is currently in the center of attention of fusion research since it seems to be one of the factors which is responsible for the LH-transition. By intrinsic rotation we understand the tendency of a fusion plasma to start rotating even in the absence of external momentum input. The toroidal velocities can reach values of kilometers per second [102]. Despite all the recent efforts, the understanding of this is only partial. Several mechanisms are proposed but no consensus on this topic exists for the moment [103]. On the level of description of MHD, pioneering work was carried out by Montgomery and coworkers [150, 151, 152, 153]. They showed that steady states in toroidal geometries imperatively contain non-vanishing velocity-fields which strongly depend on the geometry. The fact that Montgomery and coworkers showed that steady states of resistive MHD in toroidal geometries imperatively contain non-vanishing flow-fields is surprising and slightly controversial, taking into account that decades of fusion research are based on static toroidal MHD equilibria, which are only possible in the absence of viscosity and resistivity. Their studies were essentially two-dimensional, assuming symmetries in the third direction. The extension to three dimensions of these studies is important to evaluate to what extent intrinsic rotation is caused by MHD effects.

Appearance of single helicity states in the reversed field pinch. The reversed field pinch (RFP) is a toroidal fusion plasma device. The difference with respect to the tokamak geometry is that the toroidal and poloidal magnetic fields have the same order of magnitude in a RFP, whereas in a tokamak the toroidal field is several times larger than the poloidal field. This magnetic configuration leads to a much stronger tendency to develop MHD instabilities. The resulting turbulent state has for a long time demotivated the fusion community to focus on RFPs as a viable candidate for controlled fusion. Indeed, the coexistence of a large number of helical modes with different poloidal and toroidal mode numbers lead to a poor confinement quality. However, in 2000 it became clear that the plasma instabilities not only give rise to these chaotic multi-helicity states, but in some cases can lead to steady, self-organized states yielding an enhanced confinement [154]. These states are called quasi-single helicity states,

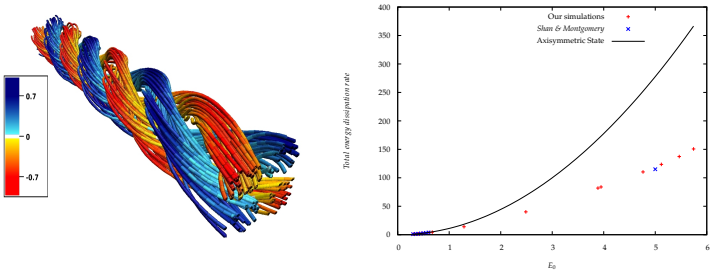

Figure 6.4: Left: helical instabilities are observed for high enouch values of the pinch ratio or Hartmann number. Right: comparison of the dissipation of the kinetic energy observed in our simulations with the results of reference [155].

since their spatial form is close to a single helical perturbation in the core of the RFP. The chaos within this structure is significantly lower than what is observed in the multiple helicity states, and the observed temperature much higher, making the RFP a more serious candidate for nuclear fusion.

6.3.2 Numerical methods to study three-dimensional MHD self-organization in toroidal geometry

Since a strong magnetic field renders the dynamics of a magnetized plasma close to two-dimensional, it is tempting to project conclusions drawn from results of purely two-dimensional investigations onto three dimensional phenomena. One mechanism of self-organization is the spin-up mechanism, discussed in the previous section, which was discovered in two-dimensional hydrodynamics [156, 149, 157]. These studies showed that turbulent fluctuations contained in non-axisymmetric boundaries tend to organize into one space-filling swirling structure. We showed in section 6.2 the influence of the shape of the boundary on the generation of swirling structures in charge neutral plasma. It is obvious that these 2D results are not directly transposable to magnetically confined toroidal plasmas, in which the imposed magnetic field is toroidally curved and helically twisted. However the possibility that a similar self-organization might take place in three-dimensions definitely triggers our curiosity.

The extension of the numerical method to three-dimensions is unavoidable if we want to investigate the self-organization of MHD flows in a toroidally confined domain. In order to investigate the precise role of the confining geometry on the plasma flow by numerical simulation, a flexible and accurate tool is therefore required, which allows to easily change the geometry. A preliminary study of such a method applied to MHD can be found in [158]. The procedure, which we already used in the studies in the previous sections to study MHD turbulence in two dimensions is based on the volume penalization technique [159], which is a specific immersed boundary method. The MHD equations are computed in a

periodic domain and the solid boundaries are modeled by a drag term,

$$\partial_t \boldsymbol{u} = ... - \frac{\chi(\boldsymbol{x})}{\eta_u}(\boldsymbol{u} - \boldsymbol{u}_0) \tag{6.13}$$

$$\partial_t \boldsymbol{b} = ... - \frac{\chi(\boldsymbol{x})}{\eta_b}(\boldsymbol{b} - \boldsymbol{b}_0), \tag{6.14}$$

where $\chi(\boldsymbol{x})$ is a mask-function which is zero in the fluid or plasma and unity in the walls, $\boldsymbol{u}_0$ and $\boldsymbol{b}_0$ are the velocity field and magnetic field which we impose in the walls. For $\boldsymbol{b} = 0$, In the limit $\eta_u \to 0$ the system tends to Navier-Stokes turbulence with no-slip boundary conditions. The extension of this method to MHD was first used in [17]. Recently, Jorge Morales, PhD student at the LMFA laboratory, performed the first simulations using this method in cylindrical and toroidal geometry, which we will now discuss.

MHD instabilities in cylindrical geometry. As a first test-case we study the confinement in a cylindrical plasma and its transition to turbulence. This case of a three-dimensional periodic cylindrical plasma within the MHD approximation was considered in Shan, Montgomery and Chen [155]. The numerical code they used was based on orthonormal basis-functions adapted to fit cylindrical or spherical boundary conditions. These Chandrasekar-Kendall eigenfunctions are a natural choice to discretize the space confined in cylindrical geometry. However, no fast transform, equivalent to the Fast-Fourier-Transform is known for these functions, so that their computation was entirely spectral. This limits the resolution of the equation to low resolution. In 1991, the maximum number of modes that could possibly used in a computation over a meaningful number of time-steps was of the order of 1000. For comparison, pseudo-spectral simulations were in the same year possible for a resolution of $240^3 \approx 1.4\ 10^7$ modes [160]. Presently, state of the art pseudo-spectral simulations are performed at a resolution of $4096^3 \approx 7\ 10^{10}$ modes. But even at their modest resolution, Shan *et al.* obtained interesting results for the dynamics induced by the typical helical structure of the magnetic field. An explanation for the performance of the method is that the first unstable modes are given directly by low-order Chandrasekar-Kendall eigenfunctions.

In Shan *et al.* the boundary conditions are chosen to be "no penetration" for the velocity and the magnetic field and zero normal vorticity and current at the wall. These conditions are implied by standard no slip conditions, but do not imply them. Physically, the magnetic field behaves as if the outer domain is a perfect conductor (zero normal magnetic field), coated on the inside by a insulating layer (zero normal current). Apparently these boundary conditions are not completely different from what is observed in fusion plasmas. The boundary conditions for the velocity do not correspond to a simple physical situation, but are in practice not very different from no-slip boundary conditions. They are in particular chosen since they are easily implemented using this type of discretization (see also [161]). The electric field is imposed by fixing the electric field at the wall. Since at the wall the values for the velocity are very small, this roughly corresponds to a fixed axial current density at the wall of value E_0/η. In the static regime, the current density will be constant throughout the cross-section S and the value of the total mean current will thus be $I_0 = SE_0/\eta$. The value of this electric field was gradually increased. At sufficiently low values

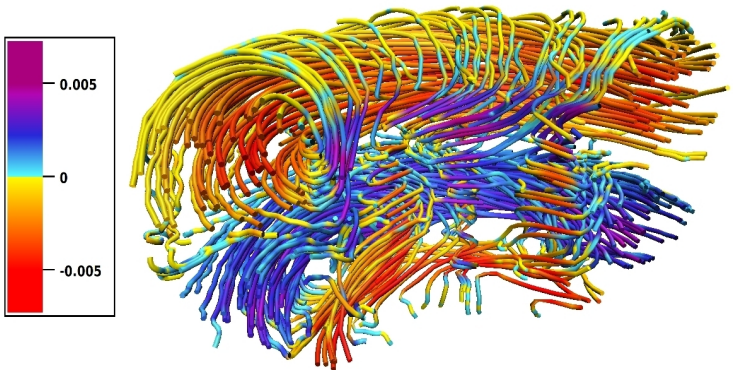

Figure 6.5: Viscoresistive instabilities generate toroidal flows. The details of the flow are determined by the geometry of the toroidal device and the magnetic field structure. Preliminary results.

of the electric field, its only influence is the generation of a mean current in the axial direction. This current logically induces a azimuthal magnetic field. The sum of the axial and azimuthal components yields a helically twisted magnetic field, similar to the magnetic geometry imposed in fusion-devices. At a certain threshold value of the electric field, the system becomes dynamically active and a helical velocity mode appears. This mode seems to appear in order to reduce the total dissipation (resistive and viscous) of the system. Apparently the system tends to a state in which the dissipation is minimized (perhaps again a manifestation of the depletion of nonlinearity). In the dynamically active regime, the $\boldsymbol{u} \times \boldsymbol{b}$ contribution to the electric field will counteract this current so that the mean value will be lower than I_0. At higher values of the electric field a multi-mode state appears, still laminar and periodic. At even higher values, the system becomes turbulent and a continuous spectrum of excited modes is observed.

Two control parameters can be identified to trigger the instability and leading to helical velocity perturbations: the pinch ratio, measuring the ratio of the poloidal magnetic field to the toroidal magnetic field, and the Hartmann number [162, 163, 99]. Our first goal was to closely reproduce the results by Shan *et al.* for as far as this is possible using the slightly different boundary conditions. This goal was reached as is shown in Figure 6.4. We illustrate the first unstable modes which appear in the cylindrical plasma and we show the quantitative agreement with [155] for the dissipation rate of the kinetic energy.

Results in toroidal geometry. The exciting study of the influence of the geometry and transport coefficients on the toroidal rotation is currently undertaken. In Figure 6.5 we show preliminary results of the flowfield generated through visco-resistive instabilities in toroidal geometry, in which the shape of the boundaries and the magnetic field are chosen similar to tokamak geometry. These results are discussed in detail in the following publication[4]. A further in-

[4]This publication has been added to the manuscript after the date of the presentation. However, it seems relevant to add it to the manuscript since the results were presented during

vestigation will focus on the appearance of quasi-single helicity states in toroidal geometry. In that study we will increase the value of the pinch ratio of the magnetic field compared to the tokamak related studies.

Magnetohydrodynamics and fusion plasmas. A word of caution is perhaps not inappropriate here. Most certainly our approach cannot be claimed to take into account all the physics observed in fusion plasmas and we do not pretend it does. In order to understand what happens *in detail* in a particular toroidal machine, incompressible MHD is certainly not a fine enough description. However, the current investigations try to describe generic mechanisms observed in fusion plasmas at the crudest level capable of reproducing some of the physics, which is MHD for some mechanisms and might be a more sophisticated description for others. As long as we do not know what can be explained by the simplest approach, it does not seem necessary to use more complex plasma descriptions.

the defense.

Intrinsic Rotation of Toroidally Confined Magnetohydrodynamics

Jorge A. Morales,[1] Wouter J. T. Bos,[1] Kai Schneider,[2] and David C. Montgomery[3]
[1]LMFA-CNRS, Ecole Centrale de Lyon-Université de Lyon, Ecully, France
[2]M2P2-CNRS & CMI, Aix-Marseille Université, Marseille, France
[3]Department of Physics and Astronomy, Dartmouth College, Hanover, New Hampshire, USA
(Received 20 July 2012; published 23 October 2012)

The spatiotemporal self-organization of viscoresistive magnetohydrodynamics in a toroidal geometry is studied. Curl-free toroidal magnetic and electric fields are imposed. It is observed in our simulations that a flow is generated, which evolves from dominantly poloidal to toroidal when the Lundquist numbers are increased. It is shown that this toroidal organization of the flow is consistent with the tendency of the velocity field to align with the magnetic field. Up-down asymmetry of the geometry causes the generation of a nonzero toroidal angular momentum.

DOI: 10.1103/PhysRevLett.109.175002 PACS numbers: 52.30.Cv, 47.65.−d, 52.65.Kj

Introduction.—The magnetic confinement of fusion plasmas is strongly influenced by turbulent fluctuations. These fluctuations degrade the quality of the confinement and thereby reduce the performance of the fusion reactor. It was discovered three decades ago [1] that, under certain circumstances, the turbulent activity is reduced, leading to a better confinement. Still today the understanding of this low-to-high-confinement transition is far from complete. There is, however, strong evidence that large toroidal velocities of the plasma are a feature that is either at the origin, or a consequence of, the mechanism that is responsible for this transition [2,3]. Large toroidal velocities, of the order of several kilometers per second, are observed even in the absence of external momentum input. Several mechanisms are put forward to explain the toroidal rotation, mostly based on the turbulent transport of toroidal momentum generated at the tokamak edge (e.g., in Refs. [4–6]). In this Letter we present a mechanism which seems to be generic, since it is observed even in one of the coarsest descriptions of a fusion plasma: viscoresistive magnetohydrodynamics (MHD).

A MHD description of fusion plasmas.—In the MHD description, the plasma is described as a charge-neutral conducting fluid. MHD, despite its low level of complexity compared to kinetic descriptions or two-fluid descriptions, already gives rise to a wealth of intricate phenomena and its analytical treatment is only possible in some simplified cases, either in the absence of velocity fields [7,8] or in the absence of nonlinear interactions [9]. We will come back to these analytical approaches, but before that, we present the equations that we consider. These are the dimensionless incompressible viscoresistive MHD equations for the velocity field $\boldsymbol{u}$ and for the magnetic field $\boldsymbol{B}$, in Alfvénic units [10],

$$\frac{\partial \boldsymbol{u}}{\partial t} - M^{-1}\nabla^2\boldsymbol{u} = -\nabla\left(P + \frac{1}{2}u^2\right) + \boldsymbol{u}\times\boldsymbol{\omega} + \boldsymbol{j}\times\boldsymbol{B}, \tag{1}$$

$$\frac{\partial \boldsymbol{B}}{\partial t} = -\nabla\times\boldsymbol{E}, \tag{2}$$

$$\boldsymbol{E} = S^{-1}\boldsymbol{j} - [\boldsymbol{u}\times\boldsymbol{B}], \tag{3}$$

$$\nabla\cdot\boldsymbol{u} = 0, \qquad \nabla\cdot\boldsymbol{B} = 0, \tag{4}$$

with the current density $\boldsymbol{j} = \nabla\times\boldsymbol{B}$, the vorticity $\boldsymbol{\omega} = \nabla\times\boldsymbol{u}$, the pressure P, and the electric field $\boldsymbol{E}$. These equations are nondimensionalized using the toroidal Alfvén speed $C_A = B_0/\sqrt{\rho\mu_0}$ as typical velocity, with B_0 the reference toroidal magnetic field at the center of the torus ($R = R_0$), ρ the density, and μ_0 the magnetic constant. The reference length L (see Fig. 1) is the diameter of the cross section for the circular case and is the minor diameter for the asymmetric D shape ($L = 1.88$ for both geometries). The dynamics are then governed by the initial and boundary conditions of the problem, and two dimensionless quantities: the viscous Lundquist number (M) and the Lundquist number (S) defined as

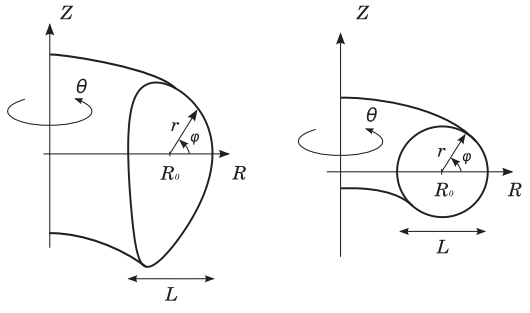

Asymmetric 'D' Circular

FIG. 1. Cross sections of the toroidal geometries considered in the present work. The toroidal angle is labeled θ and the poloidal one φ.

$$M = \frac{C_A L}{\nu}, \qquad S = \frac{C_A L}{\lambda}, \tag{5}$$

with λ the magnetic diffusivity and ν the kinematic viscosity. The ratio of these two quantities is the magnetic Prandtl number $\mathrm{Pr} = \nu/\lambda$, which we have chosen unity in the present study, thereby reducing the number of free parameters, which characterize the magnetofluid, to one, the viscous Lundquist number. Previous investigations indicate that it is the geometric mean of the viscosity and the magnetic diffusivity which determines the dynamics [11,12]. In setting the Prandtl number to one, a change in the Lundquist numbers, M or S, is equivalent to a change in the Hartmann number.

Let us now go back to the analytical description of viscoresistive MHD. In the static case in which $\boldsymbol{u} = 0$, Eq. (1) reduces to an equilibrium

$$\nabla P = \boldsymbol{j} \times \boldsymbol{B}. \tag{6}$$

In a cylindrical geometry this equilibrium can be achieved by various magnetic configurations such as the z pinch or the θ pinch [13]. In toroidal geometry it is problematic to obtain such an equilibrium, as we will now explain. We consider the case in which the driving toroidal electric field is curl-free within the plasma, over times of interest, such that $\boldsymbol{E}_\theta \sim 1/R$. Further we assume the toroidal magnetic field to obey the same scaling, which follows from the integration of Ampère's law on a toroidal loop. In the simplest case, we choose a space-uniform electrical conductivity such that the toroidal current induced by the electric field is also given by the same dependence, so that the externally imposed magnetic field and toroidal, laminar, voltage-driven current density are given by,

$$\boldsymbol{B}_0(R) = B_0 \frac{R_0}{R} \boldsymbol{e}_\theta, \qquad \boldsymbol{J}_0(R) = J_0 \frac{R_0}{R} \boldsymbol{e}_\theta. \tag{7}$$

Computing the Lorentz force resulting from these toroidal fields, taking into account the poloidal magnetic field induced by $\boldsymbol{J}_0$, results in a force field which is not curl-free [14]. Since the curl of the pressure gradient is necessarily zero, the equilibrium described by (6) becomes impossible and additional terms of Eq. (1) need to be taken into account to balance the equation. Since all other terms in (1) are proportional to (or quadratic in) the velocity, the resulting state must be dynamic. That is, a toroidal plasma, described by viscoresistive MHD, confined by curl-free toroidal electric and magnetic fields, necessarily moves.

It is true that the rationale described above depends on the choice of the electric conductivity, which was assumed to be uniform. It was however shown [15,16] that to satisfy (6) in a torus, very unusual profiles of the electrical conductivity must be assumed. We omit these rather unphysical cases and focus on the dynamical plasma behavior which results for the simplest, uniform, conductivity profile.

It follows from the foregoing that it is necessary to take into account all other terms in the MHD equations, and analytical treatment becomes impossible unless symmetries are assumed. To study the full dynamics we are obliged to solve numerically the system and this is what is done in the present investigation. Such fully three-dimensional nonstationary simulations, taking into account all relevant time and space scales, are computationally demanding and only quite recently have the necessary resources and numerical methods become available to do such simulations. Equations (1)–(4) are discretized with a Fourier pseudospectral method on a Cartesian grid. To impose the boundary conditions we use the volume-penalization technique, a method of the immersed boundary type, which we consider a good compromise between the ease of implementation, flexibility in geometry, and the numerical cost of the simulation. Results for two-dimensional MHD can be found in Ref. [17]. We recently extended this method to study the three-dimensional viscoresistive MHD equations [18], and in the present Letter we present the results of three-dimensional simulations in two toroidal geometries.

Results of numerical simulations.—Details of the numerical method are given in Ref. [18]. Simulations are carried out on a cubic domain of size 2π consisting of 256^3 grid points for the highest values of M. The initial condition for the simulations is zero magnetic fluctuations and zero velocity, and no-slip velocity boundary conditions are imposed. We consider the boundaries of the fluid domain as perfectly conducting and coated with an infinitely thin layer of insulator. Thereby the normal component at the wall of the magnetic and current density fields vanishes. We impose toroidal magnetic and current density

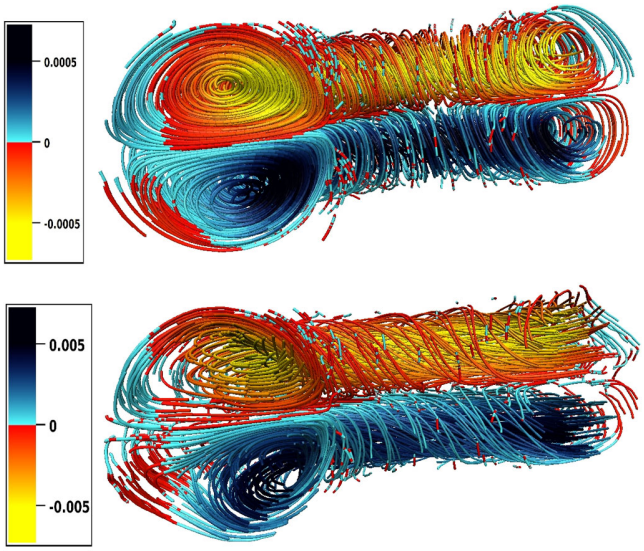

FIG. 2 (color online). Streamlines colored by the value of the toroidal velocity, u_θ for $M = 15$ (top) and $M = 150$ (bottom) in the geometry with circular cross section. Only a part of the toroidal domain is shown.

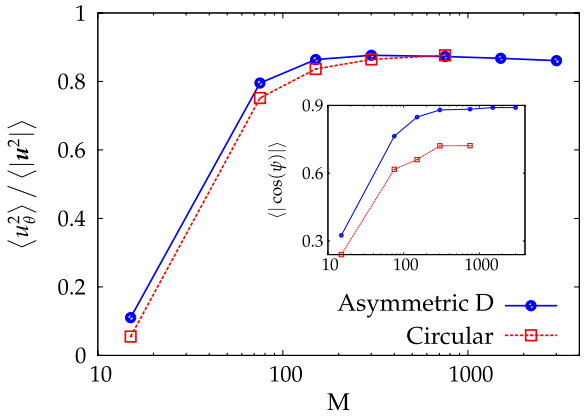

FIG. 3 (color online). The ratio of the mean-square toroidal velocity to the total mean-square velocity $\langle u_\theta^2 \rangle / \langle |\boldsymbol{u}^2| \rangle$ as a function of M. In the inset we show the average over the domain of the absolute value of the cosine of the angle between the velocity field and magnetic field.

fields given by Eq. (7). The Biot-Savart law is used to determine the poloidal magnetic field induced by the toroidal current $\boldsymbol{J}_0(R)$. All the simulations presented in this communication are performed with $B_0 = 0.8$ and $J_0 = 0.3$. This corresponds, for both geometries, to a pinch ratio $\Theta \approx 0.16$, defined as the ratio between the wall-averaged poloidal and the volume-averaged toroidal magnetic field ($\Theta = \bar{B}_\varphi / \langle B_\theta \rangle$). The only parameter that we vary is the Lundquist number M. The simulations are time dependent and they are stopped when a dynamical steady state is reached.

The results in Fig. 2 show the presence of a poloidal flow, a pair of counterrotating vortices in the r-φ plane. For small M the dynamics are dominantly poloidal, as is expected. Indeed, in the limit of vanishing nonlinearity, Bates and Montgomery [9] showed analytically that the steady state solution is a pair of poloidally rotating vortices, aligned with the toroidal direction. For nonzero nonlinearity, i.e., by increasing M, the vortices start moving in the toroidal direction, both in the opposite direction. Their toroidal velocity increases with the Lundquist number M in the two considered geometries. The three-dimensional velocity streamlines show a substantial change of topology from dominantly poloidal to dominantly toroidal flow (see Fig. 2, bottom). This is quantified in Fig. 3, where we observe that the principal direction of the flow motion is toroidal if M is raised beyond $\sim$40. The square toroidal velocity saturates for increasing M at a value of $\sim$86% of the total square velocity. This toroidal organization of the flow is consistent with the tendency of the velocity field to align with the magnetic field, as is illustrated in the inset of Fig. 3, where we compute the average (over the toroidal domain) of the absolute value of the cosine of the angle between the velocity and magnetic field. This quantity is equal to one if the velocity and magnetic field are perfectly aligned or antialigned. It is shown that the trend towards a toroidal velocity follows exactly the same M dependence as the alignment.

This tendency towards a dominant toroidal flow is similar for the torus with the asymmetric cross section as is shown in Fig. 3, while the alignment is even more pronounced. In both geometries, the generated velocity field contains non-negligible fluctuations. The quantities $\boldsymbol{u}'$ and $\boldsymbol{B}'$ denote the fluctuations around the azimuthally averaged instantaneous velocity and magnetic field, respectively. At $M = 3008$ in the D-shaped geometry, $\boldsymbol{u}'_{\rm rms}/\boldsymbol{u}_{\rm rms} = 6.7 \times 10^{-2}$, $\boldsymbol{B}'_{\rm rms}/\boldsymbol{B}_{\rm rms} = 1.5 \times 10^{-3}$ and $\boldsymbol{u}_{\rm rms}/\boldsymbol{B}_{\rm rms} = 3.2 \times 10^{-3}$. The rms values correspond here to volume averages over the toroidal domain. A detailed investigation of the spatial distribution of these fluctuations and its dependence on M will be presented elsewhere.

A fundamental difference is observed between the flows that are generated in the two geometries. The volume-averaged toroidal angular momentum is defined by

$$\langle L_\theta \rangle = \frac{1}{V} \int_V R u_\theta dV. \tag{8}$$

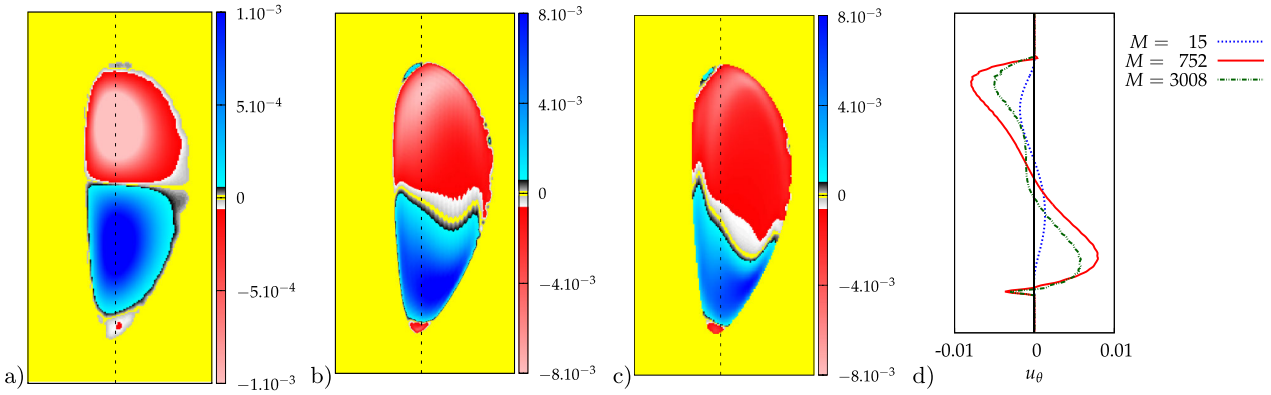

FIG. 4 (color online). Azimuthally averaged flow visualizations: toroidal velocity u_θ for $M = 15$ (a), $M = 752$ (b), and $M = 3008$ (c). (d) Toroidal velocity profiles along a vertical cut. The position of these cuts is indicated in (a), (b), (c) by a dotted vertical line.

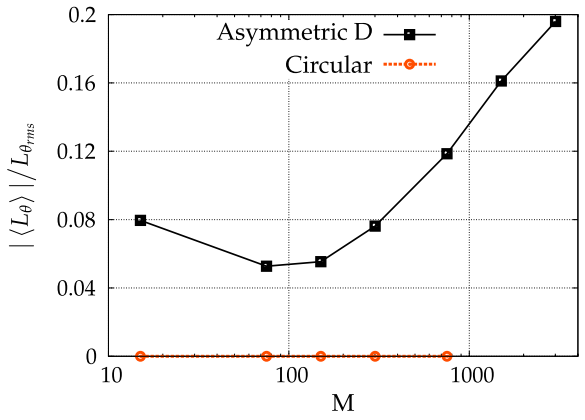

FIG. 5 (color online). Normalized toroidal angular momentum $|\langle L_\theta \rangle|/L_{\theta_{\rm rms}}$ as a function of M observed in the tori with asymmetric and symmetric cross section, respectively.

For the torus with circular cross section, this quantity is zero to a good computational approximation, due to the up-down symmetry of the observed flow. However, for the torus with asymmetric cross section this is not the case. For low M, a poloidal pair of counterrotating vortices appears (see Fig. 4 for azimuthally averaged flow visualizations, and toroidal velocity profiles along a vertical cut) as for the circular cross section. Similarly, if the viscous Lundquist number is increased, an important toroidal flow develops. Unlike the symmetric case, there is a breaking of the symmetry in the flow and the part of the flow moving in the negative direction (the red zone) becomes larger at the expense of the part of the flow which moves in the positive toroidal direction (blue zone). This symmetry breaking, illustrated in Fig. 4, leads to the development of a net toroidal flow. The toroidal angular momentum becomes hereby nonzero (see Fig. 5). Its normalized value increases significantly with the viscous Lundquist number. The observed influence of up-down symmetry is consistent with axisymmetric time-independent computations [10] and is also observed in gyrokinetic simulations and experiments [19,20].

It is presently not clear if the velocity profile observed in our simulations will change qualitatively when M is increased further and a transition to another flow topology cannot be excluded. Also have we not yet investigated the influence of the magnetic Prandtl number. It is at this point perhaps important to say that we do not know what the viscosity should be to approximate the dynamics of experiments. However, the fact that this feature is observed in fully resolved simulations of the viscoresistive MHD equations is a result of major importance, since it shows how intrinsic toroidal rotation is present in one of the coarsest global descriptions of a fusion plasma, without invoking arguments on charge non-neutrality or kinetic theory.

Conclusion.—We want to summarize the results that we obtained: considering curl-free toroidal electric and magnetic fields and constant transport coefficients, viscoresistive magnetofluids spontaneously generate velocity fields. This velocity field aligns (or antialigns) with the magnetic field, thereby generating a toroidal component. This is a nonlinear effect which becomes negligible in the limit of small Lundquist number. Furthermore, toroidal angular momentum is created, if the up-down symmetry of the torus is broken.

By its simplification, both in terms of the used model equations, as well as in terms of the parameter range chosen for the properties of the conducting fluid, our investigation should be considered academic rather than directly applicable to the detailed description of existing machines. At the same time, since MHD does give a rough description of laboratory plasmas, the mechanism that we have described should be present, at least qualitatively, in existing devices. The observed MHD self-organization thereby seems to be of major importance for the magnetically confined fusion community.

This work was supported by the contract *SiCoMHD* (ANR-Blanc 2011-045), computing time was supplied by IDRIS, project 22206.

[1] F. Wagner *et al.*, Phys. Rev. Lett. **49**, 1408 (1982).
[2] J. E. Rice, P. T. Bonoli, J. A. Goetz, M. J. Greenwald, I. H. Hutchinson, E. S. Marmar, M. Porkolab, S. M. Wolfe, S. J. Wukitch, and C. S. Chang, Nucl. Fusion **39**, 1175 (1999).
[3] J. E. Rice *et al.*, Nucl. Fusion **47**, 1618 (2007).
[4] N. Mattor and P. H. Diamond, Phys. Fluids **31**, 1180 (1988).
[5] A. G. Peeters, C. Angioni, A. Bortolon, Y. Camenen, F. J. Casson, B. Duval, L. Fiederspiel, W. A. Hornsby, Y. Idomura, T. Hein, N. Kluy, P. Mantica, F. I. Parra, A. P. Snodin, G. Szepesi, D. Strintzi, T. Tala, G. Tardini, P. de Vries, and J. Weiland, Nucl. Fusion **51**, 094 027 (2011).
[6] P. H. Diamond, C. J. McDevitt, Ö. D. Gürcan, T. S. Hahm, W. X. Wang, E. S. Yoon, I. Holod, Z. Lin, V. Naulin, and R. Singh, Nucl. Fusion **49**, 045 002 (2009).
[7] H. Grad and H. Rubin, in *Proceedings of the 2nd UN Conference on the Peaceful Uses of Atomic Energy, Geneva, 1958* (UN, Geneva, 1958), Vol. 31, p. 190.
[8] V. D. Shafranov, in *Reviews of Plasma Physics* (Consultants Bureau, New York, 1966), Vol. 2, p. 103.
[9] J. W. Bates and D. C. Montgomery, Phys. Plasmas **5**, 2649 (1998).
[10] L. P. Kamp and D. C. Montgomery, J. Plasma Phys. **70**, 113 (2004).
[11] S. Cappello and D. F. Escande, Phys. Rev. Lett. **85**, 3838 (2000).
[12] X. Shan and D. C. Montgomery, Plasma Phys. Controlled Fusion **35**, 619 (1993); **35**, 1019 (1993).
[13] J. P. Freidberg, Rev. Mod. Phys. **54**, 801 (1982).
[14] D. C. Montgomery and X. Shan, Comments Plasma Phys. Control. Fusion **15**, 315 (1994).

[15] J. W. Bates and H. R. Lewis, Phys. Plasmas **3**, 2395 (1996).
[16] D. C. Montgomery, J. W. Bates, and H. R. Lewis, Phys. Plasmas **4**, 1080 (1997).
[17] W. J. T. Bos, S. Neffaa, and K. Schneider, Phys. Rev. Lett. **101**, 235003 (2008).
[18] J. A. Morales, M. Leroy, W. J. T. Bos, and K. Schneider, http://hal.archives-ouvertes.fr/hal-00719737, V1 (2012).
[19] Y. Camenen, A. G. Peeters, C. Angioni, F. J. Casson, W. A. Hornsby, A. P. Snodin, and D. Strintzi, Phys. Rev. Lett. **102**, 125001 (2009).
[20] Y. Camenen, A. Bortolon, B. P. Duval, L. Federspiel, A. G. Peeters, F. J. Casson, W. A. Hornsby, A. N. Karpushov, F. Piras, O. Sauter, A. P. Snodin, and G. Szepesi (the TCV Team), Plasma Phys. Controlled Fusion **52**, 124 037 (2010).

Conclusion

It is hard to write a conclusion to this manuscript since a conclusion implies something final. Most of the investigations in this manuscript are not the final word on the subject. Even on a subject as old and well-discussed as isotropic turbulence, still a lot of questions are open and a fully satisfactory theory is still lacking. In complex situations such as the dynamics of fusion plasmas, the hope of such a theory is not even a goal since so many physical mechanisms play a role, one of which is the poorly understood phenomena called turbulence. Even the most academic case of isothermal, incompressible MHD confined in a toroidal geometry gives rise to a wealth of phenomena that we are far from understanding at a detailed level. Let me therefore finish this manuscript by the only appropriate concluding remarks [164]: *Further research is needed!*

References

[1] W.J.T. Bos and J.-P. Bertoglio. A single-time two-point closure based on fluid particle displacements. *Phys. Fluids*, 18:031706, 2006.

[2] W. J. T. Bos and J.-P. Bertoglio. Dynamics of spectrally truncated inviscid turbulence. *Phys. Fluids*, 18:071701, 2006.

[3] W.J.T. Bos, C. Connaughton, and F.S. Godeferd. Developing homogeneous turbulence. *Phys. D*, 241:232, 2012.

[4] W.J.T. Bos and J.-P. Bertoglio. Large scale bottleneck effect in two-dimensional turbulence. *J. Turbul.*, 10:N30, 2009.

[5] L. Fang, W.J.T. Bos, L. Shao, and J.-P. Bertoglio. Time reversibility of Navier?Stokes turbulence and its implication for subgrid scale models. *J. Turbul.*, 13:N3, 2012.

[6] W.J.T. Bos, L. Shao, and J.-P. Bertoglio. Spectral imbalance and the normalized dissipation rate of turbulence. *Phys. Fluids*, 19:045101, 2007.

[7] W.J.T. Bos, L. Chevillard, J.F. Scott, and R. Rubinstein. Reynolds number effect on the velocity increment skewness in isotropic turbulence. *Phys. Fluids*, 24:015108, 2012.

[8] W.J.T. Bos, T.T. Clark, and R. Rubinstein. Small scale response and modeling of periodically forced turbulence. *Phys. Fluids*, 19:055107, 2007.

[9] R. Rubinstein and W.J.T. Bos. On the unsteady behavior of turbulence models. *Phys. Fluids*, 21:041701, 2009.

[10] B. Favier, F. S. Godeferd, C. Cambon, A. Delache, and W. J. T. Bos. Quasi-static magnetohydrodynamic turbulence at high reynolds number. *J. Fluid Mech.*, 681:434, 2011.

[11] W.J.T. Bos, B. Kadoch, K. Schneider, and J.-P. Bertoglio. Inertial range scaling of the scalar flux spectrum in two-dimensional turbulence. *Phys. Fluids*, 21:115105, 2009.

[12] W.J.T. Bos, B. Kadoch, S. Neffaa, and K. Schneider. Lagrangian dynamics of drift-wave turbulence. *Phys. D*, 239:1269, 2010.

[13] B. Kadoch, W.J.T. Bos, and K. Schneider. Origin of Lagrangian intermittency in drift-wave turbulence. *Phys. Rev. Lett.*, 105:145001, 2010.

[14] B. Kadoch, W.J.T. Bos, and K. Schneider. Extreme Lagrangian acceleration in confined turbulent flow. *Phys. Rev. Lett.*, 100:184503, 2008.

[15] B. Kadoch, W.J.T. Bos, and K. Schneider. The influence of walls on lagrangian statistics in two-dimensional turbulence. *Phys. Fluids*, 23:085111, 2011.

[16] B. Kadoch, D. Del Castillo Negrete, W.J.T. Bos, and K. Schneider. Lagrangian statistics and flow topology in forced two-dimensional turbulence. *Phys. Rev. E*, 83:036314, 2011.

[17] S. Neffaa, W.J.T. Bos, and K. Schneider. The decay of magnetohydrodynamic turbulence in a confined domain. *Phys. Plasmas*, 15:092304, 2008.

[18] W.J.T. Bos, S. Neffaa, and K. Schneider. Rapid generation of angular momentum in bounded magnetized plasma. *Phys. Rev. Lett.*, 101:235003, 2008.

[19] W.J.T. Bos, S. Neffaa, and K. Schneider. Self-organization and symmetry-breaking in two-dimensional plasma turbulence. *Phys. Plasmas*, 17:092302, 2010.

[20] J.A. Morales, W.J.T. Bos, K. Schneider, and D.C. Montgomery. Intrinsic rotation of toroidally confined magnetohydrodynamics. *Phys. Rev. Lett. (In press)*, 2012.

[21] H. Tennekes and J.L. Lumley. *A first course in turbulence.* The MIT Press, 1972.

[22] M. Farge. Wavelet transforms and their applications to turbulence. *Annu. Rev. Fluid Mech.*, 24:395, 1992.

[23] R.H. Kraichnan. Isotropic turbulence and inertial range structure. *Phys. Fluids*, 9:1728–1752, 1966.

[24] J.G. Brasseur and S. Corrsin. Spectral evolution of the Navier-Stokes equations for low order couplings of fourier modes. In G. Comte-Bellot and J. Mathieu, editors, *Advances in Turbulence; Proceedings of the first European Turbulence Conference, Ecully, France, 1-4 july 1986*, page 152. Springer Verlag, 1987.

[25] A. Alexakis, P.D. Mininni, and A. Pouquet. Imprint of large scale flows on turbulence. *Phys. Rev. Lett.*, 95:264503, 2005.

[26] G. L. Eyink and H. Aluie. Localness of energy cascade in hydrodynamic turbulence. i. Smooth coarse graining. 21:115107, 2009.

[27] A.N. Kolmogorov. The local structure of turbulence in incompressible viscous fluid for very large Reynolds numbers. *Dokl. Akad. Nauk. SSSR*, 30:301, 1941.

[28] R.H. Kraichnan. Lagrangian-history closure approximation for turbulence. *Phys. Fluids*, 8:575, 1965.

[29] J.M. Burgers. Correlation problems in a one dimensional model of turbulence. parts i-iv. *Verhand. Kon. Ned. Akademie v. Wetenschappen*, 53:247–260; 393–406; 718–731; 732–742, 1950.

[30] R.H. Kraichnan. Lagrangian-history statistical theory for Burgers' equation. *Phys. Fluids*, 11:265, 1968.

[31] A.M. Obukhov. Structure of the temperature field in turbulent flows. *Isv. Geogr. Geophys. Ser.*, 13:58, 1949.

[32] S. Corrsin. On the spectrum of isotropic temperature fluctuations in an isotropic turbulence. *J. Appl. Phys.*, 22:469, 1951.

[33] E. Lee, M. E. Brachet, A. Pouquet, P. D. Mininni, and D. Rosenberg. Lack of universality in decaying magnetohydrodynamic turbulence. *Phys. Rev. E*, 81:016318, 2010.

[34] R.H. Kraichnan. The structure of isotropic turbulence at very high Reynolds numbers. *J. Fluid Mech.*, 5:497–543, 1959.

[35] R. H. Kraichnan. Small-scale structure of a scalar field convected by turbulence. *Phys. Fluids*, 11:945, 1968.

[36] R.H. Kraichnan. Anomalous scaling of a randomly advected passive scalar. *Phys. Rev. Lett.*, 72:1016, 1994.

[37] M. Millionschikov. On theory of homogeneous isotropic turbulence. *Dokl. Akad. Nauk SSSR*, 32:615, 1941.

[38] I. Proudman and W.H. Reid. On the decay of a normally distributed and homogeneous turbulent velocity field. *Phil. Trans. R. Soc. Lond. A*, 247:163–189, 1954.

[39] T. Tatsumi. The theory of decay process of incompressible isotropic turbulence. *Proc. R. Soc. Lond. A*, 239:16, 1957.

[40] Y. Ogura. A consequence of the zero-fourth-cumulant approximation in the decay of isotropic turbulence. *J. Fluid. Mech.*, 16:33–40, 1963.

[41] R. H. Kraichnan. Relation of fourth-order to second-order moments in stationary isotropic turbulence. *Phys. Rev.*, 107:1485, 1957.

[42] R. H. Kraichnan. Irreversible statistical mechanics of incompressible hydromagnetic turbulence. *Phys. Rev.*, 109:1407, 1958.

[43] S. Nazarenko. *Wave turbulence*, volume 825 of *Lecture notes in physics*. Springer, 2011.

[44] M. Chertkov, C. Connaughton, I. Kolokolov, and V. Lebedev. Dynamics of energy condensation in two-dimensional turbulence. *Phys. Rev. Lett.*, 99:084501, 2007.

[45] S. Goto and S. Kida. Direct-interaction approximation and Reynolds-number reversed expansion for a dynamical system. *Physica D*, 117:191, 1998.

[46] S. Goto and S. Kida. Sparseness of nonlinear coupling: importance in sparse direct-interaction perturbation. *Nonlinearity*, 15:1499, 2002.

[47] C. Brun and A. Pumir. Statistics of Fourier modes in a turbulent flow. *Phys. Rev. E*, 63:056313, 2001.

[48] H. L. Grant, R. W. Stewart, and A. Moilliet. Turbulence spectra from a tidal channel. *J. Fluid. Mech.*, 12:241, 1962.

[49] R.H. Kraichnan. Kolmogorov's hypotheses and Eulerian turbulence theory. *Phys. Fluids*, 7:1723, 1964.

[50] R.H. Kraichnan. Inertial-range transfer in two- and three-dimensional turbulence. *J. Fluid Mech.*, 47:525, 1971.

[51] R.H. Kraichnan. An almost-Markovian Galilean-invariant turbulence model. *J. Fluid Mech.*, 47:513, 1971.

[52] R. H. Kraichnan. Deviations from fluctuation-relaxation relations. *Phys. A*, 279:30, 2000.

[53] Y. Kaneda. Renormalized expansions in the theory of turbulence with the use of the Lagrangian position function. *J. Fluid. Mech.*, 107:131 – 145, 1981.

[54] Y. Kaneda. Inertial range structure of turbulent velocity and scalar fields in a lagrangian renormalized approximation. *Phys. Fluids*, 29:701–708, 1986.

[55] Y. Kaneda. Private Communication, 2011.

[56] S.A. Orszag. Analytical theories of turbulence. *J. Fluid Mech.*, 41:363, 1970.

[57] A. Pouquet, M. Lesieur, J.C. André, and C. Basdevant. Evolution of high Reynolds number two-dimensional turbulence. *J. Fluid Mech.*, 72:305–319, 1975.

[58] J.-P. Bertoglio, K. Squires, and J. Ferziger. Edqnm closure: A homogeneous simulation to support it. a quasi-homogeneous simulation to disprove it. In *Proceedings of the 1987 Summer Program of the CTR*, page 53, Stanford University, 1987.

[59] P. Sagaut and C. Cambon. *Homogeneous Turbulence Dynamics*. Cambridge University Press, 2008.

[60] R.H. Kraichnan. Convergents to turbulence functions. *J. Fluid Mech.*, 41:189, 1970.

[61] P. Langevin. Sur la théorie du mouvement brownien. *C. R. Acad. Sci. (Paris)*, 146:530, 1908.

[62] G.K. Batchelor. The effect of homogeneous turbulence on material lines and surfaces. *Proc. R. Soc. Lond. A.*, 213:349, 1952.

[63] L. Liechtenstein, F.S. Godeferd, and C. Cambon. Nonlinear formation of structures in rotating stratified turbulence. *J. Turbul.*, 6:1, 2005.

[64] W.J.T. Bos, L. Liechtenstein, and K. Schneider. Small scale intermittency in anisotropic turbulence. *Phys. Rev. E*, 76:046310, 2007.

[65] R. H. Kraichnan. Intermittency in the very small scales of turbulence. *Phys. Fluids*, 10:2080, 1967.

[66] R.H. Kraichnan and J.R. Herring. A strain-based Lagrangian-history turbulence theory. *J. Fluid Mech.*, 88:355–367, 1978.

[67] J.R. Herring and R.H. Kraichnan. A numerical comparison of velocity-based and strain-based Lagrangian-history turbulence approximations. *J. Fluid Mech.*, 91:581–597, 1979.

[68] T. Gotoh, J. Nagaki, and Y. Kaneda. Passive scalar spectrum in the viscous-convective range in two-dimensional steady turbulence. *Phys. Fluids*, 12(1):155–168, 2000.

[69] H. Chen, J.R. Herring, R.M. Kerr, and R.H. Kraichnan. Non-gaussian statistics in isotropic turbulence. *Phys. Fluids A*, 1:1844, 1989.

[70] R. H. Kraichnan. Models of intermittency in hydrodynamic turbulence. *Phys. Rev. Lett.*, 65:575, 1990.

[71] R. H. Kraichnan. Turbulent cascade and intermittency growth. *Proc. R. Soc. Lond. A*, 434:65, 1991.

[72] R. H. Kraichnan. In Eds. D.L. Dwoyer, M.Y. Hussaini, and R.G. Voight, editors, *Theoretical Approaches to Turbulence*, page 91. Springer, New York, 1985.

[73] H. Touil, M. Y. Hussaini, T. Gotoh, R. Rubinstein, and S. L. Woodruff. Development of stochastic models for turbulence. *New Journal of Physics*, (7):215, 2007.

[74] T.D. Lee. On some statistical properties of hydrodynamical and magnetohydrodynamical fields. *Q. Appl. Math*, 10:69, 1952.

[75] M. Wan, S. Oughton, S. Servidio, and W. H. Matthaeus. Generation of non-gaussian statistics and coherent structures in ideal magnetohydrodynamics. *Phys. Plasmas*, 16, 2009.

[76] S. Galtier, S.V. Nazarenko, A.C. Newell, and A. Pouquet. A weak turbulence theory for incompressible magnetohydrodynamics. *J. Plasma Phys.*, 63:447, 2000.

[77] G.I. Barenblatt. *Scaling, self-similarity, and intermediate asymptotics.* CUP, Cambridge, 1996.

[78] R.H. Kraichnan. Remarks on turbulence theory. *Adv. Math.*, 16:305, 1975.

[79] C. Cichowlas, P. Bonaïti, F. Debbasch, and M. Brachet. Effective dissipation and turbulence in spectrally truncated euler flows. *Phys. Rev. Lett.*, 95:264502, 2005. For a preliminary version of the manuscript see http://arxiv.org/ps/nlin/0410064v1.

[80] U. Frisch, S. Kurien, R. Pandit, W. Pauls, S.S. Ray, A. Wirth, and J.-Z. Zhu. Hyperviscosity, Galerkin truncation and bottlenecks in turbulence. *Phys. Rev. Lett.*, 101:144501, 2008.

[81] V. Borue and S.A. Orszag. Self-similar decay of three-dimensional homogeneous turbulence with hyperviscosity. *Phys. Rev. E*, 51:856, 1995.

[82] A.N. Kolmogorov. A refinement of previous hypotheses concerning the local structure of turbulence in a viscous incompressible fluid at high Reynolds number. *J. Fluid Mech.*, 13:82, 1962.

[83] R.H. Kraichnan. On Kolmogorov's inertial-range theories. *J. Fluid Mech.*, 62:305, 1974.

[84] F. Anselmet, Y. Gagne, E. J. Hopfinger, and R. A. Antonia. High-order velocity structure functions in turbulent shear flows. *J. Fluid Mech.*, 140:63, 1984.

[85] Y. Zhou. Interacting scales and energy transfer in isotropic turbulence. *Phys. Fluids A*, 5:2511, 1993.

[86] R.H. Kraichnan and R. Panda. Depression of nonlinearity in decaying isotropic turbulence. *Phys. Fluids*, 31:2395, 1988.

[87] M. Chertkov, A. Pumir, and B. I. Shraiman. Lagrangian tetrad dynamics and the phenomenology of turbulence. *Phys. Fluids*, 11:2394, 1999.

[88] L. Onsager. Statistical hydrodynamics. *Il Nuovo Cimento*, 6:279, 1949.

[89] G. Joyce and D. Montgomery. Negative temperature states for the two-dimensional guiding center plasma. *J. Plasma Phys.*, 10:107, 1973.

[90] D.C. Montgomery and G. Joyce. Statistical mechanics of "negative temperature" states. *Phys. Fluids*, 17:1139, 1974.

[91] D. Montgomery, W. H. Matthaeus, W. T. Stribling, D. Martinez, and S. Oughton. Relaxation in two dimensions and the "sinh-Poisson" equation. *Phys. Fluids A*, 4:3, 1992.

[92] R. Robert and J. Sommeria. Statistical equilibrium states for two-dimensional flows. *J. Fluid Mech.*, 229:291, 1991.

[93] J. Miller. Statistical mechanics of euler equations in two dimensions. *Phys. Rev. Lett.*, 65:2137–2140, 1990.

[94] A. Naso, S. Thalabard, G. Collette, P.-H. Chavanis, and B. Dubrulle. Statistical mechanics of beltrami flows in axisymmetric geometry: equilibria and bifurcations. *J. Stat. Mech.*, 2010:P06019, 2010.

[95] R. Monchaux, F. Ravelet, B. Dubrulle, A. Chiffaudel, and F. Daviaud. Properties of steady states in turbulent axisymmetric flows. *Phys. Rev. Lett.*, 96:124502, 2006.

[96] A. Pumir. A numerical study of the mixing of a passive scalar in three dimensions in the presence of a mean gradient. *Phys. Fluids*, 6:2118, 1994.

[97] A. Pumir. Anomalous scaling behaviour of a passive scalar in the presence of a mean gradient. *Europhys. Lett.*, 34:25, 1996.

[98] J.B. Taylor. Relaxation of toroidal plasma and generation of reverse magnetic fields. *Phys. Rev. Lett.*, 33:1139, 1974.

[99] S. Cappello and D. F. Escande. Bifurcation in viscoresistive MHD: The Hartmann number and the Reversed Field Pinch. *Phys. Rev. Lett.*, 85:3838, 2000.

[100] A.I. Niculescu. *VZN, a new damper concept.* BREN Editura, Bucuresti, 2010.

[101] F. Wagner *et al.* Regime of improved confinement and high beta in neutral-beam-heated divertor discharges of the ASDEX tokamak. *Phys. Rev. Lett.*, 49:1408, 1982.

[102] J.E. Rice *et al.* Inter-machine comparison of intrinsic toroidal rotation in tokamaks. *Nucl. Fusion*, 47:1618, 2007.

[103] P.H. Diamond, C.J. McDevitt, Ö.D. Gürcan, T.S. Hahm, W. X. Wang, E.S. Yoon, I. Holod, Z. Lin, V. Naulin, and R. Singh. Physics of non-diffusive turbulent transport of momentum and the origins of spontaneous rotation in tokamaks. *Nucl. Fusion*, 49(4):045002, 2009.

[104] J. A. Krommes. The gyrokinetic description of microturbulence in magnetized plasmas. *Ann. Rev. Fluid Mech.*, 44:175, 2012.

[105] S.I. Braginskii. Transport processes in a plasma. In Ed. M. A. Leontovich., editor, *Reviews of Plasma Physics, Volume 1.*, page 205. Consultants Bureau, New York, 1965.

[106] A. Hasegawa and M. Wakatani. Plasma edge turbulence. *Phys. Rev. Lett.*, 50:682, 1983.

[107] M. Wakatani and A. Hasegawa. A collisional drift wave description of plasma edge turbulence. *Phys. Fluids*, 27:611, 1984.

[108] A. Hasegawa and K. Mima. Pseudo-three-dimensional turbulence in magnetized nonuniform plasma. *Physics of Fluids*, 21:87, 1978.

[109] P.A. Davidson. *An Introduction to Magnetohydrodynamics.* Cambridge University Press, 2001.

[110] H.K. Moffatt. *Magnetic field generation in electrically conducting fluids.* Cambridge University Press, 1978.

[111] M.L. Goldstein, D.A. Roberts, and W.H. Matthaeus. Magnetohydrodynamic turbulence in the solar wind. *Anna. Rev. Astron. Astrophys.*, 33:283, 1995.

[112] D.C. Montgomery and L. Turner. Anisotropic magnetohydrodynamic turbulence in a strong external magnetic field. *Phys. Fluids*, 24:825, 1981.

[113] J.V. Shebalin, W.H. Matthaeus, and D.C. Montgomery. Anisotropy in mhd turbulence due to a mean magnetic field. *J. Plasma Phys.*, 29:525, 1983.

[114] B. Favier, F. S. Godeferd, C. Cambon, and A. Delache. On the two-dimensionalization of quasistatic magnetohydrodynamic turbulence. *Phys. Fluids*, 22:075104, 2010.

[115] H.K. Moffatt. On the suppression of turbulence by a uniform magnetic field. *J. Fluid Mech.*, 28:571, 1967.

[116] D.C. Montgomery and L. Turner. Two-and-a-half-dimensional magnetohydrodynamic turbulence. *Phys. Fluids*, 25:345, 1982.

[117] G.K. Batchelor. Small-scale variation of convected quantities like temperature in turbulent fluid. part 1. conductivity. *J. Fluid Mech*, 5:113, 1959.

[118] W.J.T. Bos, H. Touil, and J.-P. Bertoglio. Reynolds number dependency of the scalar flux spectrum in isotropic turbulence with a uniform scalar gradient. *Phys. Fluids*, 17:125108, 2005.

[119] W.J.T. Bos and J.-P. Bertoglio. Inertial range scaling of scalar flux spectra in uniformly sheared turbulence. *Phys. Fluids*, 19:025104, 2006.

[120] G.I. Taylor. The spectrum of turbulence. *Proc. Roy. Soc. Lond. A*, 164:476, 1938.

[121] C. Goepfert, J.-L. Marié, D. Chareyron, and M. Lance. Characterization of a system generating a homogeneous isotropic turbulence field by free synthetic jets. *Exp. Fluids*, 48:809–822, 2010.

[122] O. Kamps, R. Friedrich, and R. Grauer. Exact relation between eulerian and lagrangian velocity increment statistics. *Phys. Rev. E*, 79:066301, 2009.

[123] M. Holzer and E. Siggia. Skewed, exponential pressure distributions from Gaussian velocities. *Phys. Fluids A*, 5:2525, 1993.

[124] K. Yoshimatsu, N. Okamoto, K. Schneider, Y. Kaneda, and M. Farge. Intermittency and scale-dependent statistics in fully developed turbulence. *Phys. Rev. E*, 79:026303, 2008.

[125] A. Tsinober, P. Vedula, and P. K. Yeung. Random taylor hypothesis and the behavior of local and convective accelerations in isotropic turbulence. *Phys. Fluids*, 13:1974, 2001.

[126] P.K. Yeung and S.B. Pope. Lagrangian statistics from direct numerical simulations of isotropic turbulence. *J. Fluid Mech.*, 207:531, 1989.

[127] N. Mordant, P. Metz, O. Michel, and J.-F. Pinton. Measurement of Lagrangian velocity in fully developed turbulence. *Phys. Rev. Lett.*, 87:214501, 2001.

[128] G.A. Voth, A. La Porta, A.M. Crawford, J. Alexander, and E. Bodenschatz. Measurements of particle accelerations in fully developed turbulence. *J. Fluid Mech.*, 469:121, 2002.

[129] N. Mordant, J. Delour, E. Leveque, A. Arneodo, and J.-F. Pinton. Long time correlations in Lagrangian dynamics: a key to intermittency in turbulence. *Phys. Rev. Lett.*, 89:254502, 2002.

[130] M. Farge, G. Pellegrino, and K. Schneider. Coherent vortex extraction in 3d turbulent flows using orthogonal wavelets. *Phys. Rev. Lett.*, 87:054501, 2001.

[131] J. Weiss. The dynamics of enstrophy transfer in two-dimensional hydrodynamics. *Phys. D*, 48:273, 1991.

[132] W.J.T. Bos, S. Futatani, S. Benkadda, M. Farge, and K. Schneider. Role of coherent vorticity in turbulent transport in resistive drift-wave turbulence. *Phys. Plasmas*, 15:072305, 2008.

[133] Y. Kaneda. Lagranglan and eulerian time correlations in turbulence. *Phys. Fluids A*, 5:2835, 1993.

[134] C. Holland, G. R. Tynan, J. H. Yu, A. James, D. Nishijima, M. Shimada, and N. Taheri. Numerical simulations of collisional drift-wave turbulence in a magnetized plasma column. *Plasma Phys. Control. Fusion*, 49:A109, 2007.

[135] P.H. Diamond, S.-I. Itoh, K. Itoh, and T.S. Hahm. Zonal flows in plasma – a review. *Plasma Phys. Control. Fusion*, 47:35, 2005.

[136] G.R. Tynan, A. Fujisawa, and G. McKee. A review of experimental drift turbulence studies. *Plasma Phys. Control. Fusion*, 51:113001, 2009.

[137] R.H. Kraichnan. Inertial ranges in two-dimensional turbulence. *Phys. Fluids*, 10:1417, 1967.

[138] A.C. Ting, W.H. Matthaeus, and D.C. Montgomery. Turbulent relaxation processes in magnetohydrodynamics. *Phys. Fluids*, 29:3261, 1986.

[139] D. Biskamp and H. Welter. Magnetic field amplification and saturation in two-dimensional magnetohydrodynamic turbulence. *Phys. Fluids B*, 2:1787, 1990.

[140] S. Servidio, W. H. Matthaeus, and P. Dmitruk. Depression of nonlinearity in decaying isotropic mhd turbulence. *Phys. Rev. Lett.*, 100:095005, 2008.

[141] W. H. Matthaeus, A. Pouquet, P. D. Mininni, P. Dmitruk, and B. Breech. Rapid alignment of velocity and magnetic field in magnetohydrodynamic turbulence. *Phys. Rev. Lett.*, 100:085003, 2008.

[142] F. Spineanu and M. Vlad. Self-duality of the of the asymptotic relaxation states of fluids and plasmas. *Phys. Rev. E*, 67:046309, 2003.

[143] F. Bouchet and A. Venaille. Statistical mechanics of two-dimensional and geophysical flows. *Physics Reports*, In press, 2012.

[144] R. Kinney, J.C. McWilliams, and T. Tajima. Coherent structures and turbulent cascades in two-dimensional incompre ssible magnetohydrodynamic turbulence. *Phys. Plasmas*, 2:3623, 1995.

[145] S.A. Balbus and J.F. Hawley. Instability, turbulence, and enhanced transport in accretion disks. *Rev. Mod. Phys.*, 70:1, 1998.

[146] H. Ji, M. Burin, E. Schartman, and J. Goodman. Hydrodynamic turbulence cannot transport angular momentum effectively in astrophysical disks. *Nature*, 444:343, 2006.

[147] M. S. Paoletti and D. P. Lathrop. Angular momentum transport in turbulent flow between independently rotating cylinders. *Phys. Rev. Lett.*, 106:024501, 2011.

[148] C. Gissinger, J. Goodman, and H. Ji. The role of boundaries in the magnetorotational instability. *ArXiv*, page 1201.1853, 2012.

[149] H. J. H. Clercx, S.R. Maassen, and G.J.F.van Heijst. Spontaneous spin-up during the decay of 2d turbulence in a square container with rigid boundaries. *Phys. Rev. Lett.*, 80:5129, 1998.

[150] J.W. Bates and D.C. Montgomery. Toroidal visco-resisitive magnetohydrodynamic states contain vortices. *Phys. Plasmas*, 5:2649, 1998.

[151] L.P. Kamp and D.C. Montgomery. Toroidal flows in resisitive magnetohydrodynamic states. *Phys. Plasmas*, 10:157, 2003.

[152] D.C. Montgomery, J.W. Bates, and L.P. Kamp. Mhd steady states as a model for confined plasmas. *Plasma Phys. Control. Fusion*, 41:A507, 1999.

[153] L.P. Kamp and D.C. Montgomery. Toroidal steady states in visco-resistive magnetohydrodynamics. *J. Plasma Phys.*, 70:113, 2004.

[154] D. F. Escande, P. Martin, S. Ortolani, A. Buffa, P. Franz, L. Marrelli, E. Martines, G. Spizzo, S. Cappello, A. Murari, R. Pasqualotto, and P. Zanca. Quasi-single-helicity reversed-field-pinch plasmas. *Phys. Rev. Lett.*, 85:1662, 2000.

[155] X. Shan, D.C. Montgomery, and H. Chen. Nonlinear magnetohydrodynamics by Galerkin-method computation. *Phys. Rev. A*, 44:6800, 1991.

[156] S. Li, D.C. Montgomery, and W.P. Jones. Two-dimensional turbulence with rigid walls. *Theor. Comput. Fluid Dyn.*, 9:167, 1997.

[157] H.J.H. Clercx, A.H. Nielsen, D.J. Torres, and E.A. Coutsias. Two-dimensional turbulence in square and circular domains with no-slip walls. *Eur. J. Mech. B/Fluids*, 20:557, 2001.

[158] K. Schneider, S. Neffaa, and W.J.T. Bos. A pseudo-spectral method with volume penalisation for magnetohydrodynamic turbulence in confined domains. *Comp. Phys. Comm.*, 182:2, 2010.

[159] P. Angot, C.H. Bruneau, and P. Fabrie. A penalization method to take into account obstacles in viscous flows. *Numer. Math.*, 81:497, 1999.

[160] A. Vincent and M. Meneguzzi. The satial structure and statistical properties of homogeneous turbulence. *J. Fluid. Mech.*, 225:1, 1991.

[161] P.D. Mininni and D.C. Montgomery. Magnetohydrodynamic activity inside a sphere. *Phys. Fluids*, 18:116602, 2006.

[162] X. Shan and D.C. Montgomery. On the role of the Hartmann number in magnetohydrodynamic activity. *Plasma Phys. Control. Fusion*, 35:619, 1993.

[163] X. Shan and D.C. Montgomery. Global searches of Hartmann-number-dependent stability boundaries. *Plasma Phys. Control. Fusion*, 35:1019, 1993.

[164] Robert Rubinstein. Quote.

Part II

Curriculum Vitae

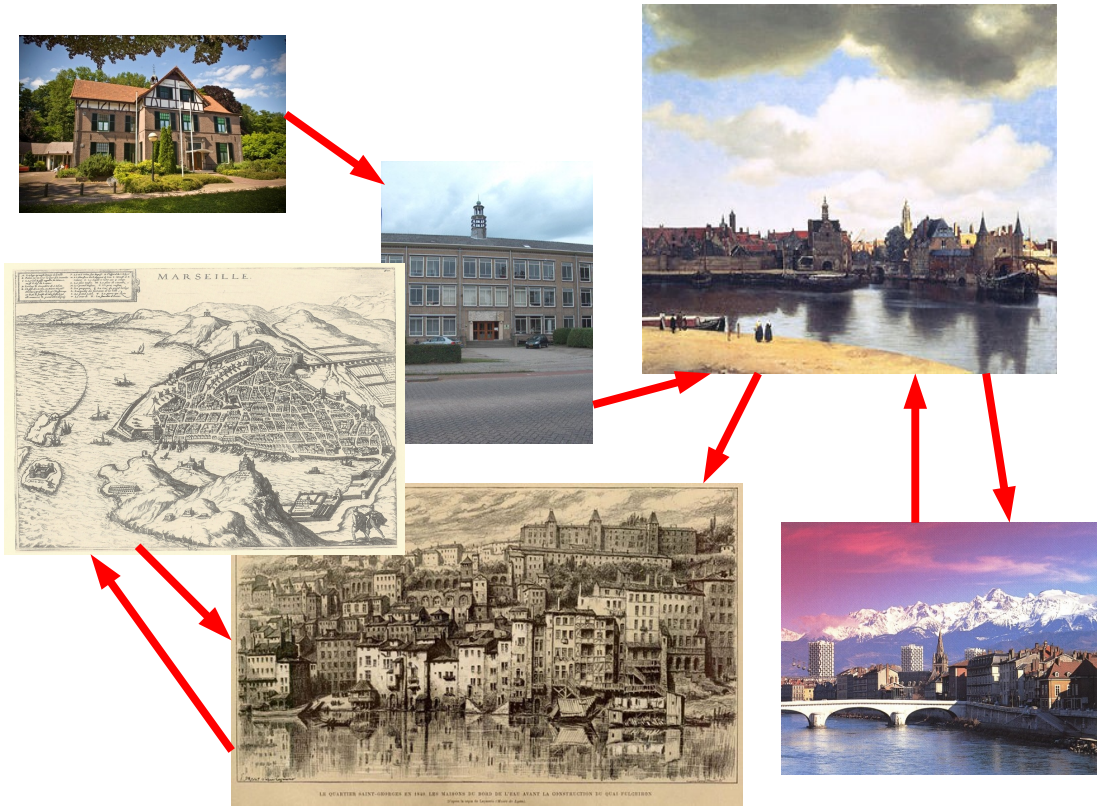

Curriculum Vitae

Personal information

Wouter J.T. Bos, born August 15th 1977 in Deventer (the Netherlands).
Married, one child
Fluent in Dutch, French, English and Spanish

Track Record

2007-	**CNRS Researcher (CR1)** LMFA, Ecole Centrale de Lyon, UCBL, INSA
2006-2007	**Postdoc**, M2P2, Marseille. ANR project: Multi-scale methods for fluid and plasma turbulence. Application to magnetically confined fusion plasmas.
2005-2006	**ATER**, Université Lyon 1. Start of a research collaboration with NASA Langley
2001-2005	**PhD in fluid mechanics** *Passive Scalar Mixing in Turbulent Flow* Supervisor: Jean-Pierre Bertoglio, Ecole Centrale de Lyon
1995-2001	**Batchelor & Master in applied physics**, Technische Universiteit Delft (Netherlands), with one year at the University Joseph-Fourier, Grenoble (France), Master in Geophysics.

Teaching

2010-	Teaching *Turbulent Mixing* (Master Recherche, Ecole Doctorale MEGA).
2004-2006	Research and teaching position (1/2 ATER) at *Université Lyon 1.*
2001-2004	Course assistant (Moniteur) at the *Ecole Centrale de Lyon.*
1998-2000	Course assistant (Vacataire) at the applied physics faculty, *Technische Universiteit Delft.*

In the following I will use the french abbreviations TP for *Travaux Pratiques* (practical work sessions), TD for *Travaux Dirigés* (tutorial classes) and CM for *Cours Magistraux* (lectures). Following the Batchelor-Master system, the three years of the Batchelor degree are indicated by (L1,2,3) and the Master degree by (M1,2).

At the different institutes (Delft University of Technology, UCBL, ISTIL, ECL), I taught:

- Turbulent mixing (CM; M2)
- Fluid Mechanics (TD, TP; L3, M1)
- Heat transfer (TD, TP; M1)
- Point Mechanics (TD, L2)
- Experimental Methods in Physics (TP; L1 ,L2)
- Experimental Electronics (TP; L1,2)
- Informatics for physisists (TP; Linux, Maple, Pascal) (L1)

The cumulative teaching load of these activities is 288 hours at Batchelor level plus 156 hours at Master level. In addition I co-developed new computer-based TP-sessions for students at the Ecole Centrale, using the commercial Computational Fluid Dynamics Code FLUENT.

Research

Fields of expertise

The remainder of this manuscript gives an approximate idea on the subjects that I have worked on the last ten years. The key topic is turbulence in both fluids and plasmas. More specifically my main contributions are in the subdomains listed below. I also show the year in which I started working on these subjects.

- Mixing (2001-)
- Spectral closure theories and turbulence modeling (2001-)
- Lagrangian statistical description of fluid flows (2007-)
- Edge turbulence modeling (in fusion devices) (2007-)
- Self-organization in magnetohydrodynamics (2008-)
- Development of numerical methods for wall bounded turbulent fluid and plasma flows (2008-)
- Depletion of nonlinearity in turbulence (2011-)
- Large Eddy Simulation techniques (2008-)
- Two-dimensional turbulent flows (2007-)

The people with whom I collaborate on these subjects can be found in the next two subsections: (co-)supervised students and external collaborators, in addition to colleagues at the LMFA laboratory (Jean-Pierre Bertoglio, Liang Shao, Fabien Godeferd, Claude Cambon, Alexandre Delache, Guillevic Lamaison, Julian Scott, Hatem Touil, Benjamin Favier).

Scientific supervision

Percentages indicate the approximate implication in the supervision.

Master Students	
L. Kacioui (30% with Claude Cambon)	2006
A. Pushkarev 100%	2009
J. Morales 100%	2009 - 2010
PhD Students	
B. Kadoch (50% with K. Schneider)	2006 - 2009
S. Neffaa (50% with K. Schneider)	2006 - 2010
L. Fang (30% final year with L. Shao)	2008 - 2009
M. Leroy (30% with K. Schneider)	2009 -
A. Pushkarev (95% with J.-P. Bertoglio)	2010 -
J. Morales (95% with J.-N. Gence)	2010 -

External Collaborations

Research collaborations over the last five years

L. Chevillard	ENS Lyon
C. Connaughton	Univ. Warwick
D. Del Castillo Negrete	Oak Ridge National Lab.
L. Fang	Ecole Centrale de Peking
S. Futatani	CEA Cadarache
F. Jacobitz	University of San Diego
B. Kadoch	IUSTI Marseille
D. Montgomery	Dartmouth College
R. Rubinstein	NASA Langley
K. Schneider	M2P2 Marseille

Project Management

Project coordinator of the project SiCoMHD (2011-2014). The project is funded by the Agence Nationale de la Recherche (ANR) in the framework of the 2011 fundamental research program (programme Blanc). The project concerns the computation of magnetohydrodynamic turbulence in wall bounded geometry with applications to geophysics, industrial flows of liquid metals and magnetically confined fusion. The project involves the Laboratories LMFA (Lyon), M2P2 (Marseille) and Cassiopee (Nice).

Scientific Production

Refereed Journal Publications: 30
Refereed conference proceedings: 23
H-factor: 7 (Web of Science February 2012)
Referee for J. Fluid Mech., Phys. Fluids, J. Turbulence, Eur. J. Mech. - B, Phys. Rev. E., Phys. Lett. A

Refereed Journal Publications

1. Wouter J.T. Bos, L. Chevillard, J.F. Scott and R. Rubinstein. Reynolds number effect on the velocity increment skewness in isotropic turbulence *Phys. Fluids*, 24:015108, 2012.
2. Le Fang, Wouter J.T. Bos, Liang Shao, and Jean-Pierre Bertoglio. Time-reversibility of navier-stokes turbulence and its implication for subgrid scale models. *J. Turbul.*, 13:1 2012.
3. Wouter J.T. Bos, Colm Connaughton, and Fabien S. Godeferd. Developing homogeneous isotropic turbulence. *Physica D*, 241:232 2012.
4. Benjamin Kadoch, Wouter J.T. Bos, and Kai Schneider. The influence of walls on lagrangian statistics in two-dimensional turbulence. *Phys. Fluids*, 23:085111, 2011.
5. Frank G. Jacobitz, Kai Schneider, Wouter J.T. Bos, and Marie Farge. Influence of initial mean helicity on homogeneous turbulent shear flow. *Phys. Rev. E*, 84:056319, 2011.
6. Benjamin Favier, Fabien S. Godeferd, Claude Cambon, Alexandre Delache and Wouter J.T. Bos. Quasi-static magnetohydrodynamic turbulence at high reynolds number. *J. Fluid Mech.*, 681:434–461, 2011.
7. Benjamin Kadoch, Diego del Castillo Negrete, Wouter J.T. Bos, and Kai Schneider. Lagrangian statistics and flow topology in forced two-dimensional turbulence. *Phys. Rev. E*, 83, 2011. http://arxiv.org/abs/1009.2819.
8. Shinpei Futatani, Wouter J.T. Bos, Diego del Castillo Negrete, Kai Schneider, and Marie Farge. Coherent vorticity extraction in resistive drift-wave turbulence: Comparison of orthogonal wavelets versus proper orthogonal decomposition. *C. R. Physique*, 12, 2011.
9. Kai Schneider, Salah Neffaa, and Wouter J.T. Bos. A pseudo-spectral method with volume penalisation for magnetohydrodynamic turbulence in confined domains. *Comp. Phys. Comm.*, 182:2–7, 2011.
10. Wouter J.T. Bos, Benjamin Kadoch, Salah Neffaa, and Kai Schneider. Lagrangian dynamics of drift-wave turbulence. *Physica D*, 239:1269–1277, 2010.
11. Le Fang, Wouter J.T. Bos, X. Zhou, Liang Shao, and Jean-Pierre Bertoglio. Corrections to the scaling of the second-order structure function in isotropic turbulence. *Acta Mech. Sin.*, 26:151–157, 2010.
12. Benjamin Kadoch, Wouter J.T. Bos, and Kai Schneider. Origin of lagrangian intermittency in drift-wave turbulence. *Phys. Rev. Lett.*, 105:145001, 2010.
13. Wouter J.T. Bos, Salah Neffaa, and Kai Schneider. Self-organization and symmetry-breaking in two-dimensional plasma turbulence. *Phys. Plasmas*, 17:092302, 2010.
14. Frank G. Jacobitz, Kai Schneider, Wouter J.T. Bos, and Marie Farge. On the structure and dynamics of sheared and rotating turbulence: Anisotropy properties and geometrical scale-dependent statistics. *Phys. Fluids*, 22:085101, 2010.
15. Wouter J.T. Bos, Benjamin Kadoch, Kai Schneider, and Jean-Pierre Bertoglio. Inertial range scaling of the scalar flux spectrum in two-dimensional turbulence. *Phys. Fluids*, 21:115105, 2009.
16. Wouter J.T. Bos and Jean-Pierre Bertoglio. Large-scale bottleneck effect in two-dimensional turbulence. *J. Turbul.*, 10:1–8, 2009.
17. Robert Rubinstein and Wouter J.T. Bos. On the unsteady behavior of turbulence models. *Phys. Fluids*, 21:041701, 2009.
18. Wouter J.T. Bos, Salah Neffaa, and Kai Schneider. Rapid generation of angular momentum in bounded magnetized plasma. *Phys. Rev. Lett.*, 101:235003, 2008.
19. Salah Neffaa, Wouter J.T. Bos, and Kai Schneider. The decay of magnetohydrodynamic turbulence in a confined domain. *Phys. Plasmas*, 15:092304, 2008.
20. Wouter J.T. Bos, Shinpei Futatani, Sadruddin Benkadda, Marie Farge, and Kai Schneider. The role of coherent vorticity in turbulent transport in resistive drift-wave turbulence. *Phys. Plasmas*, 15:072305, 2008.
21. Benjamin Kadoch, Wouter J.T. Bos, and Kai Schneider. Extreme lagrangian acceleration in confined turbulent flow. *Phys. Rev. Lett.*, 100:184503, 2008.

22. Wouter J.T. Bos, Lukas Liechtenstein, and Kai Schneider. Small-scale intermittency in anisotropic turbulence. *Phys. Rev. E*, 76:046310, 2007.
23. Wouter J.T. Bos, Timothy T. Clark, and Robert Rubinstein. Small scale response and modeling of periodically forced turbulence. *Phys. Fluids*, 19:055107, 2007.
24. Wouter J.T. Bos, Liang Shao, and Jean-Pierre Bertoglio. Spectral imbalance and the normalized dissipation rate of turbulence. *Phys. Fluids*, 19:045101, 2007.
25. Guillevic Lamaison, Wouter J.T. Bos, Liang Shao, and Jean-Pierre Bertoglio. Decay of scalar variance in isotropic tubulence in a bounded domain. *J. Turbul.*, 8:N 4, 2007.
26. Wouter J.T. Bos and Jean-Pierre Bertoglio. Inertial range scaling of scalar flux spectra in uniformly sheared turbulence. *Phys. Fluids*, 19:025104, 2007.
27. Wouter J.T. Bos and Jean-Pierre Bertoglio. Dynamics of spectrally truncated inviscid turbulence. *Phys. Fluids*, 18:071701, 2006.
28. Wouter J.T. Bos and Jean-Pierre Bertoglio. A single-time two-point closure based on fluid particle displacements. *Phys. Fluids*, 18:031706, 2006.
29. Wouter J.T. Bos, Hatem Touil, and Jean-Pierre Bertoglio. Reynolds number dependency of the scalar flux spectrum in isotropic turbulence with a uniform scalar gradient. *Phys. Fluids*, 17:125108, 2005.
30. Wouter J.T. Bos, Hatem Touil, Liang Shao, and Jean-Pierre Bertoglio. On the behavior of the velocity-scalar cross correlation spectrum in the inertial range. *Phys. Fluids*, 16:3818–3823, 2004.

Refereed Conference Proceedings

1. Alexandre Delache, Benjamin Favier, Fabien S. Godeferd, Claude Cambon, and Wouter J.T. Bos. Quasi-static magnetohydrodynamic turbulence at high reynolds number. In *Journal of Physics : Conference Series Volume 318*, page 072026, London, 2011. IOP.
2. Robert Rubinstein, Wouter J.T. Bos, and T. Gotoh. Vertex corrections and 'optimal' subgrid models for homogeneous isotropic turbulence. In *Journal of Physics : Conference Series Volume 318*, London, 2011. IOP.
3. Frank G. Jacobitz, Kai Schneider, Wouter J.T. Bos, and Marie Farge. Helical properties of sheared and rotating turbulence. In *Journal of Physics : Conference Series Volume 318*, London, 2011. IOP.
4. Wouter J.T. Bos, Robert Rubinstein, and Le Fang. Depletion of advection in turbulent scalar mixing. In *Journal of Physics : Conference Series Volume 318*, page 052037, London, 2011. IOP.
5. Benjamin Kadoch, Diego del Castillo Negrete, Wouter J.T. Bos, and Kai Schneider. Influence of flow topology on lagrangian statistics in two-dimensional turbulence. In *Journal of Physics : Conference Series Volume 318*, page 052032, London, 2011. IOP.
6. Wouter J.T. Bos and Robert Rubinstein. The role of nonlocality in unsteady turbulence. In B. Eckhardt, editor, *Advances in Turbulence XII*, Dordrecht, The Netherlands, 2009. Springer.
7. Salah Neffaa, Wouter J.T. Bos, and Kai Schneider. Zonal flows in mhd turbulence. In *Proceedings of the sixth symposium on turbulence and shear flow phenomena*, 2009.
8. Dmitry Kolomenskiy, Benjamin Kadoch, Wouter J.T. Bos, Kai Schneider, and Philippe Angot. Scalar mixing in turbulent confined flow. In B. Eckhardt, editor, *Advances in Turbulence XII*, Dordrecht, The Netherlands, 2009. Springer.
9. Frank G. Jacobitz, Wouter J.T. Bos, Kai Schneider, and Marie Farge. Anisotropy properties of rotating sheared turbulence. In *Proceedings of the sixth symposium on turbulence and shear flow phenomena*, 2009.
10. Salah Neffaa, Wouter J.T. Bos, and Kai Schneider. Spin-up in mhd turbulence. In B. Eckhardt, editor, *Advances in Turbulence XII*, Dordrecht, The Netherlands, 2009. Springer.
11. Kai Schneider, Salah Neffaa, Benjamin Kadoch, and Wouter J.T. Bos. Lagrangian intermittency and time-correlations in two-dimensional turbulence. In B. Eckhardt, editor, *Advances in Turbulence XII*, Dordrecht, The Netherlands, 2009. Springer.

12. Frank G. Jacobitz, Wouter J.T. Bos, Kai Schneider, and Marie Farge. Structural features of rotating sheared turbulence. In B. Eckhardt, editor, *Advances in Turbulence XII*, Dordrecht, The Netherlands, 2009. Springer.
13. Benjamin Kadoch, Wouter J.T. Bos, and Kai Schneider. Lagrangian statistics of two-dimensional turbulence in a square container. In B. Eckhardt, editor, *Advances in Turbulence XII*, Dordrecht, The Netherlands, 2009. Springer.
14. Wouter J.T. Bos, Laurent Chevillard, and Julian F. Scott. Reynolds number effect on the velocity increment skewness in isotropic turbulence. In *Proceedings of Euromech colloquium 512 on small scale turbulence and related gradient statistics*, 2009.
15. Salah Neffaa, Wouter J.T. Bos, and Kai Schneider. A pseudo-spectral method with volume penalisation for magnetohydrodynamic turbulence in bounded domains. In *Proceedings of the International Symposium on Frontiers of Computational Science*, 2008.
16. Robert Rubinstein and Wouter J.T. Bos. The modulated dissipation rate in periodically forced turbulence. In José M. L. M. Palma and A. Silva Lopez, editors, *Advances in Turbulence XI*, pages 553–555, Dordrecht, The Netherlands, 2007. Springer.
17. Wouter J.T. Bos and Jean-Pierre Bertoglio. Application of a two-point closure to the dispersion of particles in isotropic and sheared turbulence. In *Progress in Turbulence II*, Dordrecht, The Netherlands, 2007. Springer.
18. Wouter J.T. Bos, Liang Shao, and Jean-Pierre Bertoglio. The effect of a finite cascade time on the normalized energy dissipation. In José M. L. M. Palma and A. Silva Lopez, editors, *Advances in Turbulence XI*, pages 23–25, Dordrecht, The Netherlands, 2007. Springer.
19. Lukas Liechtenstein, Wouter J.T. Bos, and Kai Schneider. Quantifying anisotropy in stratified and rotating turbulence using orthogonal wavelets. In José M. L. M. Palma and A. Silva Lopez, editors, *Advances in Turbulence XI*, Dordrecht, The Netherlands, 2007. Springer.
20. Wouter J.T. Bos, Hatem Touil, and Jean-Pierre Bertoglio. Closure study of the reynolds number dependency of the scalar flux spectrum. In *Proceedings of the fourth symposium on turbulence and shear flow phenomena*, 2005.
21. Wouter J.T. Bos, Hatem Touil, Liang Shao, and Jean-Pierre Bertoglio. Etude de l'effet du nombre de reynolds sur le spectre du flux de scalaire. In *Actes du 17ème Congrès français de mécanique*, 2005.
22. Wouter J.T. Bos, Hatem Touil, Liang Shao, and Jean-Pierre Bertoglio. Spectral studies of scalar mixing. In H. I. Andersson and P.-A. Krogstad, editors, *Advances in Turbulence X*, pages 171–174, Barcelona, Spain, 2004. International Center for Numerical Methods in Engineering (CIMNE).
23. Wouter J.T. Bos, Hatem Touil, Liang Shao, and Jean-Pierre Bertoglio. Two-point modelling of turbulent scalar mixing and a new inertial range law. In *Turbulence, heat and mass transfer 4*, pages 895–902, New York, Wallingford (UK), 2003. Begell house inc.

Conferences without proceedings

1. Wouter J.T. Bos (2012). Depletion of nonlinearity and self-organization in turbulence and mixing New Challenges in Turbulence Research II, Les Houches, France.
2. Wouter J.T. Bos (2011). Lagrangian intermittency in drift-wave turbulence Dynamics and turbulent transport in plasmas and conducting fluids, Les Houches, France.
3. Frank G. Jacobitz, Kai Schneider, Wouter J.T. Bos, Marie Farge (2011). irect numerical simulations of homogeneous turbulent shear flow with initial mean helicity 64th Annual Meeting of the APS Division of Fluid Dynamics, Baltimore, United States.
4. Frank G. Jacobitz, Kai Schneider, Wouter J.T. Bos, Marie Farge (2011). Helicity and super-helicity in homogeneous turbulent shear flow 53rd Annual Meeting of the APS Division of Plasma Physics, Salt Lake City, United States.
5. Benjamin Kadoch, Diego Del Castillo Negrete, Wouter J.T. Bos, Kai Schneider (2011). Lagrangian statistics and flow topology in resistive drift-wave turbulence 53rd Annual Meeting of the APS Division of Plasma Physics, Salt Lake City, United States.

6. Kai Schneider, Benjamin Kadoch, Wouter J.T. Bos (2010). Is drift-wave turbulence intermittent from a Lagrangian point of view ? 63rd Annual Meeting of the APS Division of Fluid Dynamics, Long Beach, United States.
7. Benjamin Kadoch, Diego Del Castillo Negrete, Wouter J.T. Bos, Kai Schneider (2010). Influence of flow topology on Lagrangian statistics in forced 2-D turbulence 63rd Annual Meeting of the APS Division of Fluid Dynamics, Long Beach, United States.
8. Frank G. Jacobitz, Kai Schneider, Wouter J.T. Bos, Marie Farge (2010). On multiscale geometrical statistics of anisotropic homogeneous turbulence 63rd Annual Meeting of the APS Division of Fluid Dynamics, Long Beach, United States.
9. Kai Schneider, Benjamin Kadoch, Wouter J.T. Bos (2010). On Lagrangian intermittency in drift-wave turbulence 52nd Annual Meeting of the APS Division of Plasma Physics, Chicago, United States.
10. Wouter J.T. Bos (2009). Reynolds number effect on the velocity increment skewness in isotropic turbulence GDR Turbulence, Aussois, France.
11. Wouter J.T. Bos, Salah Neffaa, Kai Schneider (2009). Spin-up in MHD turbulence GDR Dynamo, Cambridge, United Kingdom.
12. Wouter J.T. Bos (2009). Physical space correlations and two-point closures Colloque Scientifique centre Henri Bénard, Ecully, France.
13. Wouter J.T. Bos, Salah Neffaa, Kai Schneider (2008). Rapid Spin-Up of MHD Turbulence 50th Annual Meeting of the APS Division of Plasma Physics, Dallas, United States.
14. Wouter J.T. Bos, Benjamin Kadoch, Kai Schneider (2008). Extreme lagrangian acceleration in confined turbulence Journée Scientifique centre Henri Bénard, Ecully, France.
15. Kai Schneider, Salah Neffaa, Wouter J.T. Bos (2008). The decay of MHD turbulence in a bounded domain 50th Annual Meeting of the APS Division of Plasma Physics, Dallas, United States.
16. Wouter J.T. Bos (2008). Generation of angular momentum in bounded two-dimensional MHD Colloque Astroflu, Ecully, .
17. Wouter J.T. Bos, Florence Raynal (2008). Lagrangian acceleration in time-periodic laminar flow GDR Turbulence, Lyon, France.
18. Kai Schneider, Benjamin Kadoch, Wouter J.T. Bos (2008). Lagrangian statistics in confined two-dimensional turbulence 61st Annual Meeting of the APS Division of Fluid Dynamics, San Antonio, United States.
19. Wouter J.T. Bos, Liang Shao, Jean-Pierre Bertoglio (2008). Déséquilibre spectral et la dissipation normalisée en turbulence GDR Turbulence, Ile d'Oléron, France.
20. Wouter J.T. Bos, Salah Neffaa, Kai Schneider (2008). Rapid Spin-Up of MHD Turbulence 61st Annual Meeting of the APS Division of Fluid Dynamics, San Antonio, United States.
21. Wouter J.T. Bos, Salah Neffaa, Kai Schneider (2008). The decay of magnetohydrodynamic turbulence in a confined domain Méthodes multi-échelles pour la turbulence plasma et fluide, Marseille, France.
22. Marie Farge, Wouter J.T. Bos, Shinpei Futatani, Sadruddin Benkadda, Kai Schneider (2008). Coherent vortex extraction in drift wave turbulence using orthogonal wavelets 50th Annual Meeting of the APS Division of Plasma Physics, Dallas, United States.
23. Wouter J.T. Bos (2008). Studies of two-dimensional turbulence Workshop on Conceptual aspects in turbulence, Vienne, Austria.
24. Wouter J.T. Bos, Liang Shao, Jean-Pierre Bertoglio (2007). Déséquilibre spectral et la dissipation normalisée en turbulence GDR Turbulence, Marseille, France.
25. Wouter J.T. Bos, Shinpei Futatani, Sadruddin Benkadda, Marie Farge, Kai Schneider (2007). Turbulent transport in drift wave turbulence: the role of coherent vorticity 49th Annual Meeting of the Division of Plasma Physics, Orlando, United States.
26. Wouter J.T. Bos, Benjamin Kadoch, Kai Schneider, Jean-Pierre Bertoglio (2007). Scaling of the velocity-scalar cross-correlation specttum in two-dimensional turbulence 60th Annual Meeting of the Divison of Fluid Dynamics, Salt Lake City, United States.

27. Wouter J.T. Bos, Jean-Pierre Bertoglio (2006). A two-point closure based on a Lagrangian timescale Euromech Fluid Mechanics Conference 6, Stockholm, Sweden.

28. Robert Rubinstein, Wouter J.T. Bos, Timothy T. Clark (2006). Small scale response in periodically forced turbulence 59th Annual Meeting of the APS Division of Fluid Dynamics, Tampa Bay, United States.

29. Wouter J.T. Bos (2006). On the universality of the normalized dissipation rate Workshop on 3D structure and Lagrangian aspects in turbulence for fluids and plasmas, Marseille, France.

30. Wouter J.T. Bos, Robert Rubinstein (2006). ForÃ§age périodique de la turbulence et réponse des petites échelles GDR Turbulence et Dynamo, Nice, France.

31. Wouter J.T. Bos, Jean-Pierre Bertoglio (2005). Dispersion de particules en turbulence avec ou sans cisaillement GDR Turbulence, Nantes, France.

32. Wouter J.T. Bos, Jean-Pierre Bertoglio (2005). Dynamique non visqueuse du spectre d'énergie cinétique dans un domaine spectral tronqué GDR Turbulence, Ecully, France.

33. Wouter J.T. Bos, Jean-Pierre Bertoglio (2005). A single-time two-point closure based on particle displacements in a scalar field NIA/ERCOFTAC workshop on Spectral theories of turbulence and their applications, Williamsburg, United States.

34. Wouter J.T. Bos, Hatem Touil, Liang Shao, Jean-Pierre Bertoglio (2004). On the velocity-scalar cross correlation spectrum Colloque Jean Mathieu, Ecully, France.

Thanks!

After finishing university I thought I knew a lot. Then, starting my PhD, I found out that the people around me knew so much more than I did. It took 4 years to learn some things about a very small part of turbulence research, in particular, thanks to Jean-Pierre Bertoglio, who not only taught me things on turbulence, but also showed me how to survive in research. After my PhD, two persons have influenced my path substantially, first Kai Schneider with his unbounded energy and enthusiasm. Secondly, Bob Rubinstein, by transmitting me some of his profound knowledge on turbulence and on Kraichnan's contributions to the field. Now, roughly ten years after the start of my PhD, despite the things that these three people have taught me, I realize that I still do not know a lot, but I also see now, that 'a lot' is a very relative concept.

Shortly after the end of my PhD, Dominique Escande visited our laboratory and gave a presentation on magnetically confined fusion research. This inspired me to dedicate a part of my energy to that field, and I still work with pleasure on the subject. I am grateful that Dominique has accepted to referee the manuscript. I also thank the other two referees, Bill Matthaeus and Annick Pouquet for having reviewed my work in detail. I thank Jean-Noël Gence for participating in the committee and more particularly for listening to my hand-waving explanations, and helping me to understand the basic mechanisms of turbulent flows. Thanks also to Jean-François Pinton for accepting to be on the committee and for almost succeeding to actually attend the presentation.

It would not have been possible for me to carry out the investigations presented in this work all by myself. I am very grateful that I could count on the contributions of Benjamin Kadoch, Salah Neffaa, Jorge Morales and Andrey Pushkarev during their PhD projects. I would also like to express my very great appreciation to my external collaborators: Laurent Chevillard, Colm Connaughton, Diego Del Castillo Negrete, Marie Farge, Shimpei Futatani, Frank Jacobitz and, in particular, to David Montgomery.

A big thanks goes to the colleagues of the LMFA and in particular to the 'turbulence' colleagues that I have collaborated with over the last ten years: Claude Cambon, Alexandre Delache, Le Fang, Benjamin Favier, Fabien Godeferd, Guillevic Lamaison, Julian Scott, Liang Shao, Hatem Touil. On a national level, I appreciated the stimulating discussions with the colleagues of the GDR turbulence.

It is a pleasure to go to work when you know that there is a place where you can relax, complain, drink coffee and have a good conversation. The laboratory microfiche facility, with its specialized documentation [100], is the perfect place for this. I want to warmly thank the colleagues that are, or were, there to share the every-day-worries and pleasures, Philippe Eyraud, Loic Méès, Cyril

Casissa, Michael Brückner, Cyril Mauger, Aurore Naso, Delphine Chareyron, Rémi Zamansky, Faouzi Laadhari, Aurélien Hémon, Andrew Lawrie, Antoine Godard and the turbomachins.

Thanks to my family and friends in Holland, France and Liverpool.

Thanks to Elena and Simon for showing me that there is more in life than work.